STARK-INDUCED OPTICAL NONLINEARITY IN GASEOUS NH_2D

and

OPTICAL WAVES IN LAYERED MEDIA

Thesis by

Pochi Albert Yeh

In Partial Fulfillment of the Requirements

for the Degree of

Doctor of Philosophy

California Institute of Technology

Pasadena, California

1978

(Submitted September 30, 1977)

ACKNOWLEDGMENT

I would like to express my deepest appreciation to my advisor, Professor A. Yariv for his superb guidance and constant encouragement, throughout the course of this research. His physical intuition led me to the directions of worthwhile research programs in physics as well as in applied physics. He taught me always with great patience, attention and care. His enlightening and instructive guidance led me to develop my research ability. I am thoroughly grateful and indebted to him for his profound influence on my professional advancement and achievement in recent years. I owe my future success to him.

I would also like to express my appreciation to Professors R. P. Feynman, J. Mathews and C. Papas for helpful discussions.

During the first part of this research I enjoyed the collaboration with Hughes Research Laboratories. In particular I would like to thank Dr. R. L. Abrams for his technical advice and helpful discussions. For the second part of this research, I would like to acknowledge Dr. A. Y. Cho of Bell Telephone Laboratories. His excellently fabricated multilayer samples made experimental observations possible.

The skillful technical assistance of D. Armstrong with the experimental apparatus is greatly appreciated. Special thanks go to Mrs. Ruth Stratton and Mrs. Verona Carpenter for their expert typing. I am also grateful to Mr. C. S. Hong for his contribution to part of this work. I wish him success in his future graduate work.

ABSTRACT

The first part of this work describes theoretical and experimental studies of Stark-induced three-wave mixing in gaseous NH_2D. Application of a dc electric field to a gaseous system destroys the basic inversion symmetry and allows two-photon mixing processes to occur. A theoretical derivation of this effect under conditions of resonantly enhanced non-linearities is given for a three-level system. Calculations are presented for mixing of a CO_2 laser with 4 GHz microwaves in the molecule NH_2D, producing single lower sideband radiation.

Experimental observation of resonantly enhanced, dc-induced, three-wave mixing in gaseous NH_2D is presented. The dependence of this effect on gas pressure, microwave frequency, applied dc field, and microwave power are presented and compared with theoretical predictions. The experiment was done at Hughes Research Laboratories by Abrams and his coworkers.

The second part of this work describes the propagation of electromagnetic waves in periodic layered media. The propagation of electromagnetic radiation in periodically stratified media is considered. Media of finite, semi-infinite and infinite extent are treated. A diagonalization of the unit cell translation operator is used to obtain exact solutions for the Bloch waves, the dispersion relations, and the band structure of the medium.

The theory of electromagnetic Bloch waves in periodic stratified media is then applied to the problems of birefringence, and group velocity in these media. The relevance of periodic media to phase matching in nonlinear mixing experiments-and to laser action in the x-ray region is discussed.

New types of guided waves such as Bragg guided waves and optical surface waves are theoretically predicted and experimentally observed.

TABLE OF CONTENTS

Part I

<u>Stark-induced Nonlinearity in Gaseous NH_2D</u>

Part II

Optical Waves in Layered Media

PART I

STARK-INDUCED NONLINEARITY IN GASEOUS NH_2D

Chapter 1

GENERAL INTRODUCTION

1-1 Introduction

The optical properties of an arbitrary medium are described by the two well-known quantities - the dielectric constant and magnetic permeability. They are defined by

$$D = \underset{\approx}{\varepsilon} E$$

$$B = \underset{\approx}{\mu} H$$

1-1

These two constants are in general functions of the field strengths. This nonlinearity has been known in the radio and microwave region of the electromagnetic spectrum for a long time. Nonlinearity in the optical region has been demonstrated by harmonic generation of light. Franken and his associates detected ultraviolet light (λ = 3471.5 Å) generated by the intense flash of a ruby laser (λ = 6943 Å) when this laser beam passed through a quartz crystal [1]. This experiment stimulated an enormous amount of both theoretical and experimental work in nonlinear optical properties. Third harmonic generation in metal vapor has been demonstrated by Miles and Harris [2]. Fifth harmonic and seventh harmonic generation of laser light in isotropic media was recently demonstrated by She and Reintjes [3]. Harmonic generation of light has been used as a source of generating short wavelength coherent light [4]. Generally speaking, the optical nonlinear effects are much smaller compared to the linear ones in most material except under resonant conditions. It takes high optical intensities to have detectable deviations from linearity. Such intensities became available only with the advent of the laser.

The nonlinear susceptibilities are in general tensors of rank 3, 4,···,etc. The linear susceptibility is a tensor of rank 2. These susceptibilities obey the same symmetry properties as the medium. As a result, nonlinear optical mixing phenomena such as parametric oscillation, frequency up-conversion and the electro-optic effect require that the medium lack an inversion symmetry. Liquids and gases in virtue of their random orientation, may possess only a microscopic inversion symmetry and hence have not been deemed appropriate for nonlinear and modulation applications. This symmetry, however, can be broken in principle by applying a dc electric field to the medium so that a gas or liquid in an electric field may be expected to display nonlinear optical properties.

To estimate the dc field-induced optical nonlinearity in a gas we carry out a quantum mechanical analysis. The analytical results are then applied to calculate the nonlinear optical constants of NH_2D which is found to be especially suitable for this application.

1-2 Previous Work on Optical Nonlinearties in Gases

Ward and New demonstrated optical third harmonic generation in gases with a focused laser beam [5]. Young and coworkers have observed the third harmonic generation in phase-matched Rb vapor [6]. Generation of vacuum ultraviolet radiation in Cd vapor has been demonstrated by Kung and coworkers [7]. Leung, Ward and Orr have demonstrated the optical third harmonic generation in cesium vapor with a two-photon resonant enhancement [8]. These works are all third harmonic generation of light in gases. DC-induced second harmonic generation in gases has been demonstrated by Finn and Ward [9]. Molecular second and third order

polarizabilities were measured by Ward and Bigio by using second harmonic generation in gases [10]. Infrared up-conversion has been demonstrated by Bloom and coworkers with two-photon resonant pumping in metal vapors [11,12]. Sorokin and coworkers [13] have demonstrated tunable coherent infrared generation based upon four-wave parametric conversion in alkali metal vapors.

Theoretical calculation of the nonlinear susceptibility using successive approximations to obtain a solution in ascending powers of the coherent perturbation was performed by Armstrong et al [14], Bloembergen and Shen [15]. Similar analysis was also carried out by Fain and Yaschin [16].

1-3 Outline of Thesis Part I

In Chapter 2 the quantum theory of the nonlinear polarizability of a general atomic system will be introduced and analyzed. Diagram technique will be introduced and discussed. Each nonlinear polarizability can be expressed in terms of a sum of several diagrams. A phenomenological equation of motion for the density matrix is introduced and analyzed. Relaxations in gases are expressed in terms of damping terms in the equation of motion.

In Chapter 3 the nonlinear polarizability due to rotational-vibrational transition in an asymmetric molecule is calculated. Some basic quantum mechanics of a rotating top is reviewed and discussed. Matrix elements for asymmetric top are calculated and selection rules are discussed.

In Chapter 4, calculations are presented for mixing of a CO_2 laser

4

with 4-GHz microwaves in the molecule NH_2D, producing single side band radiation. A general expression for the nonlinear susceptibility is derived in terms of plasma dispersion function. Pressure dependence, the dispersion behavior and the saturation effect are analyzed and discussed. Stark tuning and resonance enhancement are introduced and discussed.

In Chapter 5 the experimental measurements are presented and are compared with theory.

CHAPTER 1 REFERENCES

[1] P. A. Franken, A. E. Hill, C. W. Peters, and G. Weinreiche, Phys. Rev. Letters, 7, 118 (1961).

[2] R. B. Miles and S. E. Harris, IEEE J. QE, QE-9, 470 (1973).

[3] C. Y. She and J. Reintjes, Appl. Phys. Lett. 31, 951 (1977); C. Y. She and J. Reintjes (to be published).

[4] R. W. Waynant and R. C. Elton, Proc. IEEE, pp. 1059-1092, July 1976.

[5] J. F. Ward and G. H. C. New, "Optical third harmonic generation in gases by a focused laser beam," Phys. Rev., vol. 185, pp. 57-72, Sept. 1969.

[6] J. F. Young, G. C. Bjorklund, A. H. Kung, R. B. Miles, and S. E. Harris, "Third-harmonic generation in phase-matched Rb. vapor," Phys. Rev. Lett., vol. 27, pp. 1551-1553, Dec. 1971.

[7] A. H. Kung, J. F. Young, G. C. Bjorklund, and S. E. Harris, "Generation of vacuum ultraviolet radiation in phase-matched Cd vapor," Phys. Rev. Lett., vol. 29, pp. 985-988, Oct. 1972.

[8] K. M. Leung, J. F. Ward, and B. J. Orr, "Two-photon resonant, optical third-harmonic generation in cesium vapor," Phys. Rev. Lett., vol. 9A, pp. 2440-2448, June 1974.

[9] R. S. Finn and J. F. Ward, "DC-induced optical second-harmonic generation in the inert gases," Phys. Rev. Lett., vol. 26, pp. 285-289, Feb. 1971.

[10] J. F. Ward and I. J. Bigio, "Molecular second- and third-order polarizabilities from measurements of second-harmonic generation in gases," Phys. Rev. Lett., vol. 11A, pp. 60-66, Jan. 1975.

[11] S. E. Harris and D. M. Bloom, "Resonantly two-photon pumped frequency converter," Appl. Phys. Lett., vol. 24, pp. 229-230, March 1974.

[12] D. M. Bloom, J. Yardley, J. F. Young, and S. E. Harris, "Infrared up-conversion with resonantly two-photon pumped metal vapors," Appl. Phys. Lett., vol. 24, pp. 427-428, May 1974.

[13] P. D. Sorokin, J. J. Wynne, and J. R. Lankard, "Tunable coherent IR source based upon four-wave parametric conversion in alkali metal vapors," Appl. Phys. Lett., vol. 22, pp. 342-344, April 1973.

[14] J. A. Armstrong, N. Bloembergen, J. Ducuing, and P. S. Pershan, Phys. Rev. 127, 1918 (1962).

[15] N. Bloembergen and Y. R. Shen, Phys. Rev., 133, A37 (1964).

[16] V. M. Fain and E. Q. Yaschin, JETP, 19, pp. 474 (1964).

Chapter 2
QUANTUM THEORY OF NONLINEAR POLARIZABILITY

2-1 Introduction

In this chapter the interaction representation of quantum mechanics will be employed to find the expectation value of the dipole moment operator of an atomic system. We express the wave function of the atomic system $|\Psi>$ as an expansion in the eigenfunctions of the unperturbed system. The calculation is carried out down to second order in the perturbing potential. It is found that the nonlinear polarizability of an atomic system is the same as the scattering amplitude of the coherent fundamental processes. Therefore it can be easily represented by Feynman diagrams [1]. Since we are only interested in the optical region of the atomic transitions, nonrelativistic diagram techniques[2] will be used in this chapter. We consider the effect of radiation on an atomic system, especially the evolution of the dipole moment of an atom (or a molecule) under the radiation of three harmonic waves. In the optical regime the wavelength is about 3 or 4 orders of magnitude greater than the atomic radius. Therefore dipole approximation will be assumed throughout this chapter.

2-2 Quantum Theory of Nonlinear Polarizability

We consider the problem where an atomic system is in a certain dynamical state at time t_0 and we wish to determine its state at a later time t. In particular we wish to determine the expectation value of the dipole moment operator. We suppose that the Hamiltonian H can be written as

$$H = H_0 + H' \qquad\qquad 2\text{-}1$$

where H_0 is the unperturbed Hamiltonian whose eigenfunctions
and eigenvalues are assumed known; H' is the
perturbation Hamiltonian due to the presence of the external optical
fields. In the regime of dipole approximation. H' can be written as

$$H' = - \vec{\mu} \cdot \vec{E} \qquad\qquad 2\text{-}2$$

where $\vec{\mu}$ is the dipole moment operator and $\vec{E}$ is the classical electric
field produced by the optical waves. Without loss of generality we
will assume that the electric field consists of the superposition
of three harmonic waves. Furthermore, we will neglect the space
dependence in the dipole approximation. Thus the electric field can
be written

$$\vec{E} = \sum_{i=1,2,3} \left\{ \frac{1}{2} \vec{E}_i \, e^{-i\omega_i t} + c\cdot c\cdot \right\} \qquad\qquad 2\text{-}3$$

For the sake of simplicity in the algebraic manipulation, we define

$$\begin{aligned} \omega_{-i} &= - \omega_i \\ \vec{E}_{-i} &= \vec{E}_i^{\,*} \end{aligned} \qquad i = 1,2,3 \qquad\qquad 2\text{-}4$$

Then (2-3) can be written

$$\vec{E} = \sum_i \frac{1}{2} \vec{E}_i \, e^{-i\omega_i t} \qquad\qquad 2\text{-}5$$

Where $\displaystyle\sum_i$ means summation over ± 1, ± 2 and ± 3. This notation will be
used throughout this chapter. The dielectric polarizabilities of an
atom (or molecule) are defined as

$$\langle \mu_\alpha \rangle = \sum_i \frac{1}{2} \chi_{\alpha\beta} (\omega_i) E_{i\beta} e^{-i\omega_i t}$$

$$+ \sum_{(ij)} \frac{1}{2} \chi_{\alpha\beta\gamma} (\omega_i,\omega_j) E_{i\beta} E_{j\gamma} e^{-i(\omega_i+\omega_j)t}$$

$$+ \text{(higher order terms)} \qquad\qquad 2\text{-}6$$

Where $\langle \mu_\alpha \rangle$ is the expectation value of the α-component of the dipole moment operator. $\displaystyle\sum_{(ij)}$ means summation over the pair ij. α, β, γ are coordinate subscripts (i.e. α = x, y, z; β = x, y, z; γ = x, y, z; etc.) Summation over repeated Greek subscripts will be assumed throughout this chapter. $\chi_{\alpha\beta}(\omega)$ is the linear polarizability tensor. $\chi_{\alpha\beta\gamma}(\omega_i,\omega_j)$ is the lowest order nonlinear polarizability tensor. The expectation value of the dipole moment operator is a real number. Therefore, the following relations must hold:

$$\chi_{\alpha\beta} (-\omega) = \chi_{\alpha\beta}^{*} (\omega) \qquad\qquad 2\text{-}7$$

$$\chi_{\alpha\beta\gamma} (-\omega_i,-\omega_j) = \chi_{\alpha\beta\gamma}^{*} (\omega_i,\omega_j) \qquad\qquad 2\text{-}8$$

$$\text{etc.}$$

The expectation value of the dipole moment operator can be calculated quantum mechanically. In order to find the expectation value $\langle \mu_\alpha \rangle$ we need to know the wave function of this atomic system at time t. This can be achieved by integrating the Schrödinger equation which is given by

$$i \frac{\partial}{\partial t} |\Psi\rangle = H |\Psi\rangle \qquad\qquad 2\text{-}9$$

where we used the natural unit $\hbar = 1$.

The solution of (2-9) can be written

$$|\Psi(t)> = U(t,t_0) \mid \Psi(t_0)> \qquad \qquad 2\text{-}10$$

where $U(t,t_0)$ is the well-known evolution operator [3] which also satisfies the Schrödinger equation, i.e.

$$i \frac{\partial}{\partial t} U(t,t_0) = HU(t,t_0) \qquad \qquad 2\text{-}11$$

The use of the evolution operator in nonlinear optics has recently been suggested by Yariv [4]. Equation (2-11) can be written in its integral form

$$U(t,t_0) = -i \int_{t_0}^{t} H(\tau) U(\tau,t_0)d\tau \;\; + I \qquad \qquad 2\text{-}12$$

Using equation 2-10 and the definition of expectation value we obtain

$$<\mu_\alpha> \equiv <\Psi|\mu_\alpha|\Psi> \qquad \qquad 2\text{-}13$$

$$= <g|U^+(t,t_0) \; \mu_\alpha \; U(t,t_0)|g> \qquad \qquad 2\text{-}14$$

where

$$|g> = |\Psi(t_0) \qquad \qquad 2\text{-}15$$

and $U^+(t,t_0)$ is the Hermitian conjugate of $U(t,t_0)$. We note that $|g>$ is a normalized wave function of the atomic system at t_0. $|\Psi>$ is also a normalized wave function since $U(t,t_0)$ is a unitary operator.

By using the completeness relation of the eigenfunctions of the unperturbed system

$$\sum_{\ell} |\ell >< \ell| = I \qquad \qquad 2\text{-}16$$

where I is the unit operator, equation (2-14) can be written

$$\langle \mu_\alpha \rangle = \sum_{\ell,m} \langle g|U^+(t,t_0)|\ell \rangle \langle \ell|\mu_\alpha|m\rangle \langle m|U(t,t_0)|g\rangle \qquad \text{2-17}$$

In order to write equation (2-17) in the form of equation (2-6) we need to solve (2-12). This is usually done by successive approximation. In integrating (2-12), we take $t_0 = -\infty$ and assume that the electric field was turned on adiabatically from $t = -\infty$. In other words, for $t < 0$, $\vec{E}$ is replaced by

$$\vec{E}(t) \to \lim_{\varepsilon \to 0^+} e^{\varepsilon t} \vec{E}(t) \qquad \text{2-18}$$

This is a common procedure to get rid of the divergence at $t = -\infty$. Physically this is equivalent to neglecting the transient terms. In calculating the dielectric polarizabilities we are interested in the steady state response of the atomic system. Therefore we have to throw away all the transient terms which depend on t_0 and decay to zero eventually due to relaxation processes. This is similar to solving the steady state response of a damped oscillator driven by an external harmonic force.

By carrying out the integration and a few steps of iteration we obtain, from (2-11)

$$U(t,-\infty)_{\ell k} = e^{-iE_k t} \left\{ \delta_{\ell k} + \sum_i \frac{1}{2} \frac{(-\mu \cdot E_i)_{\ell k} \, e^{-i\omega_i t}}{(E_k + \omega_i - E_\ell + i\varepsilon)} \right.$$

$$\left. + \sum_m \sum_{ij} \left(\frac{1}{4}\right) \frac{(-\mu \cdot E_i)_{\ell m} (-\mu \cdot E_j)_{mk} \, e^{-i(\omega_i + \omega_j)t}}{(E_k + \omega_i + \omega_j - E_\ell + 2i\varepsilon)(E_k + \omega_j - E_m + i\varepsilon)} \right.$$

$$\left. + \text{(higher order terms)} \right\} \qquad \text{2-19}$$

where ℓ, m, k are indices of the eigenstates and it is assumed that ε tends to 0+. This ε is usually neglected when the optical frequencies are far away from the atomic transition frequencies. In cases of resonant scattering where the real part of the energy denominator is vanishingly small, this ε plays a very important role in averaging over the energy levels line shape functions. In doing that we have to use the following well-known relation [5].

$$\lim_{\varepsilon \to 0+} \frac{1}{x+i\varepsilon} = P.V.\left(\frac{1}{x}\right) - i\pi\delta(x) \qquad 2\text{-}20$$

we also have to know the line shape function of each energy level in order to perform the integration. We now proceed to calculate the dielectric polarizabilities. Using equation (2-19), the expectation value of μ_α (2-17) can be written as

$$
\begin{aligned}
\langle \mu_\alpha \rangle = (\mu_\alpha)_{gg} &+ \left\{ \sum_m \sum_i \frac{1}{2} \frac{(\mu_\alpha)_{gm}(-\mu_\beta)_{mg}}{E_g + \omega_i - E_m + i\varepsilon} E_{i\beta}\, e^{-i\omega_i t} + c\cdot c\cdot \right\} \\
&+ \left\{ \sum_{mn} \sum_{ij} \left[\frac{1}{4} \frac{(\mu_\alpha)_{gm}(-\mu_\beta)_{mn}(-\mu_\gamma)_{ng}}{(E_g + \omega_i + \omega_j - E_m + 2i\varepsilon)(E_g + \omega_j - E_n + i\varepsilon)} \right. \right. \\
&\qquad\qquad \left. E_{i\beta} E_{j\gamma}\, e^{-i(\omega_i+\omega_j)t} + c\cdot c\cdot \right] \\
&+ \sum_{mn} \sum_{ij} \frac{1}{4} \frac{(-\mu_\beta)_{gm}(-\mu_\alpha)_{mn}(-\mu_\gamma)_{ng}}{(E_g + \omega_j - E_n + i\varepsilon)(E_g + \omega_i - E_m - i\varepsilon)} \\
&\qquad\qquad \left. E_{i\beta}^* E_{j\gamma}\, e^{-i(-\omega_i+\omega_j)t} \right\}
\end{aligned}
$$

$$+ \text{(higher order terms)} \qquad 2\text{-}21$$

If we use the notation (2-4) and change the dummy indices i, j in (2-21), we obtain

$$\langle \mu_\alpha \rangle = (\mu_\alpha)_{gg} + \sum_i \sum_m \frac{1}{2} \left\{ \frac{(\mu_\alpha)_{gm}(-\mu_\beta)_{mg}}{E_g + \omega_i - E_m + i\epsilon} + \frac{(-\mu_\beta)_{gm}(\mu_\alpha)_{mg}}{E_g - \omega_i - E_m - i\epsilon} \right\} E_{i\beta}\, e^{-i\omega_i t}$$

$$+ \sum_{ij} \sum_{mn} \frac{1}{4} \left\{ \frac{(\mu_\alpha)_{gm}(-\mu_\beta)_{mn}(-\mu_\gamma)_{ng}}{(E_g + \omega_i + \omega_j - E_m + 2i\epsilon)(E_g + \omega_j - E_n + i\epsilon)} + \frac{(-\mu_\gamma)_{gn}(-\mu_\beta)_{nm}(\mu_\alpha)_{mg}}{(E_g - \omega_i - \omega_j - E_m - 2i\epsilon)(E_g - \omega_j - E_n - i\epsilon)} \right.$$

$$\left. + \frac{(-\mu_\beta)_{gm}(\mu_\alpha)_{mn}(-\mu_\gamma)_{ng}}{(E_g + \omega_j - E_n + i\epsilon)(E_g - \omega_i - E_m - i\epsilon)} \right\} E_{i\beta}\, E_{j\gamma}\, e^{-i(\omega_i + \omega_j)t}$$

+ (higher order terms) $\qquad$ 2-22

Comparing the definition of polarizability tensors (2-6) and equation (2-22), we obtain

$$\chi_{\alpha\beta}(\omega) = \sum_m \left\{ \frac{(\mu_\alpha)_{gm}(-\mu_\beta)_{mg}}{E_g + \omega - E_m + i\epsilon} + \frac{(-\mu_\beta)_{gm}(\mu_\alpha)_{mg}}{E_g - \omega - E_m - i\epsilon} \right\} \qquad 2-23$$

$$\chi_{\alpha\beta\gamma}(\omega_i, \omega_j) = \frac{1}{2} \sum_{mn} \left\{ \frac{(\mu_\alpha)_{gm}(-\mu_\beta)_{mn}(-\mu_\gamma)_{ng}}{(E_g + \omega_i + \omega_j - E_m + 2i\epsilon)(E_g + \omega_j - E_n + i\epsilon)} + \frac{(\mu_\alpha)_{gm}(-\mu_\gamma)_{mn}(-\mu_\beta)_{ng}}{(E_g + \omega_i + \omega_j - E_m + 2i\epsilon)(E_g + \omega_i - E_n + i\epsilon)} \right.$$

$$+ \frac{(-\mu_\gamma)_{gn}(-\mu_\beta)_{nm}(\mu_\alpha)_{mg}}{(E_g - \omega_i - \omega_j - E_m - 2i\epsilon)(E_g - \omega_j - E_n - i\epsilon)} + \frac{(-\mu_\beta)_{gn}(-\mu_\gamma)_{nm}(\mu_\alpha)_{mg}}{(E_g - \omega_i - \omega_j - E_m - 2i\epsilon)(E_g - \omega_i - E_n - i\epsilon)}$$

$$\left. + \frac{(-\mu_\beta)_{gm}(\mu_\alpha)_{mn}(-\mu_\gamma)_{ng}}{(E_g + \omega_j - E_n + i\epsilon)(E_g - \omega_i - E_m - i\epsilon)} + \frac{(-\mu_\gamma)_{gm}(\mu_\alpha)_{mn}(-\mu_\beta)_{ng}}{(E_g + \omega_i - E_n + i\epsilon)(E_g - \omega_j - E_m - i\epsilon)} \right\} \qquad 2-24$$

These are the most general expressions for dielectric polarizabilities up to second order. Although there are infinite numbers of terms in the expressions, only some dominant terms will be kept in most of the practical problems encountered. The second order polarizability tensor is the

lowest order nonlinear polarizability which is a tensor of rank three and depends upon the mixing frequencies ω_i and ω_j.

If the optical frequencies are far away from all the relevant atomic transitions, all the χ's become real and the medium becomes lossless. In this case if we consider the interaction between three waves at frequencies ω_1, ω_2 and $\omega_3 = \omega_1 + \omega_2$. The corresponding nonlinear polarizabilities satisfy the following permutation symmetry relation

$$\chi_{\gamma\alpha\beta}(\omega_1, \omega_2) = \chi_{\beta\gamma\alpha}(\omega_3, -\omega_1) = \chi_{\alpha\gamma\beta}(\omega_3, -\omega_2) \quad \text{2-25}$$

which may be easily remembered as follows: the nonlinear polarizability is invariant under the interchange of the tensor indices, provided the corresponding frequencies are also interchanged. In general there is no symmetric relation between complex nonlinear polarizabilities. Equation (2-25) can be obtained directly from (2-24) by assuming $\epsilon = 0$. This relation can also be derived by considering the work done by the three waves on the medium. In a lossless medium, we should have

$$\overline{\vec{E}_3 \cdot \frac{\partial}{\partial t} \vec{P}^{NL}_{(\omega_3 = \omega_1 + \omega_2)}} + \overline{\vec{E}_2 \cdot \frac{\partial}{\partial t} \vec{P}^{NL}_{(\omega_2 = \omega_3 - \omega_1)}} + \overline{\vec{E}_1 \cdot \frac{\partial}{\partial t} \vec{P}^{NL}_{(\omega_1 = \omega_3 - \omega_2)}} = 0 \quad \text{2-26}$$

The left hand side of (2-26) gives the nonlinear power loss due to the nonlinear polarizations. It can be easily shown that equation (2-26) leads directly to the symmetric relations (2-25).

In the limit when $\omega_i \to 0$ and $\omega_j \to 0$, equation (2-24) leads to

$$\chi_{\alpha\beta\gamma}(0,0) = \sum_{mn} \frac{1}{\omega_{ng}\,\omega_{mg}} \left\{ (\mu_\alpha)_{gm}\,(\mu_\beta)_{mn}\,(\mu_\gamma)_{ng} \right.$$

$$\left. + (\mu_\alpha)_{gm}\,(\mu_\gamma)_{mn}\,(\mu_\beta)_{ng} + (\mu_\beta)_{gm}\,(\mu_\alpha)_{mn}\,(\mu_\gamma)_{ng} \right\} \quad \text{2-27}$$

where $\omega_{ng} = E_n - E_g$ and $\omega_{mg} = E_m - E_g$.

We find that in the low frequency regime we have the following symmetry

$$\chi_{\alpha\beta\gamma} = \chi_{(\alpha\beta\gamma)} \qquad\qquad 2\text{-}28$$

where $(\alpha\beta\gamma)$ is any permutation of α,β,γ. Equation 2-28 can also be obtained from (2-25).

2-3 Diagram Representation

We have derived in the previous section the linear dielectric polarizability and the lowest order nonlinear dielectric polarizability. Equations (2-23) and (2-24) show that there are two general terms under a single summation in the polarizability tensor of rank two and there are six general terms under a double summation in the polarizability tensor of rank three. It can be proven that there are exactly n! general terms in the polarizability tensor of rank n. Diagram techniques have been introduced in particle physics to calculate the scattering amplitudes of any arbitrary order [6]. It is actually a systematic way of writing out all of the possible scattering processes and the scattering amplitude associated with each process.

It is found that the nonlinear polarizability tensors have exactly the same property. Each term in (2-23) and (2-24) can be represented by a diagram with amplitude similar to that of the Feynman diagram. The only difference from that of the Feynman diagram is that the sign of ε is not always the same as E_g which is the energy of the initial state. This is due to the fact that complex conjugate evolution

operator appears in the expectation value of μ_α (see equation 2-14).

The rules of the diagram technique are summarized below:

1. Positive ω_i means absorption of a photon.

   Negative ω_i means emission of a photon.

2. Each matrix element $(\mu_\alpha)_{\ell k}$ is represented by a vertex
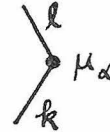
3. Each energy denominator is represented by a solid straight line $\Big|$ between two vertices.

4. The sign of ε in the energy denominator is positive if the energy denominator is below the vertex μ_α where the resulting photon is emitted (or absorbed) and is negative otherwise.

5. A numerical factor of $2(\frac{-1}{2})^{n-1}$, where n is the number of vertices.

Using these rules, the polarizability tensors in (2-23) and (2-24) can be written

$$\chi_{\alpha\beta}(\omega_i) = \sum_m \; (-1) \left\{ \qquad + \qquad \right\} \qquad 2\text{-}29$$

$$\chi_{\alpha\beta\gamma}(\omega_i, \omega_j) = \sum_{m,n} \left(\frac{1}{2}\right) \chi$$

2-30
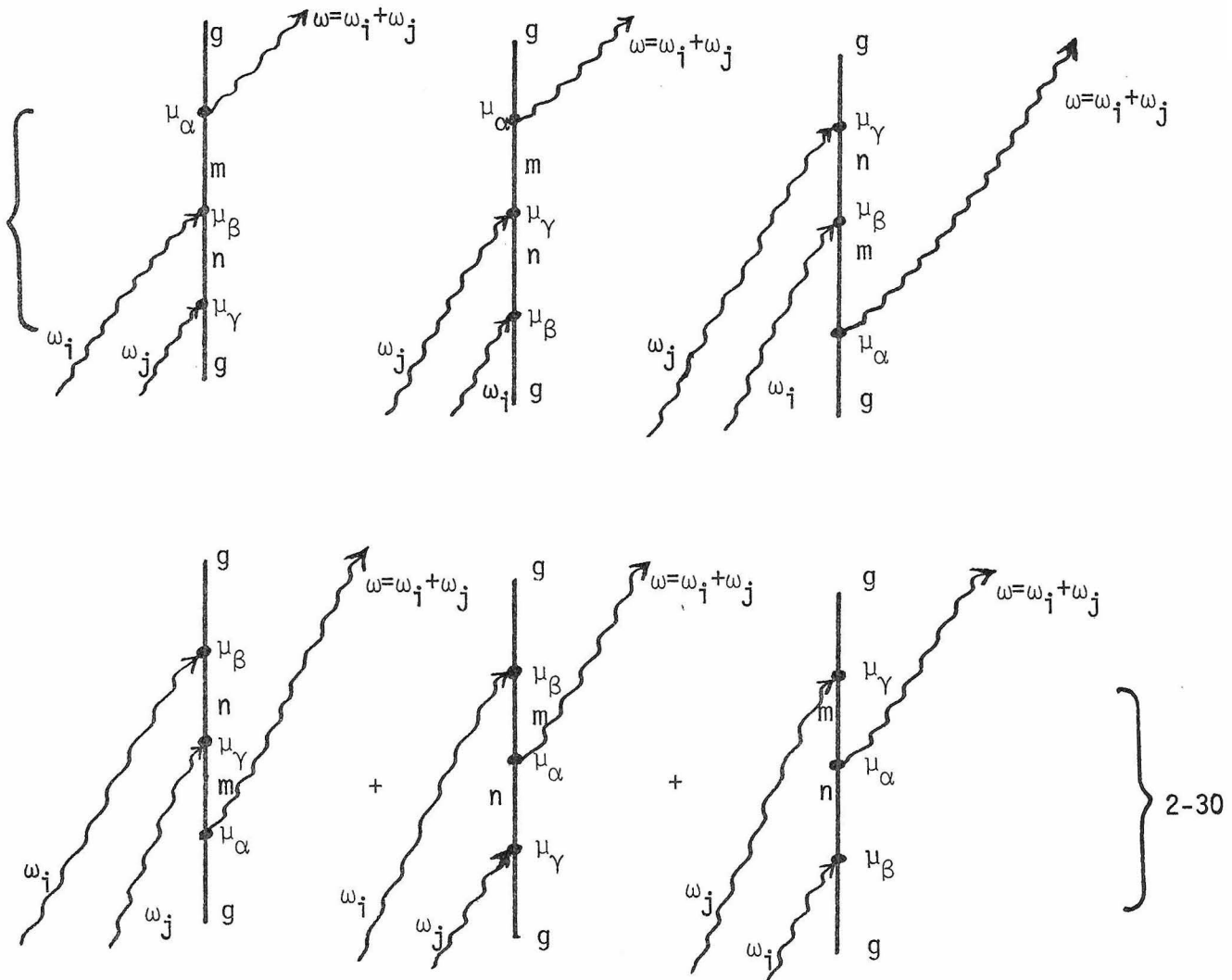
The six diagrams in $\chi_{\alpha\beta\gamma}(\omega_i, \omega_j)$ are drawn for positive ω_i and ω_j. For negative ω_i or ω_j, we simply replace the corresponding incoming photons by outgoing photons. The next higher order nonlinear polarizability tensor $\chi_{\alpha\beta\gamma\delta}(\omega_i, \omega_j, \omega_k)$ has 24 general terms under a triple summation. By using the diagram rules, $\chi_{\alpha\beta\gamma\delta}(\omega_1, \omega_2, \omega_3)$ can be written as

$$\chi_{\alpha\beta\gamma\delta}(\omega_1, \omega_2, \omega_3) = \sum_{mn\ell} \left(\frac{-1}{4}\right) \Bigg\{$$
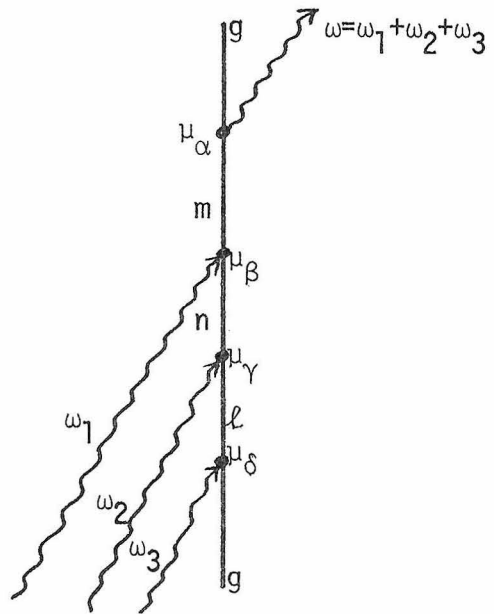
+ (23 other terms by permuting the four vertices) $\Bigg\}$

2-31

2-4 Phenomenological Equation of Motion - Density Matrix Approach

In the previous calculation we assumed that the atomic system is in some pure state at $t = t_0$. Hence the evolution of the atomic system is completely determined by the Schrödinger equation. In practice, however, the bulk nonlinear susceptibility consists of the contributions from a large number of molecules. Instead of knowing the complete wave

function of an individual molecule, we only know the equilibrium
population distribution which is usually given by the Boltzmann dis-
tribution function [7].

$$\bar{\rho}_{nn} = \bar{\rho}_{gg} \; e^{-(E_n - E_g)/kT} \qquad\qquad 2\text{-}32$$

In addition to this, the line shape function of each energy level
is also not known. The finite width of the line shape is due to
collisions, spontaneous emission, etc. [8].

Facing these two problems we have to use the density matrix
approach and find a phenomenological equation of motion for the den-
sity matrix. All those random perturbations such as collisions, spon-
taneous emissions, etc. will be lumped into a relaxation term in the
equation of motion. Thus we have the following phenomenological equa-
tion of motion [9].

$$\frac{d}{dt} \rho_{mn} = -i[H,\rho]_{mn} - \Gamma_{mn} \, (\rho_{mn} - \bar{\rho}_{mn}) \qquad\qquad 2\text{-}33$$

Where ρ_{mn} is a matrix element of the density operator ρ. m, n are the
energy level indices. $\bar{\rho}_{mn}$ is the equilibrium density matrix element
which is diagonal in the energy representation. The matrix element ρ_{mn}
is defined as

$$\rho_{mn} = \sum_s p(s) \, a_m^{(s)} \, a_n^{*(s)} \qquad\qquad 2\text{-}34$$

where we consider a mixed state as an incoherent mixture of pure states
$|\psi^{(s)}\rangle$ with a statistical weight p(s). The p(s) are real and positive

numbers satisfying $\sum_{s} p(s) = 1$. An arbitrary pure state $|\psi^{(s)}\rangle$ can

be described by a linear superposition of the unperturbed eigenfunctions

$$|\psi^{(s)}\rangle = \sum_{n} a_{n}^{(s)} |n\rangle \qquad 2\text{-}35$$

The Hamiltonian H in equation (2-33) is given by (2-1) and (2-2). The relaxation rate Γ_{mn} can be interpreted as follows: Γ_{nn} is the relaxation rate of the n-th state population and is given roughly by

$$\Gamma_{nn} \sim \frac{1}{t_{spont}} + \frac{1}{T_{inelastic}} \qquad 2\text{-}36$$

where t_{spont} is the spontaneous lifetime of the n-th state and $T_{inelastic}$ is the inelastic collision time. This is a reasonable approximation because we know that spontaneous decay and inelastic scattering will make the population tends to the equilibrium values.

$$\Gamma_{mn} = \frac{1}{2} (\Gamma_{mm} + \Gamma_{nn}) + \gamma_{mn} \qquad 2\text{-}37$$

The decay of ρ_{mm} and ρ_{nn} will also contribute to the decay of ρ_{mn}, this accounts for the first term in (2-37). There are other mechanisms which will also make ρ_{mn} decay, for example, phase-interrupintg collisions [10], velocity changing collisions [11], etc., these effects are lumped into γ_{mn}. We assume that $\gamma_{mn} = \gamma_{nm}$.

In terms of the density matrix the expectation value of the dipole moment operator is given by

$$\langle\mu_{\alpha}\rangle = Tr(\rho \, \mu_{\alpha}) = \sum_{mn} \rho_{mn} (\mu_{\alpha})_{nm} \qquad 2\text{-}38$$

If ρ_{mn} can be solved from equation (2-33), in terms of the perturbing optical fields, then the dielectric nonlinear polarizability can be

obtained from (2-6). Equation (2-33) can be solved by the method of successive approximations. We expand ρ_{mn} in terms of a power series in H' [12].

$$\rho_{mn} = \rho_{mn}^{(o)} + \rho_{mn}^{(1)} + \rho_{mn}^{(2)} + \rho_{mn}^{(3)} + \cdots \cdots \qquad 2\text{-}39$$

Substitute ρ_{mn} from (2-39) into (2-33) and equate terms with the same power of H' on both sides of the equation, we obtain

$$\frac{d}{dt} \rho_{mn}^{(o)} = -i[H_o , \rho^{(o)}]_{mn} - \Gamma_{mn}(\rho_{mn}^{(o)} - \overline{\rho}_{mn}) \qquad 2\text{-}40$$

$$\frac{d}{dt} \rho_{mn}^{(1)} = -i[H_o , \rho^{(1)}]_{mn} - i[H' , \rho^{(o)}]_{mn} - \Gamma_{mn}\rho_{mn}^{(1)} \qquad 2\text{-}41$$

$$\frac{d}{dt} \rho_{mn}^{(\ell)} = -i[H_o , \rho^{(\ell)}]_{mn} - i[H' , \rho^{(\ell-1)}]_{mn} - \Gamma_{mn}\rho_{mn}^{(\ell)} \qquad 2\text{-}42$$

If we define

$$\omega_{mn} = (E_m - E_n)/\hbar \qquad 2\text{-}43$$

and recall

$$[H_o , \rho^{(\ell)}]_{mn} = (E_m - E_n)\rho_{mn}^{(\ell)} \qquad 2\text{-}44$$

Then equation (2-42) can be written

$$\frac{d}{dt} \rho_{mn}^{(\ell)} = (-i\omega_{mn} - \Gamma_{mn})\rho_{mn}^{(\ell)} - i[H' , \rho^{(\ell-1)}]_{mn} \qquad 2\text{-}45$$

The most general solution of equation (2-45) is

$$\rho_{mn}^{(\ell)}(t) = -i \int_{-\infty}^{t} [H' , \rho^{(\ell-1)}(t')]_{mn} \, e^{i\omega_{mn}(t'-t) + \Gamma_{mn}(t'-t)} \, dt' \qquad 2.46$$

$$+ \text{ constant}$$

We are now ready to perform the successive approximation. Equation (2-46) can be integrated to obtain $\rho_{mn}^{(\ell)}(t)$ once the ℓ-1th order solution $\rho_{mn}^{(\ell-1)}(t)$ is known. After a few steps of iteration, we obtain

$$\rho_{\ell k}^{(0)} = \frac{i\Gamma_{\ell k}}{-\omega_{\ell k} + i\Gamma_{\ell k}} \quad \bar{\rho}_{\ell k} = \bar{\rho}_{kk} \, \delta_{\ell k} \qquad \qquad 2\text{-}47$$

$$\rho_{\ell k}^{(1)} = \sum_i \left(\frac{1}{2}\right) \frac{(\mu \cdot E_i)_{\ell k} \, e^{-i\omega_i t}}{-\omega_{\ell k} + \omega_i + i\Gamma_{\ell k}} (\bar{\rho}_{kk} - \bar{\rho}_{\ell\ell}) \qquad \qquad 2\text{-}48$$

$$\rho_{\ell k}^{(2)} = \sum_m \sum_{ij} \left(\frac{1}{4}\right) \frac{(-\mu \cdot E_i)_{\ell m} (-\mu \cdot E_j)_{mk} \, e^{-i(\omega_i + \omega_j)t}}{(-\omega_{\ell k} + \omega_i + \omega_j + i\Gamma_{\ell k})}$$

$$\left\{ \frac{(\bar{\rho}_{kk} - \bar{\rho}_{mn})}{(-\omega_{mk} + \omega_j + i\Gamma_{mk})} - \frac{(\bar{\rho}_{mm} - \bar{\rho}_{\ell\ell})}{(-\omega_{\ell m} + \omega_i + i\Gamma_{\ell m})} \right\} \qquad 2\text{-}49$$

The expectation value of the dipole moment operator can also be written as a similar expansion

$$\langle \mu_\alpha \rangle = \sum_{\ell k} \left\{ \rho_{\ell k}^{(0)} (\mu_\alpha)_{k\ell} + \rho_{\ell k}^{(1)} (\mu_\alpha)_{k\ell} + \rho_{\ell k}^{(2)} (\mu_\alpha)_{k\ell} \right\}$$

$$+ \text{(higher order terms)} \qquad \qquad 2\text{-}50$$

Using (2-47) - (2-50), $\langle \mu_\alpha \rangle$ can be written

$$\langle \mu_\alpha \rangle = \sum_{\ell k} \left\{ \bar{\rho}_{kk}(\mu_\alpha)_{k\ell}\delta_{\ell k} + \sum_i \left(\frac{1}{2}\right) \frac{(\mu_\alpha)_{k\ell} (-\mu_\beta)_{\ell k}}{(-\omega_{\ell k} + \omega_i + i\Gamma_{\ell k})} (\bar{\rho}_{kk} - \bar{\rho}_{\ell\ell}) E_{i\beta} \, e^{-i\omega_i t} \right.$$

$$+ \sum_m \sum_{ij} \left(\frac{1}{4}\right) \frac{(\mu_\alpha)_{k\ell}(-\mu_\beta)_{\ell m}(-\mu_\gamma)_{mk}}{(-\omega_{\ell k} + \omega_i + \omega_j + i\Gamma_{\ell k})} \left[\frac{(\bar{\rho}_{kk} - \bar{\rho}_{mm})}{(-\omega_{mk} + \omega_j + i\Gamma_{mk})} - \frac{(\bar{\rho}_{mm} - \bar{\rho}_{\ell\ell})}{(-\omega_{\ell m} + \omega_i + i\Gamma_{\ell m})} \right]$$

$$\left. E_{i\beta} E_{j\gamma} \, e^{-i(\omega_i + \omega_j)t} \right\} + \text{(higher order terms)} \qquad 2\text{-}51$$

Comparing with (2-6), we obtain the dielectric polarizability tensors
from (2-51)

$$\chi_{\alpha\beta}(\omega_i) = \sum_{\ell k} \frac{(\mu_\alpha)_{k\ell}(-\mu_\beta)_{\ell k}}{-\omega_{\ell k}+\omega_i+i\Gamma_{\ell k}} \; (\bar{\rho}_{kk} - \bar{\rho}_{\ell\ell}) \qquad\qquad 2\text{-}52$$

$$\chi_{\alpha\beta\gamma}(\omega_i,\omega_j) = \sum_{\ell km} (\tfrac{1}{2})\left\{ \frac{(\mu_\alpha)_{k\ell}(-\mu_\beta)_{\ell m}(-\mu_\gamma)_{mk}}{(-\omega_{\ell k}+\omega_i+\omega_j+i\Gamma_{\ell k})}\left[\frac{(\bar{\rho}_{kk}-\bar{\rho}_{mm})}{(-\omega_{mk}+\omega_j+i\Gamma_{mk})} - \frac{(\bar{\rho}_{mm}-\bar{\rho}_{\ell\ell})}{(-\omega_{\ell m}+\omega_i+i\Gamma_{\ell m})}\right] \right.$$

$$\left. + \frac{(\mu_\alpha)_{k\ell}(-\mu_\gamma)_{\ell m}(-\mu_\beta)_{mk}}{(-\omega_{\ell k}+\omega_j+\omega_i+i\Gamma_{\ell k})}\left[\frac{(\bar{\rho}_{kk}-\bar{\rho}_{mm})}{(-\omega_{mk}+\omega_i+i\Gamma_{mk})} - \frac{(\bar{\rho}_{mm}-\bar{\rho}_{\ell\ell})}{(-\omega_{\ell m}+\omega_j+i\Gamma_{\ell m})}\right] \right\} \; 2\text{-}53$$

We note that the second term in (2-53) is obtained from the first term
by $i \leftrightarrow j$ and $\beta \leftrightarrow \gamma$. This is due to the definition of
$\chi_{\alpha\beta\gamma}(\omega_i,\omega_j)$ (2-6) which is defined for a pair of frequencies regardless
of their order.

The results obtained in (2-52) and (2-53) are exactly identical to
those of (2-23) and (2-24) if we require $\bar{\rho}_{nn} = \bar{\rho}_{gg}\,\delta_{ng}$ and $\Gamma_{\ell g} + \Gamma_{kg} = \Gamma_{\ell k}$.
However, the results obtained from the phenomenological density matrix
equation have some significantly different meanings. Previous results
are obtained from the Schrödinger equation (2-9) by assuming a known
initial wave function $|\psi(t_o)>$ and a set of well defined energy levels. In
order to obtain a significant result near resonance, we have to perform
the line shape integration over every relevant energy level. The line
shape function of the energy levels are normally unavailable. In the
density matrix approach, we assumed that every energy level is well
defined and all the consequences due to the finite line shape are lumped
into the relaxation terms. As a result, no more line shape integration
is necessary except that of the Doppler broadening which is not included

in the relaxation terms.

The result obtained in this section will be applied to the case of three-wave mixing in NH_2D gases in the next chapter.

CHAPTER 2 REFERENCES

[1] R. P. Feynman, Quantum Electrodynamics (Benjamin, Reading, Mass.,
     1973).

[2] R. P. Feynman, Advanced Quantum Mechanics Lecture Notes, Caltech,
     Ph 205 (1973).

[3] A. Messiah, Quantum Mechanics (New York: Interscience Publishers,

[4] A. Yariv, to be published in JQE

[5] P. Roman, Advanced Quantum Theory, Addison-Wesley, Reading, Mass. 1965,pp.718.

[6] D. H. Perkins, Introduction to High Energy Physics (Addison-Wesley,
     Reading, Mass., 1972).

[7] K. Huang, Statistical Mechanics (Wiley, New York, 1963).

[8] V. B. Berestetskii, E. M. Lifshitz, L. P. Pitaevskii, Relativistic
     Quantum Theory (Pergamon Press, New York, 1973).

[9] N. Bloembergen, Nonlinear Optics (W. A. Benjamin, New York, 1965).

[10] P. R. Berman and W. E. Lamb, Jr., Phys. Rev. A $\underline{2}$, 2435 (1970).

[11] P. R. Berman and W. E. Lamb, Jr., Phys. Rev. A $\underline{4}$, 319 (1971).

[12] A. Yariv, Quantum Electronics (Wiley, New York, 1975), p. 553.

Chapter 3
NONLINEAR POLARIZABILITY OF AN ASYMMETRIC TOP

3-1 Introduction

A general expression for the second order nonlinear polarizability
tensor was derived in the previous chapter. We will now employ those
results to calculate the nonlinear polarizability tensor of an Asym-
metric Top. We will limit ourselves to the rotational-vibrational
transitions only. All the other contributions will be neglected. This
is legitimate as long as the optical waves are in resonance with
the   relevant rotational-vibrational transitions involved in the
nonlinear mixing processes.

We will review in the next section some of the basic quantum
mechanics of an asymmetric top and introduce the conventional energy
level designations for asymmetric tops. Only rotational motion will
be considered.

3-2 Quantum Mechanics of a Rigid Rotating Body

A rigid body is described by the location of its center of mass
and the orientation with respect to a coordinate system fixed in space.
The principal axes of the rigid body will be labelled $\xi\eta\zeta$. The orien-
tation of the rigid body will be defined by the three Euler angles ϕ,
θ, ψ with respect to the fixed coordinate system xyz [1]. The Hamil-
tonian of quantum mechanical rotation of the rigid body can be written [2]

$$H = \frac{J_\xi^2}{2I_a} + \frac{J_\eta^2}{2I_b} + \frac{J_\zeta^2}{2I_c} \qquad\qquad 3\text{-}1$$

where I_a, I_b, I_c are the principal moments of inertia of the rigid body; and J_ξ, J_η, J_ζ are the components of the angular momentum operator along the $\xi\eta\zeta$ axes. These angular momentum operators satisfy the commutation relations [2]

$$[J_\xi, J_\eta] = - i\hbar J_\zeta \quad , \quad \text{etc.} \qquad\qquad 3\text{-}2$$

The total angular momentum operator J^2 is given by

$$J^2 = J_\xi{}^2 + J_\eta{}^2 + J_\zeta^2 \qquad\qquad 3\text{-}3$$

It can be shown that J^2 commutes with H,

$$[H , J^2] = 0 \qquad\qquad 3\text{-}4$$

Therefore the eigenvalues of J^2 are good quantum numbers. It can be also shown that eigenvalues of J_z are also good quantum numbers.

$$[H , J_z] = 0 \qquad\qquad 3\text{-}5$$

In what follows we will describe two special cases. A rigid body with three identical moments of inertia $I_a = I_b = I_c$ is called a symmetrical top. In this case the Hamiltonian has the simple form

$$H = \frac{J^2}{2I} \qquad\qquad 3\text{-}6$$

Therefore the rotational eigenfunctions are the generalized spherical harmonics [2]

$$|JKM\rangle = \sqrt{\frac{2J+1}{8\pi^2}}\, D_{MK}^J\, (\phi,\ \theta,\ \psi) \qquad K,\ M = 0,\ \pm 1,\ \cdots \pm J \qquad 3\text{-}7$$

with eigenvalues given by

$$E = \frac{\hbar^2}{2I}\, J(J+1) \qquad\qquad 3\text{-}8$$

In equation (3-7), K and M are the eigenvalues of J_ζ and J_z respectively.

$$J_z|JKM> = M\hbar|JKM> \qquad\qquad 3\text{-}9$$

$$J_\zeta|JKM> = K\hbar|JKM> \qquad\qquad 3\text{-}10$$

For a spherical top, the energy levels have degeneracy of $(2J+1)^2$. This is due to the fact that the Hamiltonian H given by (3-6) is invariant under any rotation in both $\xi\eta\zeta$ space and xyz space. The rotational invariance in $\xi\eta\zeta$ space contribute $(2J+1)$ degeneracy in K. Another $(2J+1)$ degeneracy in M comes from the rotational invariance in xyz space.

A rigid body with an axis of symmetry has in general two identical moments of inertia. Such a body is called a symmetric top. Suppose, for example, $I_a = I_b \neq I_c$, then the Hamiltonian for rotational motion can be written

$$H = \frac{J^2}{2I_a} + \frac{J_\zeta^2}{2}\left(\frac{1}{I_c} - \frac{1}{I_a}\right) \qquad\qquad 3\text{-}11$$

The rotational eigenfunctions are still given by (3-7). The rotational eigenvalues, however, are given by

$$E = \frac{\hbar^2}{2I_a}J(J+1) + \frac{\hbar^2}{2}\left(\frac{1}{I_c} - \frac{1}{I_a}\right)K^2 \qquad\qquad 3\text{-}12$$

We notice that the degeneracy in K is partially removed. The energy levels still do not depend upon the sign of K. Therefore the degeneracy factor is $2(2J+1)$ if $K \neq 0$. This double degeneracy with respect to the sign of K is due to the fact the Hamiltonian (3-11) is invariant under reflection in a plane passing through the axis of symmetry of the rigid body (see Table 1). If all the three moments of inertia are different, the rigid body is called an asymmetric top. In this case K is no longer

a good quantum number. Only J and M are good quantum numbers. The
rotational eigenfunction can be expanded in terms of a linear combi-
nation of the symmetrical top wave function (3-7). The eigenstates
are specified by giving the value of J, and the value of K_{-1} for the
limiting prolate and K_1, for the limiting oblate symmetric top [3].
To illustrate this energy level specification, we referred to Fig. 3-1
which shows the qualtitative behavior of the asymmetric top energy
levels. The eigenfunction is given by

$$|J_{K_{-1}K_1}M> = \sum_K a_{JK} |JKM>$$
3-13

where a_{JK} are the numerical coefficients which can be determined exactly
by solving the secular equation [4].

Table 1 shows the characters of the irreducible representations
of the symmetry group $R(\theta, \phi)$, $D_{\infty h}$ and D_2 for spherical, symmetrical
and asymmetric top respectively. Fig. 3-2 shows the energy levels of
spherical, symmetrical and asymmetric top; the removal of the degeneracy
is shown as asymmetry is introduced.
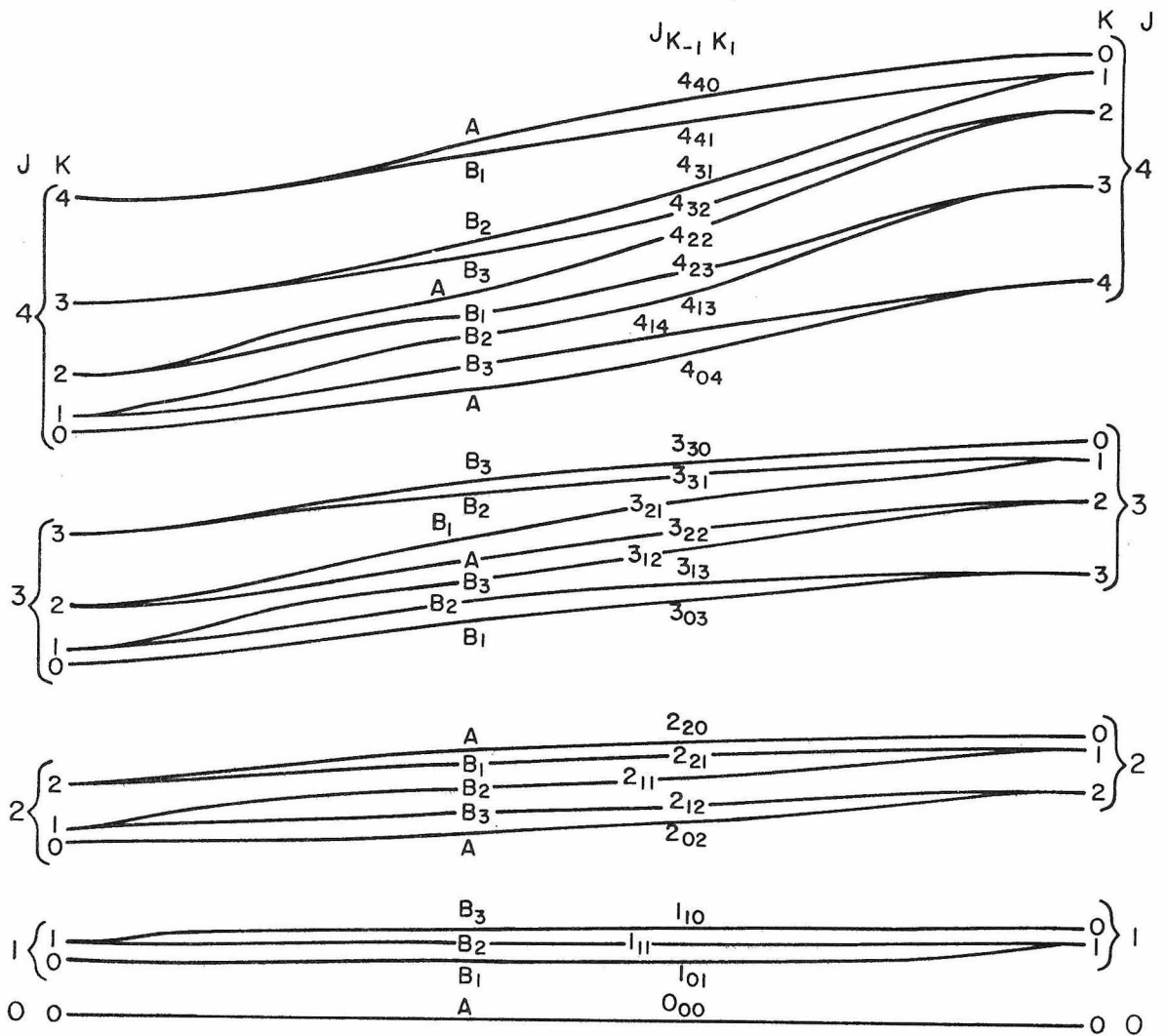
Fig. 3-1 Qualitative behavior of the asymmetric top energy levels. The left end is for a problate symmetric top and the right end is for an oblate symmetric top.
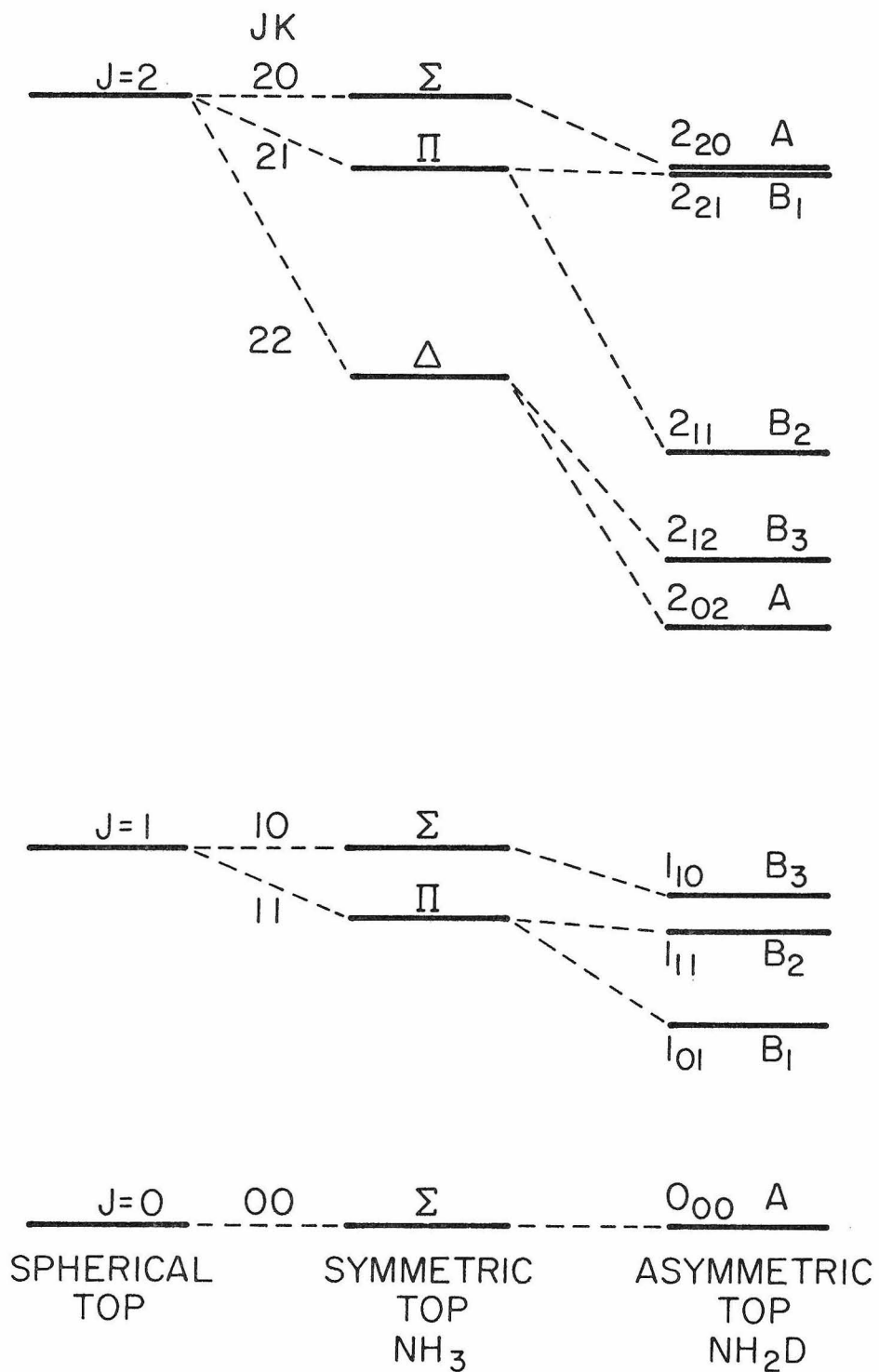
Fig. 3-2 Energy levels of tops with different symmetries.

Table 1 Character tables

$R(\theta,\phi)$	E	$\infty C(\phi)$
J = 0	1	1
J = 1	3	$\sin \frac{3}{2}\phi / \sin \frac{1}{2}\phi$
J = 2	5	$\sin \frac{5}{2}\phi / \sin \frac{1}{2}\phi$
J = 3	7	$\sin \frac{7}{2}\phi / \sin \frac{1}{2}\phi$

$D_{\infty h}$	E	$2C(\phi)$	$\infty\,\sigma_h$	i
Σ_g^+	1	1	1	1
Σ_g^-	1	1	-1	1
Σ_u^+	1	1	1	-1
Σ_u^-	1	1	-1	-1
Π_g	2	$2\cos\phi$	0	$2\cos\phi$
Π_u	2	$2\cos\phi$	0	$-2\cos\phi$
Δ_g	2	$2\cos 2\phi$	0	$2\cos 2\phi$
Δ_u	2	$2\cos 2\phi$	0	$-2\cos 2\phi$

D_2	E	C_2^ξ	C_2^η	C_2^ζ
A	1	1	1	1
B_1	1	1	-1	-1
B_2	1	-1	1	-1
B_3	1	-1	-1	1

3-3 Matrix Elements and Selection Rules

In order to calculate the nonlinear polarizability tensors we need to know the matrix element of the dipole moment operator. The rotational wave functions are in general linear combinations of the generalized spherical harmonics (see 3-13 and 3-7). Thus we have to find out first the matrix elements between these generalized spherical harmonics. In other words, we need to calculate

$$\langle J'K'M' | - \vec{\mu} \cdot \vec{E} | JKM \rangle \qquad \text{3-14}$$

where $\vec{E}$ is the electric field vector which is usually specified in the xyz space coordinate system, and $\vec{\mu}$ is the dipole moment operator which is usually specified in the body coordinate system $\xi\eta\zeta$. Let A be the rotation matrix which transforms $\xi\eta\zeta$ to xyz system. Thus we have

$$\begin{pmatrix} \mu_x \\ \mu_y \\ \mu_z \end{pmatrix} = A \begin{pmatrix} \mu_\xi \\ \mu_\eta \\ \mu_\zeta \end{pmatrix} \qquad \text{3-15}$$

where the rotation matrix is given by [1]

$$A = \begin{pmatrix} \cos\psi\cos\Phi - \cos\theta\sin\Phi\sin\psi & -\sin\psi\cos\Phi - \cos\theta\sin\Phi\cos\psi & \sin\theta\sin\Phi \\ \cos\psi\sin\Phi + \cos\theta\cos\Phi\sin\psi & -\sin\psi\sin\Phi + \cos\theta\cos\Phi\cos\psi & -\sin\theta\cos\Phi \\ \sin\theta\sin\psi & \sin\theta\cos\psi & \cos\theta \end{pmatrix} \qquad \text{3-16}$$

$$\equiv \begin{pmatrix} A_{x\xi} & A_{x\eta} & A_{x\zeta} \\ A_{y\xi} & A_{y\eta} & A_{y\zeta} \\ A_{z\xi} & A_{z\eta} & A_{z\zeta} \end{pmatrix} \qquad \text{3-17}$$

The rotation matrix (3-16) can be expressed in terms of the generalized spherical harmonics [2]

$$
A = \begin{bmatrix}
\frac{1}{2}[D^1_{11}+D^1_{1-1}+D^1_{-11}+D^1_{-1-1}] & \frac{i}{2}[D^1_{11}+D^1_{-11}-D^1_{1-1}-D^1_{-1-1}] & \frac{i}{\sqrt{2}}[D^1_{10}+D^1_{-10}] \\
\frac{-i}{2}[D^1_{11}+D^1_{1-1}-D^1_{-11}-D^1_{-1-1}] & \frac{1}{2}[D^1_{11}-D^1_{1-1}-D^1_{-11}+D^1_{-1-1}] & \frac{1}{\sqrt{2}}[D^1_{10}-D^1_{-10}] \\
\frac{-i}{\sqrt{2}}[D^1_{01}+D^1_{0-1}] & \frac{1}{\sqrt{2}}[D^1_{01}-D^1_{0-1}] & D^1_{00}
\end{bmatrix}
$$

In terms of the rotation matrix A, the matrix element (3-14) becomes

$$
<J'K'M'|-\vec{\mu}\cdot\vec{E}|JKM> = -\vec{E}\cdot<J'K'M'|A|JKM>\vec{\mu}_{body} \qquad 3\text{-}19
$$

where $\vec{\mu}_{body}$ is the dipole moment operator in the body coordinate system $\xi\eta\zeta$. Note that $\vec{\mu}_{body}$ is independent of the Euler angles Φ, θ and ψ.

From (3-19) we find that all we have to do is to calculate $<J'K'M'|D^1_{mk}|JKM>$ which is given by [2]

$$
<J'K'M'|D^1_{mk}|JKM> = \frac{8\pi^2}{2J'+1}\,(J1M\,m|J'M')\,(J1K\,k|J'K') \qquad 3\text{-}20
$$

where $(J1M\,m|J'M')$ and $(J1K\,k|J'K')$ are Clebsch- Gordan coefficients [5] (see also Table 2) and $m,k = -1,0,1$.

A typical term in a matrix element which involved in the transition from $|J'_{K'_{-1}K'_1}\,M'>$ to $|J_{K_{-1}K_1}\,M>$ is of the following form

$$
<J'_{K'_{-1}K'_1}\,M'|A_{n\nu}|J_{K_{-1}K_1}\,M> = \sum_{KK'} a^*_{J'K'}\,a_{JK}\,<J'K'M'|A_{n\nu}|JKM> \qquad 3\text{-}21
$$

where (3-13) has been used and $n = x, y, z$, $\nu = \xi, \eta, \zeta$.

Table 2   Clebsch - Gordan Coefficients $(J1M\ m|J'M')$

$(J1M\ m\|J'M')$	$m = 1$	$m = 0$	$m = -1$
$J' = J + 1$	$\left[\dfrac{(J+M+1)(J+M+2)}{(2J+1)(2J+2)}\right]^{1/2}$	$\left[\dfrac{(J-M+1)(J+M+1)}{(2J+1)(J+1)}\right]^{1/2}$	$\left[\dfrac{(J-M+1)(J-M+2)}{(2J+1)(2J+2)}\right]^{1/2}$
$J' = J$	$-\left[\dfrac{(J+M+1)(J-M)}{2J\,(J+1)}\right]^{1/2}$	$\dfrac{M}{[J\,(J+1)]^{1/2}}$	$\left[\dfrac{(J-M+1)(J+M)}{2J\,(J+1)}\right]^{1/2}$
$J' = J - 1$	$\left[\dfrac{(J-M-1)(J-M)}{2J\,(2J+1)}\right]^{1/2}$	$-\left[\dfrac{(J-M)(J+M)}{J\,(2J+1)}\right]^{1/2}$	$\left[\dfrac{(J+M)(J+M-1)}{2J\,(2J+1)}\right]^{1/2}$

If we write $A_{n\nu}$ as

$$A_{n\nu} = \sum_{mk} C_{n\nu}^{mk} \; D_{mk}^1 \; (\Phi, \theta, \psi) \qquad\qquad 3\text{-}22$$

then it follows from (3-20) that (3-21) can be written

$$\langle J'_{K'_{-1}K'_1}M' | A_{n\nu} | J_{K_{-1}K_1}M\rangle = \sum_{KK'} \sum_{mk} \frac{8\pi^2}{2J'+1} a^*_{J'K'} \; a_{JK} \; C_{n\nu}^{mk} \quad\times$$

$$(J1Kk|J'K') \; (J1Mm|J'M') \qquad\qquad 3\text{-}23$$

Because of the conservation of angular momentum (or the property of Clebsch – Gordan coefficient), the nonvanishing term must have

$$m = M' - M \qquad\qquad 3\text{-}24$$

$$k = K' - K \qquad\qquad 3\text{-}25$$

Using these m and k, (3-23) can be written

$$\langle J'_{K'_{-1}K'_1}M' | A_{n\nu} | J_{K_{-1}}K M\rangle = \alpha_{n\nu}^m \; (J',J) \; (1M\,m|J'M') \qquad\qquad 3\text{-}26$$

where

$$\alpha_{n\nu}^m \; (J',J) \equiv \frac{8\pi^2}{2J'+1} \sum_{Kk} C_{n\nu}^{mk} \; a^*_{J'\,K+k} \; a_{JK}(J1K\,k|J'\,K+k\rangle \qquad\qquad 3\text{-}27$$

These results are summarized in Table 3.

Table 3 Matrix Elements of an Asymmetric Top

		μ_ξ	μ_η	μ_ζ	
	Allowed transitions	$A \leftrightarrow B_1$ $B_2 \leftrightarrow B_3$	$A \leftrightarrow B_2$ $B_1 \leftrightarrow B_3$	$A \leftrightarrow B_3$ $B_1 \leftrightarrow B_2$	space factor
E_x	$M \to M\pm 1$	$\dfrac{i}{\sqrt{2}}\,\alpha_\xi$	$\dfrac{i}{\sqrt{2}}\,\alpha_\eta$	$\dfrac{i}{\sqrt{2}}\,\alpha_\zeta$	$x(J1M \pm 1 \mid J'\,M\pm 1)$
E_y		$\pm\dfrac{1}{\sqrt{2}}\,\alpha_\xi$	$\pm\dfrac{1}{\sqrt{2}}\,\alpha_\eta$	$\pm\dfrac{1}{\sqrt{2}}\,\alpha_\zeta$	$x(J1M \pm 1 \mid J'\,M\pm 1)$
E_z	$M \to M$	α_ξ	α_η	α_ζ	$x(J1M\ 0 \mid J'M)$

where

$$\alpha_\xi = \frac{-4\sqrt{2}\pi^2 i}{2J'+1} \sum_K \left\{ a^*_{J'K+1}\, a_{JK}\, (J1K1 \mid J'K+1) \right.$$

$$\left. + a^*_{J'K-1}\, a_{JK}\, (J1K\ -1 \mid J'\ K-1) \right\} \qquad 3\text{-}28$$

$$\alpha_\eta = \frac{4\sqrt{2}\pi^2}{2J'+1} \sum_K \left\{ a^*_{J'K+1}\, a_{JK}\, (J1K\ 1 \mid J'K+1) \right.$$

$$\left. - a^*_{J'K-1} a_{JK}\, (J1K\ -1 \mid J'\ K-1) \right\} \qquad 3\text{-}29$$

$$\alpha_\zeta = \frac{8\pi^2}{2J'+1} \sum_K a^*_{J'K}\, a_{JK}\, (J1K0 \mid J'K) \qquad 3\text{-}30$$

The selection rules are also included in Table 2. These selection rules can be obtained from the character table given in Table 1. A, B_1, B_2, B_3 are the only four irreducible representation of the symmetric group D_2 of the Hamiltonian. Each energy level of an asymmetric top is labelled by one of these four irreducible representations. The transformation properties of these four representations are also shown in the same tables. For example, if we consider a rotation of 180° around the ξ-axis, μ_ξ is unchanged, A and B_1 are also unchanged. B_2 and B_3 change sign, thus we conclude that the allowed transitions that involve μ_ξ are $A \leftrightarrow B_1$ and $B_2 \leftrightarrow B_3$.

3-4 Nonlinear Polarizability of an Asymmetric Top

We have mentioned previously that the second order nonlinear susceptibility of a medium with inversion symmetry vanishes. Therefore there is no second order nonlinear effect in gases. In order to have a nonzero second order nonlinear polarizability, it is necessary to have a nonvanishing product of the three matrix element among the three relevant energy levels involved (see 2-50). In addition to this, the summation of all the contributions from the degeneracy (usually M) should not cancel.

In this section we will show that the second order nonlinear polarizability of an asymmetric top isolated in free space with equal probability in any orientation vanishes. In order to have a nontrivial product of three matrix elements, the three energy levels involved must have different irreducible representations. Without loss of generality

we will assume that the three energy levels involved are $|B_1 \; J\rangle$, $|B_2 \; J+1\rangle$, $|B_3 \; J\rangle$ and the molecule is in its ground state $|B_1 \; J\rangle$ (see Fig. 3-3).

Consider a typical component $\chi_{zxy}(\omega_1, \omega_2)$; from (2-53) and Table 3 we have

$$\chi_{zxy}(\omega_1, \omega_2) \propto \frac{1}{2J+1} \sum_M \Bigg\{ (J,1,M,1 \mid J+1, M+1)(J+1, 1, M+1, -1)(J,1,M,0 \mid J,M)$$

$$+ (J,1,M, -1 \mid J+1, M-1)(J+1, 1, M-1, 1 \mid JM)(J,1,M,0 \mid J,M) \Bigg\}$$

$$3\text{-}31$$

From Table 3,

$$= \frac{1}{2J+1} \sum_M \Bigg\{ \left[\frac{(J+M+1)(J+M+2)}{(2J+1)(2J+2)} \right]^{1/2} \left[\frac{(J+M+1)(J+M+2)}{(2J+2)(2J+3)} \right]^{1/2} \frac{M}{\sqrt{J(J+1)}}$$

$$+ \left[\frac{(J-M+1)(J-M+2)}{(2J+1)(2J+2)} \right]^{1/2} \left[\frac{(J+1-M)(J+2-M)}{(2J+2)(2J+3)} \right]^{1/2} \frac{M}{\sqrt{J(J+1)}} \Bigg\}$$

$$3\text{-}32$$

The sum of the two terms inside the parenthesis in (3-32) is an odd function of M, so that the summation $\sum\limits_M$ gives

$$\chi_{zxy}(\omega_1, \omega_2) = 0 \qquad\qquad 3\text{-}33$$

It can be shown similarly that all the tensor components of even order nonlinear polarizabilities for a molecule with random orientation vanish.
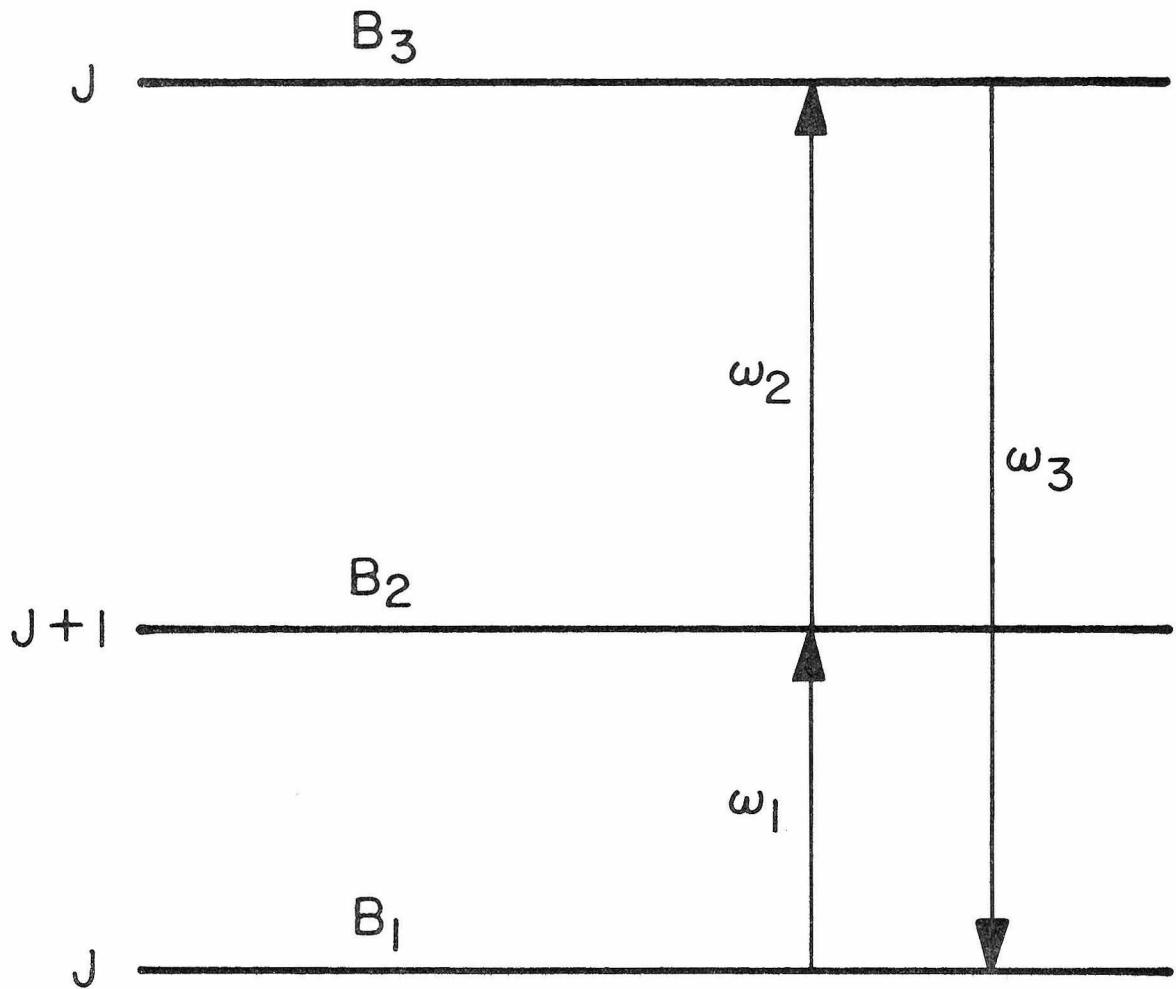
Fig. 3-3 A three-level system.

CHAPTER 3 REFERENCES

[1] H. Goldstein, <u>Classical Mechanics</u>, (Addison-Wesley, Cambridge, Mass., 1950).

[2] A. S. Davydov, <u>Quantum Mechanics</u>, (Addison-Wesley, Reading, Mass., 1968).

[3] C. H. Townes and A. L. Schawlow, <u>Microwave Spectroscopy</u>, (Dover, New York, 1975), p. 84.

[4] L. D. Landau and E. M. Lifshitz, <u>Quantum Mechanics</u>, (Addison-Wesley, Reading, Mass., 1959).

[5] M. E. Rose, <u>Elementary Theory of Angular Momentum</u>, Wiley & Sons, New York, (1957).

Chapter 4

APPLICATION TO NH_2D MOLECULE

4-1 Introduction

We have shown that an asymmetric molecule with random orientation possesses no second order nonlinear polarizability. This prohibits any three-wave mixing in molecular (or atomic) gases. Application of dc electric field to a gases system destroys the basic inversion and isotropy symmetry and allows three-wave mixing processes to occur. The general expression (2-50) derived in chapter 2 will now be applied to NH_2D molecule under the conditions of resonantly enhanced nonlinearities. Calculations are presented for mixing of a CO_2 laser with 4 GHz microwaves in the molecule NH_2D, producing single lower sideband radiation. Pressure dependence of the nonlinear susceptibility is also calculated by performing an integration over the Maxwellian velocity distribution. The dispersion behavior of the real and imaginary parts of the nonlinear susceptibility is also presented. Saturation effects are also considered.

4-2 Stark-induced Nonlinearity in NH_2D

We consider a gaseous NH_2D system in a dc electric field polarized in z-direction. The number of NH_2D molecules per unit volume is N. The application of a dc electric field to a gaseous system introuces a preferred spatial direction thus destroying the inversion and isotropy symmetry. The second order nonlinear polarization oscillating at the difference frequency $\omega_1 = \omega_3 - \omega_2$ can be related to the product of the two electric fields by

$$P_\alpha^{(2)}(t) = \text{Re}\left\{d_{\alpha\beta\gamma}(\omega_3, -\omega_2)\ E_{3\beta}\ E_{2\gamma}^*\ e^{-i(\omega_3-\omega_2)t}\right\} \qquad \text{4-1}$$

where $d_{\alpha\beta\gamma}(\omega_3, -\omega_2)$ is the corresponding nonlinear susceptibility which is related to the molecular nonlinear polarizability by

$$d_{\alpha\beta\gamma}(\omega_3, \omega_2) = N\ \chi_{\alpha\beta\gamma}(\omega_3, -\omega_2) \qquad \text{4-2}$$

Because of the applied dc field, the gaseous system now possesses an axial symmetry. The only nonvanishing second order susceptibilities are d_{zzz}, d_{zii}, d_{izi} and d_{iiz}, where i = x or y.

The NH_2D molecule has, among others, the three levels shown in Fig. 4-1, which can be Stark-tuned into simultaneous resonance with the P(20) line of the CO_2 laser [1]-[4] and microwave radiation near 4 GHz as shown. This should lead to a strong resonant mixing of the P(20) line (of frequency $\omega_3/2\pi$) and the microwave field at $\omega_2/2\pi$ = 4 GHz, giving rise to the difference frequency radiation at $\omega_1 = \omega_3 - \omega_2$ when the Stark field is near E_{dc} = 3570 V/cm. Levels 1 and 2 belong to the lowest vibrational state (ν_2 = 0) and have molecular angular momentum quantum numbers J = 4 and $|M|$ = 4. The subscripts 04 and 14 correspond to the standard asymmetric top designation [5,6]. The symbols a (asymmetric) and s (symmetric) refer to the parity of the inversion-split vibrational wave functions. The application of an electric field E_{dc} causes an admixture of the wave functions $|4_{04}a\rangle$ and $|4_{14}s\rangle$ which is due to a nonvanishing matrix element of the molecular dipole operator connecting the two states. This admixture, which will soon be shown to be responsible for the nonlinear mixing, disappears at zero dc field. The parameter Δ appearing in the expression for the wave functions corresponds
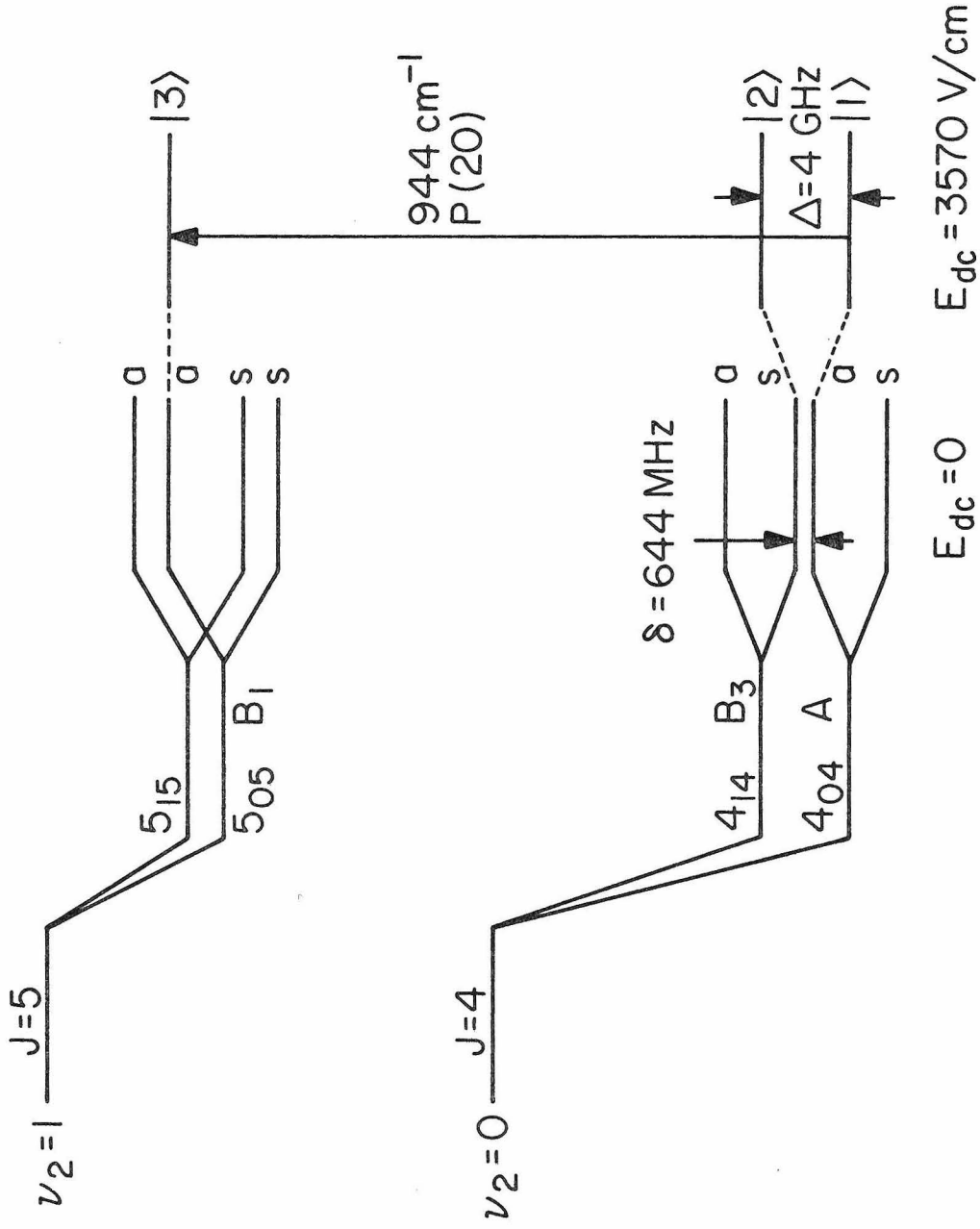
44

Fig. 4-1 The relevant energy levels of NH_2D molecule.

to the energy splitting $E_2 - E_1$ between the two low-lying states and is given by

$$\Delta = [4|<4_{04}a|\mu_z|4_{14}s>|^2(E_{dc})^2 + \delta^2]^{1/2} \qquad 4\text{-}3$$

while the admixture wave functions are

$$|1> = \frac{1}{\sqrt{2}} \ [\sqrt{1 + \delta/\Delta}|4_{04}a> + \sqrt{1 - \delta/\Delta}|4_{14}s>], \qquad 4\text{-}4$$

$$|2> = \frac{1}{\sqrt{2}} \ [\sqrt{1 - \delta/\Delta}|4_{04}a> - \sqrt{1 + \delta/\Delta}|4_{14}s >] \qquad 4\text{-}5$$

where δ is the zero splitting and μ_z is the projection of the molecular dipole moment operator along the direction of the dc field.

The expression for the nonlinear dipole moment of an NH_2D molecule depends on matrix elements which can be determined from nonlinear absorption data as well as from the data on Stark splitting. This makes possible, in principle, a precise theoretical derivation of the nonlinear mixing behavior of this molecule and of its parametric dependencies.

Applying the general results obtained from chapter 2 to the three-level system of Fig. 4-1, and keeping only the resonant terms (i.e., with near vanishing denominator), leads to the following expression for the polarization generated at $\omega_1 = \omega_3 - \omega_2$ by the applied fields at ω_2, ω_3:

$$P_\alpha^{(2)} (t) = \frac{1}{4\hbar^2} \left\{ \frac{(\mu_\alpha)_{23}(\mu \cdot E_3)_{31}(\mu \cdot E_2)_{12}}{[\omega_3 - \omega_2 - \omega_{32} + i\Gamma_{32}]} \left[\frac{(\bar{\rho}_{22} - \bar{\rho}_{11})}{[-\omega_2 + \omega_{21} + i\Gamma_{21}]} - \frac{(\bar{\rho}_{11} - \bar{\rho}_{33})}{[\omega_3 - \omega_{31} + i\Gamma_{31}]} \right] \times \right.$$

$$\left. e^{-i(\omega_3 - \omega_2)t} + c \cdot c \cdot \right\} \qquad 4\text{-}6$$

where $\overline{\rho}_{ii}$ is the equilibrium density matrix of level i with $\vec{E}_2 = \vec{E}_3 = 0$. If the NH_2D gaseous is at thermal equilibrium, we have $\overline{\rho}_{11} \cong \overline{\rho}_{22}$ and $\rho_{33} \cong 0$. Therefore the main contribution to $P_\alpha^{(2)}$ (t) comes from the second term, the one proportional to $(\overline{\rho}_{11} - \overline{\rho}_{33})$.

The energy states $|4_{04}a>$, $|14_{14}s>$ and $|5_{05}a>$ at zero dc field have the irreducible representations A, B_3 and B_1 respectively [7]. According to the selection rules described in section 3-3, the dipole moment which involved in the transition between B_3 and B_1 is μ_η. But $\mu_\eta = 0$ due to the basal symmetry of NH_2D (Note: η is the principal axis parallel to the bond direction of the two hydrogen atom in NH_2D). Thus we conclude that the matrix element $(\mu_\alpha)_{23}$ vanishes at zero dc field. It follows from (4-6) that no frequency mixing takes place at zero dc field. When $E^{dc} \neq 0$ the ground state wave function $|4_{04}a>$ is admixed into level 2 as shown in Fig. 4-1. This results in a nonvanishing matrix element $(\mu_\alpha)_{32}$ proportional to $<5_{05}a | \mu_\xi | 4_{04}a>$.

For $\vec{E}_2 || \hat{z}$, $\alpha = x$, and $\vec{E}_3 || \hat{x}$ we can show that the triple matrix product appearing in (4-6) is given by

$$(\mu_x)_{23}(\mu_x)_{31}(\mu_z)_{12} = \frac{\delta}{\Delta^2} | \mu_{I\ II}E_{dc} | \mu_{I\ II} | \mu_{I\ III} |^2 \qquad 4\text{-}7$$

where

$$\mu_{I\ II} = <4_{04}a | \mu_z | 4_{14}s> \qquad 4\text{-}8$$

$$\mu_{I\ III} = <4_{04}a | \mu_x | 5_{05}a> \qquad 4\text{-}9$$

The nonlinear mixing is thus absent, i.e., $P_x^{(2)} = 0$, at zero field ($E_{dc} = 0$) and at very high fields ($\Delta \gg \delta$).

From (4-1) and (4-6) and using that fact that at room temperature $\overline{\rho}_{22} \simeq \overline{\rho}_{11}$, we obtain

$$d_{\alpha\beta\gamma}(\omega_3, -\omega_2) = \frac{-N_1}{2\hbar^2} \cdot \frac{(\mu_\alpha)_{23} (\mu_\beta)_{31} (\mu_\gamma)_{12}}{[(\omega_3 - \omega_2) - \omega_{32} + i\Gamma_{32}] [\omega_3 - \omega_{31} + i\Gamma_{31}]} \qquad 4\text{-}10$$

where N_1 is defined as the population density of level 1 , i.e.

$$N_1 = N \overline{\rho}_{11} \qquad 4\text{-}11$$

Expression (4-10) applied to stationary molecules with energy levels at E_1, E_2 and E_3. In a gas sample we need to account for the Doppler shift of the transition energies of individual molecules. This is done by averaging the nonlinear susceptibility $d_{\alpha\beta\gamma}$ over the velocity distribution function. We will assume that the two optical waves are all propagating in y-direction so that we only take the y-component of the molecular velocity into account. The velocity distribution function is taken as a Maxwellian

$$g(v) = \frac{1}{\sqrt{2\pi}\,\sigma}\, e^{-v^2/2\sigma^2} \qquad 4\text{-}12$$

where

$$\sigma^2 = kT/m \qquad 4\text{-}13$$

We also assume that the microwave frequency ω_2 is tuned such that
$\omega_2 = \omega_{21}(v = 0)$.

The frequency off-set $\Delta\omega$ is thus due to optical waves only and is given by

$$\Delta\omega = \omega_3 - \omega_{31}(v = 0) = \omega_3 - \omega_2 - \omega_{32}(v = 0) \qquad 4\text{-}14$$

To perform the average, we need to replace ω_{31} by $\omega_{31}(1+\frac{v}{c})$ and ω_{32} by $\omega_{32}(1+\frac{v}{c})$. From now on ω_{31} and ω_{32} mean the transition frequencies for stationary molecules. From (4-10) and (4-12), the averaged $d_{\alpha\beta\gamma}$ $(\omega_3, -\omega_2)$ becomes

$$d_{\alpha\beta\gamma}(\omega_3,-\omega_2) = \frac{-N_1(\mu_\alpha)_{23}(\mu_\beta)_{31}(\mu_\gamma)_{12}}{2\hbar^2} \int_{-\infty}^{\infty} \frac{g(v)\, dv}{(\frac{-\omega_{32}}{c} v + \Delta\omega + i\Gamma)(\frac{-\omega_{31}}{c} v + \Delta\omega + i\Gamma)} \qquad 4\text{-}15$$

where we assumed $\Gamma_{13} = \Gamma_{32} \equiv \Gamma$ which is approximately the sum of the natural and pressure broadening line width. The integral in (4-15) can be separated into a difference of two plasma dispersion integrals.

$$I \equiv \int_{-\infty}^{\infty} \frac{g(v)\, dv}{(\frac{\omega_{32}}{c} v - \Delta\omega - i\Gamma)(\frac{\omega_{31}}{c} v - \Delta\omega - i\Gamma)} = \frac{c}{\sqrt{2}\sigma\omega_{21}(\Delta\omega + i\Gamma)\sqrt{\pi}} \int_{-\infty}^{\infty} \left[\frac{e^{-t^2}}{t - z_2} - \frac{e^{-t^2}}{t - z_1}\right] dt$$

$$4\text{-}16$$

where

$$z_1 = \frac{\Delta\omega + i\Gamma}{\sqrt{2}\ \sigma\ \omega_{31}} c \qquad 4\text{-}17$$

$$z_2 = \frac{\Delta\omega + i\Gamma}{\sqrt{2}\ \sigma\ \omega_{32}} c \qquad 4\text{-}18$$

We will use the following definition of plasma dispersion function suggested by Abramovitz and Stegun [8].

$$W(z) = \frac{1}{\pi i} \int_{-\infty}^{\infty} \frac{e^{-t^2}}{t - z} dt = e^{-z^2} erfc(-iz) \qquad 4\text{-}19$$

This definition is different from that of Fried and Conte [9] by a factor of $\sqrt{\pi}$ i, i.e.

$$Z(z) = \sqrt{\pi} \; i \; W(z) \qquad\qquad 4\text{-}20$$

The integral in (4-16) thus can be expressed by a difference of plasma dispersion function with two different arguments.

$$I = \frac{\pi}{2} \; \frac{c}{\sigma \; \omega_{21}(\Gamma - i\Delta\omega)} \left\{ W\left(\frac{\Delta\omega + i\Gamma}{\sqrt{2} \; \sigma \; \omega_{32}} c\right) - W\left(\frac{\Delta\omega + i\Gamma}{\sqrt{2} \; \alpha \; \omega_{31}} c\right) \right\} \qquad 4\text{-}21$$

Since $\omega_{31} \simeq \omega_{32} \gg \omega_{21}$, equation (4-21) can be approximated by the following expression

$$I = \frac{\sqrt{\pi}}{2} \; \left(\frac{c}{\sigma \; \omega_{31}}\right)^2 \; iW'\left(\frac{\Delta\omega + i\Gamma}{\sqrt{2} \; \sigma \; \omega_{31}} c\right) \qquad 4\text{-}22$$

where W' is the derivative of W with respective to its own argument.

The averaged nonlinear susceptibility $d_{\alpha\beta\gamma}$ is then

$$d_{\alpha\beta\gamma} (\omega_3, -\omega_2) = \frac{-N_1 (\mu_\alpha)_{23}(\mu_\beta)_{31}(\mu_\gamma)_{12}}{2\hbar^2} \cdot \frac{\sqrt{\pi}}{2} \; \left(\frac{c}{\sigma \; \omega_{31}}\right)^2 iW'\left(\frac{\Delta\omega + i\Gamma}{\sqrt{2} \; \sigma \; \omega_{31}} c\right) \qquad 4\text{-}23$$

We note that the argument of plasma dispersion function, $c(\Delta\omega + i\Gamma)/\sqrt{2} \; \sigma \; \omega_{31}$, is a complex number with the real part equal to the ratio of the frequency off-set to the Doppler linewidth and the imaginary part equal to the ratio of the homogeneous (spontaneous puls pressure) linewidth to the Doppler linewidth. The derivative of a plasma dispersion function

is related to itself by [10]

$$W'(z) = -2zW(z) + \frac{2}{\sqrt{\pi}} i \qquad\qquad 4\text{-}24$$

Thus the averaged nonlinear susceptibility $d_{\alpha\beta\gamma}$ can also be written

$$d_{\alpha\beta\gamma}(\omega_3, -\omega_2) = \frac{N_1 (\mu_\alpha)_{23}(\mu_\beta)_{31}(\mu_\gamma)_{12}}{2\hbar^2} \left(\frac{c}{\sigma \omega_{31}}\right)^2$$

$$\left\{1 + i\sqrt{\pi} \left(\frac{\Delta\omega + i\Gamma}{\sqrt{2} \sigma \omega_{31}} c\right) W \left(\frac{\Delta\omega + i\Gamma}{\sqrt{2} \sigma \omega_{31}} c\right)\right\} \qquad 4\text{-}25$$

At resonance, $\Delta\omega = 0$, the above expression becomes

$$d_{\alpha\beta\gamma}(\omega_3, -\omega_2) = \frac{N_1 (\mu_\alpha)_{23}(\mu_\beta)_{31}(\mu_\gamma)_{12}}{2\hbar^2} \left(\frac{c}{\sigma \omega_{31}}\right)^2$$

$$\left\{1 - \sqrt{\pi} \times e^{x^2} \text{erfc}(x)\right\} \qquad\qquad 4\text{-}26$$

where

$$x = \frac{c \Gamma}{\sqrt{2} \sigma \omega_{31}} \qquad\qquad 4\text{-}27$$

We note that Γ and N_1 are proportional to pressure if the natural line-width is negligible compared with pressure broadening linewidth.

4-3 Relation to Linear Absorption Coefficient

Although a numerical estimate of the nonlinear mixing coefficient based on (4-25) is possible, a safer procedure and one that serves as a check on the matrix elements needed to evaluate d_{xxz} (the largest co-efficient in NH_2D) is to relate it to the linear absorption coefficient

for x polarized field at ω_3. The latter can be shown, by a derivation similar to that given above, to be given by

$$\gamma_x(\Delta\omega) = \frac{4\pi N_1 |(\mu_x)_{31}|^2 \omega_{31}}{\Gamma \hbar c} \cdot \frac{c\,\Gamma}{\sqrt{2}\,\sigma\,\omega_{31}} \sqrt{\pi}\,\text{Re}\left\{W(\frac{\Delta\omega + i\Gamma}{\sqrt{2}\,\sigma\,\omega_{31}}\,c)\right\} \qquad 4\text{-}28$$

The resonant absorption coefficient is obtained from (4-28) by letting $\Delta\omega = 0$

$$\gamma_x(0) = \gamma_H \sqrt{\pi}\,x\,e^{x^2}\text{erfc}(x) \qquad 4\text{-}29$$

where x is given by (4-27) and γ_H is the absorption coefficient at high pressure ($c\Gamma >> \sigma\omega_{31}$) and is given by

$$\gamma_H = \frac{4\pi\,|\,(\mu_x)_{31}\,|^2\,\omega_{31}}{\Gamma \hbar c}\,N_1 \qquad 4\text{-}30$$

Combining (4-30) and (4-26) leads to the following expression for the resonant nonlinear susceptibility

$$d_{xxz}(\omega_3,-\omega_2) = \frac{c(\mu_z)_{12}}{8\pi\hbar}\frac{(\mu_x)_{23}}{\omega_{31}}\frac{(\mu_x)_{23}}{(\mu_x)_{13}} \cdot \frac{\pi}{2}(\frac{c}{\sigma\,\omega_{31}})\gamma_H\,[\,\frac{2}{\sqrt{\pi}}\,x - 2x^2e^{x^2}\text{erfc}(x)] \qquad 4\text{-}31$$

where x is given by (4-27).

The various constants in (4-31) are evaluated as follows: The matrix element $(\mu_z)_{12}$ is a function of the admixture and is obtained from the wavefunctions (4-4) and (4-5) as

$$(\mu_z)_{12} = \frac{\delta}{\Delta}\,<4_{04}a|\mu_z|4_{14}s> \qquad 4\text{-}32$$

where the splitting $\Delta = E_2 - E_1$ is given by (4-3). We obtain the matrix element $\langle a|\mu_z|s\rangle$ from comparing (4-3) to the experimental tuning curve of ω_{31} vs. E_{dc} [4]. This yields $\langle a|\mu_z|s\rangle = 1.14 \times 10^{-18}$ esu. At resonance $E_{dc} = 3570$ V/cm and $\delta/\Delta = 0.174$. The final result is

$$(\mu_z)_{12} = 0.174 \, a\langle|\mu|s\rangle = 0.198 \times 10^{-18} \text{ esu} \qquad 4\text{-}33$$

$(\mu_x)_{23}/(\mu_x)_{13}$ is obtained similarly and is given by

$$\frac{(\mu_x)_{23}}{(\mu_x)_{13}} = (\frac{\Delta - \delta}{\Delta + \delta})^{1/2} \qquad 4\text{-}34$$

The saturated absorption γ_H is obtained from the data on Ref. [3] for a 50:50 ND_3-NH_3 mixture as

$$\gamma_H = .028 \text{ cm}^{-1} \qquad 4\text{-}35$$

From the same data we obtain

$$\Gamma/P = 2\pi(20.1 \text{ MHz/Torr}) \qquad 4\text{-}36$$

which enables us to express the dimensionless argument x of Eq. (4-31) as

$$x = \frac{2\pi(20.1) \times 10^6 c \, P(\text{Torr})}{\sqrt{(kT/M)} \, \omega_{31}} \qquad 4\text{-}37$$

With these data we obtain

$$d_{xxz}^{\omega_1 = \omega_3 - \omega_2} = 2.31 \times 10^{-7} G(x) \text{ esu} \qquad \text{4-38}$$

$$G(x) = 2x\left[\frac{1}{\sqrt{\pi}} - x\, e^{x^2} \text{erfc}(x)\right] \qquad \text{4-39}$$

The theoretical dependence of d_{xxz} on P (4-38) is plotted in Fig. 4-2. The peak occurs at P = 2.0 Torr and has a value of

$$(d_{xxz}^{\omega_1 = \omega_3 - \omega_2})_{max} = 6.4 \times 10^{-8} \text{ esu} \qquad \text{4-40}$$

A comparison of this predicted behavior with experiment is given in the next chapter.

The coefficient d estimated above refers to the generation of sideband radiation at ω_1 by mixing CO_2 P(20) line with a microwave field ω_2 (at 4.1 GHa). It is thus appropriate to compare it to the electro-optic coefficient r_{14} of GaAs which can be used, alternatively, to generate the sideband by conventional electrooptic modulation.

Using the correspondence [11].

$$r_{j\ell k} = -\frac{2\varepsilon_0}{\varepsilon_j \varepsilon_\ell}\, d_{jk\ell} \qquad \text{4-41}$$

we have

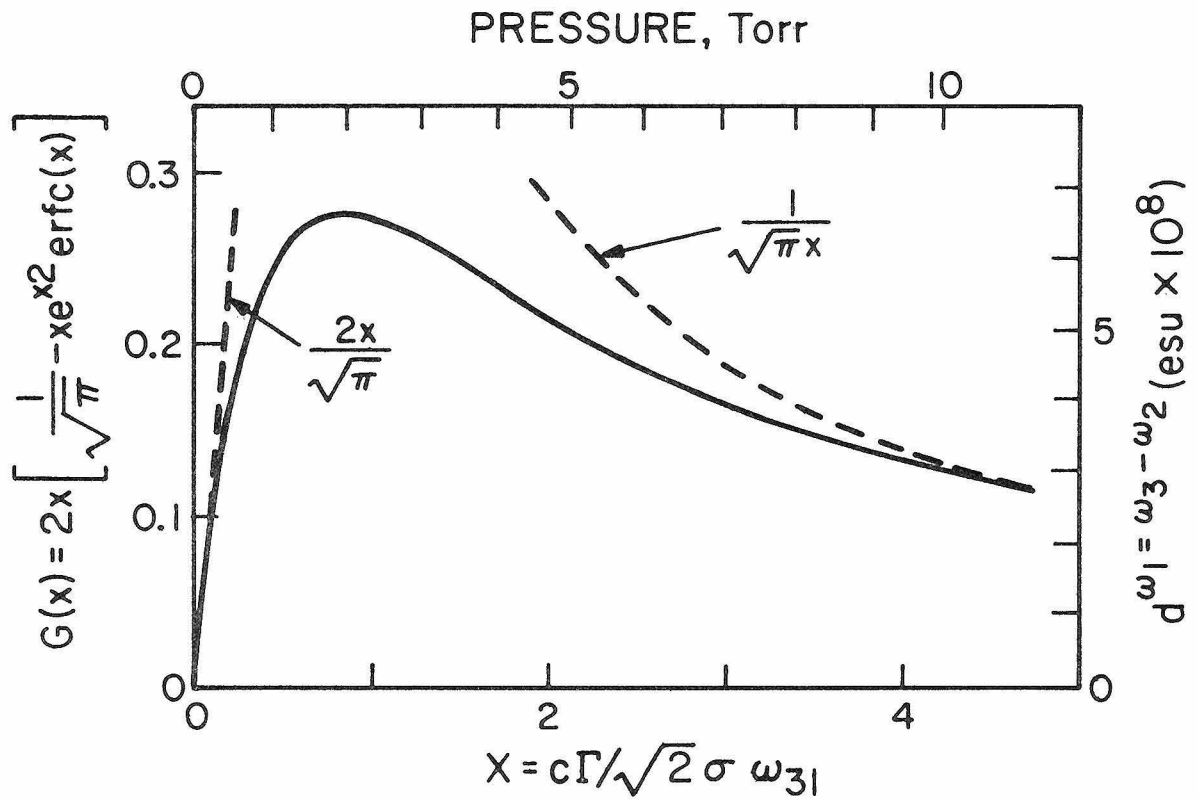$$\frac{(n^3 r)_{NH_2D}}{(n^3 r)_{GaAs}} \sim 0.8 \qquad \text{4-42}$$

Fig. 4-2 Theoretical dependence of NH_2D nonliner coefficient on pressure when the applied fields are exactly resonant with the Stark-tuned energy levels.

We reach the conclusion that for sideband generation, dc biased NH_2D at $P \simeq 2$ Torr is comparable to GaAs (which is one of the best infrared modulation materials). We must recognize, however, that this large coefficient was obtained by exploiting the resonant nature of the effect. The penalty we pay for this is that of reduced bandwidth.

Other components of the nonlinear polarizability tensor

We have mentioned that the only nonvanishing components of the second-order polarizability tensor in a system possessing axial symmetry (z-axis) are

$$d_{zzz}$$

$$d_{zxx} = d_{zyy}$$

$$d_{xzx} = d_{yzy}$$

$$d_{xxz} = d_{yyz}$$

In our special case where the $1 \leftrightarrow 2$ transition must be $\Delta M = 0$ which means if the polarization of E_2 is in x or y direction, the matrix element vanishes. This shows $d_{zxx} = d_{zyy} = d_{xzx} = 0$. Thus we have only two nonvanishing components left. Their magnitudes are related by the Clebsch - Gordan coefficients given in Table 3. For d_{xxz} , the energy state $|3>$ can have either $|M| = 5$ or $|M| = 3$ because of the x-polarization of the optical fields. While for d_{zzz} , the transition only involves $|M| = 4$. Thus we have the following relation

$$\frac{d_{xxz}}{d_{zzz}} = \frac{\frac{1}{2}\left\{(J1M1|J'M+1)^2 + (J1M-1|J'M-1)^2\right\}}{(J1M0|J'M)^2} = 2\frac{5}{9}$$

where $J' = 5$ and $J = 4$.

The absorption coefficients for x-polarized light and z-polarized light have exactly the same relation. These results are based on the assumption that the system is a three-level system.

4-4 Dispersion and Saturation

In the previous section we derived a general expression for $d_{\alpha\beta\gamma}(\omega_3,-\omega_2)$ as a function of $\Delta\omega$ and Γ. Numerical calculation was carried out for resonance nonlinear susceptibility. A real $d_{\alpha\beta\gamma}(\omega_3,-\omega_2)$ was obtained at $\Delta\omega = 0$. In general $d_{\alpha\beta\gamma}(\omega_3,-\omega_2)$ is a complex number. The real and imaginary part of $d_{\alpha\beta\gamma}$ is plotted in Fig. 4.3 as a function of $\Delta\omega$. This dispersion behavior is quite different from that of the linear susceptibility. This is due to the fact that an additional energy denominator appears in the nonlinear susceptibility. If we neglect the Doppler broadening and let d_{res} be the resonant nonlinear suscep-tibility, from (4-10) we have

$$d(\Delta\omega) = d_{res} \frac{-\Gamma^2}{(\Delta\omega+i\Gamma)^2} \qquad\qquad 4\text{-}43$$

If we rationalize the denominator of (4-43), we obtain

$$d(\Delta\omega) = \frac{[\Gamma^2-(\Delta\omega)^2] + 2i\Delta\omega\Gamma}{[(\Delta\omega)^2 + \Gamma^2]^2} \Gamma^2 d_{res} \qquad\qquad 4\text{-}44$$

We find that the real part vanishes at $\Delta\omega = \pm\,\Gamma$ and the imaginary part reaches extrema at $\Delta\omega = \pm\,\Gamma/\sqrt{3}$. These are, however, no longer true if molecular motion cannot be neglected. In general, equation (4-25) should be used if the input optical wave has a finite frequency spectrum. The curves shown in Fig. [4.3] are $d_{\alpha\beta\gamma}(\omega_3,-\omega_2)$ given by (4-25).
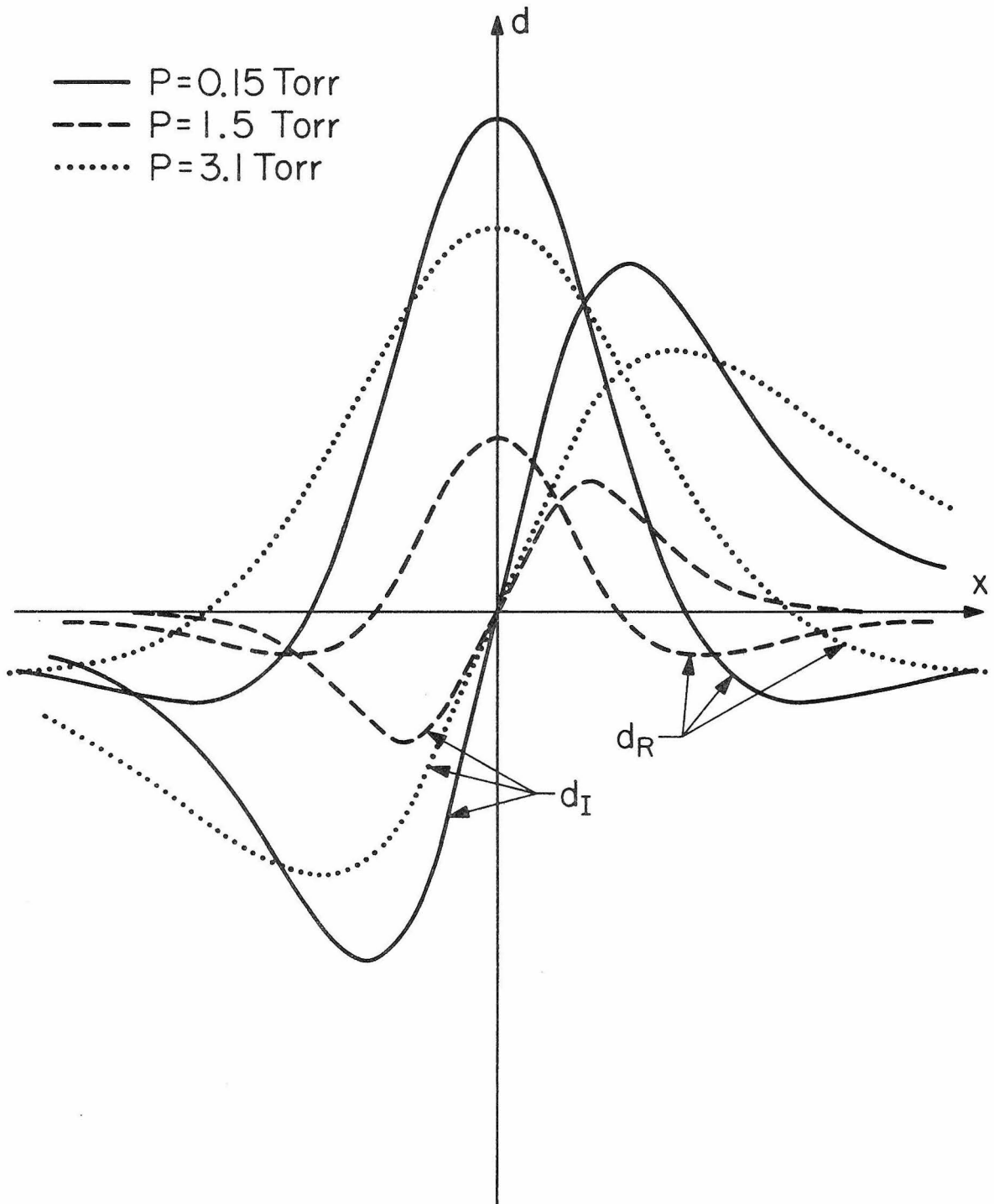
Fig. 4-3 Dispersion behavior of $d_{xxz} = d_R + id_I$ at different pressures. The horizontal coordinate is proportional to $\Delta\omega$.

In the above calculation of the nonlinear polarization at $\omega_1 = \omega_3 - \omega_2$ we only kept $E_{3\beta}E_{2\gamma}^*$ term. There are, however, other higher order terms which also oscillate at frequency $\omega_1 = \omega_3 - \omega_2$. For example, $|E_3|^2 E_{3\beta}E_{2\gamma}^*$ and $|E_2|^2 E_{3\beta}E_{2\gamma}^*$ are also oscillating at frequency $\omega_1 = \omega_3 - \omega_2$. If these terms are included in the non-linear polarization in (4-1), the resulting $d_{\alpha\beta\gamma}(\omega_3, -\omega_2)$ given by the same equation tends to decrease as $|E_2|^2$ or $|E_3|^2$ increases.

In what follows we will include the next higher terms to study the saturation effect. For the sake of simplicity in algebraic manipulation, we define d_0 as the unsaturated nonlinear susceptibility. Using the techniques described in chapter 2, we obtain

$$d = \left\{ 1 + \frac{|(\mu \cdot E_2)_{21}|^2}{4(\Delta\omega + i\Gamma)^2} + i\frac{|(\mu \cdot E_3)_{31}|^2}{4\,\Gamma(\Delta\omega + i\Gamma)} \right\}d_0 \qquad 4\text{-}45$$

where $\dfrac{\sigma\,\omega_{21}}{c} \ll \Gamma$ and $\omega_{21} \ll \omega_{31}$ are assumed.

If we now take molecular motion into account and integrate over the velocity distribution, we obtain after some mathematical manipulation

$$d = \left\{ 1 + \left(\frac{c}{\sqrt{2}\sigma\,\omega_{31}}\right)^2 \frac{|(\mu \cdot E_2)_{21}|^2}{24} \cdot \frac{\partial^2}{\partial z^2} + i\left(\frac{c}{\sqrt{2}\sigma\,\omega_{31}}\right)\frac{|\mu \cdot E_3)_{31}|^2}{8\,\Gamma}\,\frac{\partial}{\partial z} \right\}d_0(z)$$

$$4\text{-}46$$

where $d_0(z)$ is given by

$$d_0(z) = \frac{N_1(\mu_\alpha)_{23}(\mu_\beta)_{31}(\mu_\gamma)_{13}}{2\hbar^2}\left(\frac{c}{\sigma\omega_{31}}\right)^2\left\{ 1 + i\sqrt{\pi}\,z\,W(z) \right\} \qquad 4\text{-}47$$

and

$$z = \frac{\Delta\omega + i\Gamma}{\sqrt{2}\,\sigma\,\omega_{31}}\,c \qquad\qquad 4\text{-}48$$

By using the differential equation (4-24) for $W(z)$, (4-46) can be expressed in terms of $W(z)$. However, the form given by (4-46) can give us some direct physical meaning. For example, it can be shown that (4-46) can also be written

$$d = \left\{ 1 + \frac{\left|(\mu\cdot E_2)_{21}\right|^2}{24}\,\frac{\partial^2}{\partial(\Delta\omega)^2} + i\frac{\left|(\mu\cdot E_3)_{31}\right|^2}{8\,\Gamma}\,\frac{\partial}{\partial\Delta\omega} \right\} d_o(\Delta\omega,\,\Gamma) \qquad 4\text{-}49$$

This form is particularly useful because it is related to the dispersion curves shown in Fig. 4-3. The second term is negative near resonance (see Fig. 4-3). Thus we find that increasing the microwave power will tend to decrease the nonlinear susceptibility. This phenomenon is called nonlinear saturation effect. A typical dispersion behavior for the saturated nonlinear susceptibility is shown in Fig. 4-4.

In conclusion of this chapter, we have shown in detail how Stark admixing can give rise to second order optical nonlinearities in gases. We have derived an expression for the coefficient describing the mixing of an infrared and a microwave field in NH_2D. Available absorption data were used to obtain a numerical estimate for the mixing and to describe its parametric dependence.

Dispersion and saturation are also discussed. An experimental demonstration of this effect is described in chapter 5.
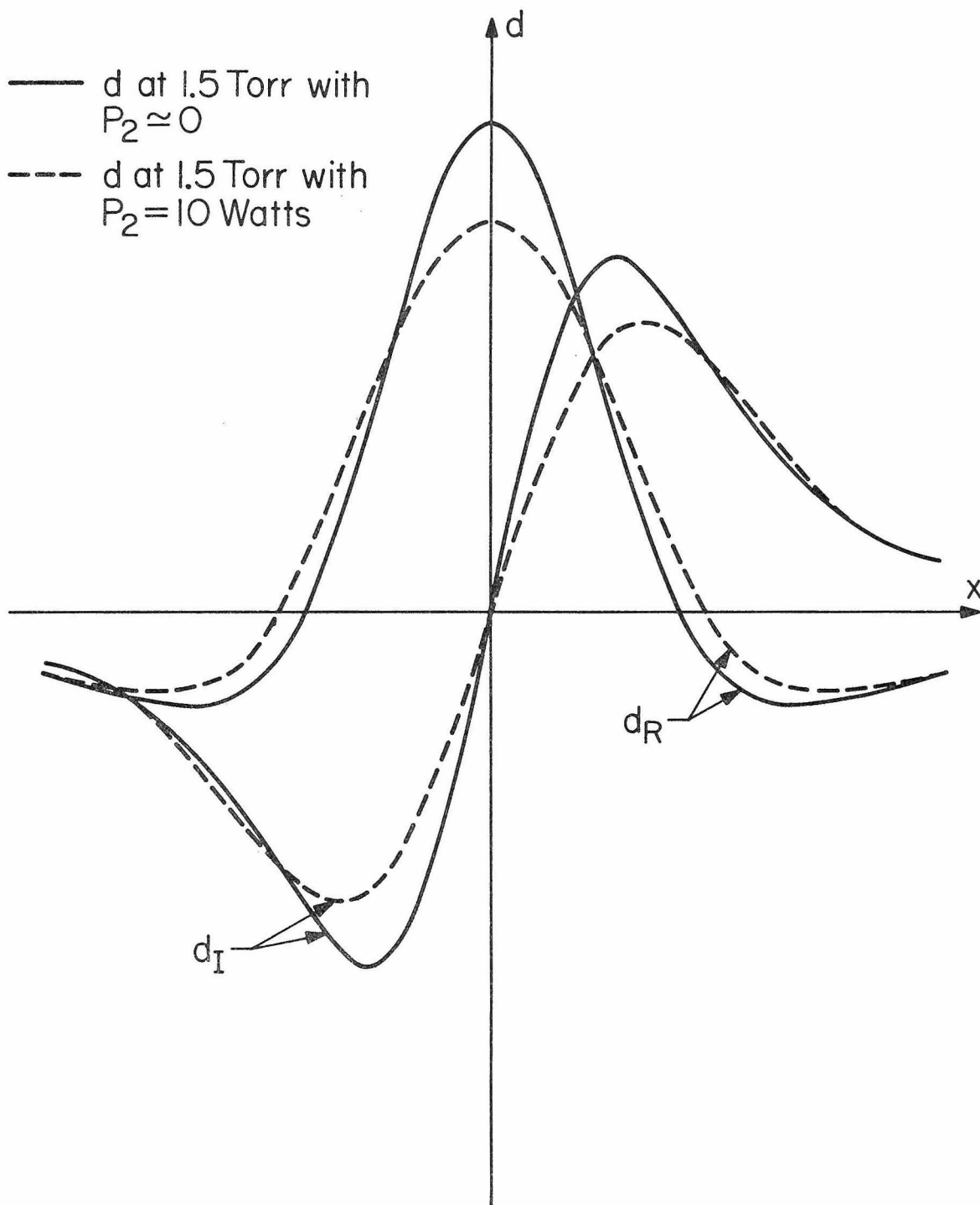
Fig. 4-4 d vs. x at 1.5 Torr with different microwave powers. x is
the real part of z.

CHAPTER 4 REFERENCES

[1] R. G. Brewer, M. J. Kelley, and A. Javan, "Precision infrared Stark spectra of $N^{14}H_2D$ using Lamb dip," Phys. Rev. Lett., vol. 23, pp. 559-563, Sept. 1969.

[2] M. J. Kelley, R. E. Francke, and M. S. Feld, "Rotational-vibrational spectroscopy of NH_2D using high-resolution laser techniques," J. Chem. Phys., vol. 53, pp. 2979-2980, Oct. 1970.

[3] T. K. Plant and R. L. Abrams, "Broadening and absorption coefficients in $N^{14}H_2D$," J. Appl. Phys., vol. 47, pp. 4006-4008, Sept. 1976. Earlier data on this absorption coefficient and pressure broadening rate were published by A. R. Johnston and R. D. S. Melville, Jr., "Stark-effect modulation of a CO_2 laser by NH_2D," Appl. Phys. Lett., vol. 19, pp. 503-506, Dec. 1971, but the more recent measurements are more accurate and substantially different.

[4] T. A. Nussmeier and R. L. Abrams, "Stark cell stabilization of CO_2 laser," Appl. Phys. Lett., vol. 25, pp. 615-617, Nov. 1974.

[5] C. H. Townes and A. L. Schawlow, Microwave Spectroscopy. New York: McGraw-Hill, 1955.

[6] See Chapter 3, section 3-2, page 29.

[7] Reference 5, p. 94 and Character table in chapter 3.

[8] M. Abramovitz and I. Stegun, Handbook of Mathematical Functions, Dover, New York (1965).

[9] B. D. Fried and S. D. Conte, The Plasma Dispersion Function, Academic Press, New York (1961).

[10] Reference 8, p. 298, equation (7.1.20).

[11] A. Yariv, <u>Quantum Electronics</u>, 2nd Ed. New York: Wiley, 1975.

Chapter 5

EXPERIMENTAL OBSERVATION

5-1 Introduction

In chapter 4 it was predicted that a resonantly enhanced non-linear mixing process in the molecule NH_2D could be induced by application of a dc electric field, where CO_2 laser radiation and microwave energy at 4 GHz below the applied laser frequency. We report here the first experimental observation of such single-sideband optical modulation, unambiguously identified through the use of a scanning Fabry-Perot interferometer (SFP). We present measurements of the dependence of the parametric signal on gas pressure, microwave frequency, applied dc field, and microwave power. The results are all in good agreement with theoretical predictions although there is some uncertainty in the quantitative comparisons due to undetermined coupling losses in the microwave structure. Qualitatively, the agreement is excellent. These experimental results are based entirely on the work of Abrams and his coworkers [1].

5-2 Experimental Apparatus

The experimental apparatus for the observation of the interaction is discussed with reference to Fig. 5-1. A frequency stabilized CW CO_2 laser beam (operating at P(20) line center) is passed through the microwave Stark cell containing the Stark-tunable gas. The cell consists of a 4-GHz ridged waveguide with an 8-mm-wide ridge width, a 1.2-mm gap, 20-cm length, and forms a resonant cavity ($Q \sim 160$). The
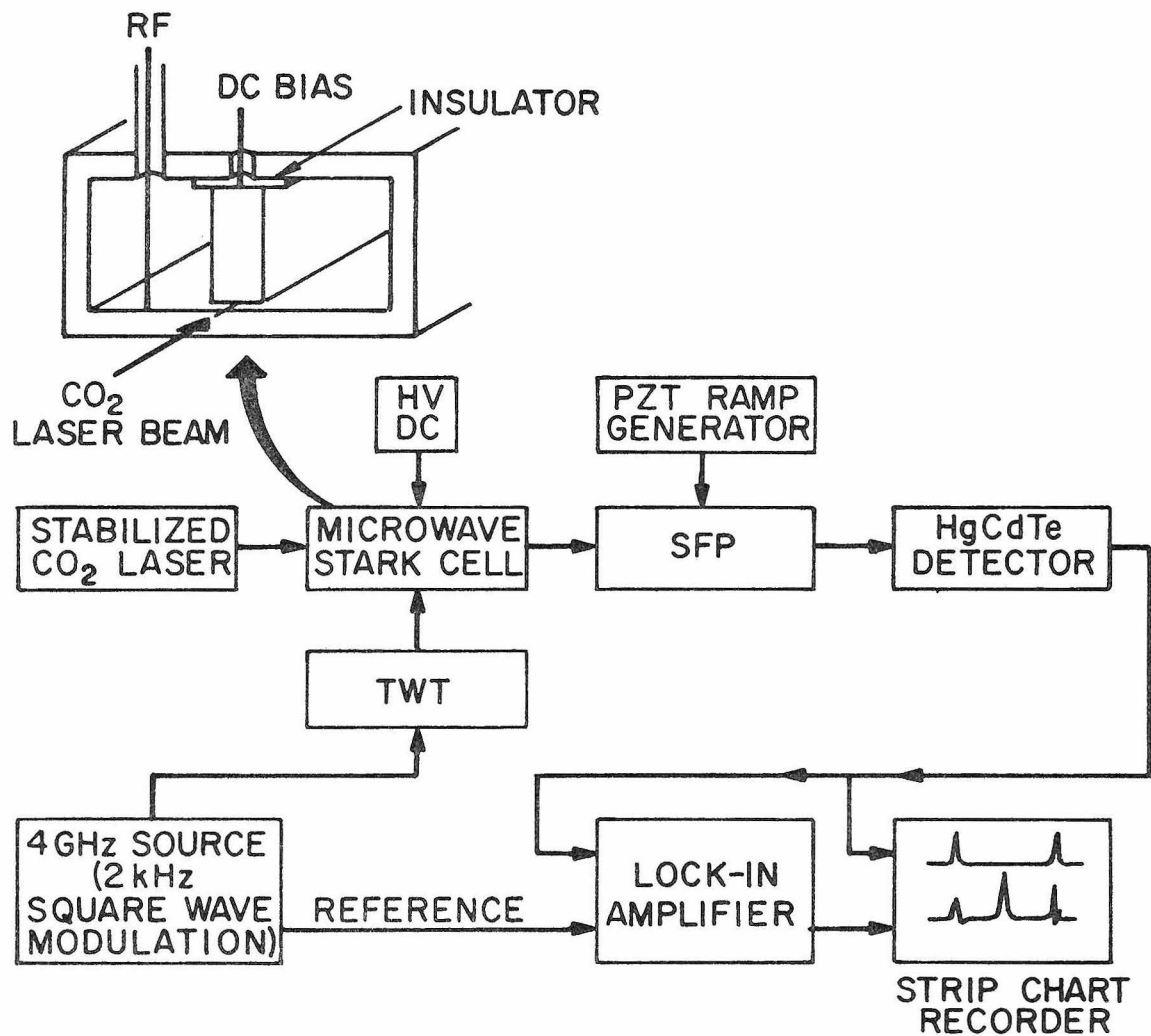
Fig. 5-1 Experimental apparatus for observation of single-sideband signal. The TWT amplifier supplies up to 4 W to the Stark cell.

ridge is insulated from the rectangular structure by a thin layer of Mylar, allowing application of a dc Stark voltage and the 4-GHz microwave signal to the ridge. The microwaves are square-wave modulated at 2 kHz, amplified in a traveling-wave tube (TWT), and coupled into the ridged waveguide by means of a probe.

The output of the Stark cell is passed through a scanning SFP and detected with a HgCdTe photodiode. The SFP performs as a narrow-bandwidth (300 MHz) optical filter that is slowly scanned through its 10-GHz free spectral range (FSR). The SFP output can then either be displayed directly on a recorder or synchronously detected at the microwave modulation frequency in a lock-in amplifier. Very small changes in the SFP output due to the presence of the microwaves were detectable with the latter method.

The NH_2D was prepared by introducing equal partial pressures of NH_3 and $\overset{|}{N}H_3$ in a mixing chamber. The resultant mixture containing 37.5 percent NH_2D was metered into the cell and the pressure monitored with a capacitance manometer.

5-3 Results

Fig. 5-2 shows the SFP output before and after lock-in detection with 1.1 torr of gas in the cell. The two outputs are simultaneously displayed on a strip chart recorder as the SFP is scanned through one full order. The upper trace shows the direct SFP signal, with the familiar pattern of a single-mode laser. This is the SFP spectrum of 10.6-μm carrier transmitted through the cell to the
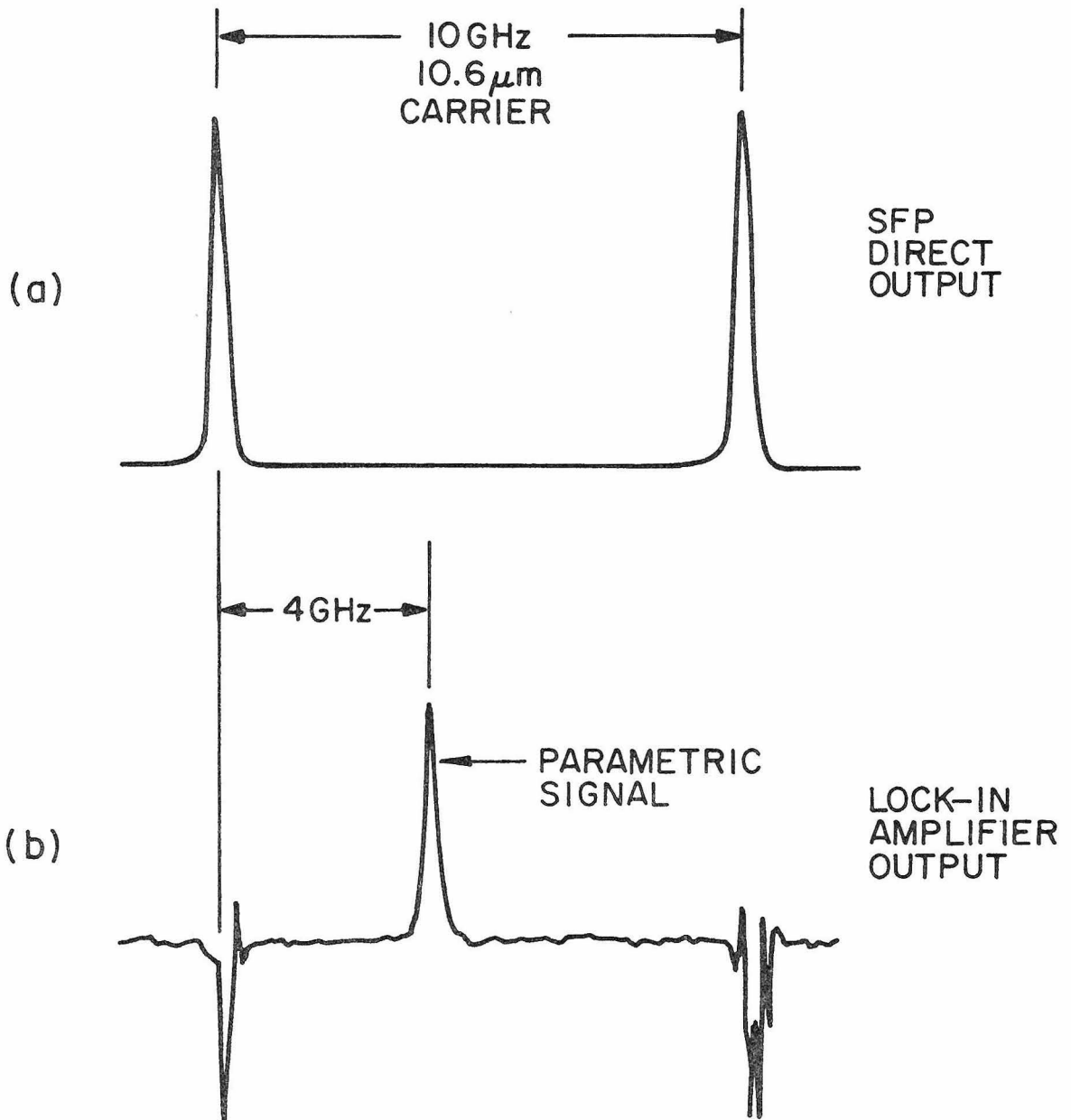
Fig. 5-2 Simultaneous signals observed. (a) Directly from the detector.
(b) After phase sensitive detection as the SFP is scanned
through one order. Note that the new feature due to the
4-GHz microwave signal appears as a single sideband 4 GHz
away from the carrier.

detector. The FSR is 10 GHz (1.5-cm plate spacing). The lower trace of Fig. [2] shows the lock-in detection output with a 30-ms time constant. Signals occur at the positions corresponding to the peaks of the direct SFP output, indicating some sort of carrier modulation as a result of the applied microwave signal. A new peak, which is the parametric signal displaced 4 GHz from the carrier, appears approximately 40 percent of the way between the two carrier peaks. Note that only a single sideband occurs, for double-sideband generation would result in two signal peaks lying between the two carrier signals. Calibration of the SFP has verified that the sideband is a lower one, as predicted, and corresponds to the difference frequency between the 10.6-μm carrier frequency and the microwave frequency. That the output is a parametric signal and not laser-induced fluorescence from the gas is substantiated by the fact that the sideband is linearly polarized and no other line is observed in the SFP output; if the output were fluorescence, unpolarized emission at several wavelengths would be expected.

The parametric signal was measured as a function of the Stark voltage as shown in Fig. 5-3. The SFP sawtooth drive was disconnected and the mirror spacing was set to transmit the peak of the parametric sideband signal for these measurements. The maximum signal occurred at a Stark voltage of 428 V with the microwave frequency set at 4.023 GHz. The full width at half-maximum (FWHM) of the signal was 28.5 V which is equivalent to a linewidth of $\sim$ 130 MHz. The linewidth of the signal is greater than the NH_2D linewidth at 1 torr
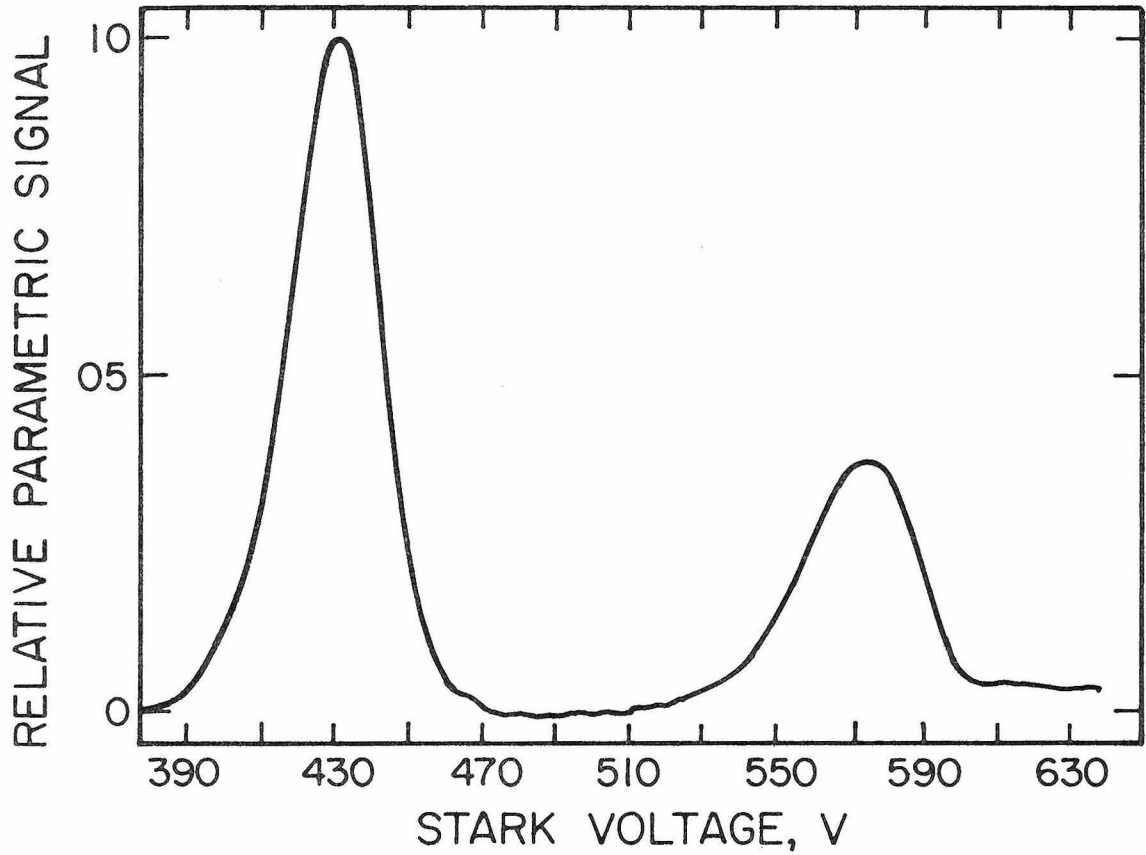
Fig. 5-3 Variation of parametric sideband signal with Stark voltage, showing interaction with $|M| = 4$ and $|M| = 3$ lines.

of 105 MHz [1] due to some inhomogeneities in the Stark gap. A measured low-pressure absorption linewidth of 100 MHz FWHM compared to the 82-MHz actual Doppler width indicates a 0.5 percent variation in the Stark-gap spacing.

The Stark voltage was increased to 600 V and the $|M| = 3$ parametric signal was seen at $\sim$ 570 V. The ratio of the $|M| = 4$ signal amplitudes was 0.414. A theoretical calculation of this intensity ratio yields a predicted signal ratio of 0.40. The agreement is well within experimental error.

The parametric signal was measured as a function of the Stark cell pressure over a range of 0-8 torr as shown in Fig. 5-4. The SFP was set to transmit the maximum signal and the microwave frequency was fixed at 4.023 GHz. The parametric signal rose slowly between 0 and 0.5 torr, then rose sharply between 0.5 and 1.5 torr, reaching a maximum at 2.4 torr. The signal slowly decreased between 3 and 8 torr. The experimental curve and theory were compared using the best current NH_2D parameters with the theoretical points also shown on Fig. 5-3. Here the experimental "effective" Doppler width of 100 MHz was used to include the effects of the gap inhomogeneities. Again, the excellent agreement enforces the theory.

The parametric conversion efficiency varied linearly with microwave power, reaching 0.2 percent at the maximum available TWT output of 4 W. Microwave power saturation effects are anticipated linewidth ($\mu \cdot E_{RF} \sim 100$ MHz). This occurs at field strength of $E_{RF} \sim 4 \times 10^4$ V/m.
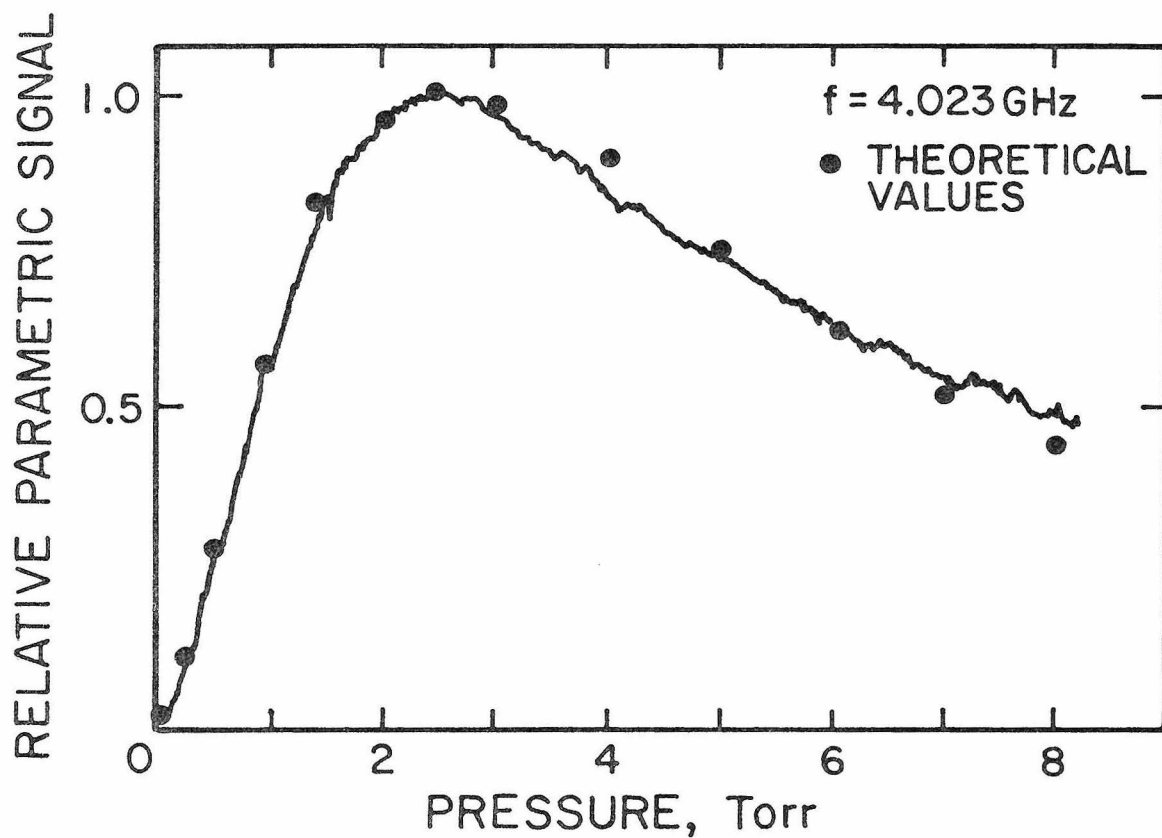
Fig. 5-4 Parametric signal versus Stark cell pressure 0 to 8 torr.
The theoretical points are calculated for a pressure-
broadening coefficient of 40.2 MHz/torr with an effective
Doppler width of 100 MHz (full linewidths at half-maximum
intensity).

Unfortunately, unknown coupling losses prevent determination of the actual field strength. In the following paragraphs we use theory, including the effects of phase mismatch and linear absorption, to calculate the theoretical conversion efficiency.

5-4 Comparison with Theory

The experiment involves traveling-wave mixing between an input CO_2 laser (ω_3) and a microwave field at ω_2 (~ 4 GHz) to generate the difference frequency at $\omega_1 = \omega_2 - \omega_3$. The interaction is described by the following coupled mode equations [3] which include the effects of optical losses and phase mismatch:

$$\frac{dA_1}{dz} = -\frac{\alpha_1}{2} A_1 - i \frac{g}{2} A_3 e^{-i\Delta kx}$$

$$\frac{dA_3}{dx} = -\frac{\alpha_3}{2} A_3 - i \frac{g}{2} A_1 e^{i\Delta kx}$$

5-1

where

$$A_i(x) = \sqrt{\frac{n_i}{\omega_i}} \; E_i(x)$$

$$g = \sqrt{\frac{\mu_0}{\varepsilon_0} \frac{\omega_1}{n_1} \frac{\omega_3}{n_3}} \; d_{xxz}^{\omega_1 = \omega_3 - \omega_2} E_2$$

$$\Delta k = k_3 - (k_1 + k_2).$$

Assuming a single input $A_3(0)$ at $x = 0$, the solution of (5-1) yields a conversion efficiency η of

$$\eta(x) \equiv \left| \frac{A_1(x)}{A_3(0)} \right|^2 = \frac{g^2}{2} \exp\left(-\left(\frac{\alpha_1 + \alpha_3}{2\gamma}x\right)\right)$$

$$\cdot[\cosh(\sqrt{\gamma}\, x \sin(\theta/2)) - \cos(\sqrt{\gamma}\, x \cos(\theta/2)] \qquad 5\text{-}2$$

where

$$\gamma^2 = \left[\Delta k^2 + g^2 - \left(\frac{\alpha_1}{2} - \frac{\alpha_3}{2}\right)^2\right]^2 + [(\alpha_1 - \alpha_3)\Delta k]^2$$

$$\theta = \tan^{-1} \frac{(\alpha_1 - \alpha_3)\Delta k}{\Delta k^2 + g^2 - (\alpha_1/2 - \alpha_3/2)^2}$$

The phase mismatch Δk occurs because both of the infrared signals travel through the cell collinearly and at the same velocity, while the microwave wavefront travels in a guided mode. For the experiment performed at Hughes Labs, Δk is given by

$$\Delta k = 2\pi/\lambda_g - 2\pi/\lambda$$

$$= 0.08 \text{ cm}^{-1} \qquad\qquad 5\text{-}3$$

where λ_g is the guide wavelength and λ is the free-space wavelength.

The maximum possible conversion efficiency occurs at a pressure of 2.4 torr. Assuming no microwave coupling losses, 4 W of input power and $Q \sim 160$ leads to $E_{RF} \sim 10^5$ V/m. At 2.4 torr, $a_3 = 0.02$ cm^{-1} (see [1]), $a_1 = 0.014$ cm^{-1}, and $g = 0.0138$ cm^{-1} giving a conversion efficiency in 20 cm of

$$\eta(20 \text{ cm}) = 1.1 \text{ percent.}$$

Due to asymmetric cavity coupling and a short $5\lambda_g/2$ cavity length, a large amount of the microwave energy is probably contained in higher order modes still present within the cavity. Assuming only 50 percent of the calculated microwave field in the lowest order mode is achieved, $E_{RF} = 5 \times 10^4$ V/m, and an efficiency of 0.27 percent is expected in the 20-cm interaction length, a value close to that observed.

CHAPTER 5 REFERENCES

[1] R. L. Abrams, C. K. Asawa, T. K. Plant, and A. E. Popa, IEEE,
     J. QE., <u>QE-13</u>, 82 (1977).

[2] T. K. Plant and R. L. Abrams, "Broadening and absorption
     coefficients in $N^{14}H_2D$," J. Appl. Phys., vol. 47, pp. 4006-
     4008, Sept. 1976.

[3] A. Yariv, <u>Quantum Electronics</u>, 2nd ed. New York: Wiley, 1975.

PART II

OPTICAL WAVES IN LAYERED MEDIA

Chapter 1

GENERAL INTRODUCTION

1.1 Introduction

Periodic optical media and specifically periodic layered struc-
tures play an important role in a number of applications. These include
multilayer coatings for both high reflection and antireflection.   This
application benefitted largely from the pioneering analysis of Abeles
[1]. Other proposals involve the use of these structures for phase
matching in nonlinear optical applications [2,3,4] and for obtaining
optical birefringence in stratified media composed of isotropic or cubic
materials [5,6].

Recent developments in the crystal growing field, especially in
molecular beam technology [7], make it possible to grow multilayer media
with well controlled periodicities and with layer thicknesses down to
$10\overset{o}{A}$. We may thus well consider the periodic optical structure as a new
optical medium to take its place along with that of, say, homogeneous
isotropic and anisotropic materials. Before proceeding with the many
applications envisaged for periodic layered media we need to understand
precisely and in detail the nature of electromagnetic wave propagation
in these media. Although a number of special cases have been analyzed,
a general theory is not available. To illustrate this situation we may
point out, as one example, that the present state of the theory does not
answer questions such as that of the direction of group and energy velo-
cities of waves in periodic media or even that of the birefringence at
arbitrary angles of incidence.

This work describes a general theory of electromagnetic propagation in periodic media. The theoretical approach is general, so that many situations considered previously will be shown to be special cases of our formalism. The theory has a strong formal similarity to the quantum theory of electrons in crystals and thus makes heavy use of the concepts of Bloch modes, forbidden gaps, evanescent waves, and surface waves.

In addition to demonstrating the application of the theory to a number of familiar problems, such as reflectivity of multilayer films, we consider in general form a variety of some experimental situations which include Bragg waveguides, birefringence and group velocity at arbitrary directions, phase matching in nonlinear optical applications, multichannel waveguides and optical surface waves. We consider also the important problem of propagation and reflection in media with periodic gain and loss alternation which is relevant to X-ray laser oscillation in artificially layered media [8].

1.2 Previous Work on Waves in Layered Media

An enormous amount of work was done on the theory of anti-reflecting and high reflecting multilayer systems as well as for monochromatic interference filters in the first half of this century [9]. However, the first general treatment of stratified media in terms of the electromagnetic theory of light was not available until 1950 when Abelés [10] introduced the matrix method to treat the propagation of light in layered media. Electromagnetic propagation in dielectric periodic layered media

was considered in detail with the direction of propagation normal to the layers by Levin [11]. Rytov [12] investigated the electromagnetic properties of a finely stratified medium. His results are general; valid for any layer thickness. However, Rytov only considered three special cases of wave propagation: propagation in a direction parallel to the layers for two polarizations, with either the electric or the magnetic vector parallel to the layers, and propagation in a direction perpendicular to the layers. Weinstein [13] derived general expressions for the transmissivity and reflectivity of multilayer coatings of any number of components, for light polarized in any way and incident at any angle. A theoretical study of the optical properties of a continuously varying medium was done by Jacobsson [14] using approximate and exact solutions of the wave equations. He showed that the general behavior of the reflection coefficient may be deduced from the reflection coefficient of a single period. Jacobsson also considered hyperbolic refractive index variation. Propagation characteristics of periodic arrays of dielectric slabs was also studied by Lewis and Hessel [15]. Dispersion curves and mode functions were used to illustrate the guiding properties of the structure. They explained those characteristics in terms of stability diagrams and equivalent network. Epstein [16] found that the equivalent index of a symmetrical period is a pure imaginary number in a stop band, while it is a real number in a pass band. Reflection from stratified anisotropic media was studied recently by Honig and den Engelsen [17] using a new method of computation which is different from that of Teitler, Henvis and Berreman [18]. Teitler-Henvis-

Berreman treatment involves solving Maxwell's equations simultaneously with a 4 x 4 matrix technique.

We note that the evanescent Bloch waves have never been studied. The historical interest in optical properties of multilayer thin films was largely confined to the use of high reflectance coatings in high resolution interferometry. Little attention, however, was paid to the guided waves in these media. During the last decade guided wave optics has become more and more important in the field of optical communication [19]. The basic circuit element in integrated optics is a thin-film waveguide which is essentially a layered medium. This has given an enormous stimulus to the study of guided waves in a general layered medium.

1.3 Outline of Thesis

In Chapter 2, the matrix method and translation operator are introduced into the electromagnetic propagation in periodic layered media. Bloch waves and dispersion relation are derived by diagonalizing the unit cell translation operator. The concept of phase velocity and group velocity in layered media are introduced and analyzed. Birefringence and double refraction are also studied. Numerical results for interesting special cases are presented and discussed.

In Chapter 3, the mode theory of electromagnetic waves in layered media is studied. Attention is confined to guided modes in either finite or infinite structures. The concept of Regge poles [20] is employed to explain the relation between modes and the poles of reflectivity spectrum in β-space. Optical surface waves are introduced and analyzed. The

analogy between solid state physics and optics of periodic layered media is emphasized and discussed.

In Chapter 4, Bragg reflectors are introduced and analyzed. Numerical results for some interesting cases are presented and discussed. A new type of waveguide, the Bragg waveguide, is introduced and analyzed. Mode characteristics are derived and numerical results are given and discussed. The wavelength selectivity of Bragg waveguides is discussed. The leakage due to finite number of periods in the Bragg reflector is analyzed. Thickness matching is introduced in the optimum design of Bragg waveguides. Some other Bragg waveguide structures are also presented and discussed.

In Chapter 5, the dispersion due to periodic stratification is introduced. Application of this dispersion to compensate for the material dispersion in nonlinear optical mixing is introduced and analyzed. Normal processes and Umklapp processes [21] are explained in terms of phonon-phonon scattering. Distributed feedback soft X-ray lasers in artificially layered media are considered and analyzed.

In Chapter 6, the propagation of electromagnetic waves in cylindrically layered media is presented and analyzed. A concept of Bragg waveguiding is extended into the cylindrical regime. Bragg fiber is designed according to the optimization procedures. Mode characteristics and leak spectrum are presented and discussed.

In Chapter 7, some experimental observation of Bragg waveguiding and surface wave propagation is described.

References - Chapter 1

1. F. Abelés, Ann. de Physique $\underline{5}$, 596, 706 (1950).

2. A. Ashkin and A. Yariv, Bell Labs. Tech. Memo MM-61-124-46 (November 13, 1961).

3. N. Bloembergen and A. J. Sievers, Appl. Phys. Lett. $\underline{17}$, 483 (1970).

4. C. L. Tang and P. P. Bey, IEEE J. Quantum Electr. $\underline{QE-9}$, 9 (1973).

5. S. M. Rytov, Zh. Eksp. Teor. Fiz. $\underline{29}$, 605 (1955) [Sov. Phys. JETP $\underline{2}$, 466 (1956).]

6. J. P. van der Ziel, M. Ilegems, and R. M. Mikulyak, Appl. Phys. Lett. $\underline{28}$, 735 (1976).

7. A. Y. Cho and J. R. Arthur, Progress in Solid State Chemistry, Vol. 10, Part 3, pp. 157-191 (Pergamon Press, 1975).

8. A. Yariv, Appl. Phys. Lett. $\underline{25}$, 105 (1974).

9. See, for example, O. S. Heavens, Optical Properties of Thin Solid Films (Dover, New York, 1954).

10. F. Abeles, Ann. de Physique $\underline{5}$, 596, 706 (1950).

11. M. L. Levin, J. Tech. Phys. (USSR) $\underline{81}$, 1399 (1948).

12. S. M. Rytov, Sov. Phys. JETP $\underline{2}$, 446 (1956).

13. W. Weinstein, J. Opt. Soc. Am. $\underline{37}$, 576 (1947).

14. R. Jacobsson, Arkiv för Fysik $\underline{31}$, nr. 14, 191 (1965).

15. L. R. Lewis and A. Hessel, IEEE Trans. Microwave Theory and Techniques, March, 276 (1971).

16. L. I. Epstein, J. Opt. Soc. Am. $\underline{42}$, 806 (1952).

17. E. P. Honig and D. den Engelsen, Optica Acta $\underline{24}$, 89 (1977).

18. S. Teitler and B. W. Henvis, J. Opt. Soc. Am. $\underline{60}$, 830 (1970). Also, D. W. Berreman, J. Opt. Soc. Am. $\underline{62}$, 502 (1972).

19. See, for example, IEEE J. Quantum Electr. <u>QE-13</u>, Special Issue on Integrated Optics, 1977.

20. See, for example, A. Yariv, <u>Quantum Electronics</u>, 2nd ed. (Wiley, New York, 1977), p. 425.

21. See, for example, C. Kittel, <u>Introduction to Solid State Physics</u>, 3rd ed. (Wiley, New York, 1965).

Chapter 2

BLOCH FORMULATION OF ELECTROMAGNETIC PROPAGATION IN LAYERED MEDIA

2.1 Introduction

Bloch wave function was introduced in 1928 to describe the electron motion in crystals [1]. A crystalline solid is characterized by its translational symmetry. If we ignore all the other symmetry except the translational symmetry, the entire symmetry classification of an electron wave function in the crystal can be given by Bloch's theorem [2]. The irreducible representations can be completely labeled by specifying the crystal momentum K to each wave function. In one-dimensional cases we have

$$\psi_K(x + \Lambda) = e^{iK\Lambda} \, \psi_K(x) \tag{2.1}$$

This property allows us to write the most general wave function in the form

$$\psi_K(x) = U_K(x) \, e^{iKx} \tag{2.2}$$

where U_K is a periodic function of x

$$U_K(x + \Lambda) = U_K(x) \tag{2.3}$$

Electromagnetic propagation in a periodic layered medium has exactly the same property as electron motion in a one-dimensional periodic square well potential field [3]. Therefore, we expect that all the interesting properties of electrons in solids should have their counterparts in the optics of periodic layered media. For example, the stop bands and pass bands of a periodic layered medium are equivalent to the forbidden bands

and allowed bands of a crystalline solid respectively. Furthermore, we will later show that the electronic surface states of crystals also have their optical analog--optical surface states--in periodic layered media. Phase velocities, group velocities and energy velocities for optical Bloch waves will be carefully studied. Although the phase velocity for electrons in a crystal is not an important quantity in solid state physics, the phase velocities for optical waves are very important in interference and nonlinear mixing.

In addition to the above properties, periodic layered media also exhibit the birefringence properties in a manner similar to a uniaxial crystal [4].

2.2 The Matrix Method and the Translation Operator

For the sake of clarity in introducing the basic concepts, we will consider first the simplest type of periodically stratified medium. The extension to the more general case is presented in Appendix A. The stratified medium treated in what follows consists of alternating layers of different indices of refraction. The index of refraction profile is given by

$$n(x) = \begin{cases} n_2 & 0 < x < b \\ n_1 & b < x < \Lambda \end{cases} \tag{2.4}$$

with

$$n(x + \Lambda) = n(x) \tag{2.5}$$

where the x-axis is normal to the interfaces and Λ is the period. The geometry of the structure is sketched in Fig. 2.1. The distribution of some typical field components can be written as
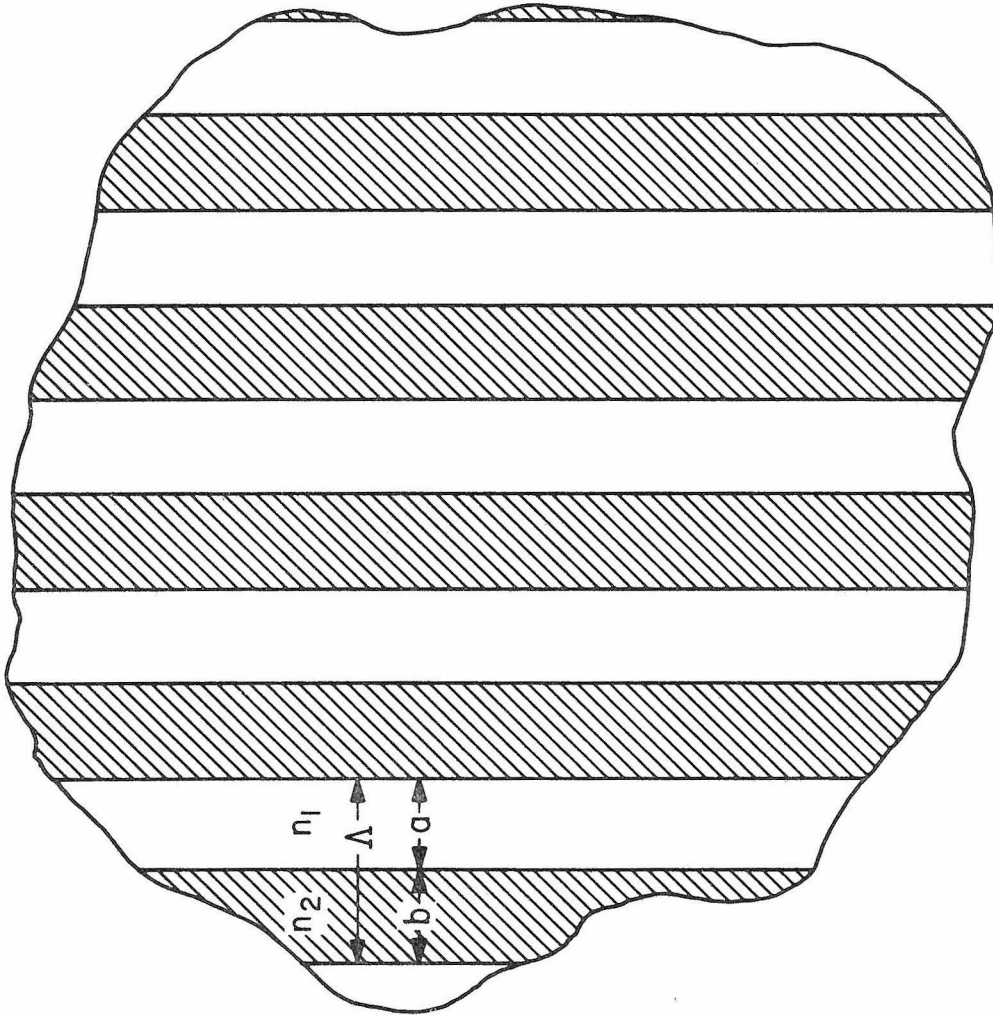
84

Fig. 2.1 A portion of a typical periodic stratified medium.

$$E(x,z) = E(x) \, e^{i\beta z} \tag{2.6}$$

The electric field distribution within each homogeneous layer can be expressed as a sum of an incident plane wave and a reflected plane wave. The complex amplitudes of these two waves constitute the components of a column vector. The electric field in the α layer of the nth unit cell can thus be represented by a column vector

$$\begin{pmatrix} a_n^{(\alpha)} \\ b_n^{(\alpha)} \end{pmatrix} \tag{2.7}$$

As a result, the electric field distribution in the same layer can be written as

$$E(x,z) = \left\{ a_n^{(\alpha)} \, e^{ik_{\alpha x}(x-n\Lambda)} + b_n^{(\alpha)} \, e^{-ik_{\alpha x}(x-n\Lambda)} \right\} e^{i\beta z} \tag{2.8}$$

with

$$k_{\alpha x} = \sqrt{(\tfrac{\omega}{c} n_\alpha)^2 - \beta^2} \qquad \alpha = 1,2 \tag{2.9}$$

The column vectors are not independent of each other. They are related through the continuity conditions at the interfaces. As a matter of fact, only one vector (or two components of two different vectors) can be chosen arbitrarily. In the case of TE modes (E vector in y-z plane) imposing continuity of E and $\partial E/\partial x$ at the interface (see Fig. 2.2) leads to

$$a_{n-1} + b_{n-1} = e^{-ik_{2x}\Lambda} c_n + e^{ik_{2x}\Lambda} d_n \tag{2.10}$$

$$ik_{1x}(a_{n-1} - b_{n-1}) = ik_{2x}(e^{-ik_{2x}\Lambda} c_n - e^{ik_{2x}\Lambda} d_n) \tag{2.11}$$

$$e^{-ik_{2x}a} c_n + e^{ik_{2x}a} d_n = e^{-ik_{1x}a} a_n + e^{ik_{1x}a} b_n \tag{2.12}$$
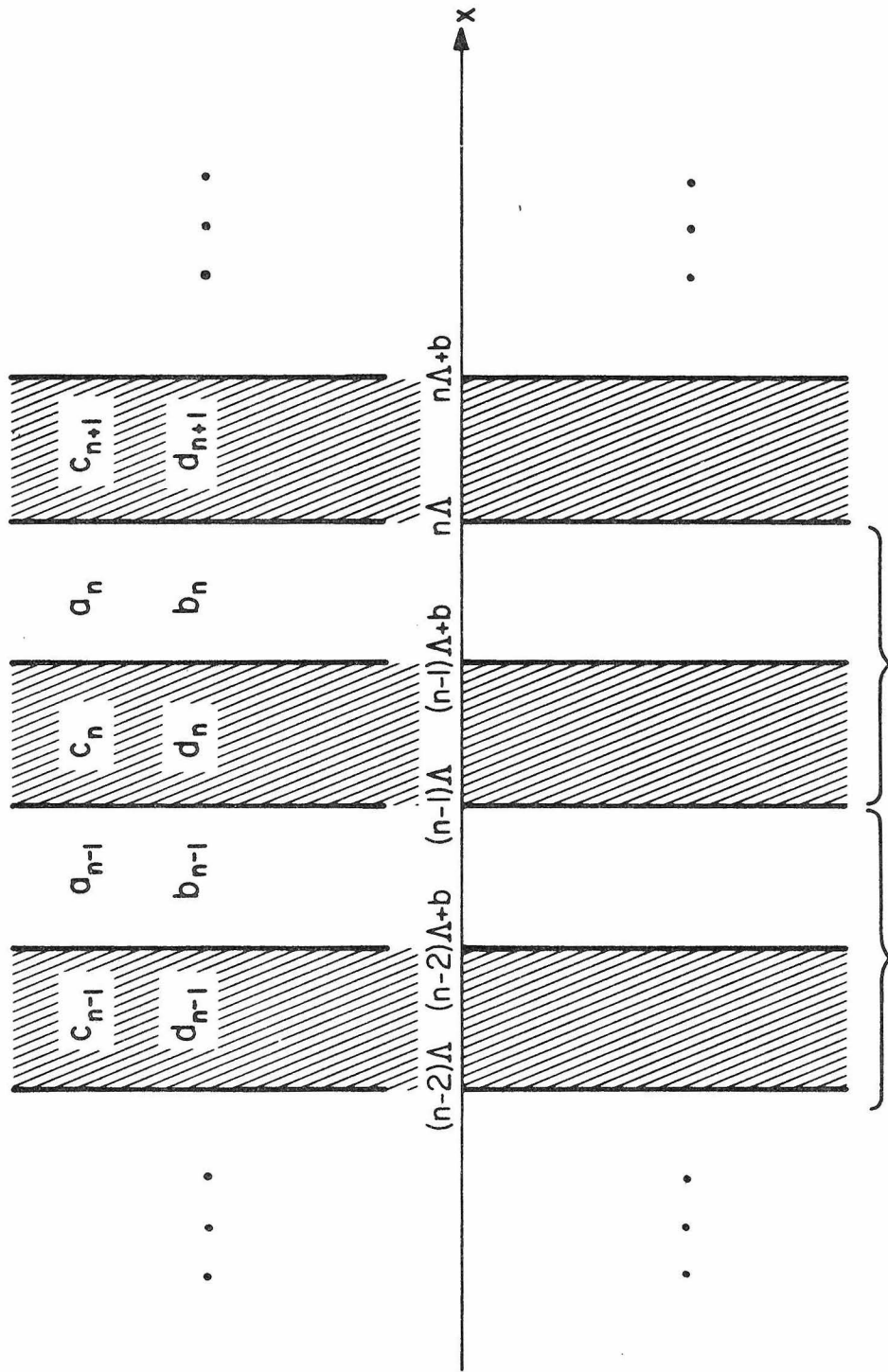
Fig. 2.2 Plane wave amplitudes associated with the nth unit cell and its neighboring cells.

$$ik_{2x}(e^{-ik_{2x}a}c_n - e^{ik_{2x}a}d_n) = ik_{1x}(e^{-ik_{1x}a}a_n - e^{ik_{1x}a}b_n) \tag{2.13}$$

The four equations in (2.10) to (2.13) can be rewritten as the following two matrix equations:

$$\begin{pmatrix} 1 & 1 \\ 1 & -1 \end{pmatrix} \begin{pmatrix} a_{n-1} \\ b_{n-1} \end{pmatrix} = \begin{pmatrix} e^{-ik_{2x}\Lambda} & e^{ik_{2x}\Lambda} \\ \dfrac{k_{2x}}{k_{1x}}e^{-ik_{2x}\Lambda} & -\dfrac{k_{2x}}{k_{1x}}e^{ik_{2x}\Lambda} \end{pmatrix} \begin{pmatrix} c_n \\ d_n \end{pmatrix} \tag{2.14}$$

$$\begin{pmatrix} e^{-ik_{2x}a} & e^{ik_{2x}a} \\ e^{-ik_{2x}a} & -e^{ik_{2x}a} \end{pmatrix} \begin{pmatrix} c_n \\ d_n \end{pmatrix} = \begin{pmatrix} e^{-ik_{1x}a} & e^{ik_{1x}a} \\ \dfrac{k_{1x}}{k_{2x}}e^{-ik_{1x}a} & -\dfrac{k_{1x}}{k_{2x}}e^{ik_{1x}a} \end{pmatrix} \begin{pmatrix} a_n \\ b_n \end{pmatrix} \tag{2.15}$$

where we define

$$\begin{aligned} a_n &\equiv a_n^{(1)} \\ b_n &\equiv b_n^{(1)} \\ c_n &\equiv a_n^{(2)} \\ d_n &\equiv b_n^{(2)} \end{aligned} \tag{2.16}$$

By eliminating

$$\begin{pmatrix} c_n \\ d_n \end{pmatrix}$$

the matrix equation

$$\begin{pmatrix} a_{n-1} \\ b_{n-1} \end{pmatrix} = \begin{pmatrix} A & B \\ C & D \end{pmatrix} \begin{pmatrix} a_n \\ b_n \end{pmatrix} \tag{2.17}$$

is obtained. The matrix elements are

$$A = e^{-ik_{1x}a} \left[\cos k_{2x}b - \frac{1}{2} i \left(\frac{k_{2x}}{k_{1x}} + \frac{k_{1x}}{k_{2x}} \right) \sin k_{2x}b \right] \tag{2.18}$$

$$B = e^{ik_{1x}a} \left[-\frac{1}{2} i \left(\frac{k_{2x}}{k_{1x}} - \frac{k_{1x}}{k_{2x}} \right) \sin k_{2x}b \right] \tag{2.19}$$

$$C = e^{-ik_{1x}a} \left[\frac{1}{2} i \left(\frac{k_{2x}}{k_{1x}} - \frac{k_{1x}}{k_{2x}} \right) \sin k_{2x}b \right] \tag{2.20}$$

$$D = e^{ik_{1x}a} \left[\cos k_{2x}b + \frac{1}{2} i \left(\frac{k_{2x}}{k_{1x}} + \frac{k_{1x}}{k_{2x}} \right) \sin k_{2x}b \right] \tag{2.21}$$

and according to (2.9) can be viewed as functions of β. The matrix in (2.17) is the <u>unit cell translation matrix</u> which relates the complex amplitudes of the incident plane wave a_{n-1} and the reflected plane wave b_{n-1} in one layer of a unit cell to those of the equivalent layer in the next unit cell. Because of the fact that this matrix relates the fields of two equivalent layers with the same index of refraction, it is unimodular, i.e.,

$$AD - BC = 1 \tag{2.22}$$

It is important to notice that the matrix which relates $\begin{pmatrix} c_{n-1} \\ d_{n-1} \end{pmatrix}$ to $\begin{pmatrix} c_n \\ d_n \end{pmatrix}$ is different from the matrix in (2.17). These matrices, however, possess the same trace (see Appendix A). As will be shown later, the trace of the translation matrix is directly related to the band structure of the stratified periodic medium.

The matrix elements (A,B,C,D) for TM waves (H-vector in yz-plane) are slightly different from those of the TE waves. They are given by:

$$A_{TM} = e^{-ik_{1x}a}[\cos k_{2x}b - \frac{1}{2}i(\frac{n_2^2\, k_{1x}}{n_1^2\, k_{2x}} + \frac{n_1^2\, k_{2x}}{n_2^2\, k_{1x}})\sin k_{2x}b] \quad (2.23)$$

$$B_{TM} = e^{ik_{1x}a}[-\frac{1}{2}i(\frac{n_2^2\, k_{1x}}{n_1^2\, k_{2x}} - \frac{n_1^2\, k_{2x}}{n_2^2\, k_{1x}})\sin k_{2x}b] \quad (2.24)$$

$$C_{TM} = e^{-ik_{1x}a}[\frac{1}{2}i(\frac{n_2^2\, k_{1x}}{n_1^2\, k_{2x}} - \frac{n_1^2\, k_{2x}}{n_2^2\, k_{1x}})\sin k_{2x}b] \quad (2.25)$$

$$D_{TM} = e^{ik_{1x}a}[\cos k_{2x}b + \frac{1}{2}i(\frac{n_2^2\, k_{1x}}{n_1^2\, k_{2x}} + \frac{n_1^2\, k_{2x}}{n_2^2\, k_{1x}})\sin k_{2x}b] \quad (2.26)$$

As noted above, only one column vector is independent. We can choose it, as an example, as the column vector of the n_1-layer in the zeroth unit cell. The remaining column vectors of the equivalent layers are given as

$$\begin{pmatrix} a_n \\ b_n \end{pmatrix} = \begin{pmatrix} A & B \\ C & D \end{pmatrix}^{-n} \begin{pmatrix} a_o \\ b_o \end{pmatrix} \quad (2.27)$$

By using (2.22), the above equation can be simplified to

$$\begin{pmatrix} a_n \\ b_n \end{pmatrix} = \begin{pmatrix} D & -B \\ -C & A \end{pmatrix}^{n} \begin{pmatrix} a_o \\ b_o \end{pmatrix} \quad (2.28)$$

The column vector for the n_2-layer can always be obtained by using equation (2.15); more generally we can specify the field uniquely by specifying any a_i and b_j.

2.3 Bloch Waves and Band Structures

The periodically stratified medium is equivalent to a one-dimensional lattice which is invariant under the lattice translation. The lattice

translation operator T is defined by

$$Tx = x + \ell\Lambda \tag{2.29}$$

where ℓ is an integer; it follows that

$$TE(x) = E(T^{-1}x) = E(x-\ell\Lambda) \tag{2.30}$$

The ABCD matrix derived in the previous section is a representation of the unit cell translation operator. According to the Floquet theorem, a wave propagating in a periodic medium is of the form [5]

$$E_K(x,z) = E_K(x) \, e^{iKx} \, e^{i\beta z} \tag{2.31}$$

where $E_K(x)$ is periodic with a period Λ, i.e.,

$$E_K(x + \Lambda) = E_K(x) \tag{2.32}$$

The subscript K indicates that the function $E_K(x)$ depends on K. The constant K is known as the Bloch wave number. The problem at hand is thus that of determining K and $E_K(x)$.

In terms of our column vector representation, and from (2.8), the periodic condition (2.32) for the Bloch wave is simply

$$\begin{pmatrix} a_n \\ b_n \end{pmatrix} = e^{iK\Lambda} \begin{pmatrix} a_{n-1} \\ b_{n-1} \end{pmatrix} \tag{2.33}$$

It follows from (2.17) and (2.33) that the column vector of the Bloch wave satisfies the following eigenvalue problem:

$$
\begin{pmatrix} A & B \\ C & D \end{pmatrix} \begin{pmatrix} a_n \\ b_n \end{pmatrix} = e^{-iK\Lambda} \begin{pmatrix} a_n \\ b_n \end{pmatrix} \tag{2.34}
$$

The phase factor $\exp(-iK\Lambda)$ is thus the eigenvalue of the translation matrix (A,B,C,D) and is given by

$$
e^{-iK\Lambda} = \frac{A+D}{2} \pm \sqrt{\left(\frac{A+D}{2}\right)^2 - 1} \tag{2.35}
$$

The eigenvectors corresponding to the eigenvalues (2.35) are obtained from (2.34) and are

$$
\begin{pmatrix} a_0 \\ b_0 \end{pmatrix} = \begin{pmatrix} B \\ e^{-iK\Lambda} - A \end{pmatrix} \tag{2.36}
$$

times any arbitrary constant. The Bloch waves which result from (2.36) can be considered as the eigenvectors of the translation matrix with eigenvalues $e^{\pm iK\Lambda}$ given by (2.35). The two eigenvalues in (2.35) are the inverse of each other, since the translation matrix is unimodular. Equation (2.35) is the dispersion relation among ω, β, and K. It can be written as

$$
K(\beta,\omega) = \frac{1}{\Lambda} \cos^{-1}\left(\frac{A+D}{2}\right) \tag{2.37}
$$

Regimes where $\left|\frac{A+D}{2}\right| < 1$ correspond to real K and thus to propagating Bloch waves, when $\left|\frac{A+D}{2}\right| > 1$, $K = \frac{m\pi}{\Lambda} + iK_i$ and has an imaginary part K_i so that the Bloch wave is evanescent. These are the so-called "forbidden" bands of the periodic medium. The band edges are the regimes where

$$\left|\frac{A+D}{2}\right| = 1.$$

According to (2.8) and (2.33) the final result for the Bloch wave in the n_1-layer of the nth unit cell is

$$E_K(x) \, e^{iKx} = \{[a_0 e^{ik_{1x}(x-n\Lambda)} + b_0 e^{-ik_{1x}(x-n\Lambda)}] \, e^{-iK(x-n\Lambda)}\} \, e^{iKx} \quad (2.38)$$

where a_0 and b_0 are given by Eq. (2.36). This completes the solution of the Bloch waves.

The band structure for a typical stratified periodic medium as obtained from (2.37) is shown in Figs. 2.3 and 3.4 for TE and TM waves, respectively. It is interesting to notice that the TM "forbidden" bands shrink to zero when $\beta = \frac{\omega}{c} n_2 \sin \theta_B$ with θ_B as the Brewster angle, since at this angle the incident and reflected waves are un-coupled. The dispersion relation ω vs K for the special case $\beta = 0$, i.e., normal incidence, is shown in Fig. 2.5.

2.4 Phase Velocity and Group Velocity

We have derived some of the important characteristics of Bloch waves propagating in a periodic stratified medium. An exact expression for the dispersion relation among K, β, and ω was derived. This dispersion relation can be represented by contours of constant frequency in the β-K plane as in Fig. 2.6.

It can be seen that these contours are more or less circular with only a slight ellipticity. The origin corresponds to the contour of zero frequency. In the long wavelength regime ($\lambda \gg \Lambda$), these are similar to the dispersion curves of electromagnetic waves in a
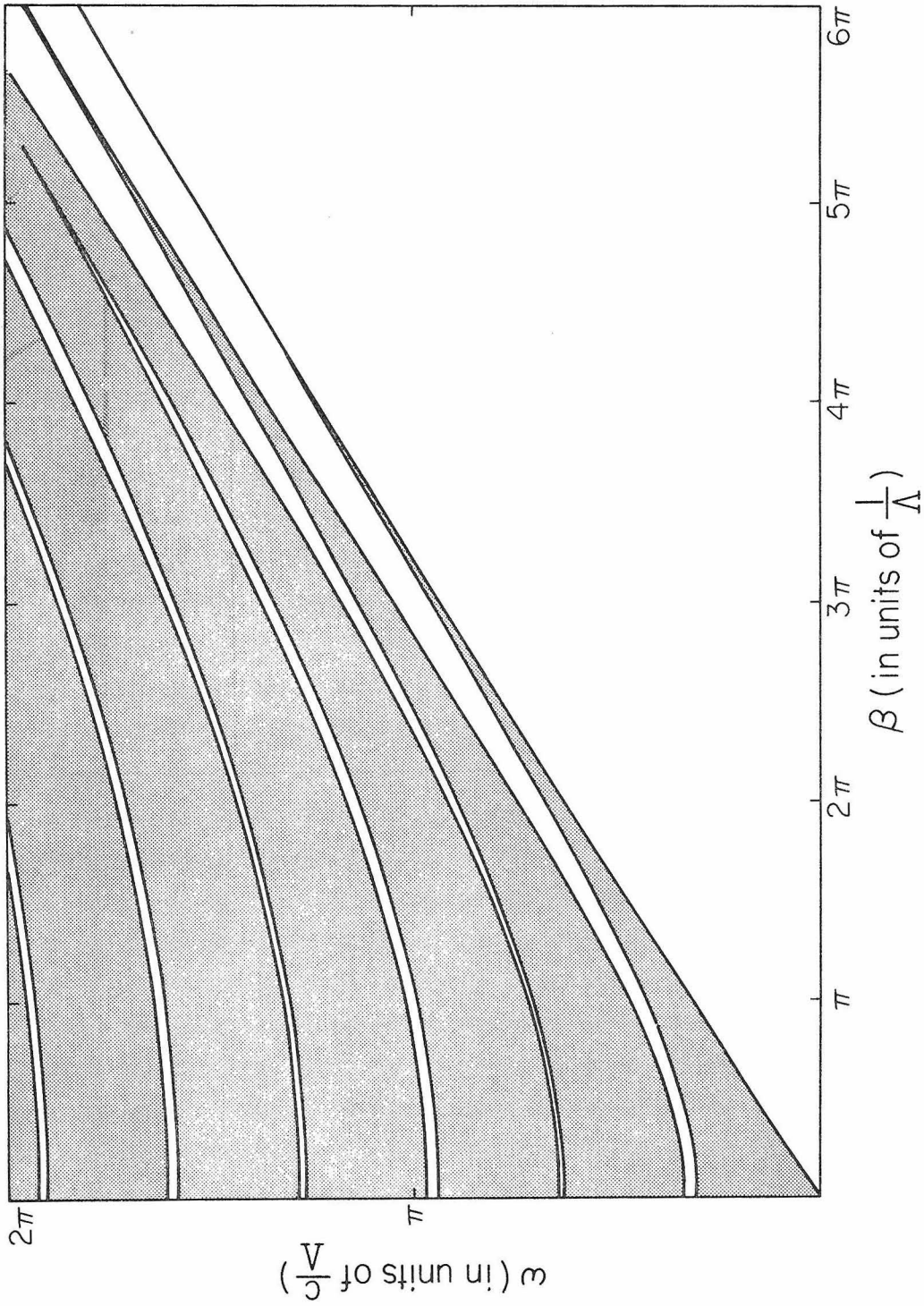
Fig. 2.4 TM waves ($\vec{H}$ perpendicular to the direction of periodicity). band structure in the ω-β plane. The dashed line is

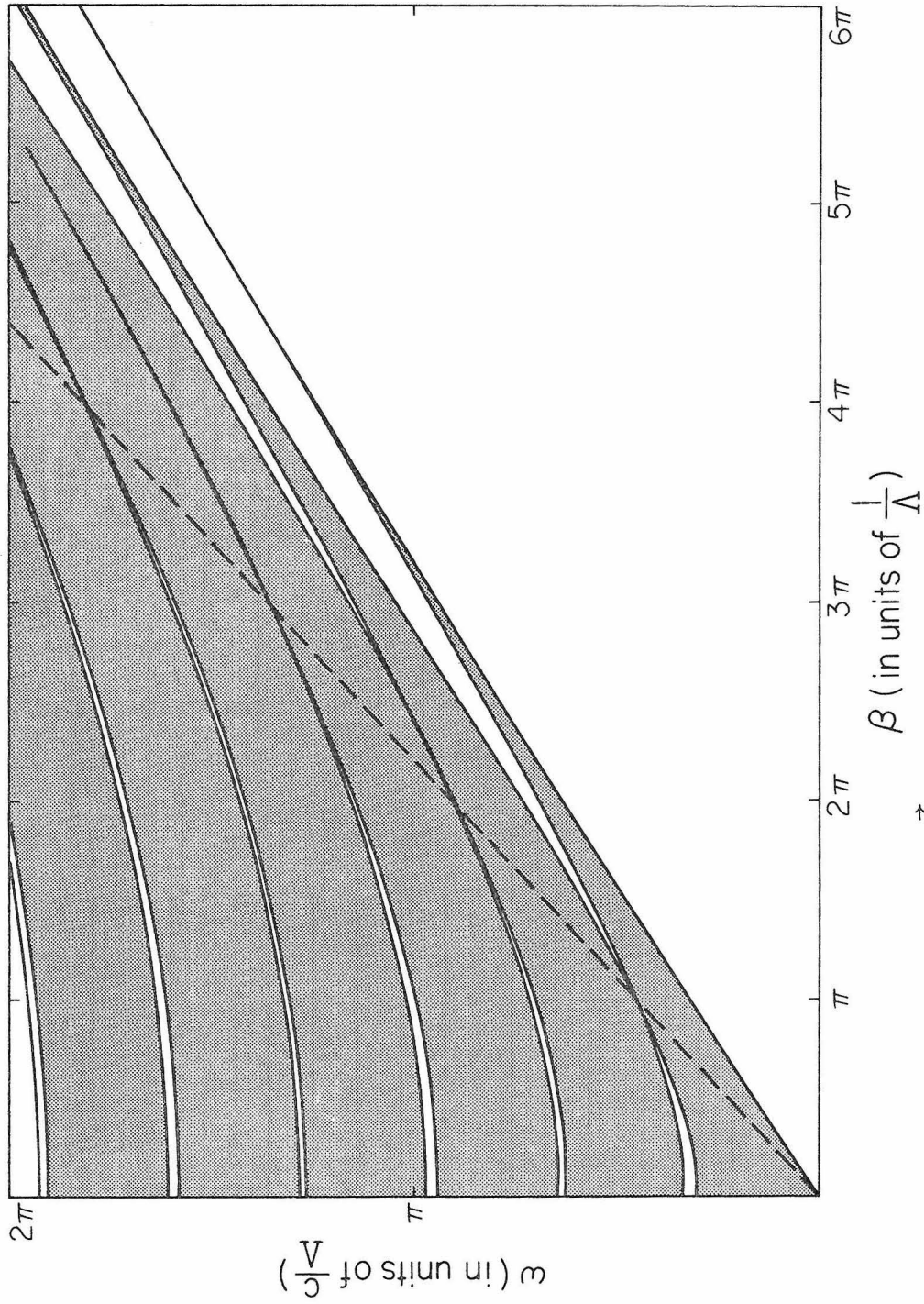$$\beta = \frac{\omega}{c} n_2 \sin \phi_B.$$ The dark zones are the allowed bands.

Fig. 2.3 TE waves (E perpendicular to the direction of periodicity) band structure in the ω-β plane. The dark zones are the allowed bands.
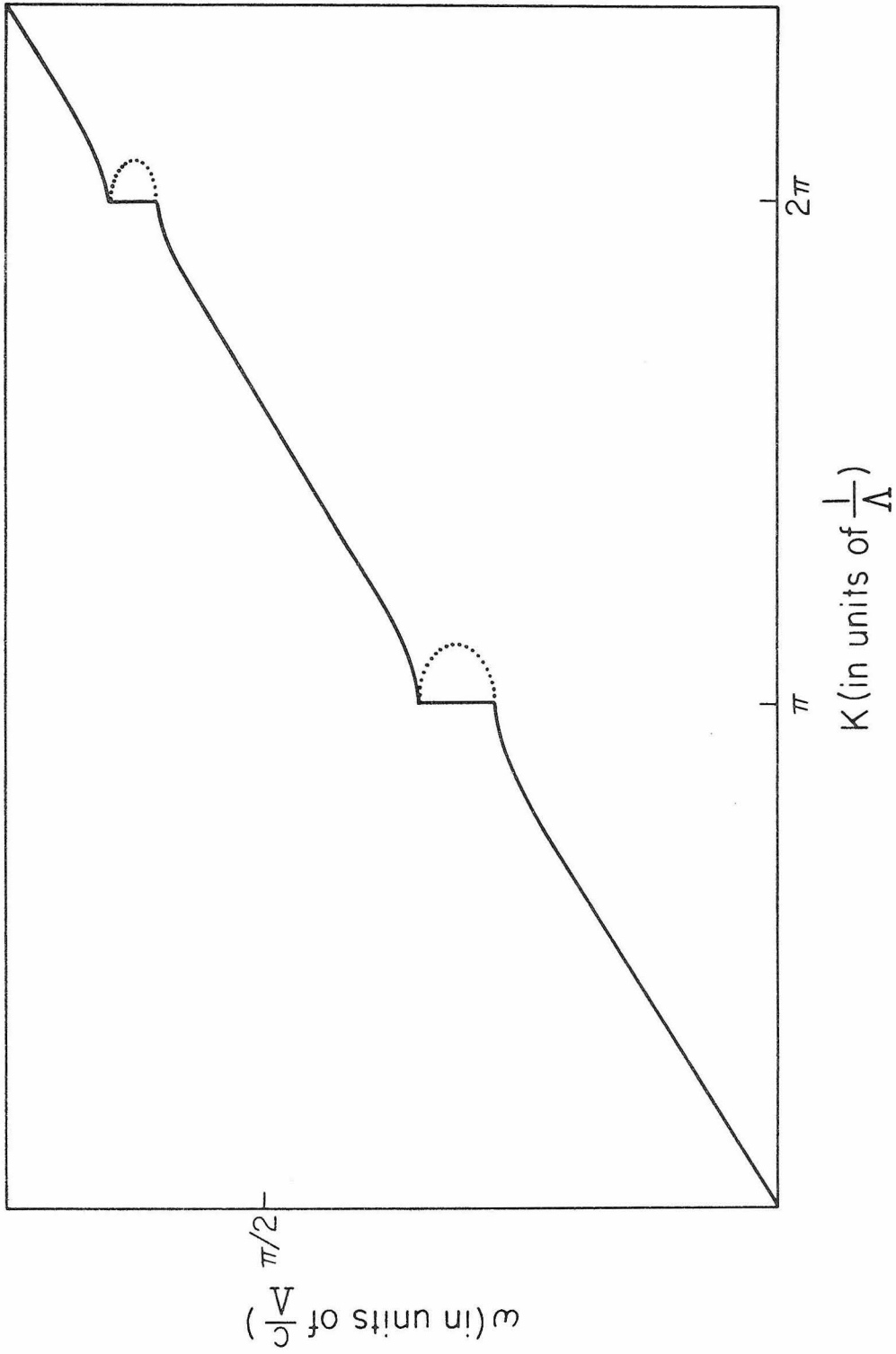
Fig. 2.5 Dispersion relation between ω and K when β = 0 (normal incidence). Dotted curves are the imaginary part of K in arbitrary scales.
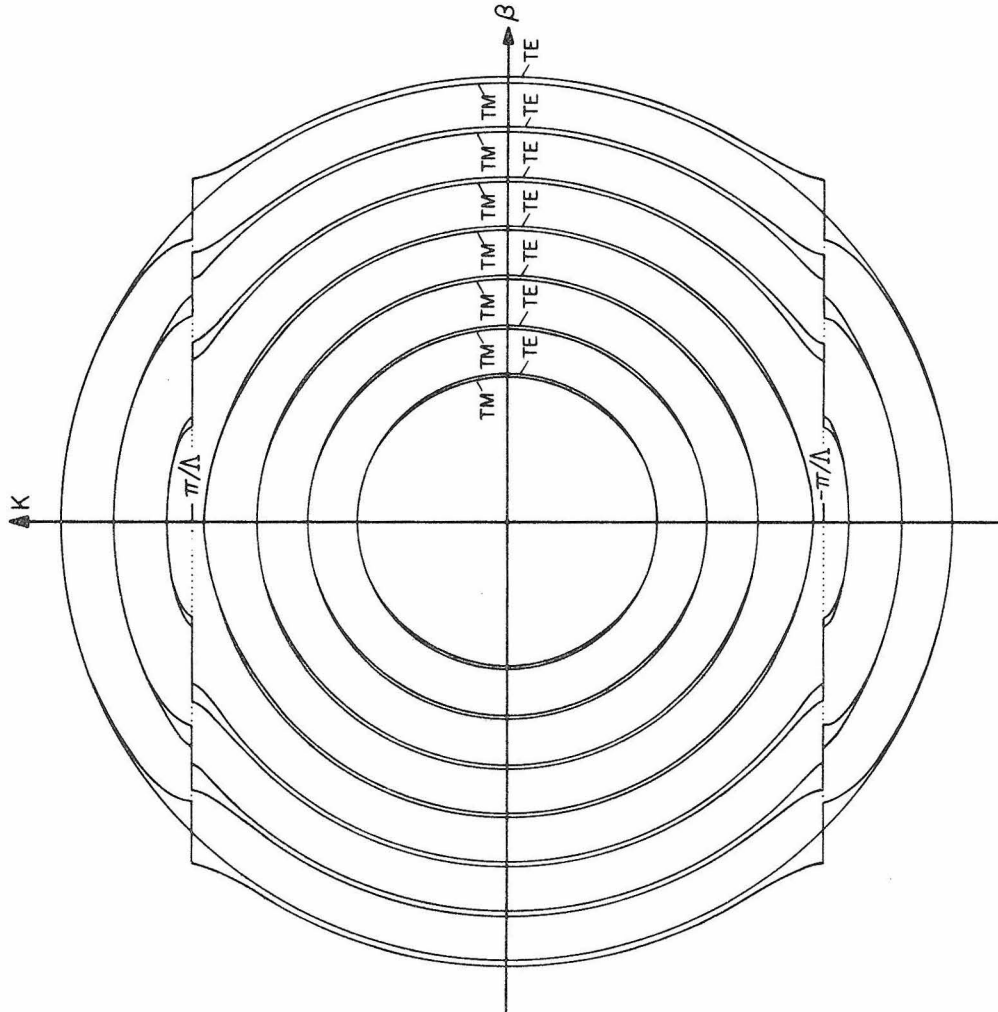
Fig. 2.6 Contours of constant frequency in β-K plane.

negative uniaxial crystal. The birefringence property of a periodic stratified medium will be discussed further in the next section. These contours become distorted and modified at shorter wavelengths and near the boundaries of the Brillouin zone (KΛ = ℓπ) where the wavelength is comparable with the dimension of a unit cell and the electromagnetic waves interact strongly with the periodic medium.

The concepts of phase and group velocities in periodic layered media are subtle and require careful examination. Let us start by reviewing some of the relevant results which were derived in Section 2.2.

The electromagnetic Bloch wave is given by

$$\vec{E}(x,z,t) = \vec{E}_K(x)e^{iKx}e^{i\beta z}e^{-i\omega t} \tag{2.39}$$

where $\vec{E}_K(x)$ is a periodic function of x with period Λ and is given by Eq. (2.38). The dispersion relation between K, β and ω is given by

$$\cos(K\Lambda) = \frac{1}{2}(A+D)$$
$$= \cos k_{1x}a \cos k_{2x}b - \Delta \sin k_{1x}a \sin k_{2x}b \tag{2.40}$$

where A and D are given respectively by equations (2.18), (2.21), (2.23) and (2.26) and

$$\Delta = \begin{cases} \dfrac{1}{2}\left(\dfrac{k_{2x}}{k_{1x}} + \dfrac{k_{1x}}{k_{2x}}\right) & \text{TE waves} \\[3mm] \dfrac{1}{2}\left(\dfrac{n_2^2 k_{1x}}{n_1^2 k_{2x}} + \dfrac{n_1^2 k_{2x}}{n_2^2 k_{1x}}\right) & \text{TM waves} \end{cases} \tag{2.41}$$

$$k_{1x} = \sqrt{(\frac{\omega}{c} n_1)^2 - \beta^2} \qquad (2.42)$$

$$k_{2x} = \sqrt{(\frac{\omega}{c} n_2)^2 - \beta^2} \qquad (2.43)$$

It is important to notice that the Bloch wave number K given by (2.40) is not uniquely defined to the extent that any integer multiple of $2\pi/\Lambda$ can be added to it. The reduced Brillouin zone scheme commonly used in solid state physics is no longer useful as far as the phase velocity of an electromagnetic Bloch wave is concerned. If $E_K(x)$ is expanded in a Fourier series

$$\vec{E}_K(x) = \sum_n \vec{e}_K^{(n)} e^{in \frac{2\pi}{\Lambda} x} \qquad (2.44)$$

the Bloch wave (2.39) can be written as a linear superposition of an infinite number of partial plane waves which are the so-called "space harmonics." From (2.39) and (2.44) we have

$$\vec{E}(x,z,t) = \sum_n \vec{e}_K^{(n)} e^{i(K+n \frac{2\pi}{\Lambda})x} e^{i\beta z} e^{-i\omega t} \qquad (2.45)$$

where $\vec{e}_K^{(n)}$ are constant. Thus the multivalued nature of the Bloch wave number embodies the existence of the whole set of space harmonics. If the periodicity is removed, i.e., $n_1 = n_2 \equiv n$ then the Bloch mode should become an ordinary plane wave and K should be equal to $k_x = \frac{\omega}{c} n\cos\theta$. Equation (2.40) in this case reads

$$\cos K\Lambda = \cos[k_x(a+b)] = \cos k_x\Lambda \qquad (2.46)$$

so that when $n_1 - n_2 \ll n_1$, the principal value of K, can be chosen as that nearest to k_{1x} or k_{2x}. We can insure that K satisfies the

above condition by choosing it in such a way that

$$|\vec{e}_K^{(o)}| \geq |\vec{e}_K^{(n)}|$$ (2.47)

for all n or equivalently by choosing K such that the integral

$$\frac{1}{\Lambda} \int_0^\Lambda \vec{E}_K(x)dx \equiv <\vec{E}_K>$$ (2.48)

has a maximum value.

Having a proper choice of the Bloch wave number K we are now in a position to define the phase velocity of a Bloch wave. It is defined as

$$V_p = \frac{\omega}{\sqrt{K^2 + \beta^2}}$$ (2.49)

The phase velocity defined above is strictly speaking the phase velocity of the fundamental (n = 0) space harmonic which is a plane wave of the form

$$\vec{E}(x,z,t) = <\vec{E}_K>e^{iKx} e^{i\beta z}e^{-i\omega t}$$ (2.50)

In the long wavelength regime where the whole structure behaves as if it were homogeneous, the fundamental space harmonic is the dominant part of the Bloch wave and can be taken alone as a very good approximation of the whole wave.

The group velocity for a Bloch wave packet is given by

$$\vec{V}_g = \left(\frac{\partial \omega}{\partial K}\right)_\beta \hat{a}_x + \left(\frac{\partial \omega}{\partial \beta}\right)_K \hat{a}_z$$ (2.51)

In a homogeneous medium the group velocity represents the velocity of energy flow of a quasi-monochromatic wave and is thus parallel to the

Poynting vector which is a constant vector in a homogeneous lossless medium. The Poynting vector of a Bloch wave given by (2.39) is a periodic function of x. The group velocity (2.51) of the same wave, however, is a constant vector. The discrepancy is due to the fact that in a periodic medium the power flow is a periodic function of the space coordinates. We will show, however, that the averaged velocity of energy flow defined as

$$
\vec{V}_e = \frac{\dfrac{1}{\Lambda} \displaystyle\int_0^\Lambda (\text{Poynting vector})\ dx}{\dfrac{1}{\Lambda} \displaystyle\int_0^\Lambda (\text{Energy density})\ dx}
\tag{2.52}
$$

is exactly equal to the group velocity as given by (2.51) (see Appendix B). This endows the concept of group velocity as defined by (2.51) with a rigorous meaning. It is an extremely useful concept since it now makes it possible to consider the propagation of confined finite aperture beams in a layered medium. The space averaged Poynting vector and energy density are particularly useful in the long wavelength regime where the medium can be considered as a quasi-homogeneous and anisotropic medium.

2.5 Birefringence and Double Refraction

In this section we review the birefringence which results from the medium periodicity. We start by reviewing in the context of our present discussion the birefingent behavior of bulk anisotropic media.

The index of refraction of light propagating in an anisotropic medium depends on its state of polarization. Given a direction of propagation in the medium, there are in general two eigenpolarizations with

two respective eigenphase velocities. The directions of eigenpolarization and their corresponding indices of refraction for a plane wave of the following form

$$\vec{E}(\vec{r},t) = \vec{E}e^{i(\frac{\omega}{c} n\vec{s}\cdot\vec{r}-\omega t)} \qquad (2.53)$$

are given by the following well-known formulae [6]

$$\frac{s_x^2}{n^2-\varepsilon_x/\varepsilon_0} + \frac{s_y^2}{n^2-\varepsilon_y/\varepsilon_0} + \frac{s_z^2}{n^2-\varepsilon_z/\varepsilon_0} = \frac{1}{n^2} \qquad (2.54)$$

$$E_i = \frac{n^2 s_i (\vec{s}\cdot\vec{E})}{n^2-\varepsilon_i/\varepsilon_0} \qquad i = x,y,z \qquad (2.55)$$

where $\varepsilon_x, \varepsilon_y, \varepsilon_z$ are the principal dielectric constants and $\vec{s}$ is a unit vector along the direction of polarization.

Equation (2.54) (also known as Fresnel's equation of wave normals) can be solved for the eigen-indices of refraction, while equation (2.55) gives the directions of polarization.

It is important to notice that equation (2.54) is in fact the dispersion relation between ω and $\vec{k}$. If we define $\vec{k}$ as $(\omega/c)n\vec{s}$ for the plane wave given by (2.53), then equation (2.54) can be written as

$$\frac{k_x^2}{k^2- \frac{\omega^2}{c^2}\frac{\varepsilon_x}{\varepsilon_0}} + \frac{k_y^2}{k^2- \frac{\omega^2}{c^2}\frac{\varepsilon_y}{\varepsilon_0}} + \frac{k_z^2}{k^2- \frac{\omega^2}{c^2}\frac{\varepsilon_z}{\varepsilon_0}} = 1 \qquad (2.56)$$

where

$$k^2 = k_x^2 + k_y^2 + k_z^2 \qquad (2.57)$$

Equation (2.56) describes a surface of two shells in $\vec{k}$-space known as the normal surface. The two shells of the normal surface have only four points in common. The two lines which go through the origin at these points are known as the optic axes. Given a direction of propagation, there are in general two k values which are the intersections of the direction of propagation and the normal surface. These two k values correspond to two different phase velocities ω/k of the waves propagating along the chosen direction.

Equation (2.56) can also be derived directly from the wave equation

$$\vec{\nabla} \times (\vec{\nabla}\times\vec{E}) + \mu\overset{=}{\varepsilon}\ \frac{\partial^2}{\partial t^2}\vec{E} = 0 \tag{2.58}$$

Substitution for $\vec{E}$ from (2.53) gives, if we also recall $\vec{k} = \frac{\omega}{c}\,n\vec{s}$:

$$\vec{k} \times (\vec{k}\times\vec{E}) + \omega^2\ \mu\overset{=}{\varepsilon}\ \vec{E} = 0 \tag{2.59}$$

or equivalently

$$\begin{pmatrix} \omega^2\mu\varepsilon_x - k_y^2 - k_z^2 & k_x k_y & k_x k_z \\[2mm] k_y k_x & \omega^2\mu\varepsilon_y - k_x^2 - k_z^2 & k_y k_z \\[2mm] k_z k_x & k_z k_y & \omega^2\mu\varepsilon_z - k_x^2 - k_y^2 \end{pmatrix} \begin{pmatrix} E_x \\[2mm] E_y \\[2mm] E_z \end{pmatrix} = 0 \tag{2.60}$$

In order to have a nontrivial plane wave solution, the determinant of

the matrix in (2.60) must vanish. This gives us equation (2.61) which
is equivalent to the dispersion relation (2.56), if we recall that
$c^2 = 1/\mu\varepsilon_0$.

$$\det \begin{vmatrix} \omega^2\mu\varepsilon_x - k_y^2 - k_z^2 & k_x k_y & k_x k_z \\ k_y k_x & \omega^2\mu\varepsilon_y - k_z^2 - k_x^2 & k_y k_z \\ k_z k_x & k_z k_y & \omega^2\mu\varepsilon_z - k_x^2 - k_y^2 \end{vmatrix} = 0$$

(2.61)

Of particular interest is the uniaxial crystal with a normal surface
consisting of a sphere and an ellipsoid of revolution. If we set
$\varepsilon_y = \varepsilon_z$ in equation (2.56), the equation breaks into two factors, giving

$$\begin{cases} \dfrac{k_x^2}{n_o^2} + \dfrac{k_y^2 + k_z^2}{n_e^2} = \dfrac{\omega^2}{c^2} & (2.62) \\[4ex] \dfrac{k_x^2}{n_o^2} + \dfrac{k_y^2 + k_z^2}{n_o^2} = \dfrac{\omega^2}{c^2} & (2.63) \end{cases}$$

where

$$n_e^2 = \varepsilon_x/\varepsilon_o$$

$$n_o^2 = \varepsilon_y/\varepsilon_o \qquad (2.64)$$

The section of the normal surface by the coordinate plane $k_y = 0$ is a
circle and an ellipse (see Fig. 2.7). The line joining the origin and
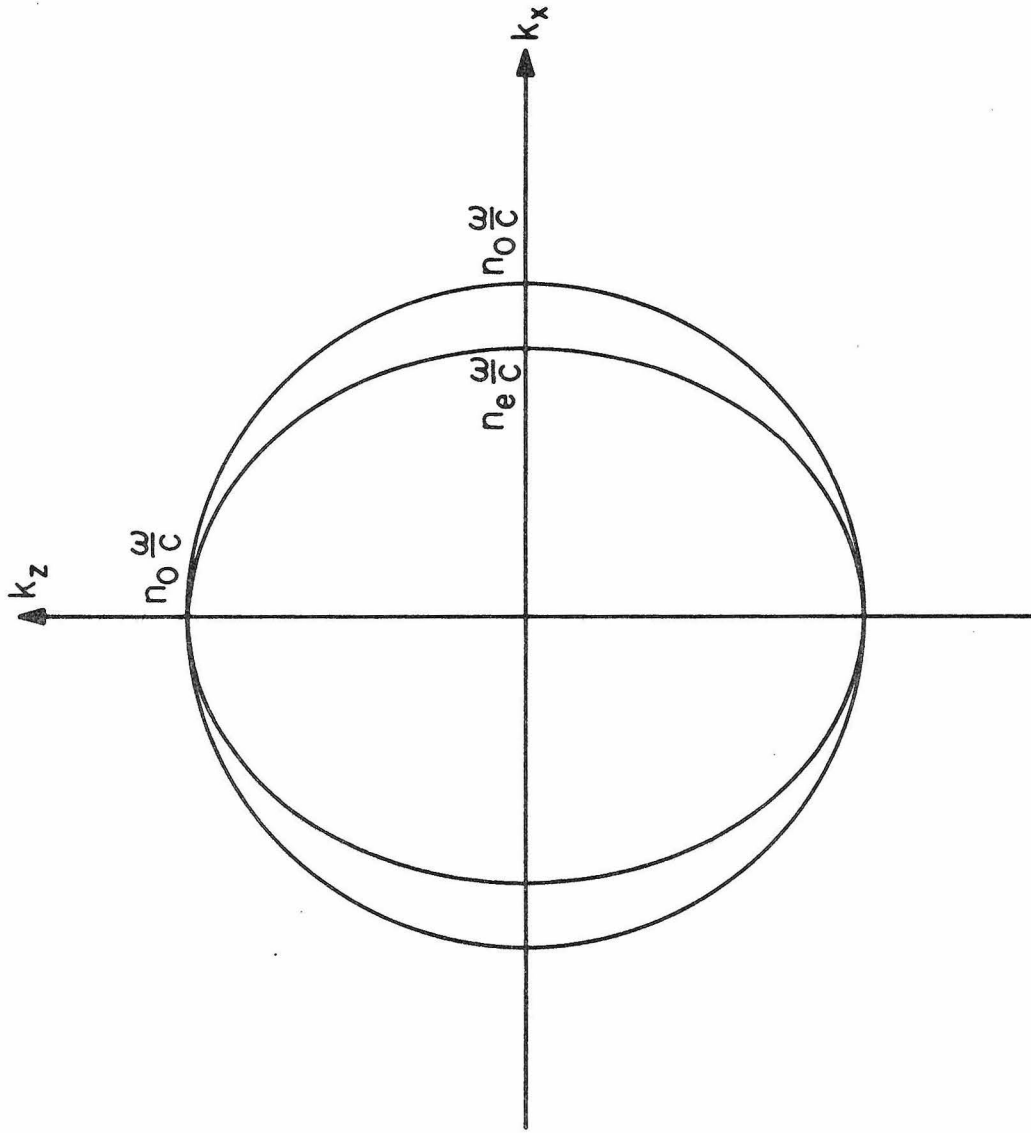
Fig. 2.7 Section of normal surface in k_x-k_z plane.

the osculating points of the circle and the ellipse is the optic axis.

It can easily be shown that the vectors $\vec{E}$ and $\vec{H}$ always lie in the tangent plane of the normal surface. As a result the Poynting vector $\vec{S}$ defined by

$$\vec{S} = \vec{E} \times \vec{H} \tag{2.65}$$

is always parallel to the group velocity which is given by

$$\vec{v}_g = \nabla_{\vec{k}}\omega(\vec{k}) \tag{2.66}$$

To prove that $\vec{S}$ and $\vec{v}_g$ are parallel we start from equation replacing $\partial/\partial t$ by $-i\omega$ rewrite it as

$$\vec{k}(\vec{k}\cdot\vec{E}) - \vec{E}(\vec{k}\cdot\vec{k}) + \omega^2\, \mu\overline{\overline{\epsilon}}\vec{E} = 0 \tag{2.67}$$

$$+ \omega^2\mu\overline{\overline{\epsilon}}\, \vec{E} = 0 \tag{2.68}$$

If we multiply both sides of this equation by $\vec{E}$, we obtain, using $\epsilon_{ij} = \epsilon_{ji}$

$$2\delta\vec{k}\cdot[\vec{k}(\vec{E}\cdot\vec{E})-\vec{E}(\vec{k}\cdot\vec{E})]+\delta\vec{E}\cdot[\vec{k}(\vec{E}\cdot\vec{k})-\vec{E}(\vec{k}\cdot\vec{k})+\omega^2\mu\overline{\overline{\epsilon}}\vec{E}] = 0 \tag{2.69}$$

The second term vanishes according to (2.67) and the first term can be written as $2\delta\vec{k}\cdot[\vec{E} \times (\vec{k} \times \vec{E})]$. Hence, we have, using $\vec{H} = 1/\omega\mu\, \vec{k} \times \vec{E}$,

$$\delta\vec{k}\cdot(\vec{E} \times \vec{H}) = 0 \tag{2.70}$$

i.e., $\vec{E} \times \vec{H}$ is perpendicular to $\delta\vec{k}$ which is an arbitrary infinitesimal vector in the tangent plane of the normal surface. The group velocity $\vec{v}_g$ defined by (2.66) is also perpendicular to the normal surface, thus proving our statement.

Let us now consider the propagation of electromagnetic waves in a medium consisting of infinitely alternating layers of two different homogeneous and isotropic substances. Although each individual layer is isotropic, the whole structure behaves as an anisotropic medium. TE waves and TM waves are found to propagate with different effective phase velocities and the periodic medium is birefringent. This phenomenon is well known in an anisotropic homogeneous crystal and is used in the electrooptic modulation of light and in a variety of polarizing applications.

The electromagnetic properties of a periodic laminated structure have been studied by Rytov [7], who limited his treatment to cases in which the direction of propagation is either parallel or normal to the layers. In the present analysis we use the Bloch wave formalism of Section 2.2 to obtain the exact birefringence behavior of a periodic medium for waves propagating in an arbitrary direction.

It was shown above that the only dynamical variables needed to describe a monochromatic plane wave propagating in a periodic stratified medium are ω, β, and K. The generalized wave vector is defined as

$$\vec{\kappa} = \hat{a}_x K + \hat{a}_z \beta \tag{2.71}$$

The dispersion relation between ω and $\vec{\kappa}$ is given by equation (2.40).

If the period Λ is sufficiently small compared with the wavelength then the whole structure behaves as if it were homogeneous and uniaxially anisotropic. The wave given by (2.39) thus behaves as if it were a plane wave of the form given by (2.50).

In Figure 2.6 the contours of constant ω are plotted in the K-β plane. These are sections of the normal surfaces with the K-β plane for various frequencies. It is evident from inspection that at the long wavelength limit ($\lambda \gg \Lambda$) the dispersion of a layered medium is qualitatively similar to that of a negative uniaxial crystal.

To demonstrate this analogy we take the limit of $k_{1x}a \ll 1$, $k_{2x}b \ll 1$ and $K\Lambda \ll 1$ and expand all the transcendental functions in (2.40). After neglecting higher order terms we obtain

$$\frac{K^2}{n_o^2} + \frac{\beta^2}{n_o^2} = \frac{\omega^2}{c^2} \qquad \text{TE} \qquad (2.72)$$

$$\frac{K^2}{n_o^2} + \frac{\beta^2}{n_e^2} = \frac{\omega^2}{c^2} \qquad \text{TM} \qquad (2.73)$$

with

$$n_o^2 = \frac{a}{\Lambda} n_1^2 + \frac{b}{\Lambda} n_2^2 \qquad (2.74)$$

$$\frac{1}{n_e^2} = \frac{a}{\Lambda} \cdot \frac{1}{n_1^2} + \frac{b}{\Lambda} \cdot \frac{1}{n_2^2} \qquad (2.75)$$

Equations (2.66) and (2.67) represent the two shells of the normal surface in the K-β plane. One surface (2.72) applies to a TE wave and is a sphere while the TM normal surface (2.73) is an ellipsoid of revolution. TE waves thus are formally analogous to the so-called ordinary waves in a uniaxial crystal, while TM waves are the extraordinary waves. The normal surface becomes more complicated at higher frequencies. It consists of two oval surfaces osculating each other at the intersections with the K axis, as long as the frequency is below the first forbidden gap.

For frequencies higher than the forbidden gap, the oval surfaces break into several sections. The break points occur at

$$K = m \frac{\pi}{\Lambda} \quad , \quad m = \text{integer} \tag{2.76}$$

which is the Bragg condition for the quasi-plane wave (2.50).

Double Refraction at a Boundary

Consider a plane wave incident on the surface of a semi-infinite periodic stratified medium. If the incident wave is a mixture of TE and TM waves, double refraction takes place. This can be easily seen from the normal surface in the β-K plane. A very important kinematic property of refraction at a plane interface between two dielectric media is the fact that β, the tangential component of the wave vectors, must be equal for both the incident and refracted waves. Given a β value, the two shells of the normal surface in general yields two K values, thus giving rise to two refracted waves as shown in Figure 2.8. The two refracted waves are in general both extraordinary waves in the sense that their phase velocities, i.e., effective indices, depend on β.

However, at the long wavelength regime where $\lambda \gg \Lambda$, TE waves become ordinary waves while TM waves remain extraordinary. If the wave vector of the incident wave is denoted by $\vec{k}_o$, and θ is the angle of incidence, the projection of the wave vector along the boundary plane is given by

$$\beta = k_o \sin \theta \tag{2.77}$$

The transverse wave vectors in the medium are determined either
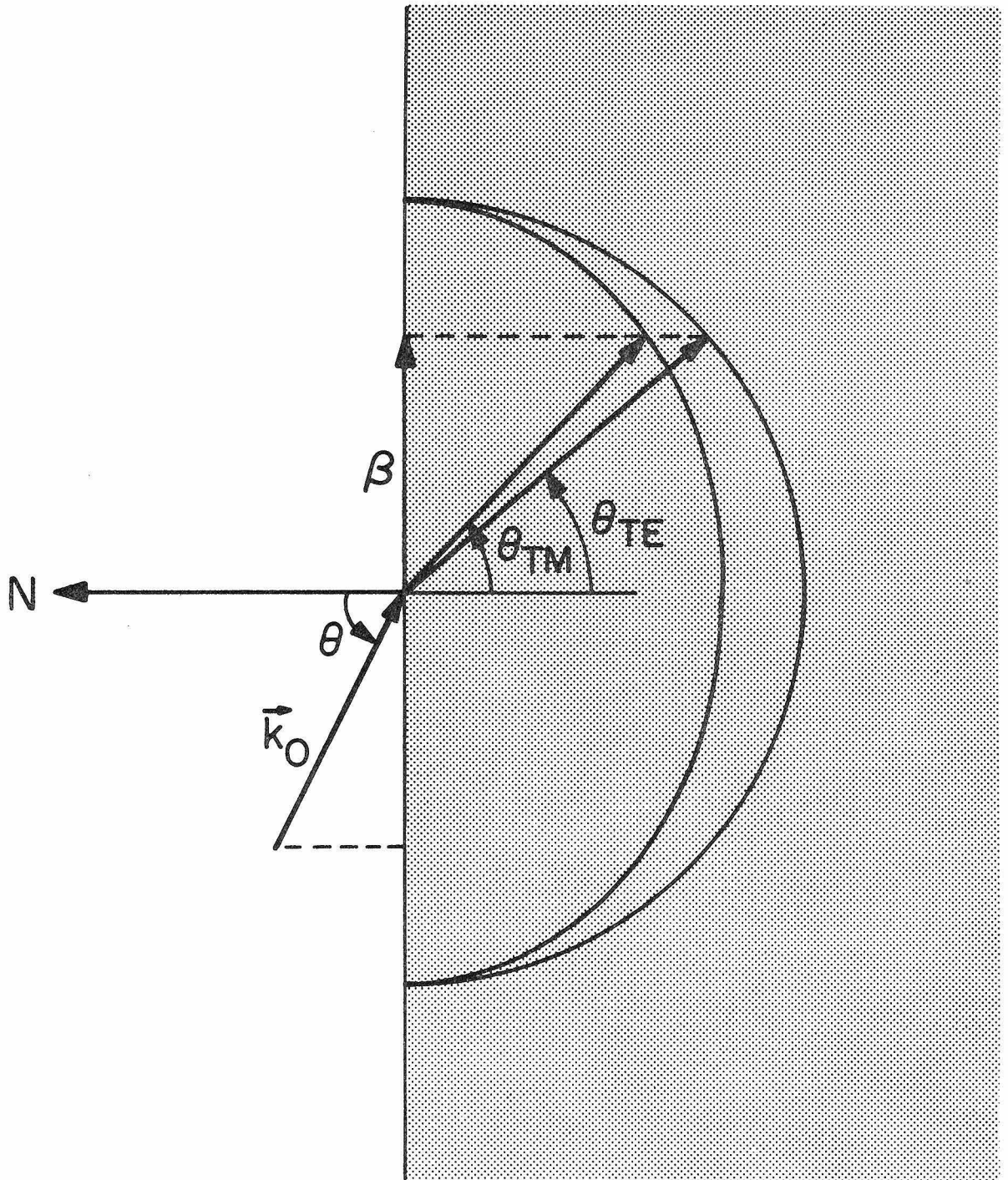
Fig. 2.8 Double refraction at the boundary of a periodic stratified medium.

graphically from Figure 2.8, or analytically from the dispersion relation (2.40). The angles of refraction are given by

$$\tan \theta_{TE} = \frac{\beta}{K_{TE}} \tag{2.78}$$

$$\tan \theta_{TM} = \frac{\beta}{K_{TM}} \tag{2.79}$$

The angles given by (2.78) and (2.79) are the directions normal to the wavefronts of the refracted waves. The directions of energy flow are obtained by taking the normals to the normal surface.

The effect of double refraction is very pronounced near the zone boundaries where the medium is very dispersive and the bandgap is different for TE and TM modes. At the edge of the bandgap the group velocity which is parallel to the normal to the curve, is along the z axis and has no component normal to the interfaces. This is consistent with the fact that at or inside the gap the reflectivity is unity so that no power can flow along the x direction.

References - Chapter 2

1. F. Bloch, Z. Physik $\underline{52}$, 555 (1928).

2. See, for example, C. Kittel, <u>Introduction to Solid State Physics</u>, 3rd ed. (Wiley, New York, 1967).

3. D. Kossel, J. Opt. Soc. Am. $\underline{56}$, 1434 (1966).

4. J. P. van der Ziel, M. Ilegems, and R. M. Mikulyak, Appl. Phys. Lett. $\underline{28}$, 735 (1976).

5. See, for example, J. Mathews and R. L. Walker, <u>Mathematical Methods of Physics</u>, 2nd ed. (W. A. Benjamin, New York, 1970).

6. See, for example, M. Born and E. Wolf, <u>Principles of Optics</u> (Macmillan, New York, 1964).

7. S. M. Rytov, Soviet Physics JETP $\underline{2}$, 446 (1956).

Chapter 3

OPTICAL MODES IN LAYERED MEDIA

3.1 Introduction

We have derived in Chapter 2, the eigenmodes of electromagnetic waves in an infinite periodic layered medium. Bloch waves and band structures are obtained by using the concept of translation operator. In the practical world the real structures are all finite in the number of periods. In order to solve the eigenmodes of finite structures, we have to match the boundary conditions at the surfaces of the layered media. Conventional methods involve matching the plane wave solutions at each interface. This results in solving a large number of linear simultaneous equations. A systematic approach is to use the matrix method described in Section 2.2. This new method is based on the fact that every interface is now replaced by a 2×2 matrix which is much easier to deal with. As a result of the successive matrix multiplication, we obtain a linear relation between the fields on both sides of a finite layered medium:

$$
\begin{pmatrix} A_a \\ B_a \end{pmatrix} = \begin{pmatrix} m_{11} & m_{12} \\ m_{21} & m_{22} \end{pmatrix} \begin{pmatrix} A_s \\ B_s \end{pmatrix}
\tag{3.1}
$$

The matrix contains all the information of the layered medium. A_a, B_a are the amplitudes of plane waves on the air side of the structure, A_s, B_s are those of the substrate side. This matrix has a modulus of k_{sx}/k_{ax} and becomes unimodular when $n_a = n_s$, where n_a and n_s are the

refractive indices of the air and substrate respectively. We will assume $n_s > n_a$ throughout this thesis, unless otherwise specified.

The reflectivity coefficient is given by

$$r = \left(\frac{B_a}{A_a}\right)_{B_s=0} = \left(\frac{m_{21}}{m_{11}}\right) \tag{3.2}$$

Given a structure, the reflectivity depends on β and ω for both TE and TM waves:

$$r = r(\beta,\omega) \tag{3.3}$$

In the next section we will show that the zeros and poles of reflectivity coefficient play an important role in the mode theory of layered media.

3.2 Regge Poles and Optical Modes

A basic problem in high energy physics is that the poles in the scattering amplitude, which are assumed to dominate the scene, correspond to exchange of particles carrying definite angular momentum [1]. In other words, a resonance scattering corresponds to an eigenstate of the composite system. It was suggested by Regge [2] in 1959 to treat the angular momentum as a continuous complex variable. In particle scattering, the angular momentum corresponds to the impact parameter, while in the optics of layered media the angle of incidence (or equivalently, β) is the corresponding variable. We can now extend the β variable into a complex variable and search for the zeros and poles of the reflection coefficient which correponds to the scattering amplitude. In general, the poles occur at complex values of β, and each of these poles corresponds

either to a guided mode or a continuum mode or a leaky mode. It is important to notice that at the poles of the reflection coefficient the reflectivity is infinite. In order to fulfill the finiteness of the electromagnetic field, the solution of the Maxwell equation consists of outgoing waves only. We will now discuss these poles in terms of two categories:

(a) $\beta > \frac{\omega}{c} n_s$ (guided modes)

In this region both k_{sx} and k_{ax} are pure imaginary. Outgoing waves with imaginary propagation constant are evanescent waves. Therefore, the optical energy is guided by the structure and propagating parallel to the layers.

(b) β = complex (leaky modes)

These modes are referred to as "leaky modes" [3] since they correspond to a flow of energy away from the layered medium. These modes have β's with positive imaginary part. As a result, the wave attenuates in the direction of propagation which may account for the energy outflow. However, the transverse k vectors k_{sx} and k_{ax} have a negative imaginary part which makes the field "blow up" at infinity, hence these modes do not belong to the proper eigenvalue spectrum [4].

In addition to these poles there are solutions with standing waves along the x axis existing for all $0 < \beta < \frac{\omega}{c} n_s$. They are divided into two categories:

(a) $\frac{\omega}{c} n_a < \beta < \frac{\omega}{c} n_s$ (substrate modes)

These modes have a pure imaginary k_{ax}, hence the field is evanescent in the air. In the substrate the field is a standing wave. The energy is flowing in the direction of propagation. Since the major part of the energy is in the substrate, these modes are called substrate modes.

(b) $0 < \beta < \frac{\omega}{c} n_a$ (air mode)

These modes have both real k_{sx} and k_{ax}, hence the fields are standing on both sides of the structure with their energy flowing in the z-direction.

There are also solutions with pure imaginary β. These modes are evanescent waves in the z-direction. Since we are only interested in the propagating waves in the z-direction, these evanescent modes will not be discussed in this chapter.

3.3 Guided Waves

Multilayer waveguides are becoming increasingly important in integrated optics. The 2-channel dielectric waveguide has been studied extensively in the theory of branching waveguides [5,6], which is used in fabricating mode selectors, switches and directional couplers in integrated optics [7]. The analytic treatment for the general N-channel waveguide, however, suffers from the serious difficulty of solving an eigenvalue problem involving a 4N x 4N matrix, and has relied heavily on numerical techniques.

In the present analysis we employ the matrix method described in

Section 2.2 which involves only the manipulation of 2 x 2 matrices. Of particular interest is the Periodic Multichannel Dielectric Waveguide (PMDW) which consists of a stack of dielectric layers of alternating indices of refraction. Analytic expressions for the mode dispersion relations and field distributions can be obtained by the matrix method.

We are looking for guided waves propagating in the positive z direction. Two important periodic multichannel waveguides will be considered in the following.

(a) Symmetric Type

Consider the simplest kind of symmetric PMDW with the index of refraction given by

$$n(x,z) = \begin{cases} n_2 & m\Lambda \leq x \leq m\Lambda + b \\ & (m=0,1,2,.,\ldots,N-1) \\ n_1 & \text{otherwise} \end{cases} \tag{3.4}$$

with

$$n_1 < n_2 \tag{3.5}$$

The geometry of the waveguide is sketched in Figure 3.1. We will limit our analysis to TE waves only. It was shown in Section 2.2 that the translation matrix T which relates the field vector in one period to that of the next one is given by

$$T = \begin{pmatrix} A & B \\ C & D \end{pmatrix} \tag{3.6}$$

where, after defining $-ik_{1x} = q$, $k_{2x} = p$

$$A = e^{qa}[\cos pb - \frac{1}{2}(\frac{p}{q} - \frac{q}{p})\sin pb] \tag{3.7}$$
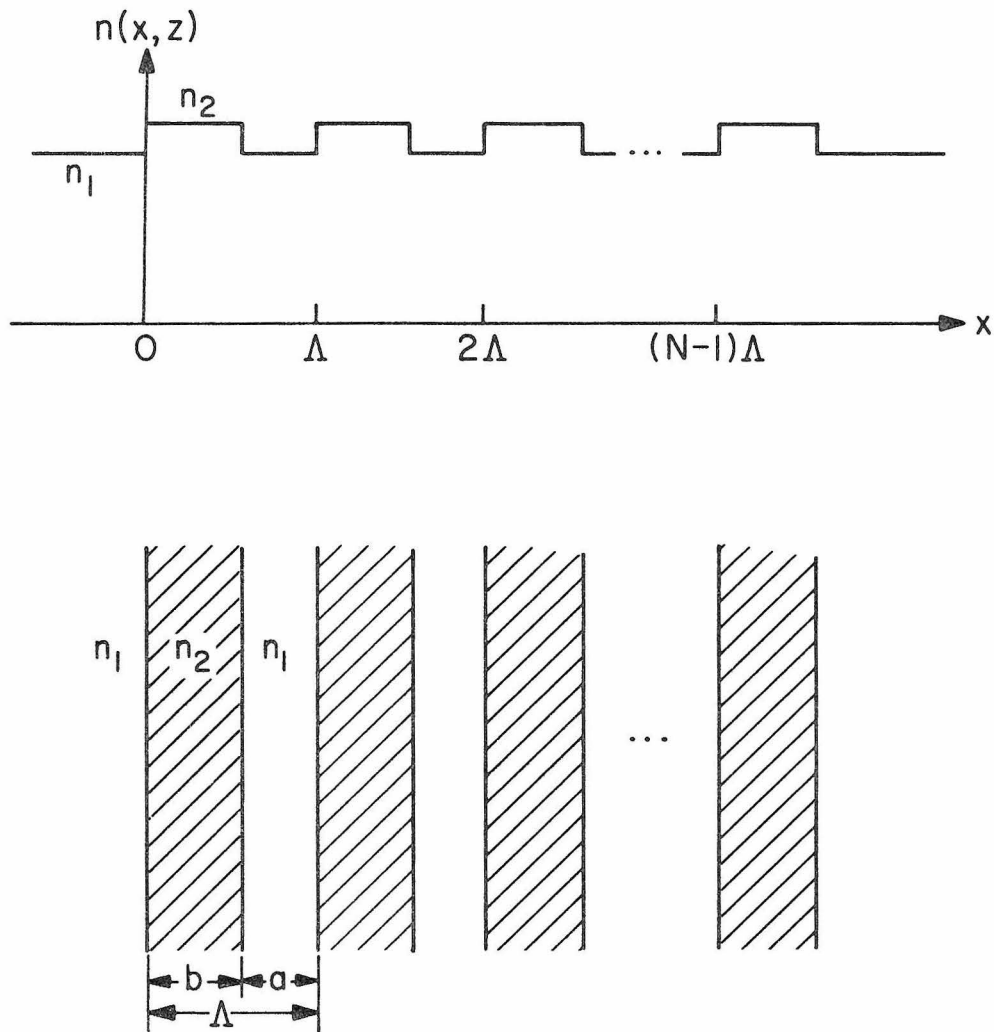
Fig. 3.1 Section view of a typical N-channel symmetric waveguide.

$$B = e^{-qa}[-\frac{1}{2}(\frac{p}{q} + \frac{q}{p})\sin pb] \tag{3.8}$$

$$C = e^{qa}[\frac{1}{2}(\frac{p}{q} + \frac{q}{p})\sin pb] \tag{3.9}$$

$$D = e^{-qa}[\cos pb + \frac{1}{2}(\frac{p}{q} - \frac{q}{p})\sin pb] \tag{3.10}$$

with

$$q = \sqrt{\beta^2 - (\frac{\omega}{c}n_1)^2} = -ik_{1x} \tag{3.11}$$

$$p = \sqrt{(\frac{\omega}{c}n_2)^2 - \beta^2} = k_{2x} \tag{3.12}$$

Since we are interested in guided waves only, the fields must be evanescent in the n_1 layer. The matrix equation (3.1) for this case can be written

$$\begin{pmatrix} A_a \\ B_a \end{pmatrix} = \begin{pmatrix} A & B \\ C & D \end{pmatrix}^N \begin{pmatrix} A_s \\ B_s \end{pmatrix} \tag{3.13}$$

We set $A_a = B_s = 0$ in (3.13); since only outward radiating waves can be present in a waveguide the mode dispersion relation is immediately obtained

$$A(\frac{\sin NK\Lambda}{\sin K\Lambda}) - (\frac{\sin(N-1)K\Lambda}{\sin K\Lambda}) = 0 \tag{3.14}$$

where we have used the Chebyshev identity (Appendix C) to obtain the matrix element m_{11} of the Nth power of a unimodular matrix.

If the left-hand side of (3.14) is plotted using (2.37) as a function of β for a given frequency ω, the zeros are the mode propagation constants (β's). It can be shown mathematically that there are exactly N zeros in each allowed band where $K\Lambda$ varies from $m\pi$ to $(m+1)$ and none

elsewhere (see Appendix C). Physically the waveguide can be considered as a system of N interacting slab waveguides. The N modes are simply due to the splitting of an N-fold degenerate band as the separations between the N identical slab waveguides are reduced from infinity. Each confined mode of the single slab waveguide thus gives rise to a band with N nondegenerate modes. The dispersion relation (ω vs β) is shown in Figs. 3.2 and 3.3.

(b) Asymmetric Type

Consider a simple asymmetric N-channel waveguide with the following index of refraction

$$n(x,z) = \begin{cases} n_a & x < 0 \\ n_2 & m\Lambda \leq x < m\Lambda + b \\ & \quad (m=0, 1, 2, \ldots, N-1) \\ n_1 & \text{otherwise} \end{cases} \qquad (3.15)$$

The grand matrix which relates $\binom{A_a}{B_a}$ to $\binom{A_s}{B_s}$ in this case is easily obtained from the continuity condition and is given by

$$M = \begin{pmatrix} \frac{1}{2}(1+\frac{q}{q_a}) & \frac{1}{2}(1-\frac{q}{q_a}) \\ \frac{1}{2}(1-\frac{q}{q_a}) & \frac{1}{2}(1+\frac{q}{q_a}) \end{pmatrix} \begin{pmatrix} A & B \\ C & D \end{pmatrix}^N \qquad (3.16)$$

Similarly, the mode dispersion relation is given by

$$(A + \frac{q_a-q}{q_a+q} C) \frac{\sin NK\Lambda}{\sin K\Lambda} - \frac{\sin(N-1)k\Lambda}{\sin k\Lambda} = 0 \qquad (3.17)$$

The eigenvalues β are determined as in the symmetric case (3.14). The
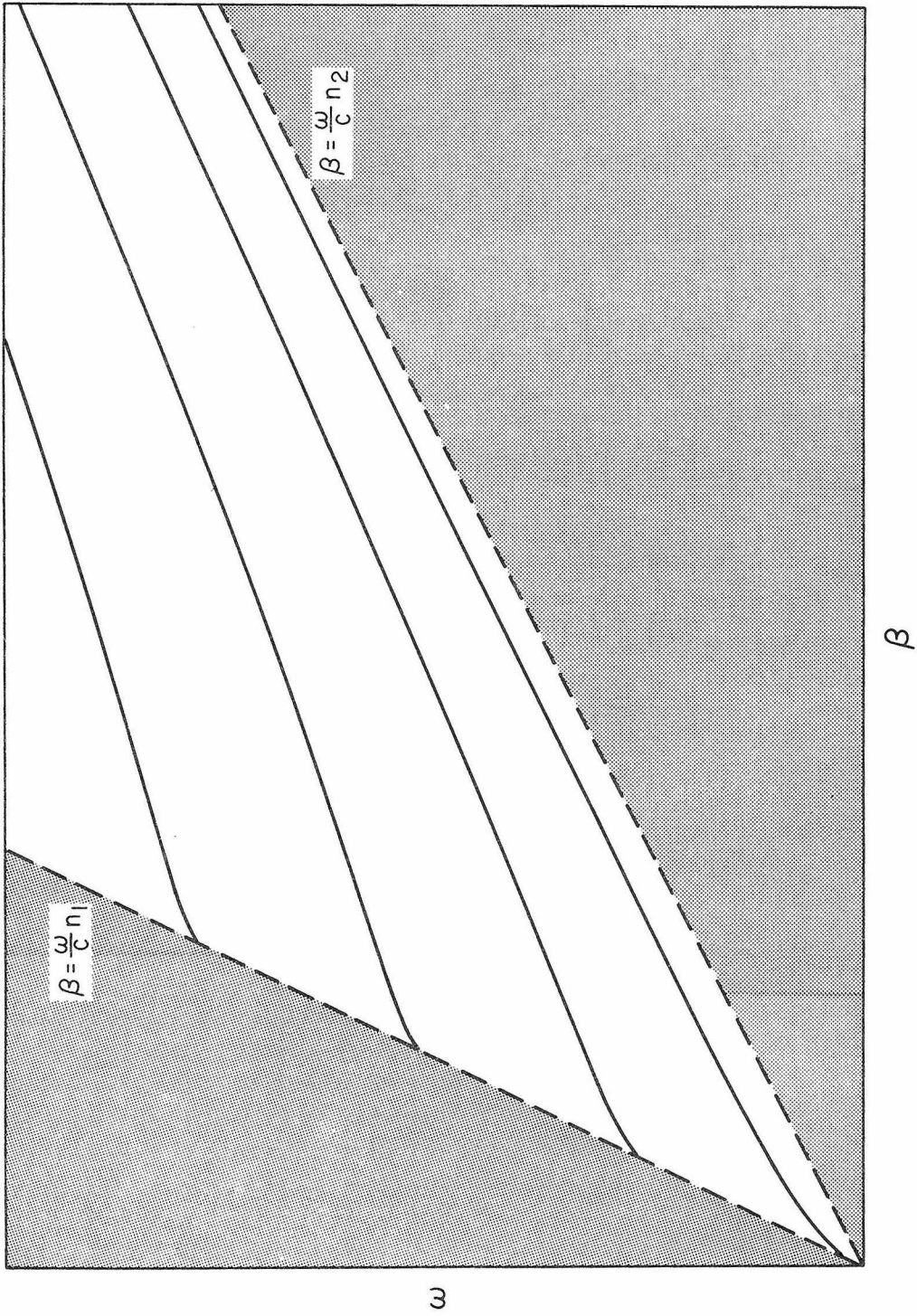
Fig. 3.2 Dispersion curves for the confined modes of a typical single

channel waveguide (N=1).

$\beta = \frac{\omega}{c} n_2$
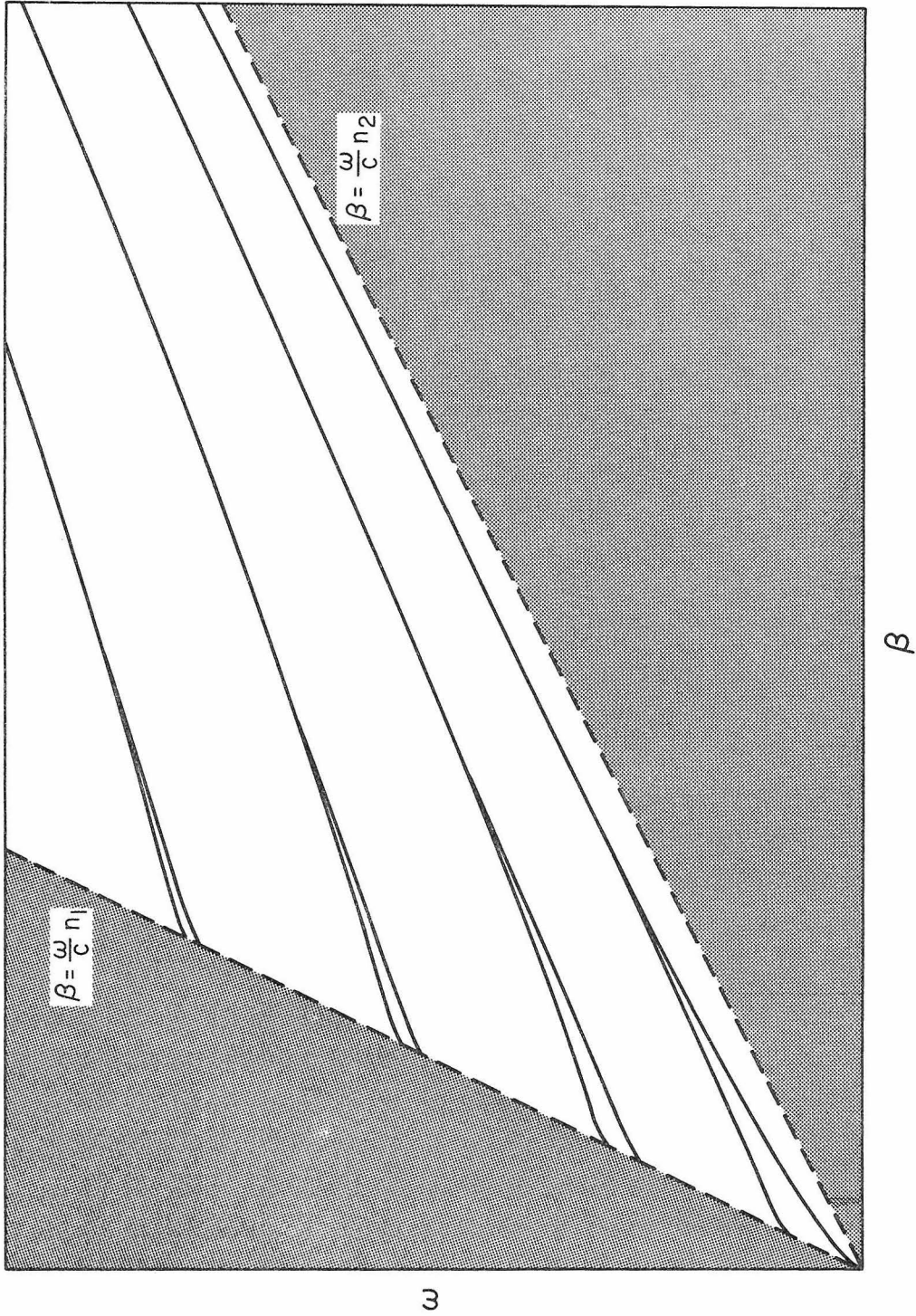
$\beta = \frac{\omega}{c} n_1$

β

Fig. 3-3 Dispersion curves for the confined modes of a typical

2-channel waveguide (N=2). Notice the splitting in

comparison with Fig. 3.2.

above equation can be reduced to equation (3.14) which is the mode condition for a symmetric N-channel waveguide by setting $n_a = n_1$.

Associated with each β of a confined mode at a given frequency, there is a corresponding Bloch K vector given by (2.37). Instead of having all eigenvalues (β's) in the allowed band, an asymmetric periodic N-channel waveguide can have some eigenvalues (β's) with corresponding complex K and thus be in the "forbidden" band. These modes can be traced in terms of perturbation theory to the unperturbed modes of the surface channels in terms of perturbation theory. The characteristics of those modes are the localization of energy near the surface. Eingevalues (β's) of the confined modes as a function of the separation between the neighboring channels are shown in Figs. 3.4 and 3.5 for two typical waveguiding structures. The band edges of the infinite periodic medium are also shown in the same figures. For small separation, all the modes have their eigenvalues in the allowed bands. There are exactly N β-levels in a complete band. At infinite separation the β-levels consist of an (N-1)-fold degenerate state and one nondegenerate state. The (N-1)-fold degenerate state will split into a band of (N-1) levels when the separation is finite. <u>Those (N-1) levels are always in the allowed band regardless of separation. The crossing between the nondegenerate state and the band edge happens at some critical separation a_c.</u> The surface modes only exist when the separation is larger than a_c. The properties of surface mode will be discussed more thoroughly in the next section.
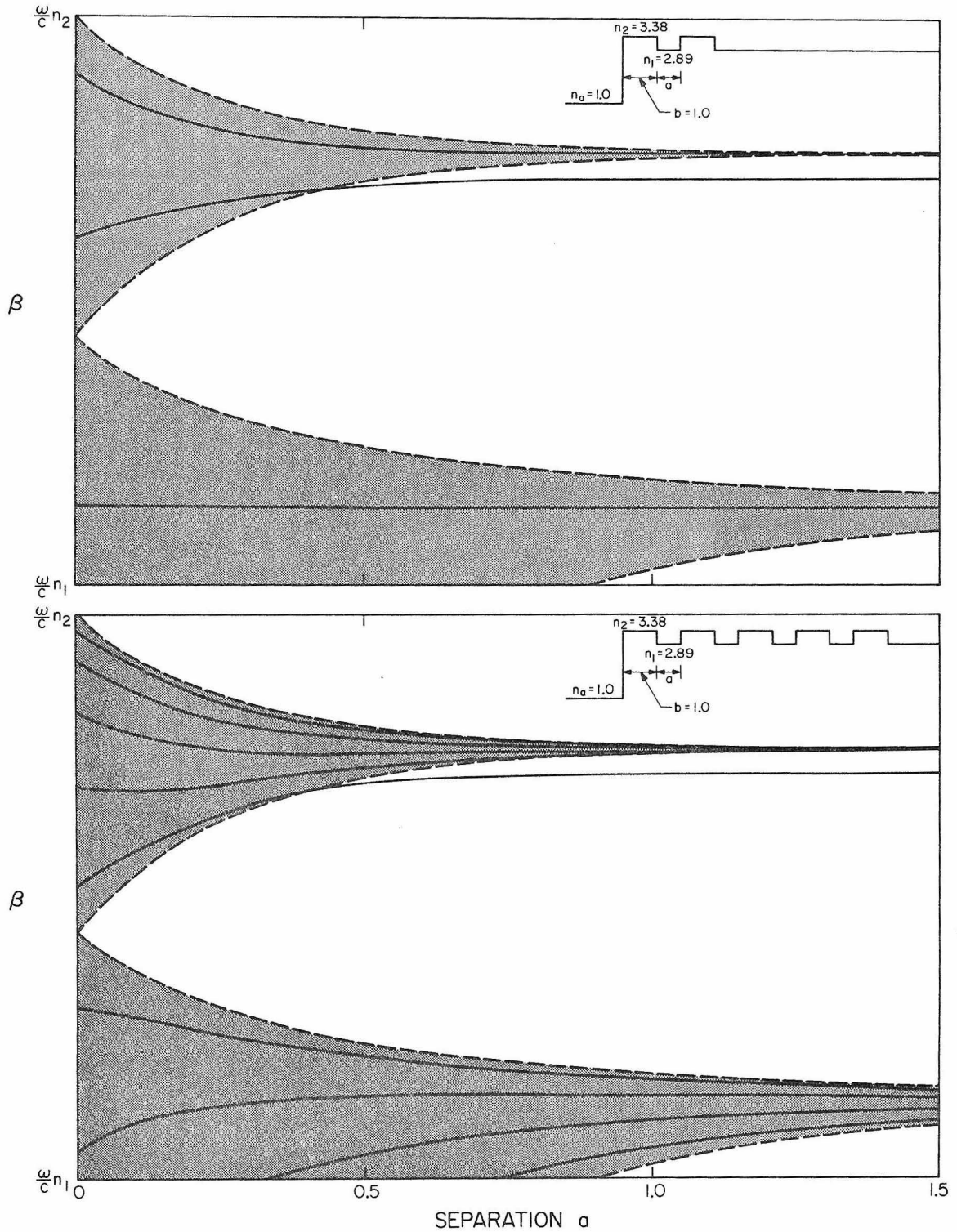
Fig. 3.4 β vs separation for two asymmetric multichannel waveguides with N=2 (upper diagram) and N=5 (lower diagram) at $\omega = \frac{3}{4} \pi \frac{c}{a}$. The dark zones are the allowed bands. Dashed curves are the band edges. The inset shows the refractive index profile.
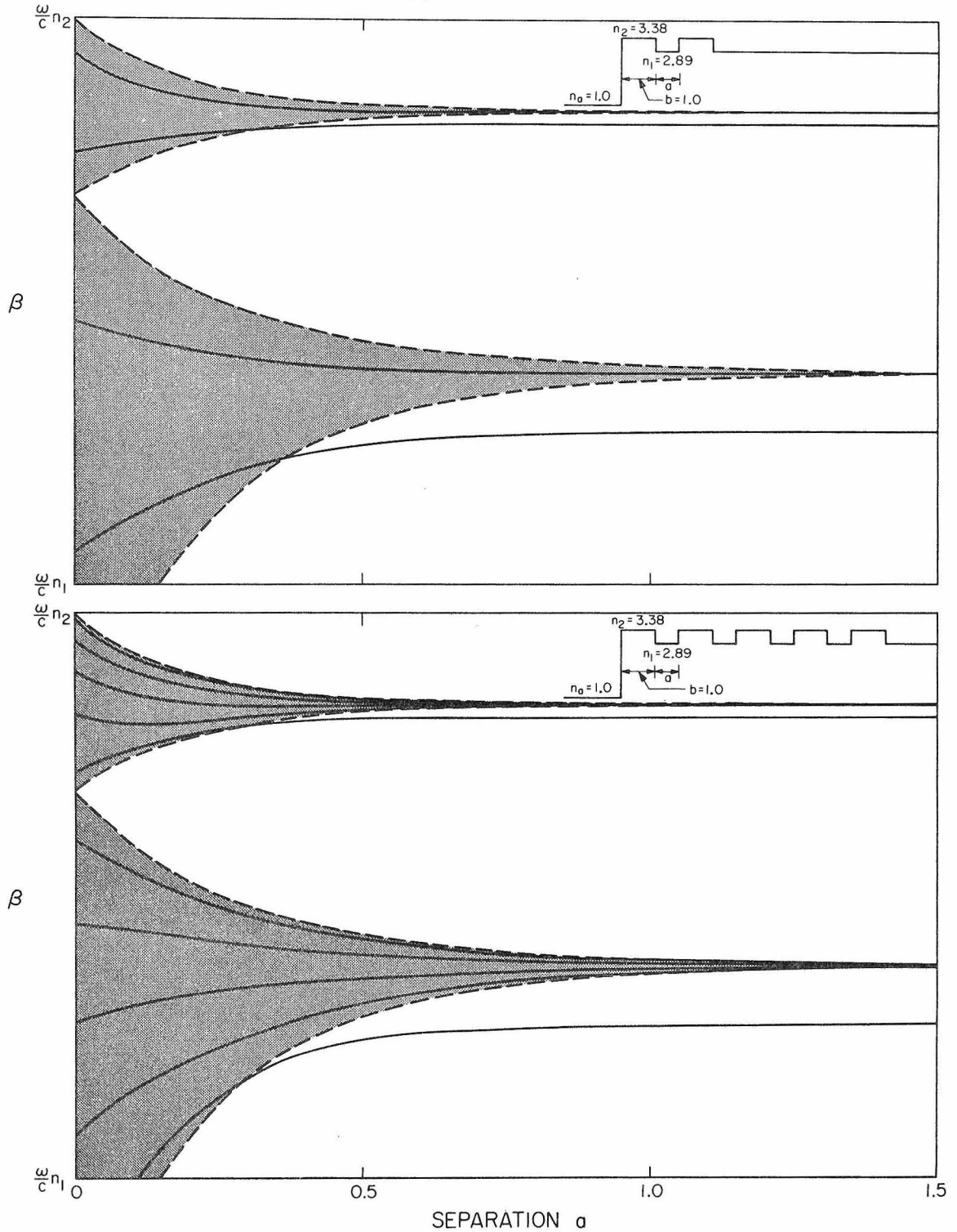
Fig. 3.5 β vs separation for two asymmetric multichannel waveguides with N=2 (upper diagram) and N=5 (lower diagram) at $\omega = \pi \frac{c}{a}$. The dark zones are the allowed bands. Dashed curves are the band edges. The inset shows the refractive index profile.

The transverse field distributions for a few typical periodic multichannel asymmetric dielectric waveguides are shown in Figs. 3.6 and 3.7 with N = 2 and 5, respectively. Only the confined modes in the first allowed band which corresponds to the lowest order modes of the uncoupled individual channel waveguide are shown. As we know, there are exactly N modes in each complete group. The modes will be designated as TE_{mn} and TM_{mn} with n as the band index (n = 0,1,2,$\cdots$) and m as the mode index (m = 0,1,2,$\cdots$,N-1). There are exactly (m+nN) zero crossings in the transverse field distribution for the mnth mode with n zero crossings in each guiding channel and m zero crossings in the (N-1) separation layers. The field can have at most one zero crossing in each separation layer where the wave is evanescent.

The field distribution depends strongly on the index of refraction of the superstrate n_a when n_a is near n_1. The variation for the fundamental mode is shown in Figs. 3.8 and 3.9 for N = 2 and 5, respectively. There is a drastic change of the field distribution for the surface channel when n_a is varied slightly from n_1. This phenomenon will be very useful in branching waveguide if a superstrate material with electrooptic effect can be found so that n_a can be tuned slightly around n_1 by applying a dc field

$$n_a = n_a(E^{DC} = 0) + \alpha E^{DC} \qquad (3.18)$$
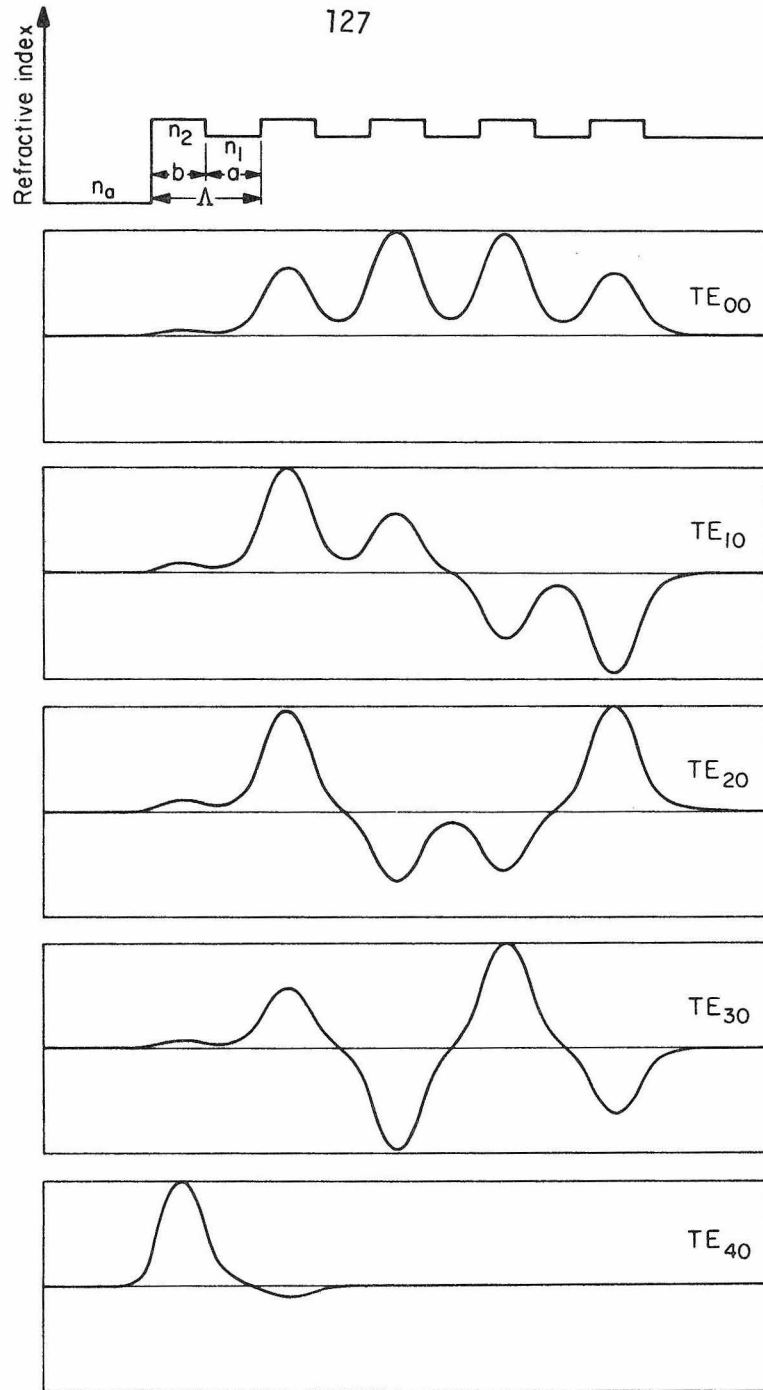
with

$$n_a(E^{DC} = 0) = n_1 \qquad (3.19)$$

This drastic change of the field distribution due to slight variation of n_a can be used in electrooptic modulation [8].
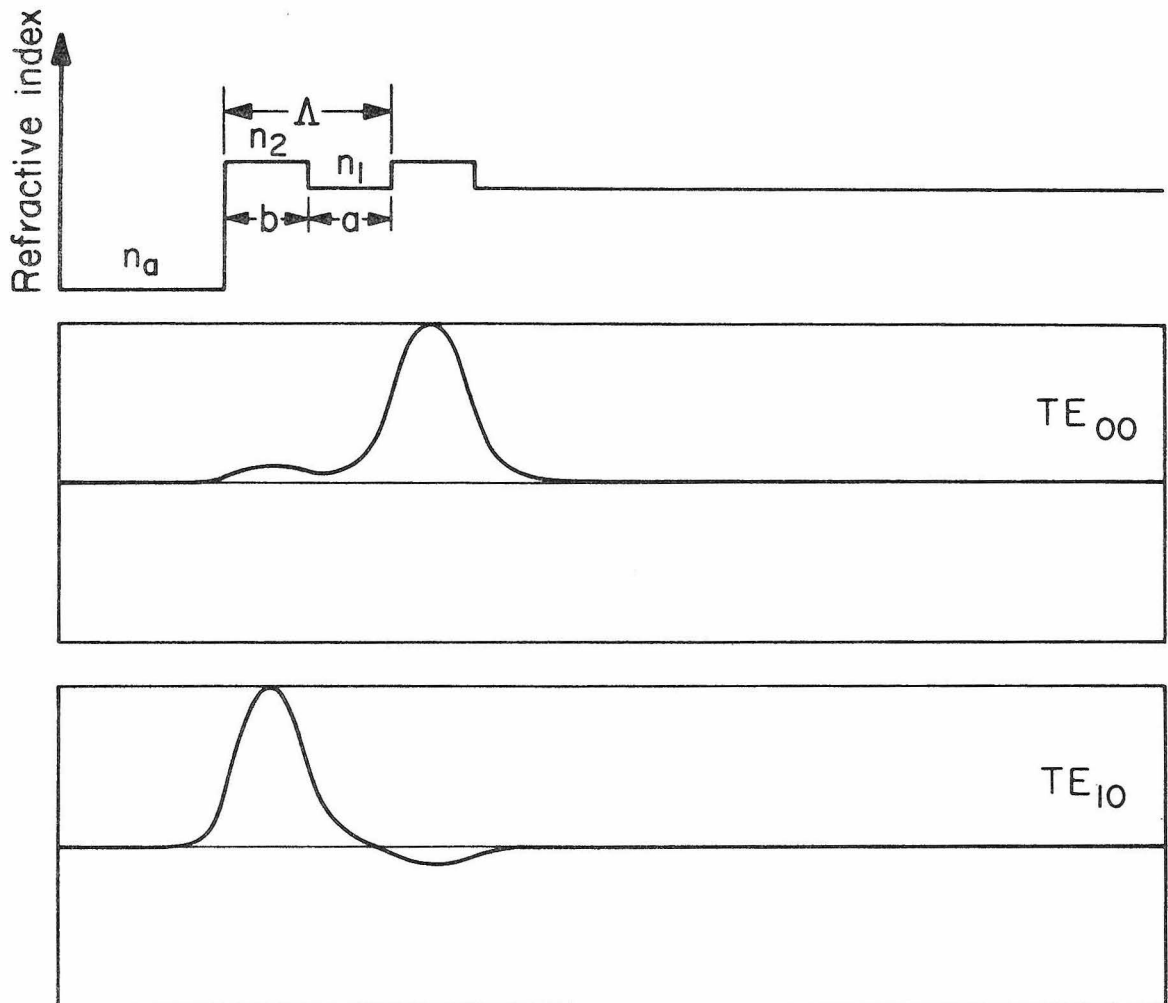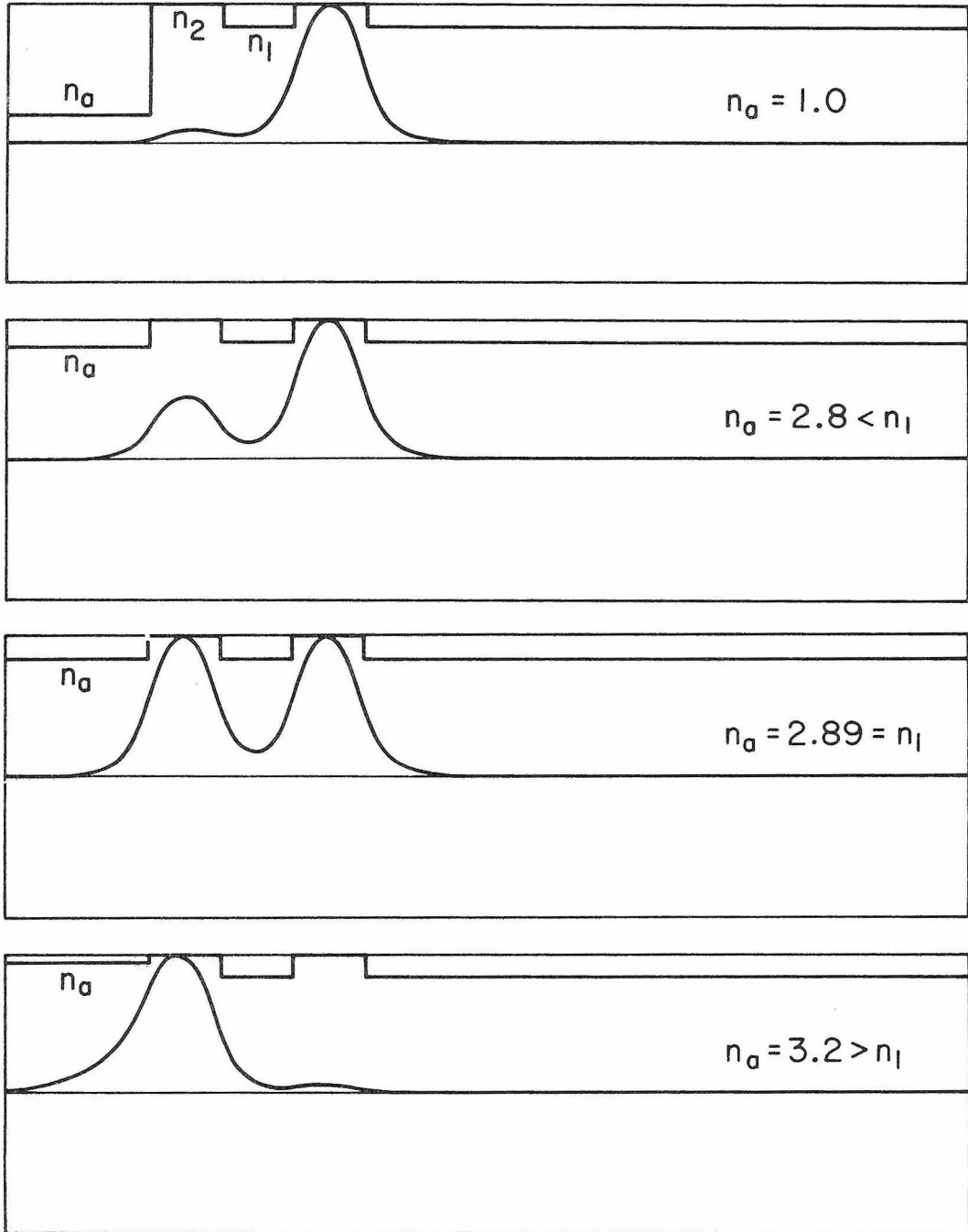
Transverse field distribution

Fig. 3.6   Transverse field distribution for the confined modes in the

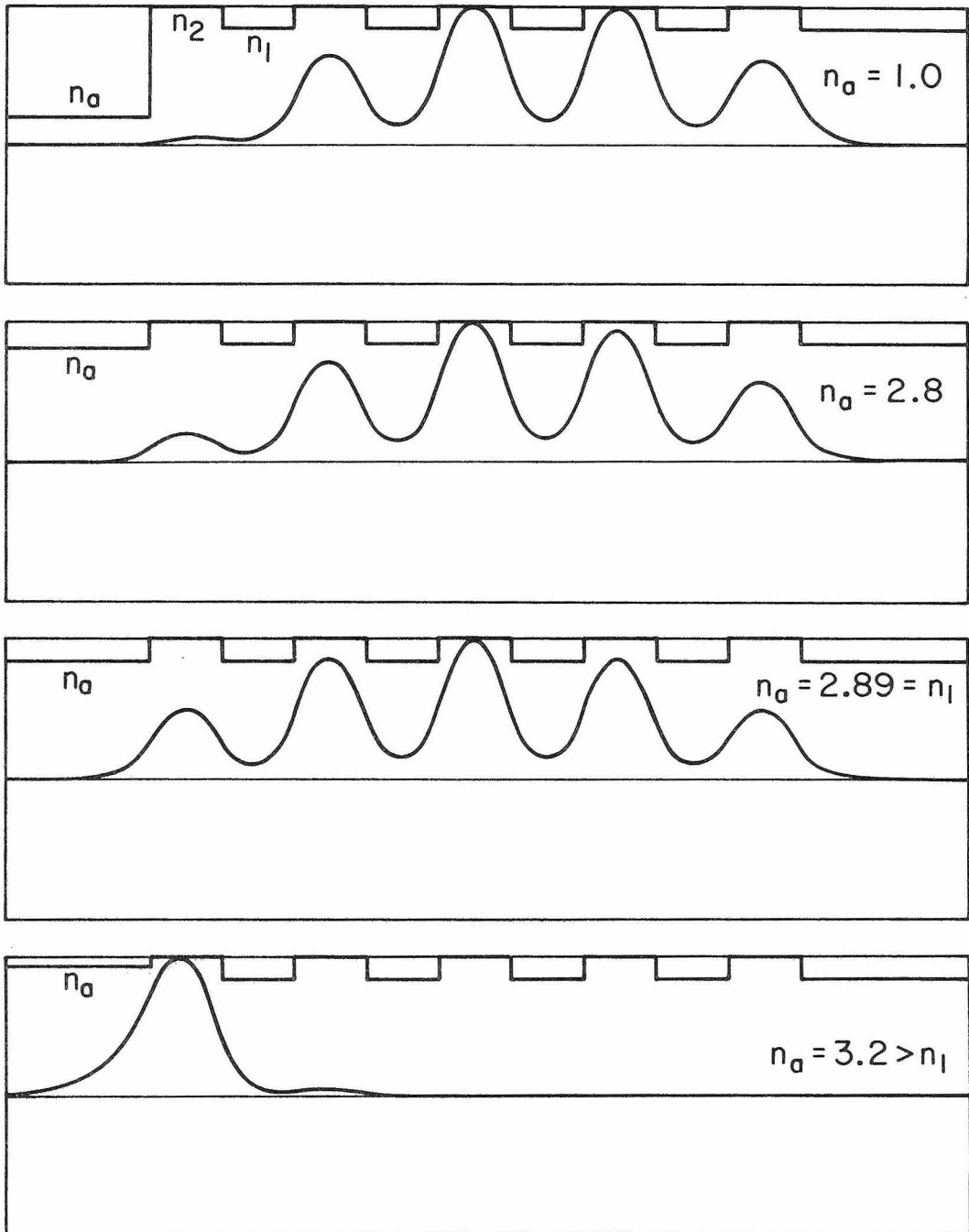first band of a 2-channel waveguide.

Transverse field distribution

Fig. 3.7 Transverse field distribution for the confined modes in the first band of a 5-channel waveguide.

Transverse field distribution

Fig. 3.8 Transverse field distribution for the TE_{00} mode of a 2-channel waveguide at various n_a's.

Transverse field distribution

Fig. 3.9 Transverse field distribution for the TE_{00} mode of a 5-channel waveguide at various n_a's.

In the above analysis we assumed that the refractive index of the substrate $n_s = n_1$ for simplicity of calculation. This is the reason why only one surface mode is found. In general, if $n_1 \neq n_s < n_2$, two surface modes will exist. This is similar to the surface states in a crystal where the number of surface states is equal to the number of surface atoms. Here the number of surface modes is equal to the number of surface channels.

It has been shown in the above analysis that there are exactly N modes in each band. However, not all the modes need be confined. A confined mode must have its propagation constant β satisfy

$$\beta_{min} < \beta < \beta_{max} \qquad (3.20)$$

with

$$\beta_{max} = \frac{\omega}{c} n_2 \qquad (3.21)$$

$$\beta_{min} = \max(\frac{\omega}{c} n_a, \frac{\omega}{c} n_s) \qquad (3.22)$$

so that the wave is propagating in the guiding channels and evanescent in the substrate and cladding regions. For large enough separation between channels the whole band of β-levels will fall between β_{max} and β_{min} so that all the N modes are confined. As the guiding channels are brought closer together, the β-levels "repel" each other. As a result some of the modes will find their β-value expelled from the confined region in β space. Those modes are transformed into radiation modes ($\beta < \beta_{min}$). The transition is shown in Figs. 3.4 and 3.5.

3.4 Electromagnetic Surface Wave

It is the purpose of this section to investigate electromagnetic surface waves guided by the boundary of a semi-infinite periodic multi-layer dielectric medium. The surface wave, by definition, is a wave bounded by the interface between two semi-infinite systems. For example, the ripple phenomenon in water is a surface wave guided by the interface between air and water. Another interesting kind of surface wave is the electronic surface state which has been extensively studied in solid state physics. The electromagnetic surface state was considered in an approximate manner by Arnaud and Saleh [9]. In this paper, the band theory of the periodic dielectric medium is employed to study the surface wave with an eigenvalue in the "forbidden" band.

The existence of a surface state can be explained as follows: In Section 2.3 we have shown that, at a given frequency, there are regions of β, for which K is complex and $K = \frac{m\pi}{\Lambda} \pm iK_i$. For an infinite periodic medium the exponential intensity variation cannot exist, and we refer to these regions as "forbidden". If the periodic medium is semi-infinite, the exponentially damped solution is a legitimate solution near the interface and the field envelope decays as $\exp(-K_i x)$ where x is the distance from the interface.

The existence of surface states can also be argued using perturbation theory. According to perturbation theory, the periodic multi-layer dielectric medium which consists of alternating layers of different indices of refraction can be considered as a system of interacting waveguides. These waveguides are identical to each other except for the one near the surface. The interaction strength between the waveguides

depends on the separation between the neighboring waveguides due to overlap of the evanescent field distributions. When the separation is infinite, there is no interaction and the guides can be considered as independent of each other. The eigenvalues (β's) thus fall into two groups: One is an infinitely degenerate state, the other is a nondegenerate state which corresponds to the extreme guide near the surface. As the waveguides are brought together, the interaction between the waveguides causes the eigenvalues to split. The splitting is shown in Figures 3.4 and 3.5. As the eigenvalues split, the allowed energy band for the infinite structure is fully occupied by the levels originating in the infinitely degenerate level. As a result, the nondegenerate level corresponding to the waveguide near the surface will be expelled out of the allowed energy band. The only place where this state can be accommodated is in the forbidden gap. The field distribution for this state is localized near the surface because of he fact that the corresponding eigenvalue is in the "forbidden" band, i.e., $K = \frac{m\pi}{\Lambda} + iK$.

To investigate the properties of the surface modes consider a semi-infinite periodic multilayer dielectric medium consisting of alternating layers of different indices of refraction. The distribution of the indices of refraction is

$$
n(x,z) = \begin{cases} n_a & x \leq 0 \\ n_2 & m\Lambda \leq x < m\Lambda + b \\ n_1 & m\Lambda + b \leq x < (m+1)\Lambda \quad (m=0,1,2,\cdots) \end{cases} \tag{3.23}
$$

The geometry of the structure is sketched in Figure 3.10. We look for the possibility of waves propagating in the positive z direction. Since the structure is semi-infinite, we are only interested in the surface wave as far as guiding is concerned. For the sake of definiteness we consider the case of TE surface modes where the electric field is polarized in the y direction. The electric field distribution (TE) obeys the wave equation

$$\frac{\partial^2}{\partial x^2} E(x) + \frac{\omega^2}{c^2} n^2(x) E(x) = 0 \tag{3.24}$$

We take the solution in the following form:

$$E(x) = \begin{cases} \alpha e^{q_a x} & x \leq 0 \\ E_K(x) e^{iKx} & x \geq 0 \end{cases} \tag{3.25}$$

where q_a is given by

$$q_a = \sqrt{\beta^2 - (\frac{\omega}{c} n_a)^2} \tag{3.26}$$

and α is a constant.

In order to be a guided wave, the constant K in (3.25) must be complex so that the field decays as x goes to infinity. This is possible only when the propagating conditions (i.e., β) in the periodic medium correspond to a "forbidden" band. Another condition is that E(x) and its x derivative be continuous at the interface with medium "a". This gives us the condition for surface modes:
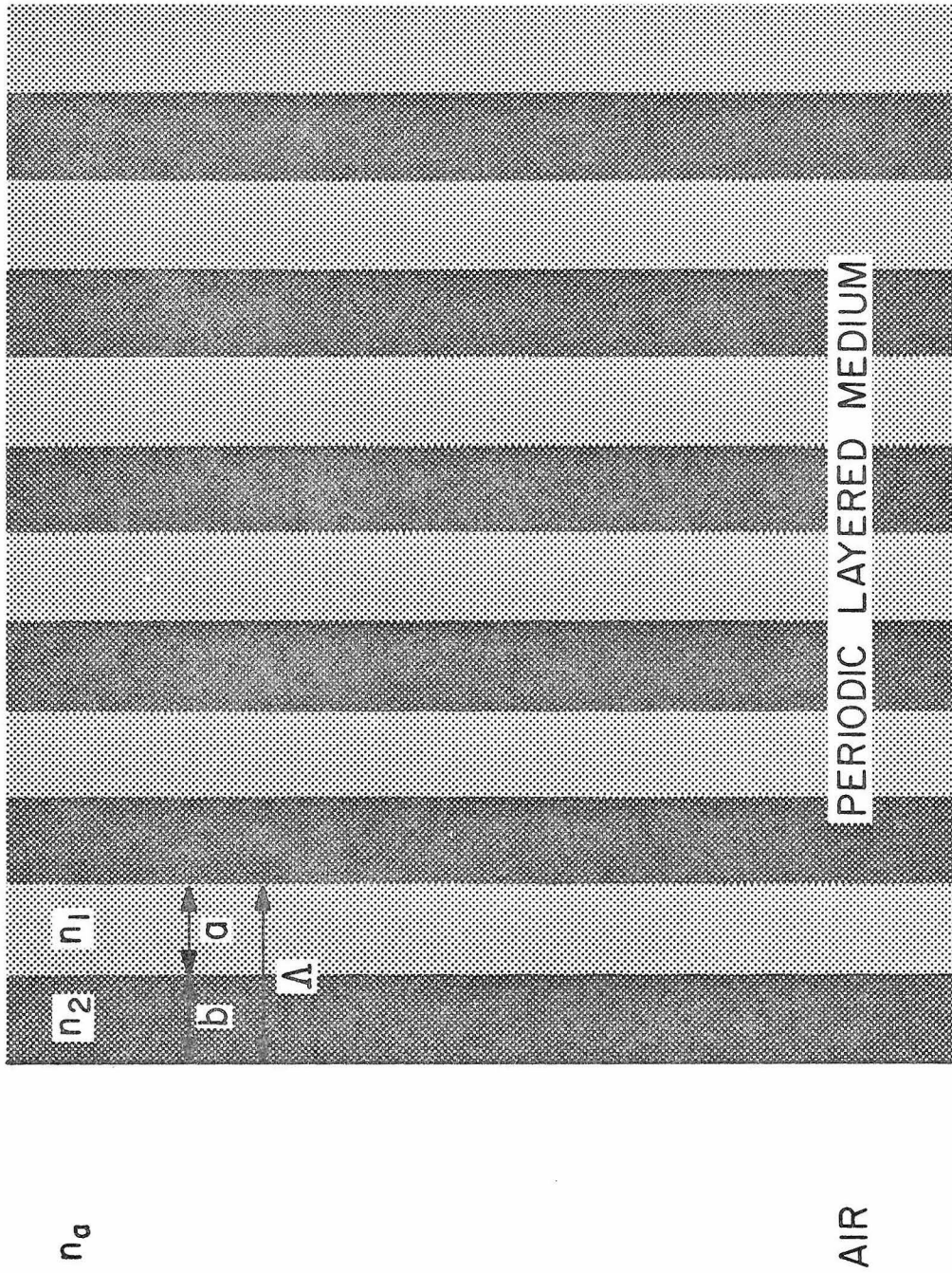
Fig. 3.10 A semi-infinite periodic stratified medium.

$$q_a = q \frac{e^{-iK\Lambda} - A - B}{e^{-iK\Lambda} - A + B} \qquad (3.27)$$

The field distributions of some typical surface waves are shown in Figures 3.11 and 3.12. It is evident that the energy is more or less concentrated in the first few periods of the semi-infinite periodic medium. It can easily be shown that

$$\frac{\text{Energy in the first period}}{\text{Energy in the whole semi-infinite periodic structure}} = (1 - e^{-2K_i\Lambda})$$

$$(3.28)$$

where K_i is the imaginary part of K. Generally, speaking, the fundamental surface wave has the highest K_i and hence the highest degree of localization. The fundamental surface wave may happen to be in the 0th or the 1st forbidden gap. It depends on the magnitude of the index of refraction n_a. For n_a less than n_1 which is a case of practical interest, (n_a = index of refraction of air) the fundamental surface wave has a Bloch wave vector in the first forbidden gap. This is due to the fact that when the waveguides are separated infinitely from each other the singlet state has an eigenvalue β lower than that of the infinitely degenerate state.

The field distribution in each period is similar to that of the distribution in the preceding period except that the amplitude is reduced by a factor of $(-1)^m e^{-K_i\Lambda}$, where m is the integer corresponding to the mth forbidden gap.
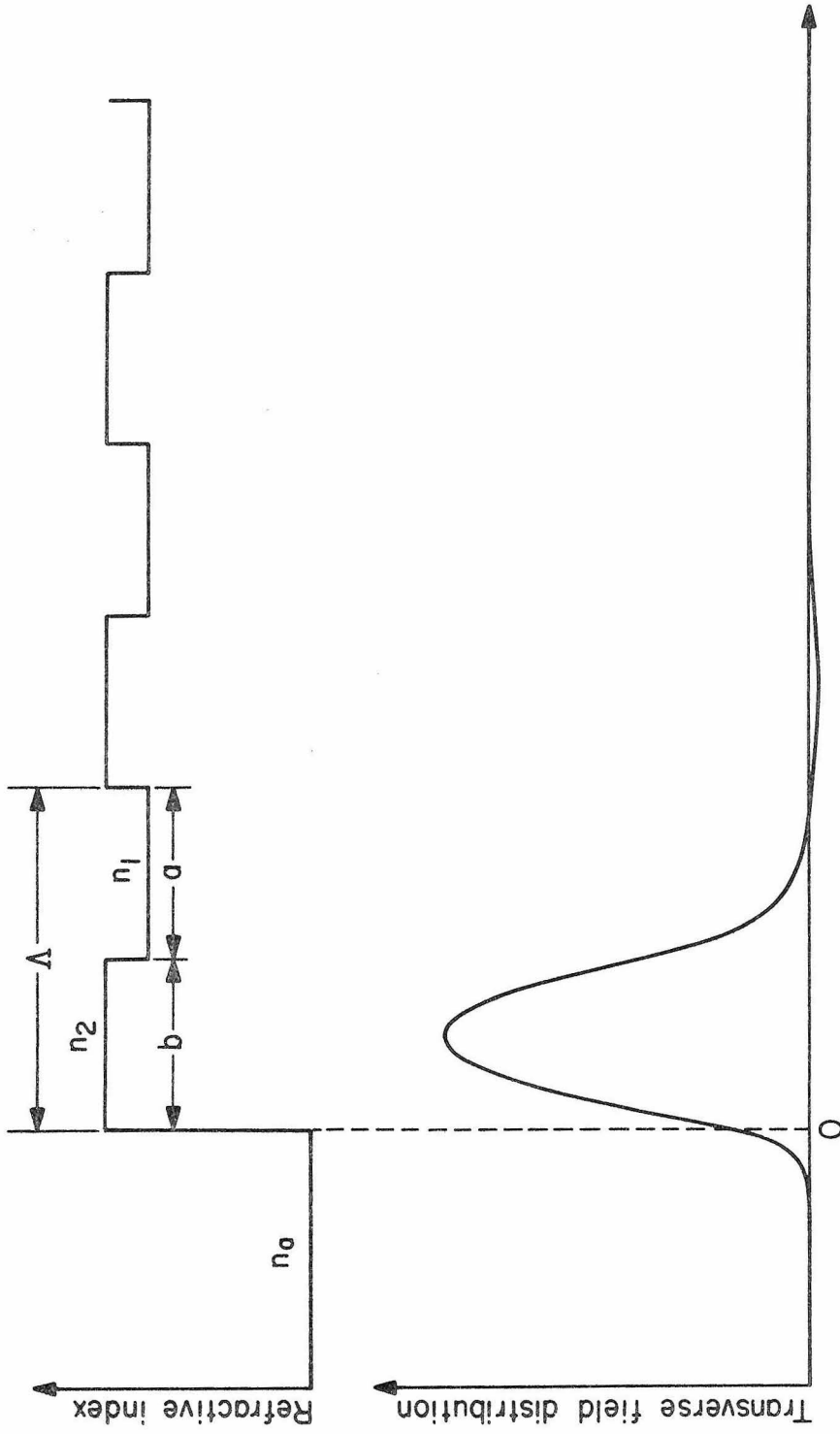
Fig. 3.11 Transverse field distribution for a typical fundamental surface mode guided by the surface of a semi-infinite periodic stratified medium.
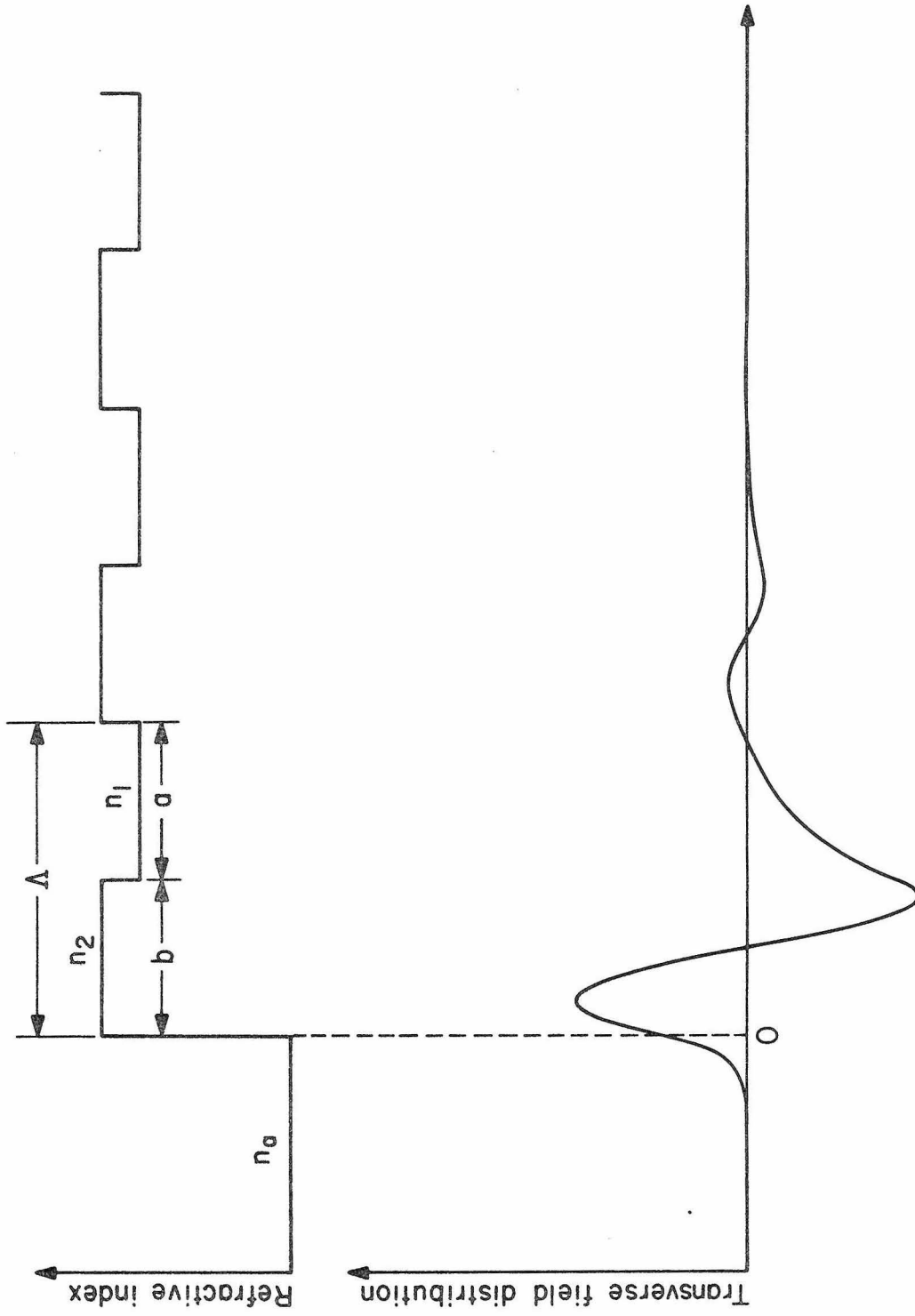
Fig. 3.12 Transverse field distribution for a typical higher order surface mode guided by a semi-infinite periodic stratified medium.

We have derived the mode condition for the surface wave by matching the boundary condition between an evanescent wave and a decaying Bloch wave. This electromagnetic surface wave is almost completely analogous to the surface state in solid state physics. The existence of the surface mode in a semi-infinite structure is independent of the separation between waveguides, because the allowed band is always fully occupied. However, in a finite system, the allowed band is not fully occupied. As a result, the surface wave appears only when the separation is <u>large</u> enough so that one of the eigenvalues falls within the "forbidden" gap (see Figures 3.4 and 3.5). This state of affairs is quite different from that of electronic surface states in crystals where, according to Shockley [10], surface levels appear only when the interatomic distance becomes small enough so that the boundary curves of the allowed energy bands have crossed. The number of surface modes equals the number of modes that can be guided by the waveguide near the surface. This is very comprehensible in terms of perturbation theory.

The surface mode can still be guided when $n_2 < n_1$, however, the local extrema occur in the regions with index n_1 where the x dependence is sinusoidal. This is a general property of evanescent wave. The field distribution profile can bend at most once in the region where the wave is evanescent. The bending corresponds to a local minimum of the magnitude of field distribution. Because of the fact that $\frac{1}{E} (\frac{\partial^2 E}{\partial x^2})$ is always positive, for $E > 0$ the field distribution profile is concave upward, while for $E < 0$ the field distribution profile is concave downward. This makes it impossible for $|E(x)|$ to possess a local maximum in the region where the wave is evanescent.

In the above analysis we assumed $\frac{\omega}{c} n_1 < \beta < \frac{\omega}{c} n_2$ so that the field is propagating (i.e., has a sinusoidal x-profile) in the higher index medium while being evanescent in the lower index medium. However, this condition is not necessary. Surface waves exist also when $\beta < \frac{\omega}{c} n_{1,2}$. The analysis in this case is exactly the same as that above except that q has to be replaced by $-ik_{1x}$. The guiding, however, is not as tight as that of the former case, since the Bloch waves decay faster whenever there is a region where the wave is evanescent.

The surface wave does not exist, however, when $\beta > \frac{\omega}{c} n_{1,2}$ since in this case $\frac{1}{E} \frac{\partial^2 E}{\partial x^2} > 0$ everywhere so that if the field is evanescent in the homogeneous medium "a", it will increase without bound in the periodic medium and vice versa.

3.5 Optical Interface Modes

It is well known in semiconductor physics that electronic interface states exist at the interface between two semiconductors [8]. This has been extensively studied in the area of solid state devices where the junctions are the main feature of these devices. It is not difficult to believe that optical interface states can also exist at the interface between two periodic layered media.

In what follows, we will derive the dispersion relation for the interface modes. The analysis is similar to that of the surface modes except that the air is now replaced by another layered medium. The distribution of the refractive index is given by

$$
n(x,z) = \begin{cases} n_1 & m\Lambda + b \leq x < (m+1)\,\Lambda \\[6pt] n_2 & m\Lambda \leq x < m\Lambda + b \\[6pt] n_3 & -(m+1)\Lambda' \leq x < -m\Lambda' - c \\[6pt] n_4 & -m\Lambda' - c \leq x < -m\Lambda' \\[6pt] & \qquad (m = 0,1,2,3,\cdots) \end{cases} \tag{3.29}
$$

The geometry of the structure is sketched in Figure 3.13.

We again look for the possibility of guided propagation in the positive z direction. Since the structure is infinite, we are interested only in the interfacial waves as far as guiding is concerned. We will again analyze this problem for TE waves only. The analysis for TM waves is similar. We take the solution of the wave equation in the following form:

$$
E(x) = \begin{cases} E_K(x)\, e^{iKx} & x \geq 0 \\[10pt] E_{K'}(x)\, e^{-iK'x} & x \leq 0 \end{cases} \tag{3.30}
$$

In order to be a guided wave, the Bloch wave numbers K and K' must be complex so that the field decays as x goes to infinity.
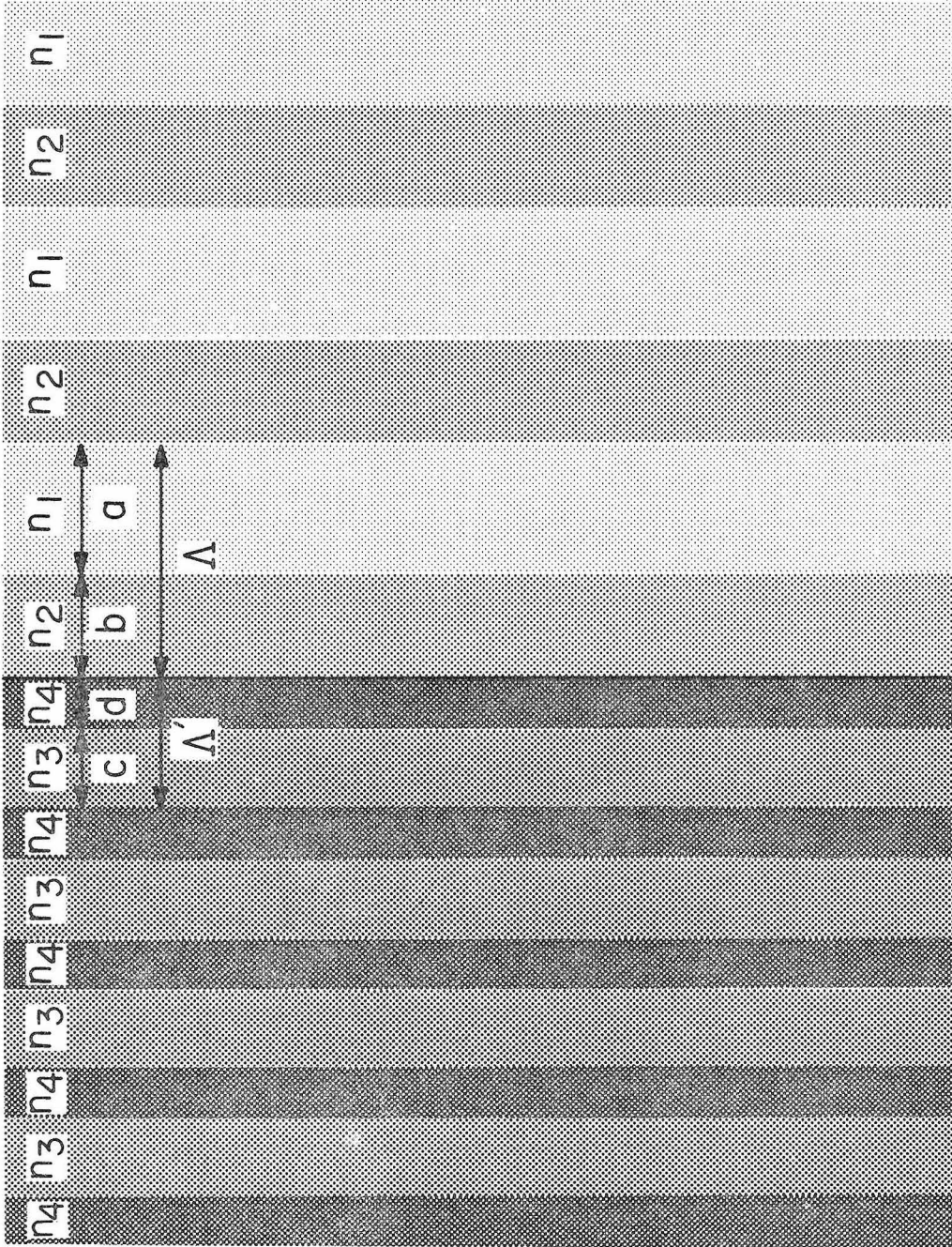
141

Fig. 3.13 Interface between two periodic layered media.

$$K = m\pi/\Lambda + iK_i$$

$$K' = m'\pi/\Lambda' + iK_i'$$

(3.31)

This is possible only when the "forbidden" bands of both layered media have some overlap and the propagation condition (i.e., β) has to be in these overlap regions. Another condition is that $E(x)$ and its x derivative be continuous at the interface. This gives us the dispersion relation:

$$-(-ik_{3x})(\frac{e^{-iK'\Lambda'} - A' - B'}{e^{-iK'\Lambda'} - A' + B'}) = (-ik_{1x})(\frac{e^{-iK\Lambda} - A - B}{e^{-iK\Lambda} - A + B})$$

(3.32)

The optical energy of these interface modes is also localized near the interface. A special case of particular interest is when $n_3 = n_1$, $n_4 = n_2$, $c = a$, and $d = b$. Under these conditions (3.32) becomes

$$(e^{-iK\Lambda} - A + B)(e^{-iK\Lambda} - A - B) = 0$$

(3.33)

The modes can be divided into two categories: (a) even modes with their maxima right at the interface, (b) odd modes with their node at the interface. Typical field distributions of this structure are shown in Figure 3.14. In general, the solution of (3.32) or (3.33) forms a discrete set of spectrum (β's). It is even possible that there is no solution of (3.32) for some particular cases.

3.6 Leak Consideration for Surface Waves

Because of the finite number of periods in the structure, the intensity of the substrate is not exactly zero (i.e., the surface modes

Fig. 3.14 An odd interface mode.

are leaky). This loss results in the attenuation of the surface mode in the direction of propagation. The following calculation is to find out the attenuation coefficient α for each surface mode. The time-averaged flux of energy is given by the real part of the complex Poynting vector

$$S = \frac{1}{2} \text{Re}(E \times H^*) \tag{3.34}$$

To evaluate the total power flow P, we integrate the z-component of S over the cross sectional area A:

$$P = \int_A S_z \, dxdy \tag{3.35}$$

The power loss due to flowing of energy into the substrate is given by

$$P_{loss} = \int_W S_x \, dzdy \tag{3.36}$$

where w is the wall area. The power flow along the guide can be written

$$P(z) = P_0 \, e^{-\alpha z} \tag{3.37}$$

Thus the attenuation coefficient is given by

$$\alpha = -\frac{1}{P} \left(\frac{dP}{dz}\right) \tag{3.38}$$

where $-\left(\frac{dP}{dz}\right)$ can be interpreted as the power loss per unit length of the guide. By combining (3.35), (3.36), and (3.37) we obtain

$$\alpha = \frac{S_x}{\int S_z \, dx} \tag{3.39}$$

In calculating the attenuation coefficient α, we have to use the unperturbed mode solution to evaluate the denominator of (3.39). However, we cannot use the unperturbed S_x, because for a guided mode $S_x = 0$. Nevertheless, S_x can be estimated by decomposing S_x into an outgoing part and an incoming part and taking the outgoing part as S_x. This procedure is legitimate because there is actually no incoming wave in a real structure.

Using the field distribution given in the previous section, we obtain

$$\int_{-\infty}^{N\Lambda} S_z \, dx = \frac{c\beta}{2\omega} \left\{ \frac{1}{2q_a} + \frac{1}{2} (F_1 a + F_2 b) \right\} \tag{3.40}$$

where

$$F_1 = \frac{1 - e^{-2(N+1)K_i\Lambda}}{1 - e^{-2K_i\Lambda}} \left[(1 + \frac{q_a^2}{k_2^2}) + \frac{\sin k_2 b}{k_2 b} \cos k_2 b (1 - \frac{q_a^2}{k_2^2}) \right]$$
$$- 2 \frac{q_a}{k_{2x}} \frac{\sin^2 k_2 b}{k_2 b} \tag{3.41}$$

$$F_2 = \frac{1 - e^{-2(N+1)K_i\Lambda}}{1 - e^{-2K_i\Lambda}} e^{-2K_i\Lambda} \left[(1 + \frac{q_a^2}{k_{1x}^2}) + \frac{\sin k_{1x} a}{k_{1x} a} \cos k_{1x} a (1 - \frac{q_a^2}{k_{1x}^2}) \right.$$
$$\left. - 2 \frac{q_a}{k_{1x}} \frac{\sin^2 k_{1x} a}{k_{1x} a} \right] \tag{3.42}$$

S_x is given by

$$S_x = \frac{c k_{2x}}{2\omega} \frac{1}{4} (1 + \frac{q_a^2}{k_{2x}^2}) e^{-2NK_i\Lambda} \tag{3.43}$$

Here we assume that the substrate has a refractive index of n_2. The attenuation coefficient α is thus given by

$$\alpha = \frac{k_{2x}}{4\beta} \left(1 + \frac{q_a^2}{k_{2x}^2}\right) \left\{\frac{1}{2q_a} + \frac{1}{2} (F_1 a + F_2 b)\right\}^{-1} e^{-2NK_i \Lambda} \tag{3.44}$$

For large number N, $e^{-2(N+1)K_i \Lambda}$ may be neglected in F_1, F_2. Thus we see that α decays as $e^{-2NK_i \Lambda}$ as N increases:

$$\alpha \underset{N \to \infty}{\sim} e^{-2NK_i \Lambda} \tag{3.45}$$

A typical case is shown in Figure 3.15.
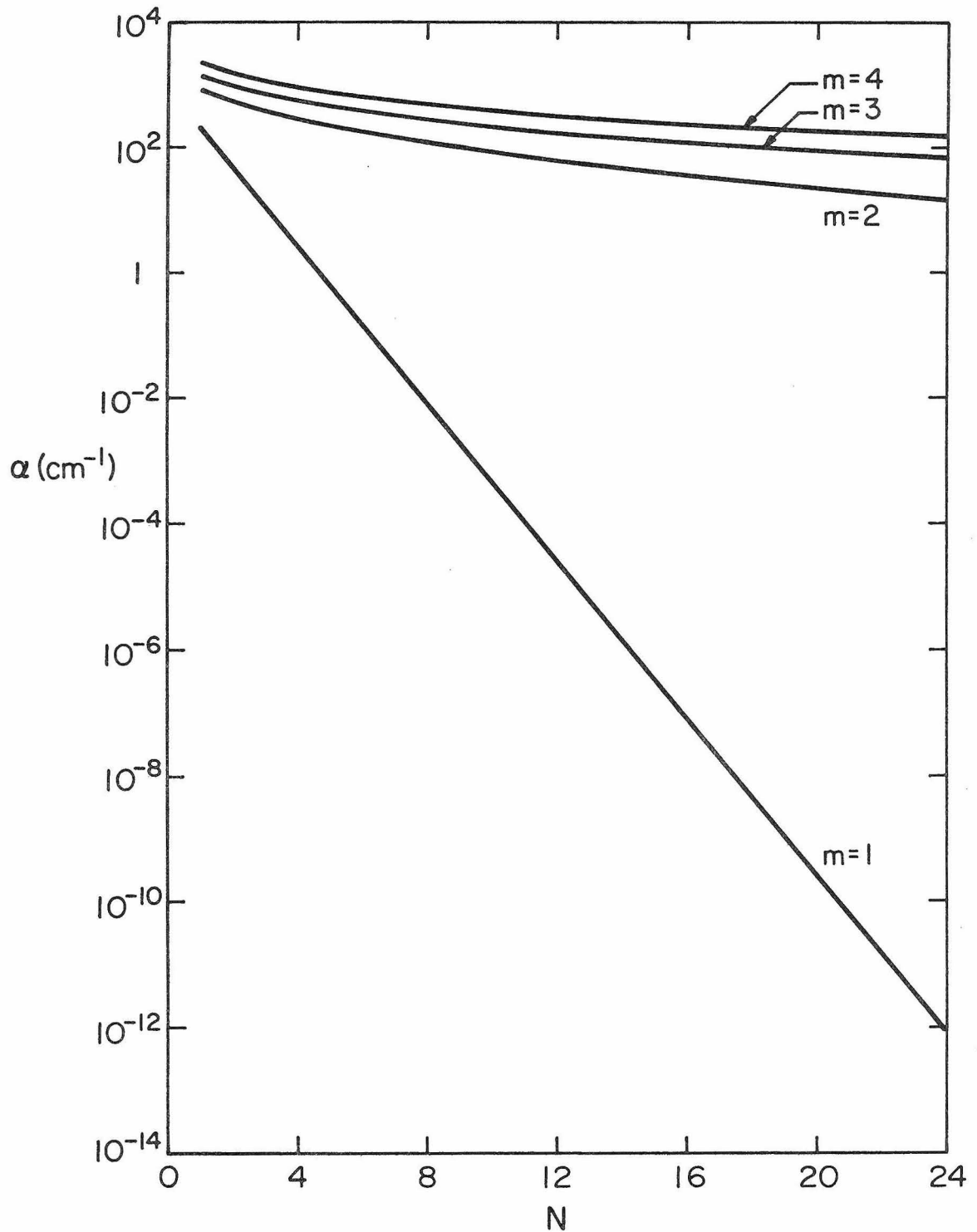
Fig. 3.15   Attenuation coefficient α vs. number of periods N for the

four surface modes supported by a periodic layered medium.

References - Chapter 3

1. S. C. Frautschi, <u>Regge Poles and S-Matrix Theory</u> (W. A. Benjamin, New York, 1963).

2. T. Regge, Nuov. Cim. <u>14</u>, 951 (1959).

3. See, for example, R. E. Collin and F. J. Zucker, <u>Antenna Theory</u> (McGraw-Hill, New York, 1969).

4. See, for example, R. E. Collin, <u>Field Theory of Guided Waves</u> (McGraw-Hill, New York, 1960).

5. H. Yajima, Proc. Symp. Optical and Acoustical Micro-Electronics, New York, April 1974.

6. L. B. Stotts, Optics Comm. <u>17</u>, 133 (1976).

7. S. Somekh, E. Garmire, A. Yariv, H. Garvin, R. Hunsperger, Appl. Phys. Lett. <u>22</u>, 46 (1973).

8. A. B. Buckman, J. Opt. Soc. Am. <u>66</u>, 30 (1976).

9. J. A. Arnaud and A.A.M. Saleh, Appl. Opt. <u>13</u>, 2343 (1974).

10. W. Shockley, Phys. Rev. <u>56</u>, 317 (1939).

Chapter 4
BRAGG WAVEGUIDES

4.1 Introduction

Optical dielectric waveguides with a slab configuration are capable of supporting lossless confined modes provided the index of refraction of the inner layer exceeds the indices of the two bounding media. This condition is necessary to obtain an imaginary transverse propagation constant which corresponds to an evanescent decay of the mode field in the bounding media.

There are many practical situations where it is desirable or necessary to guide power in a layer with a lower index than that in the two bounding media. A prime example of such a case is the waveguide laser in which the inner layer is air. This situation leads to lossy (leaky) modes whose loss constant increases as the third power of the reciprocal thickness of the inner layer.

In a Bragg waveguide the conventionally used substrate is replaced by a periodic layered medium. The use of Bragg reflection in waveguiding was first suggested by Fox [1] and recently by Yeh and Yariv [2]. It is shown that confined guiding with arbitrarily low loss is possible even when the guiding layer possesses an index of refraction which is <u>lower</u> than that of the periodic layered substrate. The propagation may be considered formally as that of a plane wave zigzagging inside the guiding (n_g) layer and undergoing total internal reflection at the interface ($x = -t$) with the low index medium (n_a) and Bragg reflection at the

interface (x = 0) with the layered medium. Bragg total reflection happens only when the incidence angle satisfies the Bragg condition, or more exactly, that the propagation conditions inside the periodic layered medium fall within one of the optical "forbidden" gaps.

The introduction of Bragg waveguides opens a new dimension for light propagation in integrated optics. It is now possible to guide a light wave in a low refractive index film. Before we study the mode properties of a Bragg waveguide, we will first show some important characteristics of Bragg reflectors in the following section.

4.2 Bragg Reflector

Periodic perturbation in a dielectric medium has been used extensively in fabricating distributed feedback lasers [3,4] (DFB) and distributed Bragg reflection lasers [5] (DBR). Corrugation over the guiding layer is the usual way of providing periodic perturbation. The optical fields are determined by using the coupled-mode theory [6], which is a very good approximation as long as the perturbation is small. In the case of square well alternation, which corresponds to the layered medium described above, an exact solution is obtained by our matrix method.

Consider a periodically stratified medium with N unit cells. The geometry of the structure is sketched in Figure 4.1. The coefficient of reflection is given by

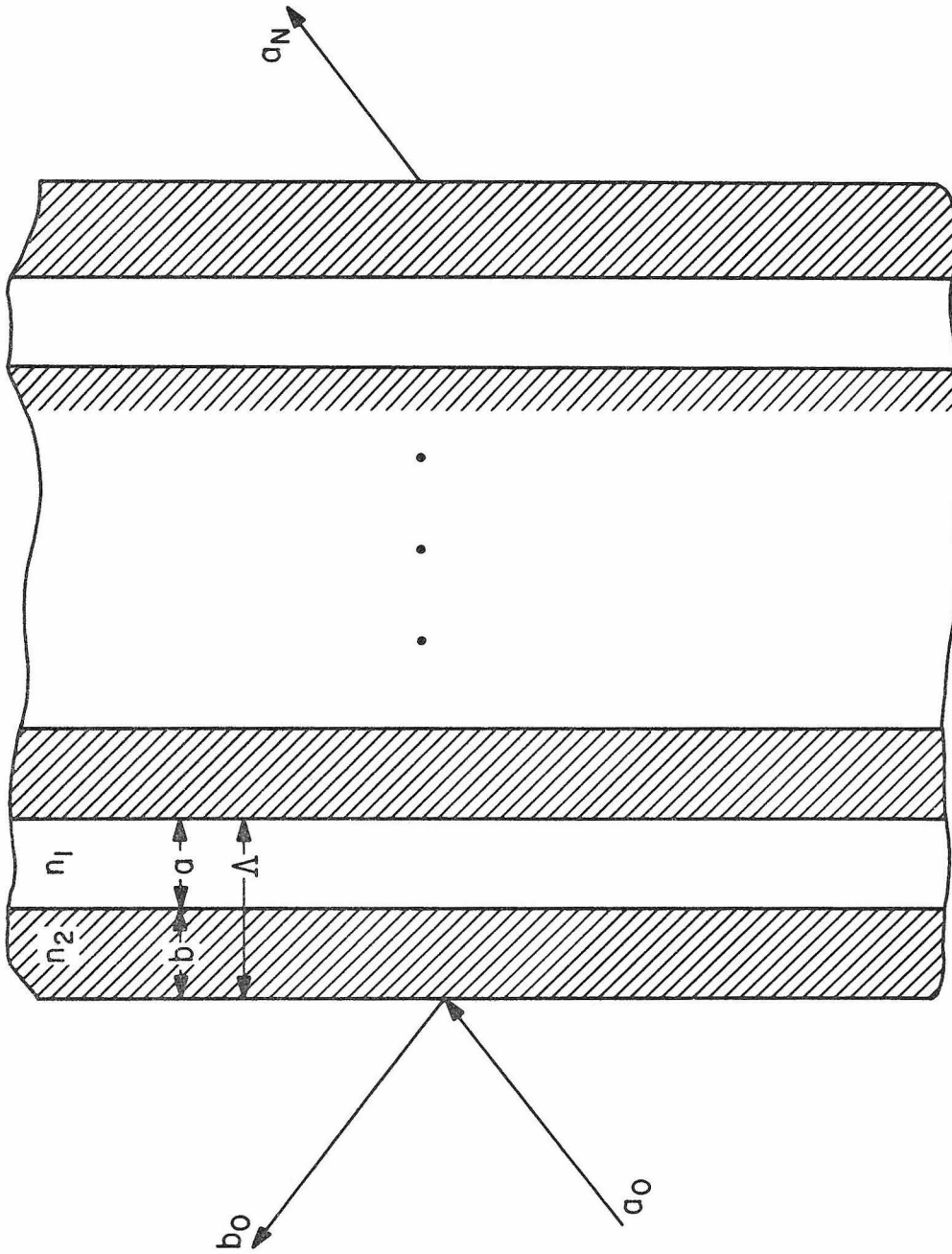$$r_N = \left(\frac{b_0}{a_0}\right)_{b_N=0} \tag{4.1}$$

Fig. 4.1   Geometry of a typical N-period Bragg reflector.

From (2.27) we have the following relation

$$\begin{pmatrix} a_0 \\ b_0 \end{pmatrix} = \begin{pmatrix} A & B \\ C & D \end{pmatrix}^N \begin{pmatrix} a_N \\ b_N \end{pmatrix} \tag{4.2}$$

The Nth power of an unimodular matrix can be simplified by the following matrix identity [7] (see Appendix D)

$$\begin{pmatrix} A & B \\ C & D \end{pmatrix}^N = \begin{pmatrix} AU_{N-1} - U_{N-2} & BU_{N-1} \\ CU_{N-1} & DU_{N-1} - U_{N-2} \end{pmatrix} \tag{4.3}$$

where

$$U_N = \frac{\sin(N+1)K\Lambda}{\sin K\Lambda} \tag{4.4}$$

with K given by Equation (2.37).

The coefficient of reflection is immediately obtained from (4.1), (4.2), and (4.3) as

$$r_N = \frac{CU_{N-1}}{AU_{N-1} - U_{N-2}} \tag{4.5}$$

The reflectivity is obtained by taking the absolute square of r_N

$$|r_N|^2 = \frac{|C|^2}{|C|^2 + (\frac{\sin K\Lambda}{\sin NK\Lambda})^2} \tag{4.6}$$

We have in (4.6) an analytic expression of the reflectivity of a multilayer reflector. The term $|C|^2$ is directly related to the reflectivity of a single unit cell by

$$|r_1|^2 = \frac{|C|^2}{|C|^2 + 1} \tag{4.7}$$

or

$$|C|^2 = \frac{|r_1|^2}{1 - |r_1|^2} \tag{4.8}$$

The $|r_1|^2$ for a typical Bragg reflector is usually much less than 1. As a result $|C|^2$ is roughly equal to $|r_1|^2$. The second term in the denominator of (4.6) is a fast varying function of K, or alternatively, of β and ω. Therefore it dominates the structure of the reflectivity spectrum. Between any two "forbidden" bands there are exactly (N-1) nodes where the reflectivity vanishes. The peaks of the reflectivity occur at the centers of the "forbidden" bands. There are exactly (N-2) side lobes which are all under the envelope $|C|^2/[|C|^2 + (\sin K\Lambda)^2]$. At the band edges $K\Lambda = m\pi$ and the reflectivity is given by

$$|r_N|^2 = \frac{|C|^2}{|C|^2 + (\frac{1}{N})^2} \tag{4.9}$$

In the "forbidden" gap $K\Lambda$ is a complex number

$$K\Lambda = m\pi + iK_i\Lambda \tag{4.10}$$

The reflectivity formula of (4.6) becomes

$$|r_N|^2 = \frac{|C|^2}{|C|^2 + (\frac{\sinh K_i\Lambda}{\sinh NK_i\Lambda})^2} \tag{4.11}$$

For large N the second term in the denominator approaches zero exponentially as $e^{-2(N-1)K_i\Lambda}$. It follows that the reflectivity in the forbidden gap is near unity for a Bragg reflector with a substantial number of periods.

TE and TM waves have different band structures and different re-flectivities. For TM waves incident at the Brewster angle there is no reflected wave. This is due to the vanishing of the dynamical factor $|C|^2$ at that angle.

The reflectivity for some typical Bragg reflectors as a function of frequency and angle of incidence are shown in Figures 4.2 and 4.3.

4.3 Theory of Bragg Waveguides

In what follows we will show that, in principle, lossless propagation is possible in a low index slab provided the bounding media with indices of refraction larger than that of the inner slab are periodic. The model analyzed below assumes stratified periodic media. The use of stratified media in dielectric waveguiding has been proposed by Ash [8] who, however, did not consider the case of confined propagation in low index materials.

Referring to Figure 4.4, we consider the case where $n_a < n_g < n_1, n_2$. In the case of TE modes the only field components are E_y, H_x, and H_z. Each of these components, say E_y, satisfies the wave equation

$$\frac{\partial^2 E_y}{\partial z^2} + \frac{\partial^2 E_y}{\partial x^2} + \frac{\omega^2}{c^2} n^2(x) E_y = 0 \qquad (4.12)$$

If we take $E_y(x,y,z) = E(x)\exp(i\beta z)$ the wave equation becomes

$$\frac{\partial^2 E(x)}{\partial x^2} + (\frac{\omega^2}{c^2} n^2(x) - \beta^2) E(x) = 0 \qquad (4.13)$$

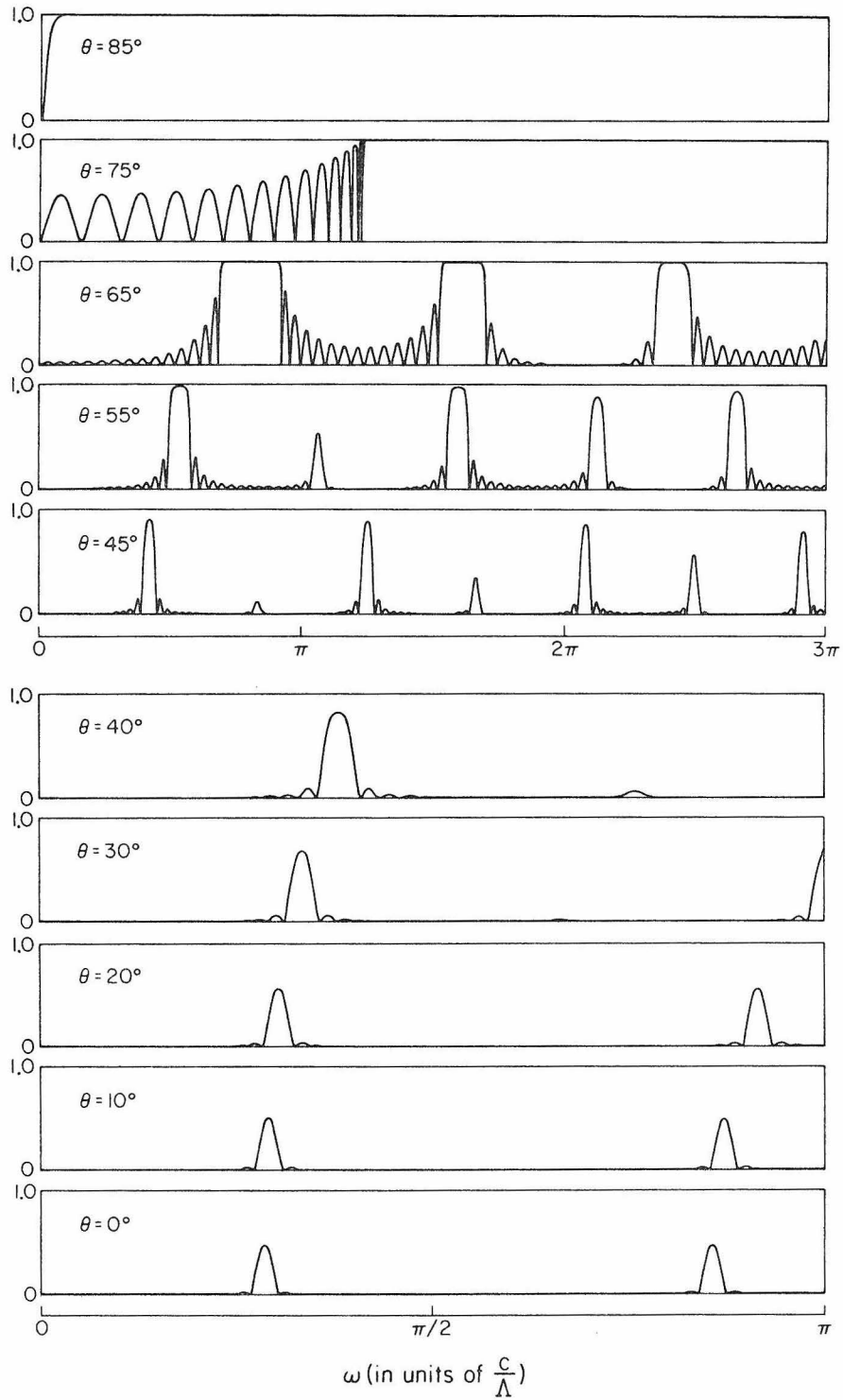We take a solution in the form

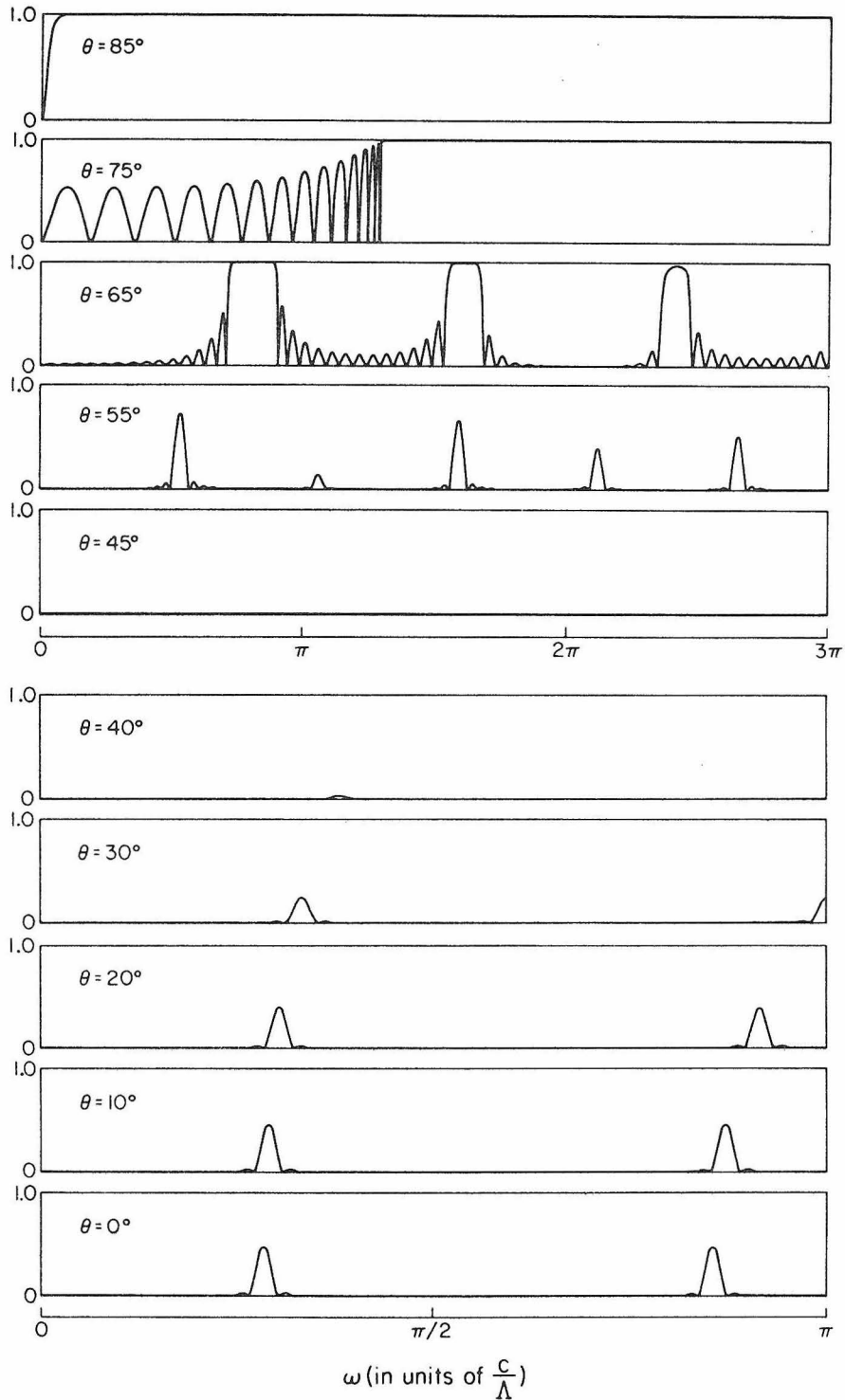Fig. 4.2 TE waves reflectivity spectrum of a 15-period Bragg reflector at various angles of incidence.

Fig. 4.3 TM waves reflectivity spectrum of a 15-period Bragg reflector
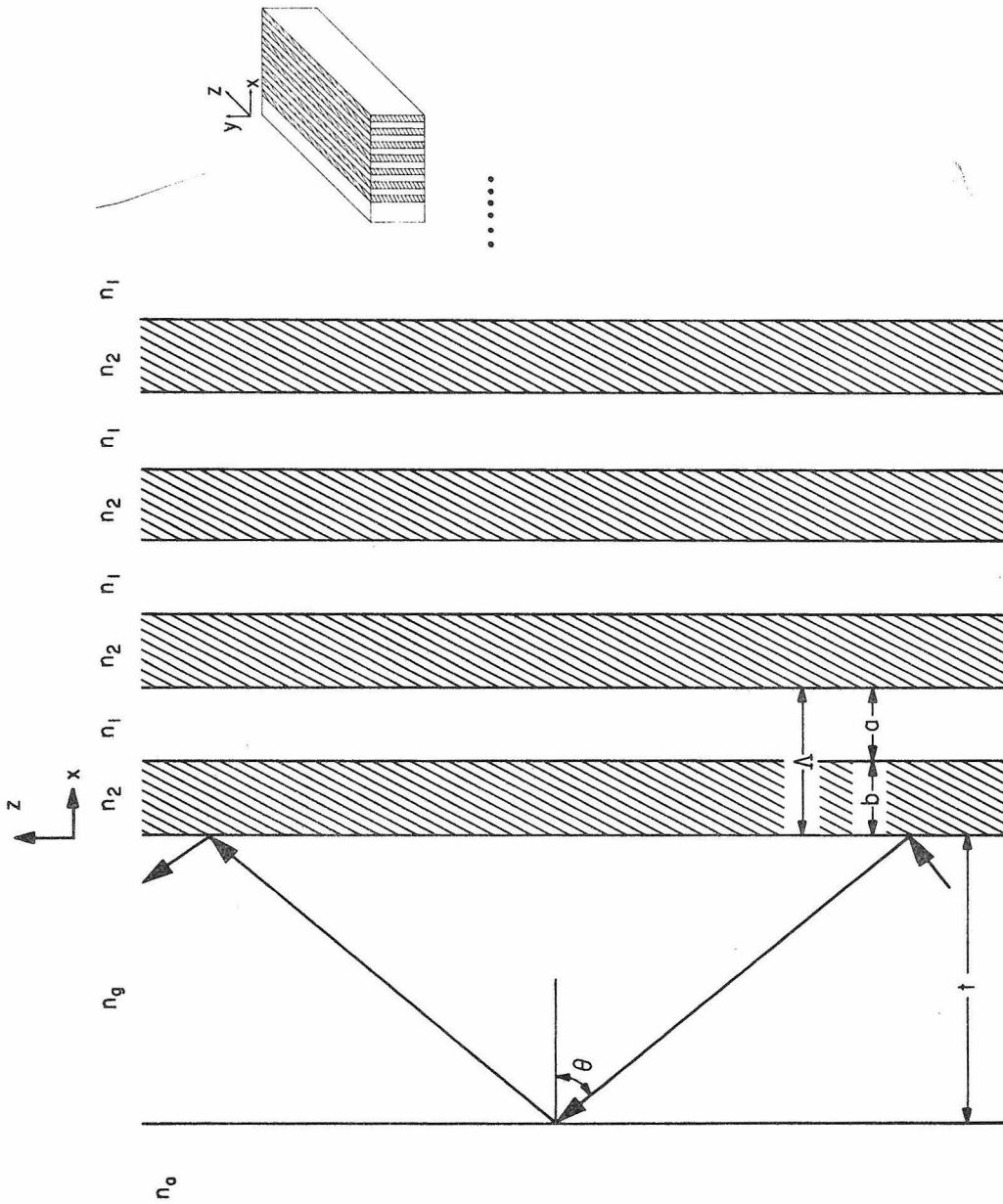at various angles of incidence.

Fig. 4.4 A Bragg reflection (slab) waveguide $(\partial/\partial y = 0)$.

$$E(x) = \begin{cases} \text{(i)} \quad e^{q_a(x+t)} & x < -t \\ \\ \text{(ii)} \quad c_1\cos(k_g x) + c_2\sin(k_g x) & -t \leq x < 0 \\ \\ \text{(iii)} \quad E_K(x)e^{iKx} & 0 \leq x \end{cases} \tag{4.14}$$

where

$$q_a = \sqrt{\beta^2 - (\tfrac{\omega}{c}\, n_a)^2} \quad, \qquad k_g = \sqrt{(\tfrac{\omega}{c}\, n_g)^2 - \beta^2} \tag{4.15}$$

The assumed solution in regions (i) and (ii) of Eq. (4.14) is identical to that of conventional slab dielectric waveguides [9]. The new feature in this case is the form of the wave $E_K(x)\, e^{iKx}$ in the stratified periodic medium where $E_K(x)\, e^{iKx}$ is given by (2.38).

It is important to notice that the sign in front of the square root in (2.35) has to be the same as that of $(A+D)/2$. This ensures that the Bloch wave is evanescent in the positive x direction.

To obtain the solution for the mode of the waveguide of Figure 4.4, we match the fields and their x derivatives at $x = 0$ and $x = -t$. The result, using (2.36), (2.38), and (4.14) is the dispersion relation

$$k_g \left(\frac{q_a \cos k_g t - k_g \sin k_g t}{q_a \sin k_g t + k_g \cos k_g t} \right) = -ik_{1x}\, \frac{e^{-ik\Lambda}_- \; A - B}{e^{-ik\Lambda}_- \; A + B} \tag{4.16}$$

The left side of (4.16) contains only parameters of the guiding (n_g) and substrate (n_a) layers, while the right side depends only on parameters of the periodic medium. For confined propagation β, q_a, and k_g are real so that the left side of (4.16) is a real number. The right side is

real _only_ when the propagating conditions in the periodic medium fall within one of the forbidden gaps, i.e., when $(\frac{A+D}{2})^2 > 1$. It follows that _confined lossless_ modes of the composite waveguide (Figure 4.4) exist. Operationally we may solve for the eigenmode by starting with some value of $\beta < \frac{\omega}{c} n_g$. This (for a given ω) determines k_g, q_a, k_{1x}, and k_{2x}. If the resulting values of A and D correspond to a forbidden gap $((\frac{A+D}{2})^2 > 1)$, then the right side of (4.16) is a (fixed) real number. We then proceed to adjust the thickness of the guiding layer t until an equality results. A simple physical description of the mathematical procedure just outlined is as follows: For _confined_ and _lossless_ mode propagation complete reflection must take place at the interface (see Figure 4.4) between the guiding layer and the layered medium. This indeed occurs only when the zigzagging wave is incident on the interface under conditions corresponding to that of a forbidden gap.

Also important is the fact that the evanescent decay is nearly complete in several periods so that practical structures with, say, ten unit cells are a good approximation to the semi-infinite layered medium assumed in the analysis.

A symmetric waveguide composed of a low index slab, say air, separating two semi-infinite periodic media is of course also possible. Such a waveguide can be constructed by replacing the structure to the left of plane "a" (where $\frac{dE}{dx} = 0$) the structure to the right. The field distribution is then even symmetric about plane a. The result of such a procedure is shown in Figure 4.6. Such a structure can be used as the waveguide for gaseous lasers.
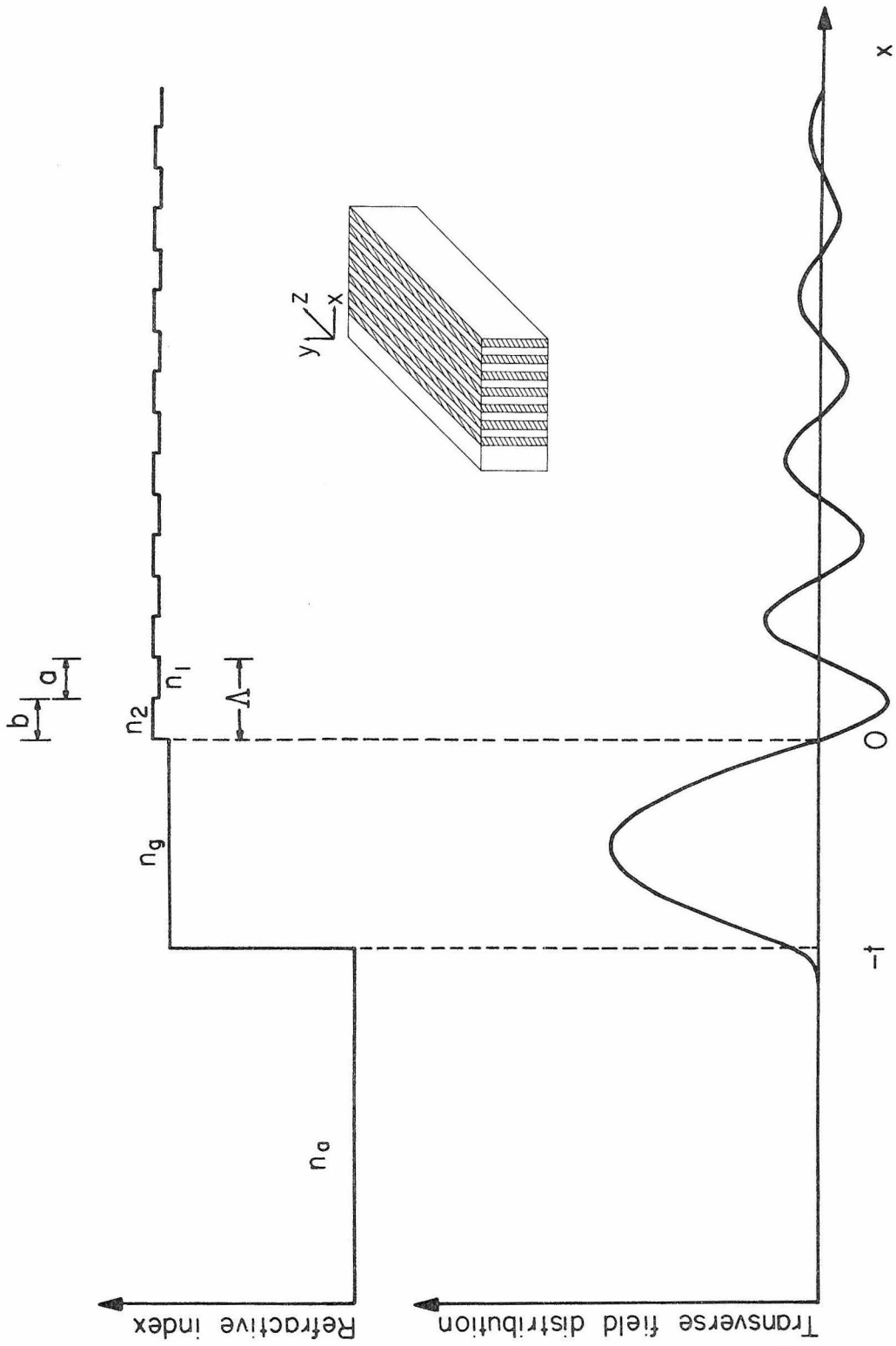
Fig. 4.5 Transverse field distribution of the fundamental modes of a typical Bragg reflection (slab) waveguide.
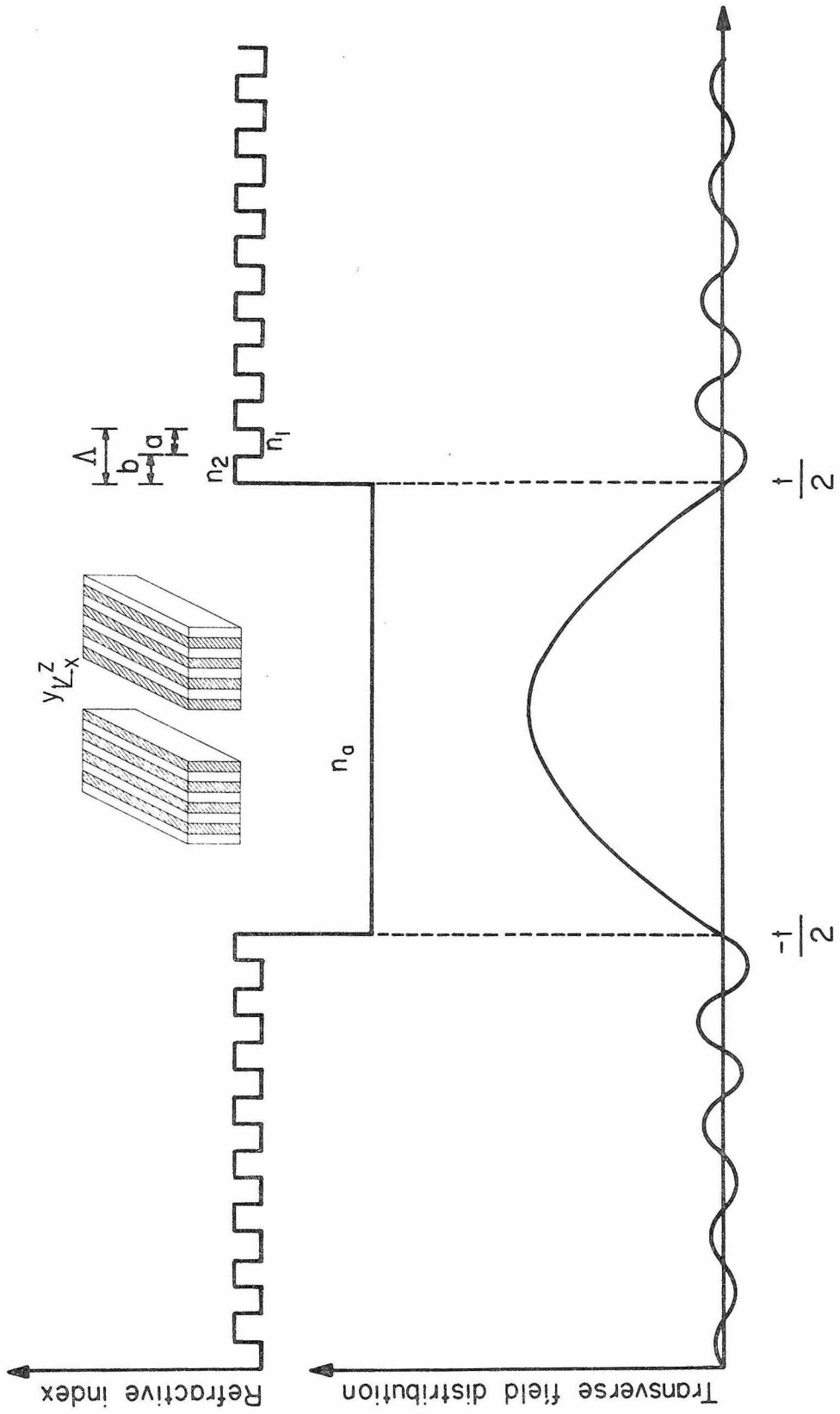
161

Fig. 4.6 Transverse field distribution of the fundamental mode of a typical Bragg reflection waveguide with air as the guiding channel.

Mathematically, the mode conditions for the TE modes of the symmetric Bragg waveguide can easily be shown to be

$$-ik_{1x}\left(\frac{e^{-iK\Lambda}-A-B}{e^{-iK\Lambda}-A+B}\right) = \begin{cases} -k_a\tan(k_a\ t/2) & \text{even TE modes} \\[1em] k_a\cot(k_a\ t/2) & \text{odd TE modes} \end{cases} \tag{4.17}$$

where

$$k_a = \sqrt{(\frac{\omega}{c}\ n_a)^2-\beta^2} \tag{4.18}$$

The Bragg waveguides described above should display strong discrimination against higher order transverse modes, i.e., modes with a larger number of nodes in the central guiding region. This is due to the fact that the existence of a given mode requires, as discussed above, the simultaneous fulfillment of the transverse resonance condition within the guiding layer and the Bragg condition in the layered media. If the waveguide is designed so that these conditions are satisfied for a given transverse mode, they will not be satisfied by other transverse modes, except accidentally. We can show that if the waveguide is designed for the fundamental transverse mode (s=0) then in order that the sth mode exist as well, the condition

$$\frac{\Lambda^2}{t^2} = \frac{\ell}{s}\quad , \qquad \ell = 1,2,3\ \cdots \tag{4.19}$$

need very nearly be satisfied. In equation (4.19) it was assumed that $(n_1-n_2)/n_1 \ll 1$.

4.4 Mode Characteristics

The mode dispersion relations (4.16), (4.17), and (4.18) give us the relations between ω, β, and t, with n_a, n_g, n_1, n_2, a, and b as parameters. In a conventional waveguide the β's for confined modes can vary continuously from $\frac{\omega}{c} \max(n_a, n_s)$ to $\frac{\omega}{c} n_g$, where n_s is the refractive index of the substrate. In a Bragg waveguide, however, the β for confined modes can only vary within the optical forbidden bands, i.e., $|\frac{A+D}{2}| > 1$. A typical mode dispersion with ω fixed is shown in Figure 4.7. It is interesting to note that there are some thickness regions where no confined mode exists. This is due to the fact that the existence of a confined Bragg mode requires, as discussed above, the simultaneous fulfillment of the transverse resonance condition (4.16) and the Bragg condition $|\frac{A+D}{2}| > 1$.

We will use a GaAlAs Bragg waveguide as an example throughout this section. The light wavelength is 1.15 μm of the He-Ne laser. The waveguide structure consists of a guiding layer of $Al_{0.38}Ga_{0.62}As$ with thickness t, and a periodic layered substrate consists of alternating layers of GaAs and $Al_{0.2}Ga_{0.8}As$. At this wavelength, $n_1 = 3.35$, $n_2 = 3.43$, $n_g = 3.24$, $n_a = 1.0$ [11].

The result of the calculation for TE waves is shown in Figure 4-8. These t vs β curves are the mode characteristics of the Bragg waveguide. We notice that β is no longer ranging from $\frac{\omega}{c} \max(n_a, n_s)$ to $\frac{\omega}{c} n_g$ for the waveguide modes. Instead, β varies from β_{min} to β_{max} where the Bloch wave in the substrate becomes evanescent, or equivalently, $K_i > 0$. Also shown in the same figure is the K_i vs β curve. We notice that K_i is
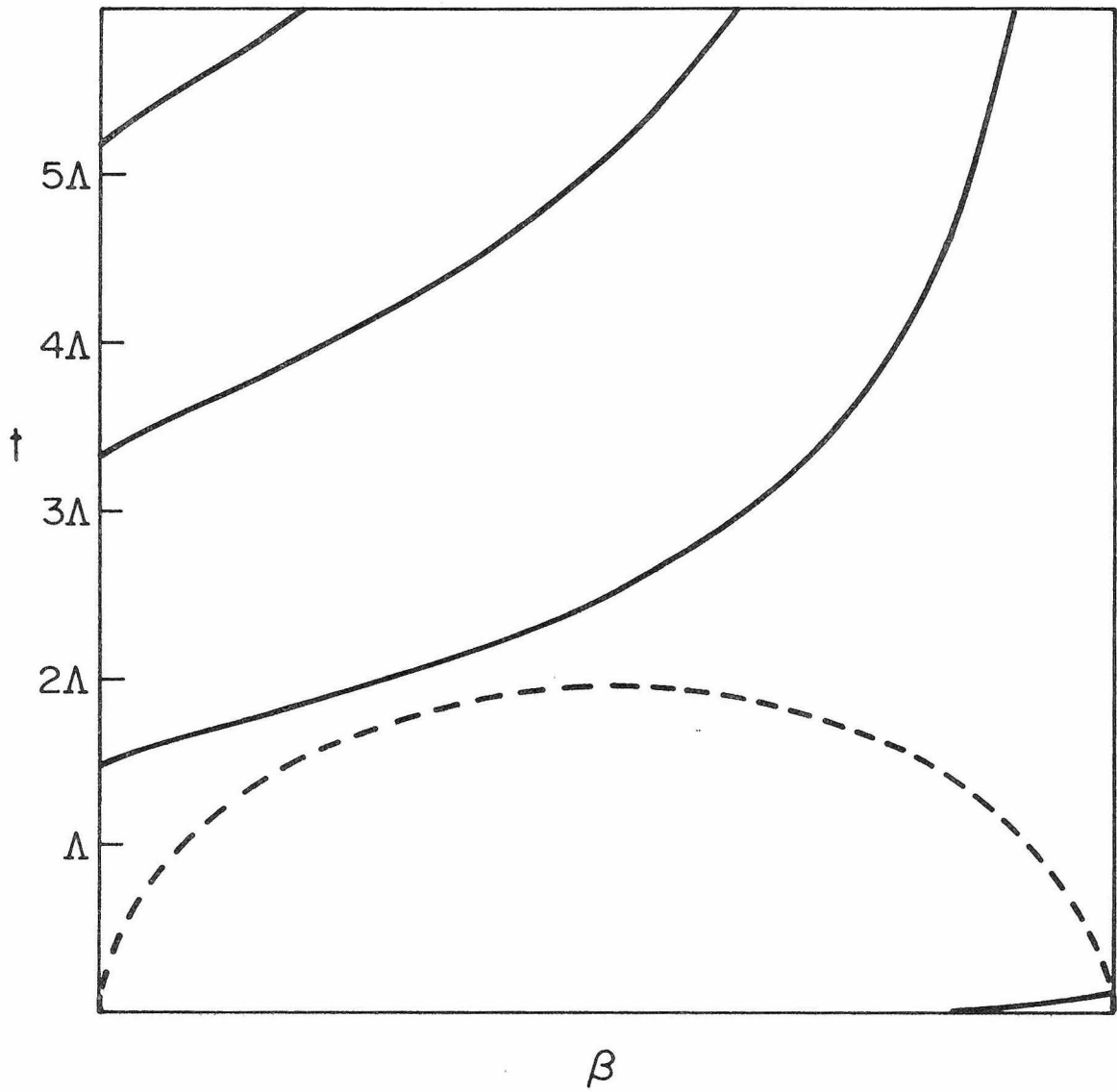
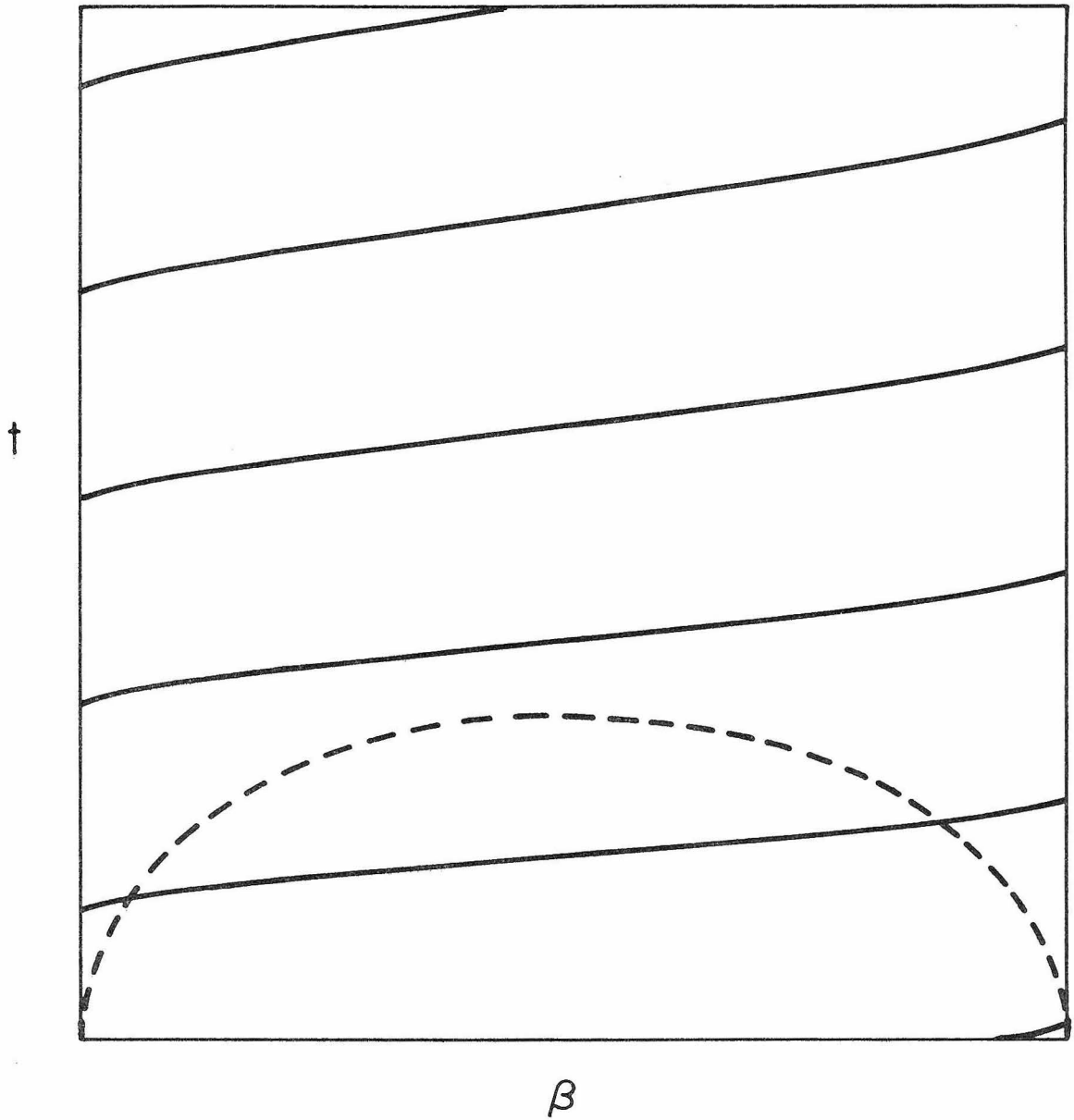Fig. 4.7   t vs. β for a typical Bragg waveguide.

Fig. 4.8 t vs β for another typical Bragg waveguide.

maximum at the center of the forbidden gap. The magnitude of K_i measures the decaying speed of the light wave in the periodic layered substrate. For $\beta \geq \beta_{max}$ or $\beta \leq \beta_{min}$, the waveguide modes are turned into Bloch substrate modes.

We also notice that for the same β, the thicknesses of different modes are equally spaced. The thickness difference between the neighboring modes is exactly a half wavelength,

$$\Delta t = \frac{1}{2}(\frac{2\pi}{k_g}) \tag{4.20}$$

This property can be easily seen from the mode dispersion relations (4.16), (4.17), and (4.18), which are invariant under the following transformation:

$$t \rightarrow t' = t + \frac{1}{2}(\frac{2\pi}{k_g}) \tag{4.21}$$

The Bragg waveguide mode at $t = 0$ is essentially an electromagnetic surface wave bound by the surface of the periodic layered medium, which was discussed in Section 3.4.

A single mode Bragg waveguide can be constructed according to the mode characteristics shown in Figure 4.7 at a thickness which is a few times larger than the wavelength. A conventional waveguide at such a thickness and index discontinuities would support several transverse modes.

4.5 Optimum Bragg Waveguide

As we already know that the Bragg waveguide modes decay as $e^{-K_i x}$ into the periodic layered substrate, in order to get the best degree of

confinement, it is desirable to find a Bragg reflector with layer thicknesses such that K_i has its maximum possible value. In other words, the optimum thicknesses a,b of the alternating layers are such that

$$\left(\frac{\partial K_i}{\partial a}\right) = \left(\frac{\partial K_i}{\partial b}\right) = 0 \tag{4.22}$$

It can be shown that (4.22) is equivalent to

$$k_{1x}a = k_{2x}b = \pi/2 \tag{4.23}$$

In other words, a Bragg reflector has its maximum stopping power for a given incidence condition when each layer is a quarter-wave plate at that incidence condition.   At this optimum condition the decay factor is given

$$e^{iK\Lambda} = -\left(\frac{k_{1x}}{k_{2x}}\right) \tag{4.24}$$

Here we assume that $|k_{2x}| > |k_{1x}|$ and $\mu_2 = \mu_1$. The reflection coefficient r of a semi-infinite Bragg reflector consisting of alternating layers of high and low refractive indices with the same optical quarter wave thickness is given by

$$r = -1 \tag{4.25}$$

Thus we see that the field must vanish at the surface of the Bragg reflector. The mode dispersion relation at this optimum condition is given by

$$q_a = -k_g \cot k_g t \tag{4.26}$$

The field distribution for an optimum Bragg waveguide mode is shown in Figure 4.9. We note that the field has its maxima and minima exactly at the layer interfaces. This property can be proved rigorously by using the mathematical optimization procedure which will be given in the latter half of this section.

Referring to Figure 4.10a, we consider the following problem: Given the material of the structure with indices of refraction $n_a < n_g < n_1 < n_2$, we are to find the locations of the interfaces x_n, $n=1,2,3,\cdots$, such that the guided Bragg mode has the highest degree of confinement. To solve this problem we consider a general interface between two media. Let ξ be the location of the interface and n,n' are the indices of refraction on the left and right side, respectively. Furthermore, we assume that $E(x)$ is the electric field distribution for TE waves in the region $x < \xi$ which is completely determined by the boundary condition at $x = -\infty$. The electric field distribution in the region $x > \xi$ is given by

$$E = A \cos k'x + B \sin k'x \tag{4.27}$$

where $k' = \sqrt{(\frac{\omega}{c} n')^2 - \beta^2}$ and A,B are constants. The boundary conditions require that the tangential components of E and H are continuous at $x = \xi$. The result, using (4.27), is given by

$$A \cos k'\xi + B \sin k'\xi = E(\xi) \tag{4.28}$$

$$-k'A \sin k'\xi + k'B \cos k'\xi = \frac{\mu'}{\mu} \left(\frac{dE}{dx}\right)_\xi \tag{4.29}$$
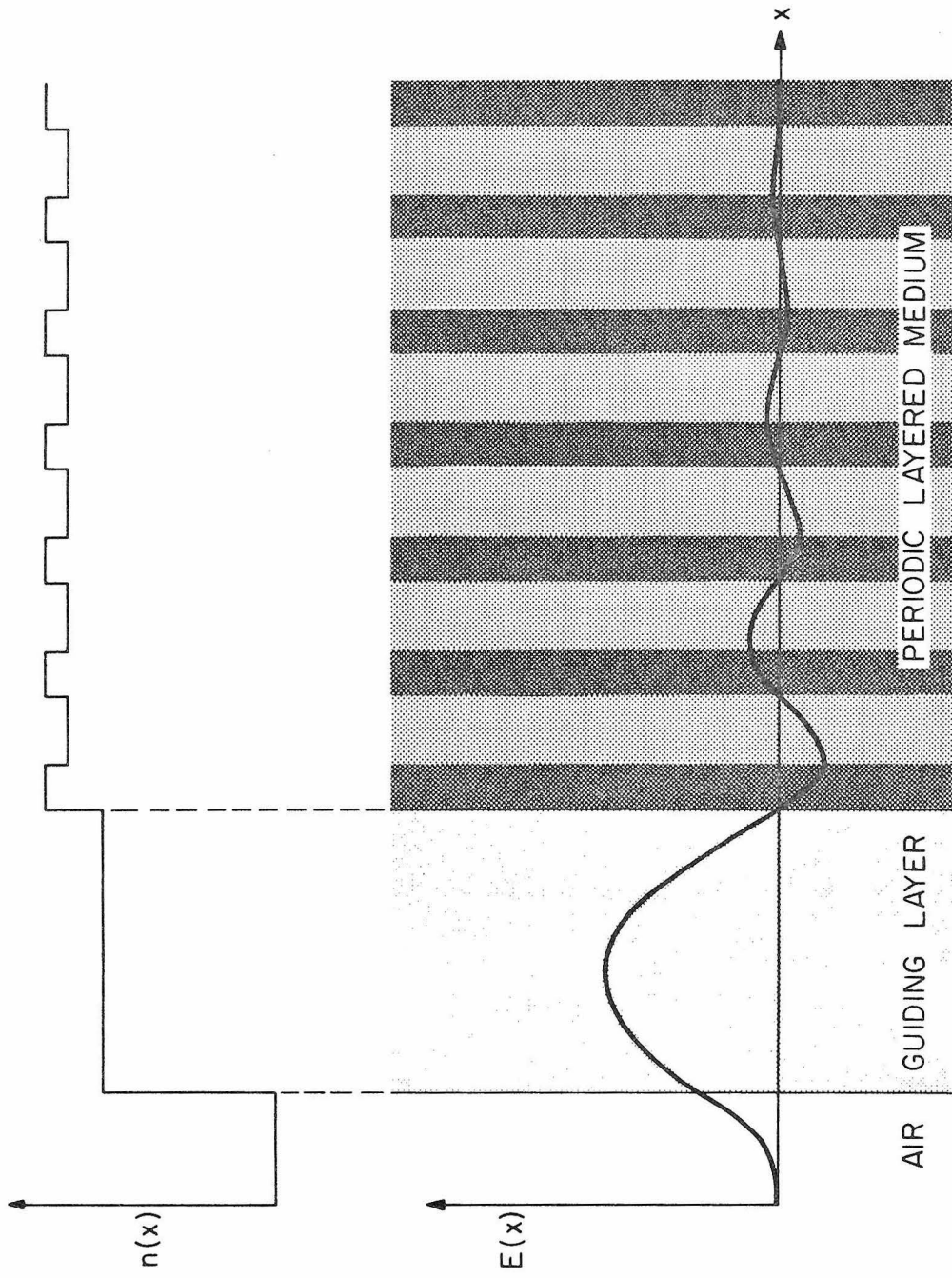
Fig. 4.9 An optimum Bragg waveguide mode.

where μ and μ' are the magnetic permeabilities. Solving for A and B from (4.28) and (4.29), we get

$$A = \cos k'\xi\, E(\xi) - \frac{\mu'}{\mu}\, \frac{\sin k'\xi}{k'}\, (\frac{dE}{dx})_\xi \qquad (4.30)$$

$$B = \sin k'\xi\, E(\xi) + \frac{\mu'}{\mu}\, \frac{\cos k'\xi}{k'}\, (\frac{dE}{dx})_\xi \qquad (4.31)$$

We note that A and B depend on ξ . The field energy on the right hand side of the interface is proportional to (A^2+B^2). In order to get the best degree of confinement, we need to find a location ξ such that (A^2+B^2) is minimized. By carrying out the algebraic manipulation we obtain from (4.30) and (4.31)

$$\frac{\partial}{\partial\xi}(A^2+B^2)_{TE} = \frac{1}{2}[1 - (\frac{k\mu'}{k'\mu})^2]\, E(\xi)(\frac{dE}{dx})_\xi \qquad (4.32)$$

where $k = \sqrt{(\frac{\omega}{c} n)^2 - \beta^2}$. A similar expression for TM waves is given by

$$\frac{\partial}{\partial\xi}(A^2+B^2)_{TM} = \frac{1}{2}[1 - (\frac{k\varepsilon'}{k'\varepsilon})^2]\, H(\xi)(\frac{dH}{dx})_\xi \qquad (4.33)$$

We see that the field energy is optimized whenever either the electric field or the magnetic field vanishes at the interface. In order to find whether these extrema are maxima or minima, we have to inspect the signs of the second order derivatives. By carrying out the differentiation on (4.32) and (4.33), we obtain, using the wave equation

$$\frac{\partial^2}{\partial\xi^2}(A^2+B^2)_{TE} = \frac{1}{2}[1 - (\frac{k\mu'}{k'\mu})^2][(\frac{dE}{dx})^2_\xi - k^2E^2(\xi)]$$ (4.34)

$$\frac{\partial^2}{\partial\xi^2}(A^2+B^2)_{TM} = \frac{1}{2}[1 - (\frac{k\epsilon'}{k'\epsilon})^2][(\frac{dH}{dx})^2_\xi - k^2H^2(\xi)]$$ (4.35)

The results (4.32) through (4.35) can be summarized as follows:

TE Waves

(a) $\quad \frac{k}{\mu} < \frac{k'}{\mu'}$

Minimization of $(A^2 + B^2)$ occurs at $E(\xi) = 0$.

(b) $\quad \frac{k}{\mu} > \frac{k'}{\mu'}$

Minimization of $(A^2 + B^2)$ occurs at $(\frac{dE}{dx})_\xi = 0$.

TM Waves

(a) $\quad \frac{k}{\epsilon} < \frac{k'}{\epsilon'}$

Minimization of $(A^2 + B^2)$ occurs at $H(\xi) = 0$.

(b) $\quad \frac{k}{\epsilon} > \frac{k'}{\epsilon'}$

Minimization of $(A^2 + B^2)$ occurs at $(\frac{dH}{dx})_\xi = 0$.

It can be shown that the field amplitude decreases by a factor of $\frac{k\mu'}{k'\mu}$ (or $\frac{k\epsilon'}{k'\epsilon}$ for TM waves) at the optimized condition for $\frac{k}{\mu} < \frac{k'}{\mu'}$ (or $\frac{k}{\epsilon} < \frac{k'}{\epsilon'}$ for TM waves). This is illustrated in Figure 4.10 for TE waves. Thus we find that in a stack of alternating high and low refractive index layers the optimum layer thicknesses for best confinement are quarter-wave thicknesses. The field vanishes at the interfaces with low index media

ϵ ϵ'

μ μ'

$E = E(x)$ $E = A\cos k'x + B\sin k'x$

$x = \xi$
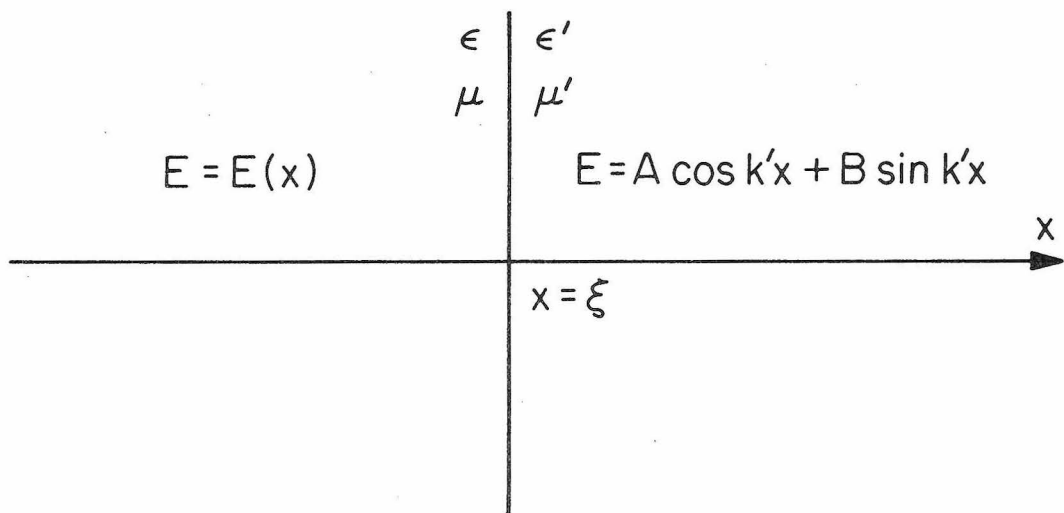
(a)
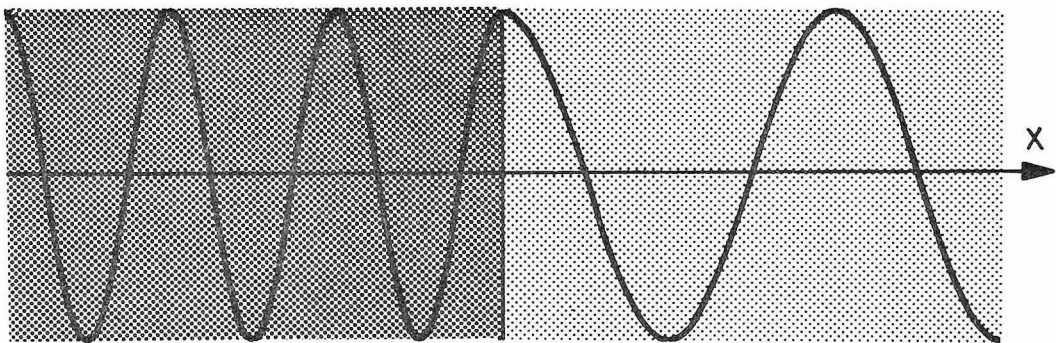
(b)
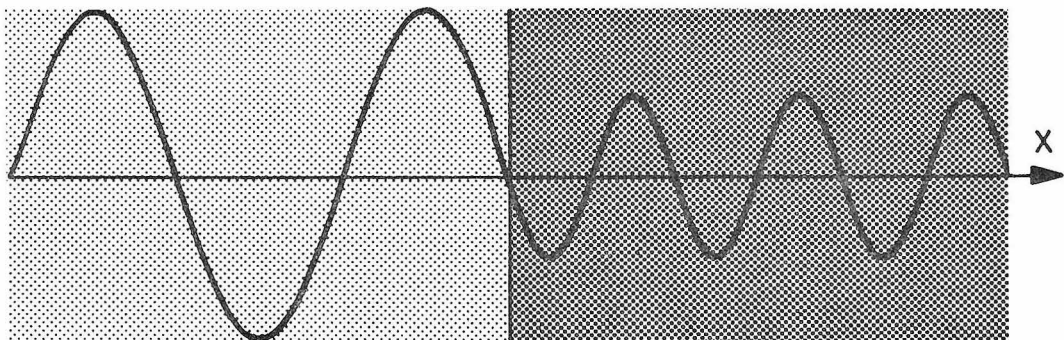
(c)

Fig. 4.10   (a)   A general interface at $x = \xi$.   (b)   Transition from high index material to low index material.   (c)   Transition from low index material to high index material.

on its left hand side and reaches maximum at the interfaces with low index media on its right hand side. Each period is exactly a half-wave plate. The field amplitude decreases by a factor of $e^{iK\Lambda}$ given by

$$e^{iK\Lambda} = \begin{cases} -\dfrac{k_1\mu_2}{k_2\mu_1} & \text{TE waves} \\[4mm] -\dfrac{k_1\varepsilon_2}{k_2\varepsilon_1} & \text{TM waves} \end{cases} \qquad (4.36)$$

This approach in designing a Bragg waveguide will later be extended to the cylindrical regime to study the Bragg fibers.

4.6 Leak Consideration

We now discuss the loss due to the finite number of periods in the periodic layered substrate. All the above derivations are based on the assumption that the periodic layered substrate is of infinite extent. In practice, it is impossible to fabricate an infinite number of periods, although the current molecular beam technology can fabricate as many layers as needed. Usually the time invested in the growth is proportional to the number of periods. Typical growth rate is about 1 μm/hr. The growth rate is so slow that the layer thickness can be precisely controlled [12].

In what follows, we will calculate the attenuation coefficient of the Bragg waveguide due to the resulting losses into the substrate. The analysis will be similar to that of the surface waves. However, we will limit ourselves to the interesting case of optimum Bragg waveguides.

We consider an optimum Bragg waveguide with N periods in the periodic layered substrate. The attenuation coefficient is again given by

$$\alpha = \frac{S_x(x=N\Lambda)}{\displaystyle\int_{-\infty}^{N\Lambda} S_z \, dx} \tag{4.37}$$

Without loss of generality we will consider TE wave only. Also, we assume all the layers are pure dielectric materials so that all the magnetic permeabilities are equal to μ_0. The electric field distribution can be written

$$E_y = \begin{cases} \sin k_g t \, e^{f_a(x-t)} & x \le -t \\[2mm] -\sin k_g x & -t \le x \le 0 \\[2mm] -\dfrac{k_g}{k_2} \sin k_{2x} x & 0 \le x \le b \\[2mm] -\dfrac{k_g}{k_2} \cos k_{1x}(x-b) & b \le x \le \Lambda \\[2mm] \left(\dfrac{k_g}{k_2}\right)\left(\dfrac{k_1}{k_2}\right) \sin k_2(x-\Lambda) & \Lambda \le x \le \Lambda + b \end{cases} \tag{4.38}$$

$$\text{etc.}$$

The thickness of the guiding layer is given by equation (4.26). Using (4.38) and (3.34) we obtain

$$\int_{-\infty}^{N\Lambda} S_z \, dx = \frac{c\beta}{2\omega} \left\{ \frac{1}{2} t - \frac{\tan k_g t}{2k_g} + F\left(\frac{k_g}{k_{2x}}\right)^2 \frac{\Lambda}{2} \right\} \tag{4.39}$$

where

$$F = \frac{1 - e^{-2NK_i\Lambda}}{1 - e^{-2K_i\Lambda}} \tag{4.40}$$

By using (4.26), (4.39) can be simplified further as

$$\int_{-\infty}^{N\Lambda} S_z dx = \frac{c\beta}{2\omega} \{\frac{1}{2} t + \frac{1}{2\tilde{q}_a} + \frac{1}{2} \Lambda (\frac{k_g}{k_{2x}})^2 F\} \tag{4.41}$$

The outflowing flux S_x at $x = N$ is given by

$$S_x = \frac{ck_{2x}}{2\omega} \cdot \frac{1}{4} (\frac{k_g}{k_{2x}})^2 e^{-2(N-1)K_i\Lambda} \tag{4.42}$$

where we have assumed that the substrate material is the same as layer 2, so that $n_s = n_2$. Combining (4.41) and (4.42) we obtain the attenuation coefficient

$$\alpha = \frac{k_{2x}}{2\beta} (\frac{k_g}{k_{2x}})^2 \frac{e^{-2(N-1)K_i\Lambda}}{t + \frac{1}{q_a} + \Lambda(\frac{k_g}{k_{2x}})^2 F} \tag{4.43}$$

Again, we see that the attenuation coefficient decreases exponentially as N becomes large.

A typical curve for α vs N is shown in Figure 4.11. It is important to notice that the attenuation coefficient we have just calculated accounts for the radiation loss due to finite number of periods only. In practice, there are losses due to surface scatterings, bulk absorptions, and bending losses.
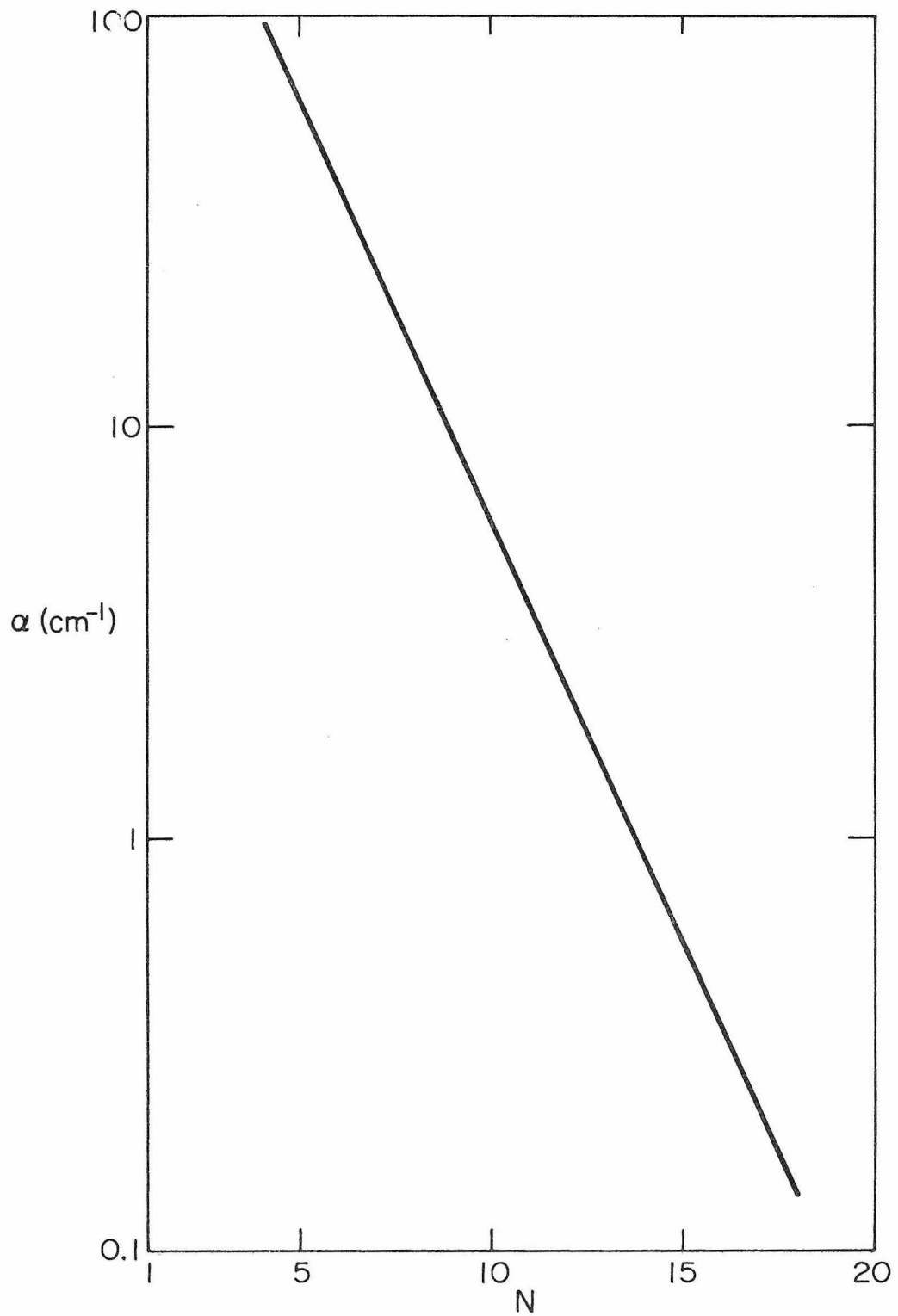
Fig. 4.11 α vs. N for a Bragg waveguide.

4.7 Other Bragg Waveguide Structures

A waveguide composed of a low index slab separating two semi-infinite periodic layered media is of course also possible. The most general Bragg waveguide has an index profile shown in Figure 4.12. The mode dispersion relations for such a waveguide can be derived by the same method as described in Section 4.3, and is given by

$$k_g \left(\frac{-\Gamma_{34} \cos k_g t - k_g \sin k_g t}{-\Gamma_{34} \sin k_g t + k_g \cos k_g t} \right) = \Gamma_{12} \tag{4.44}$$

or, equivalently,

$$\tan k_g t = \frac{k_g (\Gamma_{12} + \Gamma_{34})}{\Gamma_{12}\Gamma_{34} - k_g^2} \tag{4.45}$$

where

$$\Gamma_{12} \equiv -ik_{1x} \frac{e^{-iK\Lambda} - A - B}{e^{-iK\Lambda} - A + B} \tag{4.46}$$

$$\Gamma_{34} \equiv -ik_{3x} \frac{e^{-iK'\Lambda'} - A' - B'}{e^{-iK'\Lambda'} - A' + B'} \tag{4.47}$$

and A', B', K', Λ' are the parameters of the left side periodic layered medium corresponding to A, B, K, Λ, respectively.

Mathematically Γ_{12} and $-\Gamma_{34}$ are the logarithmic derivatives of the Bloch waves at x = 0 and x = -t respectively. A special case of particular interest is the symmetric Bragg waveguide where $n_3 = n_1$, $n_4 = n_2$, c = a and d = b. Such a structure can be used as the waveguide for gaseous lasers.
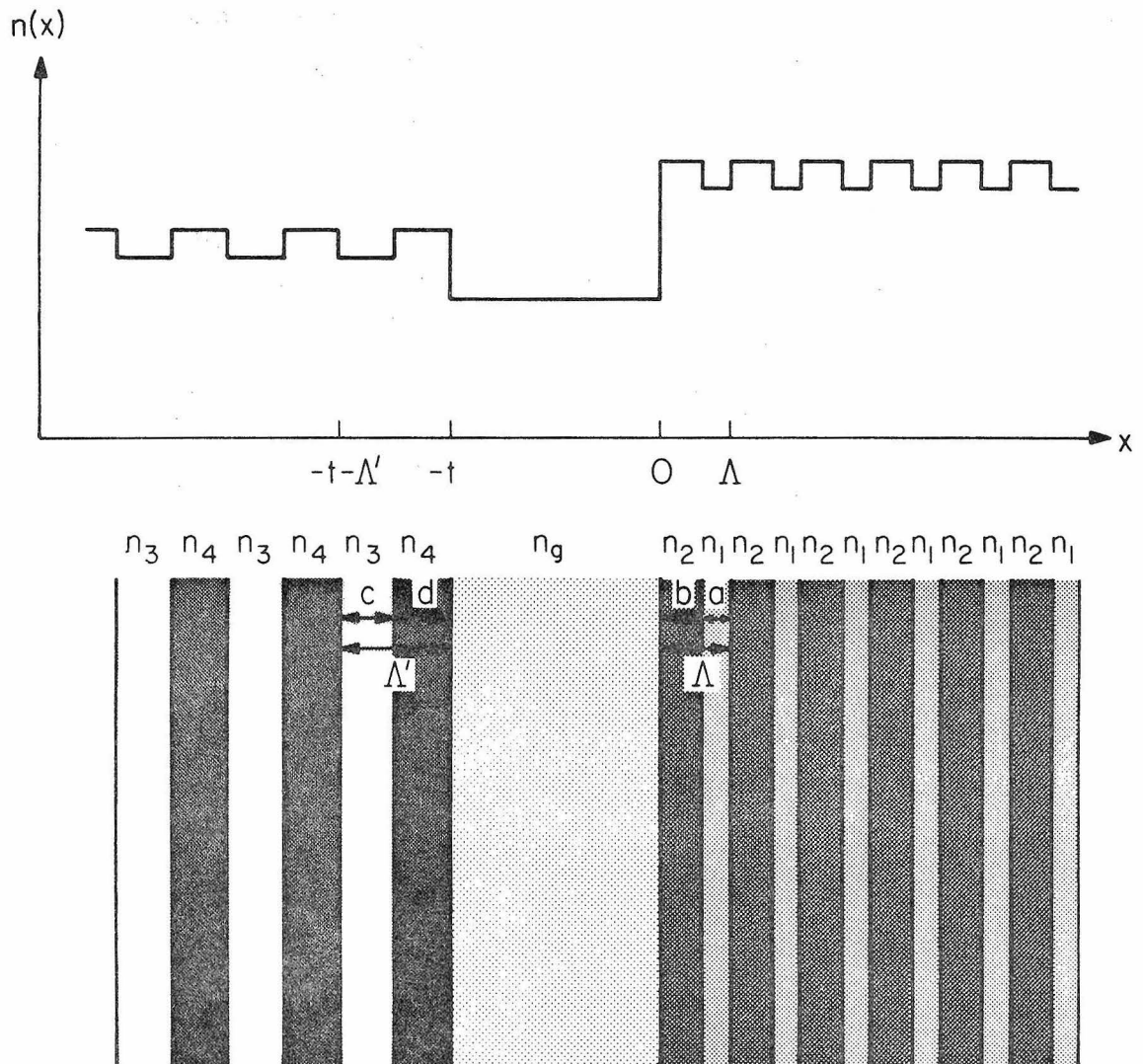
Fig. 4.12   Geometry of a double Bragg waveguide.

The mode condition for the symmetric Bragg waveguide can be obtained from (4.45) by setting $\Gamma_{34} = \Gamma_{12}$ and is given by

$$
\Gamma_{12} = \begin{cases} -k_g \tan(\frac{1}{2} k_g t) & \text{even modes} \\[2ex] k_g \cot(\frac{1}{2} k_g t) & \text{odd modes} \end{cases} \tag{4.48}
$$

If we let $n_3 = n_4 = n_a < n_g$, the left side medium becomes homogeneous and Γ_{34} becomes $-q_a$ according to (4.47). Thus we get the dispersion relations for the slab Bragg waveguide (4.16).

In order for a double-Bragg waveguide to support a confined mode two Bragg conditions plus a phase resonance condition have to be satisfied simultaneously. This is not generally possible. However, under appropriate conditions a double-Bragg waveguide can support confined modes. It is evident that confined modes exist only when there is some overlap between the optical forbidden bands of the two periodic layered media. Because of the additional Bragg condition, a double-Bragg waveguide has the desired capability of mode discrimination. If a double-Bragg waveguide is designed to support a given confined transverse mode, it will not in general be able to support other transverse modes, except accidentally.

Another special case of particular interest is the double-Bragg waveguide structure with $t = 0$, which is exactly the interface mode discussed in Section 3.5.

References - Chapter 4

1. A. J. Fox, Proc. IEEE 62, 644 (1974).

2. P. Yeh and A. Yariv, Opt. Comm. 19, 427 (1976).

3. K. Aiki, M. Nakamura, J. Umeda, A. Yariv, A. Katzir and H. W. Yen, Appl. Phys. Lett. 27, 145 (1975).

4. H. C. Casey, Jr., S. Somekh and M. Ilegems, Appl. Phys. Lett. 27, 142 (1975).

5. F. K. Reinhart, R. A. Logan and C. V. Shank, Appl. Phys. Lett. 27, 45 (1975).

6. A. Yariv, IEEE J. Quant. Electr. QE-9, 919 (1973).

7. M. Born and E. Wolf, Principles of Optics (MacMillan, New York, 1964), p. 67.

8. E. A. Ash, "Grating Surface Waveguides", presented at the Int. Microwave Symposium, Newport Beach, Calif., May 1970.

9. A. Yariv, Quantum Electronics (Wiley, New York, 1975).

10. P. K. Tien, Appl. Opt. 10, 2395 (1971).

11. H. C. Casey, Jr., D. D. Sell and M. B. Panish, Appl. Phys. Lett. 24, 63 (1974).

12. A. Y. Cho, Appl. Phys. Lett. 19, 467 (1971).

Chapter 5
OTHER TOPICS IN LAYERED MEDIA

5.1 Introduction

We have derived some of the important characteristics of Bloch waves propagating in a periodic layered medium. The results are applied in this chapter to the problems of periodicity dispersion, phase matching in nonlinear mixing experiments and to laser action in the soft x-ray region. Periodicity dispersion is the dispersion introduced by the periodic stratification without regarding any material dispersion. Under appropriate conditions this dispersion can compensate the material dispersion. As a result, the whole layered medium becomes dispersionless in some region of the frequency spectrum.

Phase matching is an important problem in nonlinear optics. In order to get high conversion efficiency, perfect phase matching is needed. However, most material exhibits some kind of dispersion. Perfect phase matching in gases can be achieved by adding buffer gases with different dispersion behavior into the mixing medium. Phase matching in crystalline solids can be achieved by employing the birefringence property of the crystal [1]. In this chapter we will describe how to apply the periodicity dispersion to get perfect phase matching.

5.2 Periodicity Dispersion

In this section we treat analytically and quantitatively the periodicity dispersion. We obtain expressions for the locations and sizes of the bandgaps. We will limit our derivation to the case of normal

incidence. The extension of our result to the general case will be given in the last part of this section.

Instead of using n_1, n_2, a and b, a new set of more convenient parameters will be defined in the following.

$$\Delta = \frac{1}{2} \left(\frac{n_2}{n_1} + \frac{n_1}{n_2} \right) \tag{5.1}$$

$$\bar{n} = \frac{n_1 a + n_2 b}{\Lambda} \tag{5.2}$$

$$\nu = \frac{n_1 a - n_2 b}{\Lambda} \tag{5.3}$$

In terms of these new parameters, the dispersion relation (2.37) can be written as

$$\cos K\Lambda = \left(\frac{\Delta+1}{2} \right) \cos \bar{n} \frac{\omega}{c} \Lambda - \left(\frac{\Delta-1}{2} \right) \cos \nu \frac{\omega}{c} \Lambda \tag{5.4}$$

By using the following identity

$$\cos x = 1 - 2 \sin^2 \frac{x}{2} \tag{5.5}$$

eq. (5.4) can be written as

$$\sin^2 \frac{K\Lambda}{2} = \left(\frac{\Delta+1}{2} \right) \sin^2 \frac{\bar{n}\omega}{2c} \Lambda - \left(\frac{\Delta-1}{2} \right) \sin^2 \frac{\nu\omega}{2c} \Lambda \tag{5.6}$$

This equation is especially useful when $\nu \ll \bar{n}$. In the event when $\nu = 0$ ($n_1 a = n_2 b$) equation (5.6) gives us the explicit form of ω as a function of K.

The locations of band edges can be obtained from (5.6). If we set $K\Lambda = m\pi$, we obtain

$$\sin^2(\frac{\bar{n}\omega}{2c}\Lambda) = \begin{cases} (\frac{\Delta-1}{\Delta+1})\sin^2(\frac{\nu\omega}{2c}\Lambda) & K\Lambda = 2\ell\pi \\ \\ 1 - (\frac{\Delta-1}{\Delta+1})\cos^2(\frac{\nu\omega}{2c}\Lambda) & K\Lambda = (2\ell+1)\pi \end{cases} \tag{5.7}$$

where ℓ is an integer. If $\nu << \bar{n}$ which is normally true, equation (5.7) can be solved by the method of successive approximation. The results for the upper and lower band edge frequencies after one iteration are given by

$$\omega_{u,\ell} \approx \begin{cases} \frac{c}{\bar{n}\Lambda}\{2\ell\pi \pm 2\sin^{-1}[\sqrt{\frac{\Delta-1}{\Delta+1}}\sin(\frac{\nu}{\bar{n}}\ell\pi)]\} & K\Lambda = 2\ell\pi \tag{5.8} \\ \\ \frac{c}{\bar{n}\Lambda}\{(2\ell+1)\pi \pm 2\sin^{-1}[\sqrt{\frac{\Delta-1}{\Delta+1}}\cos(\frac{\nu}{\bar{n}}(\ell+1/2)\pi] & K\Lambda = (2\ell+1)\pi \end{cases}$$

Consider a stratified medium consisting of alternating layers of the same optical thickness which is the case when $\nu = 0$, all the even order bandgaps shrink to zero. While the odd order bandgaps have a maximum constant value

$$\Delta\omega_{max} = \frac{4c}{\bar{n}\Lambda}\sin^{-1}\sqrt{\frac{\Delta-1}{\Delta+1}} \tag{5.9}$$

and the centers of the bandgaps are all on the same straight line

$$\omega = \frac{c}{\bar{n}}K \tag{5.10}$$

The vanishing of the even order bandgaps is due to the fact that each layer becomes a half-wave layer at the even-order Bragg conditions so that reflections from two adjacent interfaces are out of phase by an odd multiple of π. The dispersion relation for this special case is shown in Fig. 5.1.

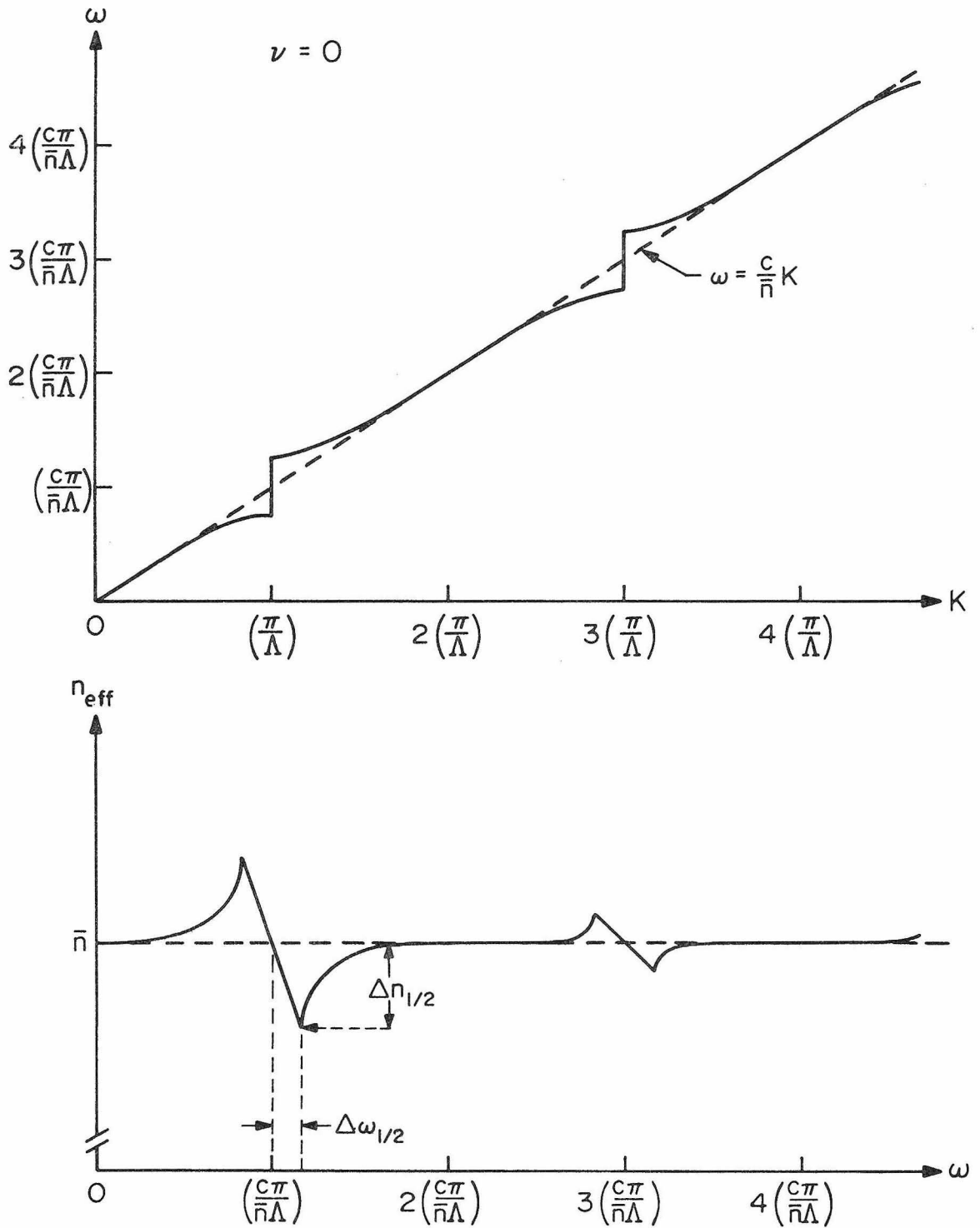Fig. 5.1 Periodicity dispersion when $n_1a = n_2b$ (or $\nu = 0$).

In the general case when $\nu \neq 0$, the degeneracy is removed and there
is, in general, a finite bandgap at $K\Lambda = 2\ell\pi$. The band edges of each
forbidden gap are always on both sides of the straight line
$\omega = cK/\bar{n}$. The bandgap sizes vary roughly periodically as a function
of the Bragg-order for even orders and odd orders separately. This
can be seen from either (5.8) or Figure 5.2, which is a plot of both
sides of eq. (5.7) and gives a graphic solution of the locations of
band edges. The bandgaps are given approximately by

$$\Delta\omega_{gap} = \begin{cases} \frac{4c}{\bar{n}\Lambda} \sin^{-1} \sqrt{\frac{\Delta-1}{\Delta+1}} \sin(\frac{\nu}{n} \ell\pi) & K\Lambda = 2\ell\pi \\[3mm] \frac{4c}{\bar{n}\Lambda} \sin^{-1} \sqrt{\frac{\Delta-1}{\Delta+1}} \cos[\frac{\nu}{n} (\ell+1/2)\pi] & K\Lambda = (2\ell+1)\pi \end{cases} \tag{5.11}$$

In the usual case of inclined incidence ($\beta \neq 0$), all the above results are
applicable provided Δ, $\bar{n}$ and ν are defined by

$$\Delta = \begin{cases} \frac{1}{2} (\frac{n_2\cos\theta_2}{n_1\cos\theta_1} + \frac{n_1\cos\theta_1}{n_2\cos\theta_2}) & \text{TE waves} \\[3mm] \frac{1}{2} (\frac{n_1\cos\theta_2}{n_2\cos\theta_1} + \frac{n_2\cos\theta_1}{n_1\cos\theta_2}) & \text{TM waves} \end{cases} \tag{5.12}$$

$$\bar{n} = \frac{n_1 a\cos\theta_1 + n_2 b\cos\theta_2}{\Lambda} \tag{5.13}$$

$$\nu = \frac{n_1 a\cos\theta_1 - n_2 b\cos\theta_2}{\Lambda} \tag{5.14}$$

where

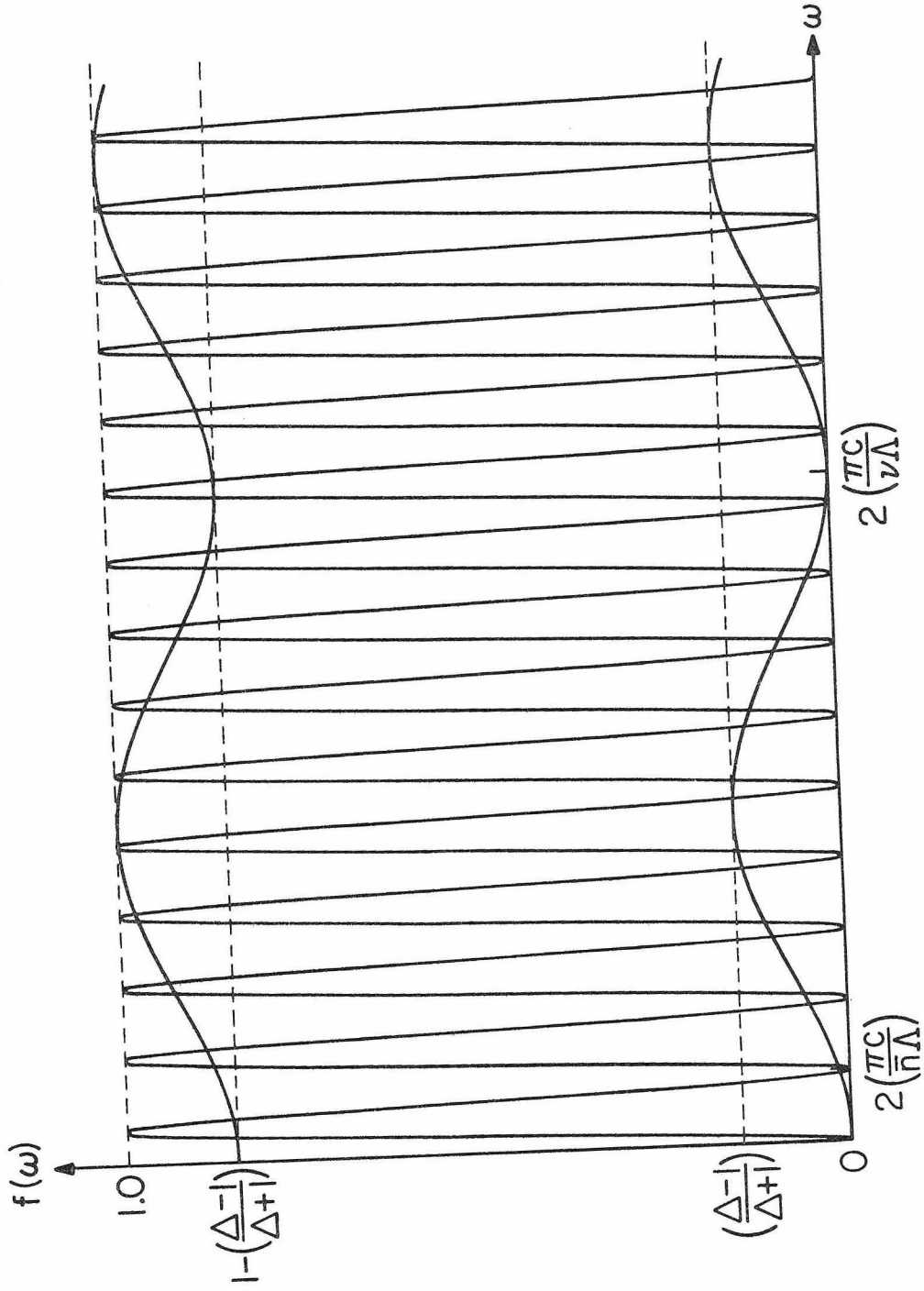$$\cos\theta_1 = \frac{ck_{1x}}{n_1 \omega} \tag{5.15}$$

Fig. 5.2 Graphic method of finding band edges and gap sizes.

$$\cos\,\theta_2 = \frac{ck_{2x}}{n_2\,\omega} \tag{5.16}$$

It can be seen from (5.8) that the locations of the bandgaps are shifted toward higher frequencies and the sizes of the bandgaps become larger at inclined incidence.

5.3 Generalized Phase Matching of Nonlinear Processes

Phase-matched enhancement of nonlinear mixing processes in a periodic stratified medium was proposed by Ashkin and Yariv [2], Bloembergen and Sievers [3], and recently by Tang and Bey [4]. Experimental evidence for this effect has been demonstrated recently by van der Ziel et al and Ilegems [5].

In the following we present a general theory of phase matching in a periodic stratified medium. In our approach we employ the Bloch electromagnetic wave functions and their space harmonics.

Let us consider three interaction electromagnetic waves in a periodic stratified medium. The electric fields are given by their Bloch expressions

$$\vec{E}^{(\omega_\ell)}(x,z,t) = \vec{E}^{K_\ell}(x)\,e^{iK_\ell x}\,e^{i\beta_\ell z}\,e^{-i\omega_\ell t} \quad , \quad \ell = 1,2,3 \tag{5.17}$$

with
$$\omega_3 = \omega_1 + \omega_2 \tag{5.18}$$

The y-dependence is again suppressed for the sake of simplicity in illustration. Let the two media comprising the layered structure possess nonlinear optical properties which cause the two waves at ω_1 and ω_2 to generate a polarization $P(\omega_3)$ at ω_3 with a complex amplitude

$$P_i^{(\omega_3)}(x,z) = d_{ijk}E_j^{(\omega_1)}(x,z)E_k^{(\omega_2)}(x,z) \tag{5.19}$$

The nonlinear coupling coefficient d_{ijk}, reflecting the symmetry of the medium, is a periodic function of x

$$d_{ijk}^{\omega_1 + \omega_2 \to \omega_3}(x+\Lambda) = d_{ijk}^{\omega_1 + \omega_2 \to \omega_3}(x) \tag{5.20}$$

The power flowing into wave at frequency ω_3 from $E^{(\omega_1)}$ and $E^{(\omega_2)}$ is given by $\vec{E}^{(\omega_3)} \frac{\partial}{\partial t} \vec{P}^{(\omega_3)}$ which is proportional to

$$\langle K_3 | d | K_1 K_2 \rangle = \iint d_{ijk}(x) E_i^{K_1}(x) E_j^{K_2}(x) (E_k^{K_3}(x))^* e^{i(K_1+K_2-K_3)x} e^{i(\beta_1+\beta_2-\beta_3)z} dxdz \tag{5.21}$$

where the superscript of $d_{ijk}(x)$ is dropped and the integration is over the interaction region. Each of the periodic functions in the integrand may be expanded in a Fourier series

$$d_{ijk}(x) = \sum_m D_{ijk}^m e^{im\frac{2\pi}{\Lambda}x} \tag{5.22}$$

$$E_i^{K_1}(x) = \sum_n A_i^n e^{in\frac{2\pi}{\Lambda}x} \tag{5.23}$$

$$E_j^{K_2}(x) = \sum_\ell B_j e^{i\ell\frac{2\pi}{\Lambda}x} \tag{5.24}$$

$$E_k^{K_3}(x) = \sum_p C_k^p e^{ip\frac{2\pi}{\Lambda}x} \tag{5.25}$$

Thus

$$\langle K_3 | d | K_1 K_2 \rangle = (2\pi)^2 \sum_{m,n,\ell,p} D_{ijk}^m A_i^n B_j^\ell (C_k^p)^* \delta[K_1+K_2-K_3+(m+n+\ell-p)\frac{2\pi}{\Lambda}]$$

$$\times \delta(\beta_1+\beta_2-\beta_3) \tag{5.26}$$

We see that the nonlinear mixing is allowed only when the following two conditions are satisfied.

$$\beta_3 = \beta_1 + \beta_2 \tag{5.27}$$

$$K_3 = K_1 + K_2 + s \frac{2\pi}{\Lambda} \qquad s = m+n+\ell-p \tag{5.28}$$

By analogy with the corresponding phonon-phonon collisions in solid state physics, one may classify the allowed nonlinear processes into the two categories described in the next section.

5.4 Normal Processes and Umklapp Processes

(A) Normal Nonlinear Processes (s = 0)

Normal nonlinear processes in a homogeneous medium require either no dispersion or anomalous dispersion. The dispersion in a periodic stratified medium can be separated into two factors which are, the natural dispersion of the material itself and the additional dispersion due to artificially periodic stratification. The latter was discussed and analyzed in Section 5.1.

A typical periodicity dispersion is shown in Figure 5.3. An analytic study of the periodicity dispersion was given in Section 5.1. It can be seen from Figure 5.4, in which the periodicity dispersion is superposed on top of the natural dispersion, that the natural dispersion, due say, to some absorption resonance at ω_0, is modified by the periodicity dispersion. As a result, phase matching can be achieved in a spectral region where it would be impossible if the medium were homogeneous. This can be explained as follows: In order to achieve phase matching in a piece-wise homogeneous medium, the dispersion function $n(\omega)$ in the relevant spectral region cannot increase monotonically.
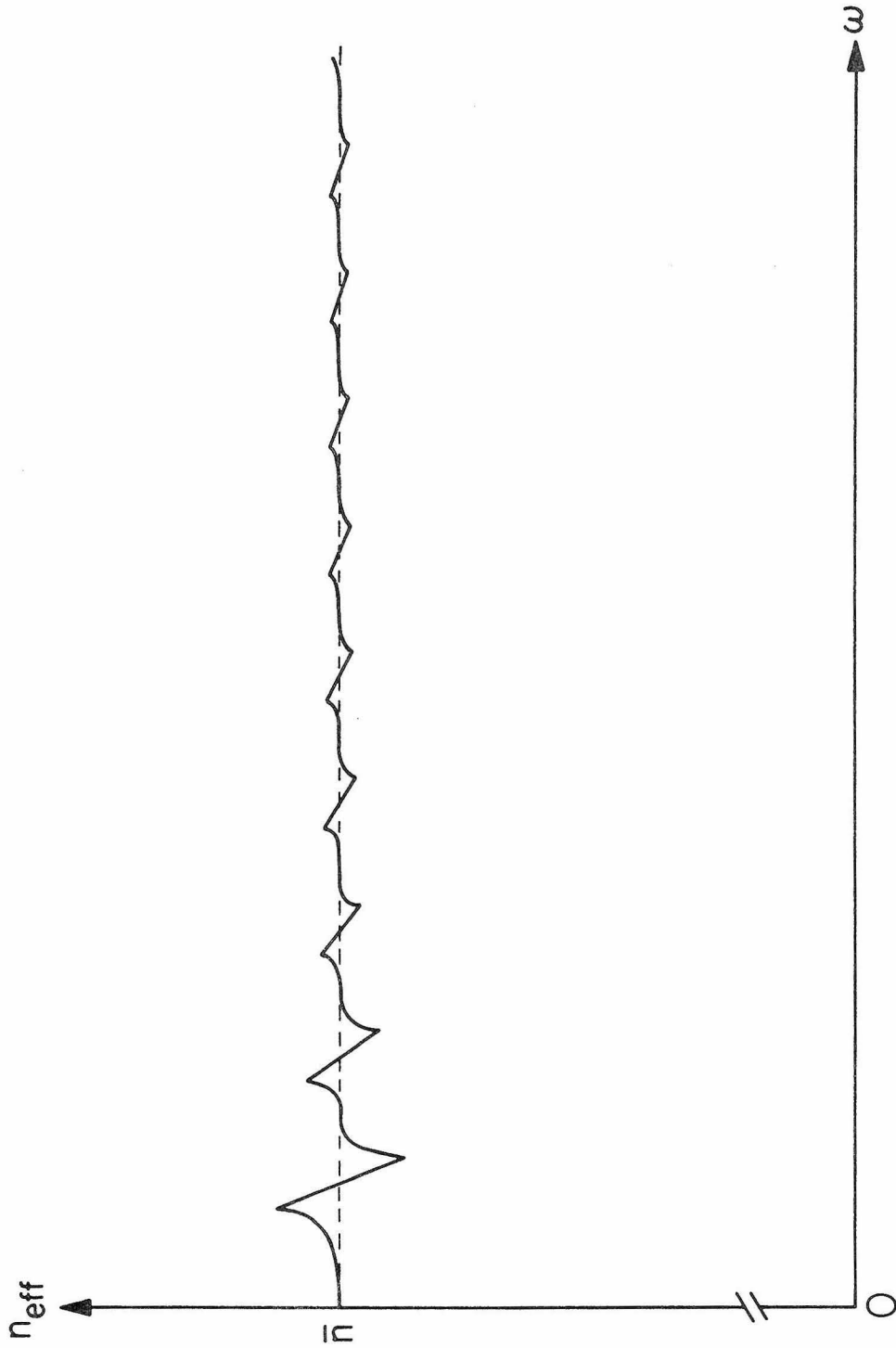
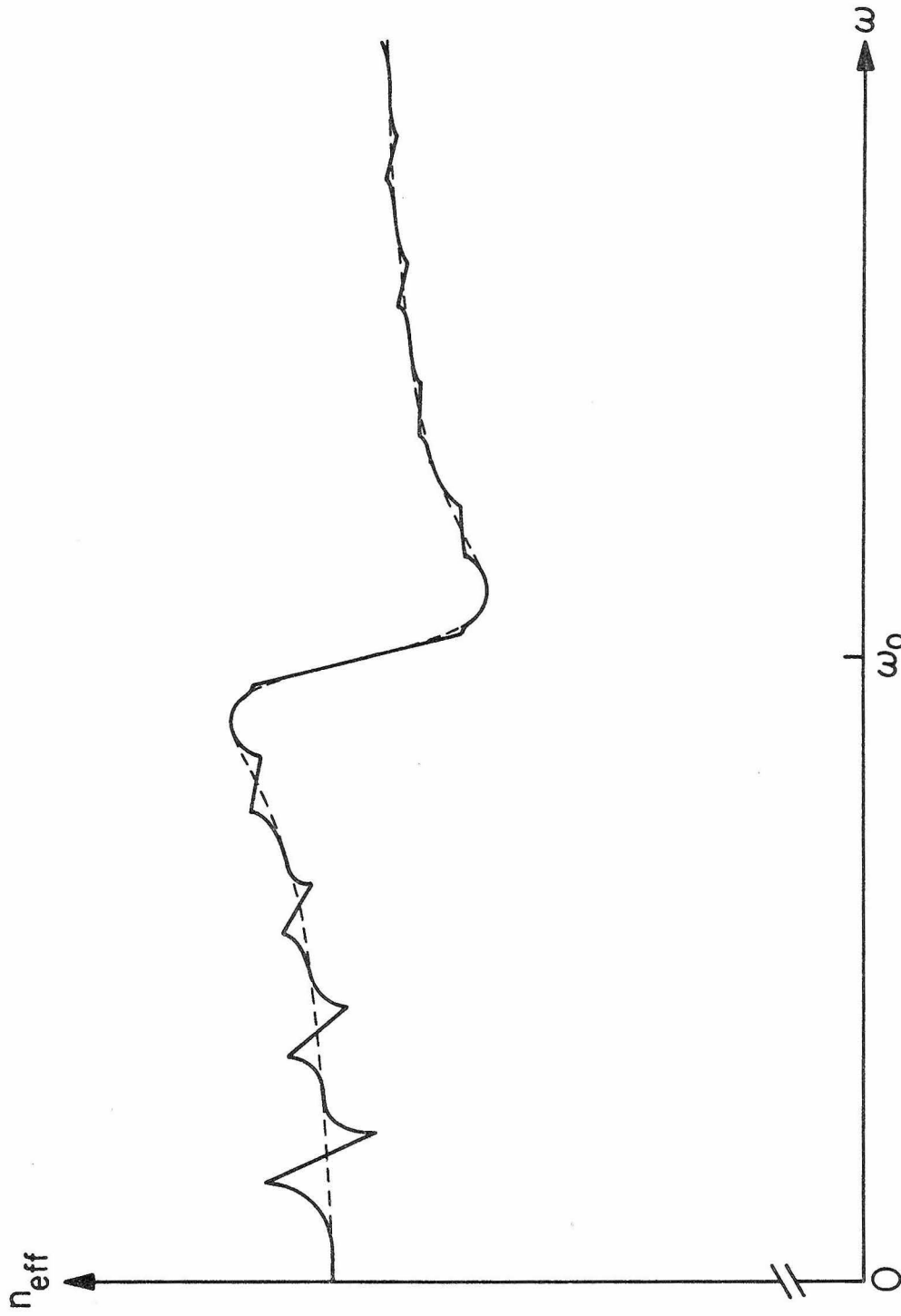Fig. 5.3 A typical periodicity dispersion n_{eff} vs. ω.

Fig. 5.4 A typical overall dispersion n_{eff} vs. ω.

The monotony of the dispersion is removed when the periodic stratification is introduced, since, as shown in Figure 5.4, the change in index due to periodicity changes sign near a Bragg resonance frequency. It is therefore possible to select the parameters of the periodic structure so that phase matching is achieved in a given triplet of waves.

It is interesting to get an expression for the maximum change in the effective index of the refraction which is achievable by periodicity dispersion. To be specific we derive an expression for the maximum index deviation $\Delta n_{1/2}$ as defined in Figure 5.1.

For simplicity let us consider the case of normal incidence ($\beta=0$). The effective index of refraction is obtained from (2.49) and the relation $v_p = c/n_{eff}$

$$n_{eff}(\omega) = \frac{cK(\omega)}{\omega} \tag{5.29}$$

Far from Bragg resonances the effective index is equal to $\bar{n}$ where

$$\bar{n} = \frac{n_1 a + n_2 b}{\Lambda} \tag{5.30}$$

The maximum deviation of n_{eff} from $\bar{n}$ occurs at the band edges. The band edge frequencies can be approximated according to the second of (5.8) by

$$\omega_{u,\ell} \stackrel{\sim}{=} \frac{c}{\bar{n}\Lambda} \left[(2\ell+1)\pi \pm 2\sqrt{\frac{\Delta-1}{\Delta+1}} \right] \tag{5.31}$$

$$\Delta \stackrel{\sim}{\sim} 1 , \quad \frac{\nu}{\bar{n}} (\ell+1/2)\pi \ll 1 \tag{5.32}$$

The maximum index deviation $\Delta n_{1/2}$ is thus

$$\Delta n_{1/2} = n_{eff}(\omega_\ell) - \bar{n} = \frac{cK(\omega_\ell)}{\omega_\ell} - \bar{n} \tag{5.33}$$

At the (odd) band edges (ω_u, ω_ℓ) we have

$$K(\omega_\ell)\Lambda = (2\ell+1)\pi \qquad (5.34)$$

so that

$$\Delta n_{1/2} = \frac{c(2\ell+1)\pi}{\omega_\ell \Lambda} - \bar{n} \qquad (5.35)$$

Substituting (5.31) for ω_ℓ in the last expression and using the fact that $\Delta - 1 \ll 1$ leads to

$$\Delta n_{1/2} = \frac{2\bar{n}}{(2\ell+1)\pi} \sqrt{\frac{\Delta-1}{\Delta+1}} \qquad (5.36)$$

From (5.31) we find that the width of the gap is

$$\Delta\omega_{1/2} \equiv \frac{1}{2}(\omega_u - \omega_\ell) \simeq \frac{2c}{\bar{n}\Lambda}\sqrt{\frac{\Delta-1}{\Delta+1}} \qquad (5.37)$$

If the amount of natural dispersion that needs to be overcome in a given process is less than $\Delta n_{1/2}$ given by (5.36), the normal nonlinear processes can achieve perfect phase matching by introducing the periodic stratification.

Phase matching can also be achieved by utilizing the birefringence property of the periodic medium. The difference in the refractive indices of the ordinary waves and extraordinary waves is given by

$$n_o - n_e = \frac{4ab}{\Lambda^2} \frac{n_e^2}{n_o + n_e} (\Lambda^2 - 1) \qquad (5.38)$$

However, this quantity is much smaller compared with $\Delta n_{1/2}$ (5.36) for $\Delta - 1 \ll 1$.

(B) <u>Umklapp Nonlinear Processes (s ≠ 0)</u>

An Umklapp nonlinear process can be thought of as the generation of a wave at the mixed frequency (such as $\omega_3 = \omega_1 + \omega_2$) with, simultaneously, a Bragg reflection. The additional momentum in this process is obviously provided by the periodic stratified medium (or, in other words, transferred to the periodic stratified medium). Umklapp phase-matched nonlinear processes can take place in any dispersive medium under appropriate conditions. For example, the phase mismatch due to the normal dispersion of the material can always be compensated by the crystal momentum, i.e., choosing the period so that (5.28) is satisfied for some combination of m, n, ℓ, p. The missing wave momentum is thus provided by the periodicity of the integrand in (5.21). It can come from either the Fourier component of the nonlinear coefficient, i.e., m ≠ 0, or the space harmonics of the Bloch waves, or both. The Umklapp nonlinear process is thus a way to achieve phase matching when the periodicity dispersion (5.36) is not big enough to compensate the material dispersion.

Traditionally this process can be thought of an interaction between the space harmonics of the Bloch waves (5.22- 5.25), since the rate of power transfer will involve, according to (5.26), the amplitudes of the space harmonics.

5.5 DFB Soft X-Ray Lasers in Periodic Stratified Media

In this section we consider the possibility of using a layered structure as a medium for x-ray laser. The huge pump intensities which

will be required to overcome the ordinary photoelectric losses in the x-ray region will limit the pumped region to very small volumes. Under these conditions the use of an external resonator structure seems highly unlikely. One proposal advanced earlier [6] was to use the periodicity of natural crystal to provide oscillation feedback by Bragg reflection. In what follows we consider the possibility of obtaining Bragg x-ray laser action in artificial layered media. In such media we have the freedom of tailoring the period exactly so that the Bragg condition is satisfied at the oscillation wavelength. In addition no crystals exist in which the unit cell dimensions are comparable to oscillation wavelengths of, say, 100Å.

We will thus consider a layered medium in which one of the layers provides gain at some frequency ω. Since the presence of gain or loss can be represented by the use of complex indices of refraction we need to extend the analysis of part I to the case of media with complex indices. The coefficient of reflectivity of the N layered structure is given as in (33) of part I by

$$r_N = \frac{CU_{N-1}}{AU_{N-1} - U_{N-2}} \tag{5.39}$$

while the transmission is

$$t_N = \frac{1}{AU_{N-1} - U_{N-2}} \tag{5.40}$$

The complex indices of refraction are taken as

$$\hat{n}_1 = n_1 + i\kappa_1 \tag{5.41}$$

$$\hat{n}_2 = n_2 + i\kappa_2 \tag{5.42}$$

The imaginary part of a refractive index is directly related to the bulk loss constant (or gain) by the following relation.

$$\alpha_{1,2} = 2\kappa_{1,2}\frac{\omega}{c} \tag{5.43}$$

Consider next a periodic stratified medium with alternating gain and loss layers ($\alpha_1 > 0$, $\alpha_2 < 0$).

Such a structure could result if we were to fabricate, as an example, an artificial layered medium composed alternately of two media-- 1 and 2 and then pump it by an incoherent x-ray beam or an intense laser source. Since the layers are different the effect of the pump can be to produce an inversion in layer 2, say, at some characteristic x-ray frequency. We thus have a situation where x-ray radiation of the characteristic frequency is amplified in layer 2 but is absorbed by the photoelectric effect in layer 1. We will show next that if the unit cell (i.e. the alternation period) length Λ is chosen near the Bragg value $\ell\lambda_g/2$ then oscillation may result. The determination of the threshold pumping requires an exact formulation of the electromagnetic problem. This becomes possible with the aid of the Bloch formalism developed in Chapter 2.

We choose n_1 and n_2 as well as α_1 as parameters, take the layer thicknesses a = b = $\Lambda/2$ and investigate the reflectivity r_N of a 10 period slab (N = 10) as a function of $\omega\Lambda/c$ and α_2. The contour plot of $|r_N|$ in the α_2-ω plane are shown in Figure 5.5. A series of points where $|r_N| = \infty$ are found in the lower half plane ($\alpha_2 < 0$). The coordinates of these poles correspond to the threshold gains and the oscillation frequencies of the laser. The number of poles is exactly N, which is

the number of periods. The pole trajectory in the α_2-ω plane indicates that the pole nearest the bandgap has the lowest threshold gain. The threshold gain α_{2t} is approximately equal to loss α_1 for modes whose frequency is far away from the bandgap. However, it is much less than the loss when the oscillation is near the bandgap. In our example $|\alpha_{2t}| \simeq \alpha_1/3$. This theoretical result can be explained as follows: The power dissipation per unit area is proportional to

$$J = \int \alpha(x) \, E^2(x) \, dx \qquad (5.44)$$

where

$$\alpha(x) = \begin{cases} \alpha_1 > 0 & \text{Layer 1} \\ \alpha_2 < 0 & \text{Layer 2} \end{cases} \qquad (5.45)$$

If the lasing mode intensity distribution can have its maxima in the gain layers and minima in the loss layers, power generation (J<0) is possible even when the integrated loss is positive, or in other words when

$$\int \alpha(x)dx > 0 \qquad (5.46)$$

In the conventional Fabry-Perot laser where $\alpha(x) = $ constant, power generation requires a net positive gain (negative loss)

$$\alpha L < 0 \qquad (5.47)$$

That means the laser medium of the conventional laser has to be pumped until the gain conquers the loss. However, in a periodic multilayer laser the gain constant of the gain layer does not have to be larger

than the loss constant of the loss layer assuming the same layer thickness. This is similar to the "Borrmann effect" of an x-ray propagating in a crystal [7]. This finding is of large significance to x-ray lasers, since it should make possible significant reductions in the threshold pumping requirements.

The field distribution near oscillation of a typical multilayer x-ray laser is shown in Figure 5.6. Notice that the local maxima of the field amplitude are all located in the gain layers. The parameters correspond to the low threshold pole of Figure 5.5.
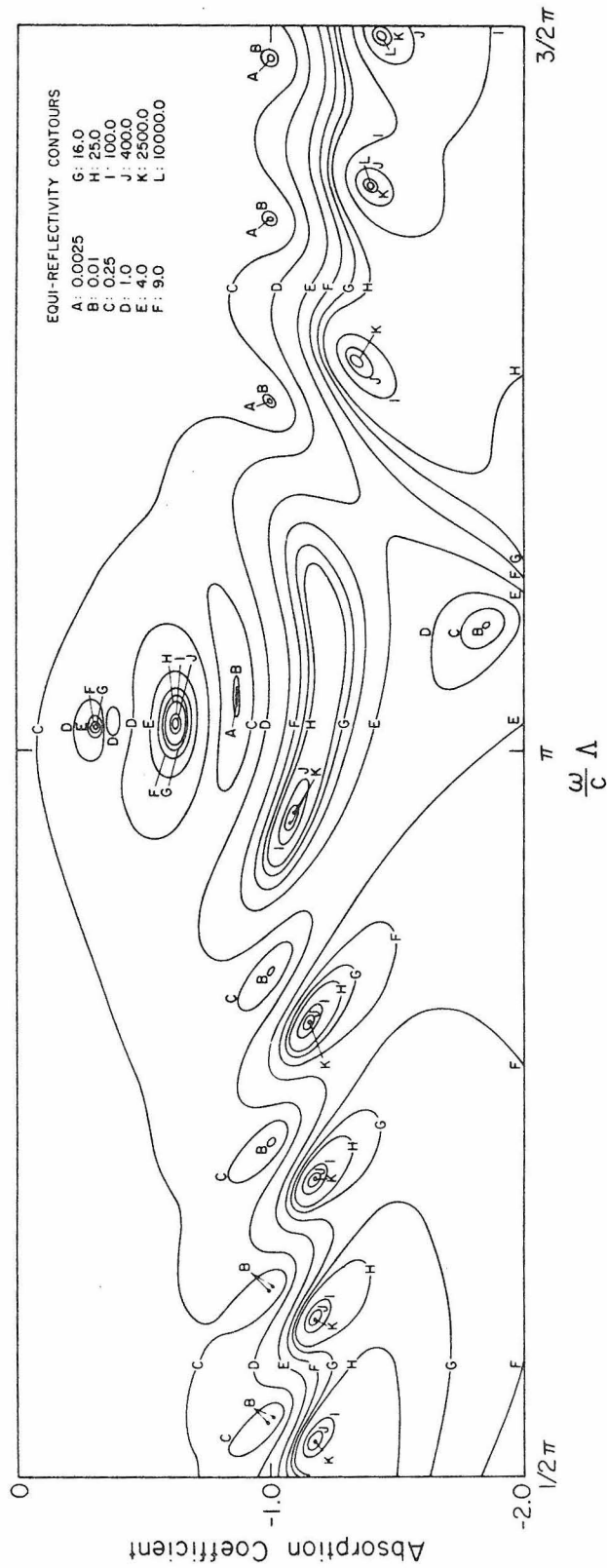
EQUI-REFLECTIVITY CONTOURS

A: 0.0025   G: 16.0
B: 0.01   H: 25.0
C: 0.25   I: 100.0
D: 1.0   J: 400.0
E: 4.0   K: 2500.0
F: 9.0   L: 10000.0

Absorption Coefficient

$\frac{\omega}{c} \Lambda$

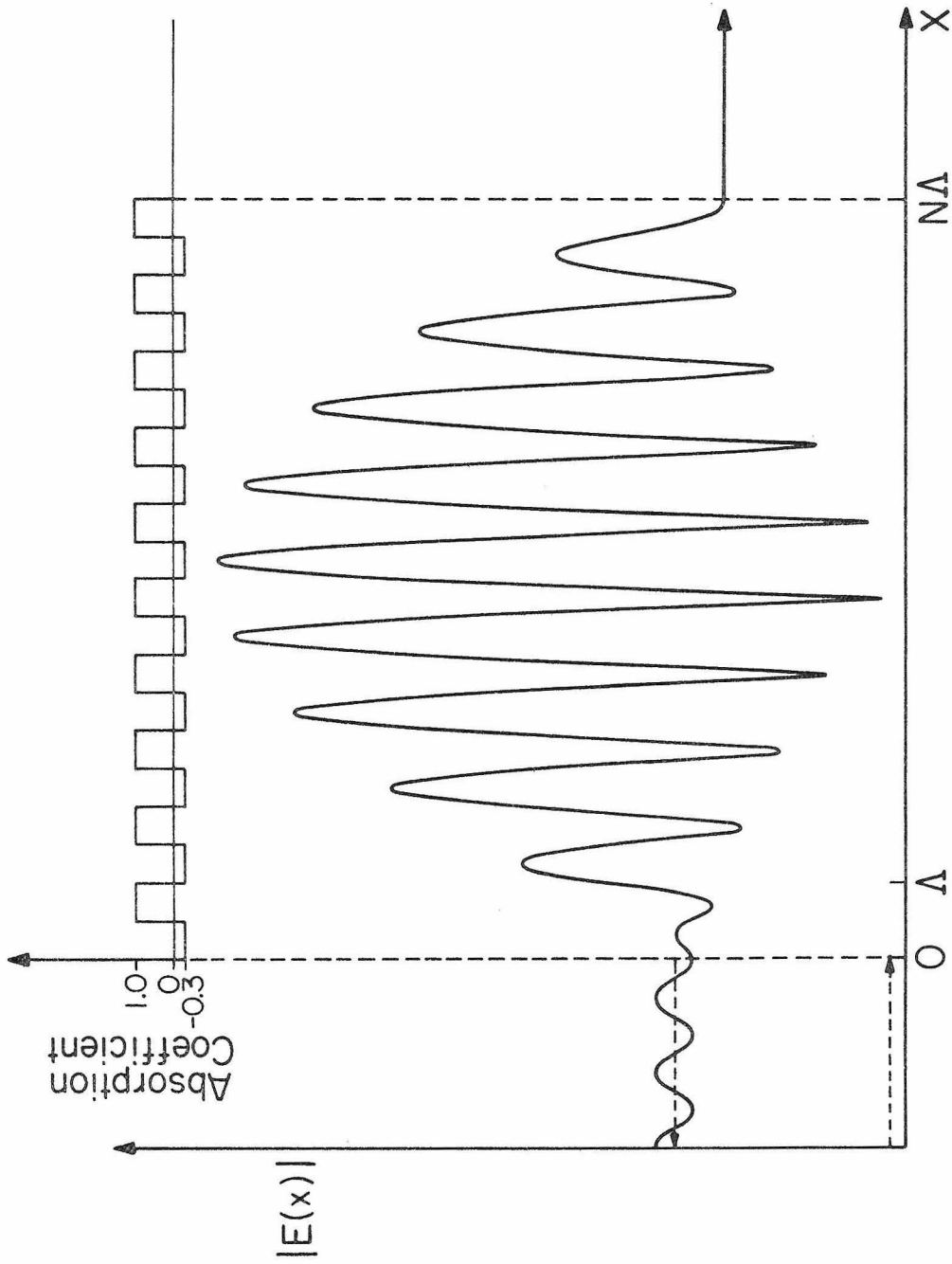Fig. 5.5 Contours of equal reflectivity in $\omega - \alpha_2$ plane.

Fig. 5.6 Field distribution near oscillation. The dashed arrows indicate incident and reflected waves respectively. The solid arrow at the right hand side indicates the transmitted wave. The inset in the upper part is the gain-loss profile.

References - Chapter 5

1. See, for example, A. Yariv, Quantum Electronics, 2nd ed. (Wiley, New York, 1975), p. 423.

2. A. Ashkin and A. Yariv, Bell Labs. Tech. Memo MM-61-124-46 (November 13, 1961).

3. N. Bloembergen and A. J. Sievers, Appl. Phys. Lett. 17, 483 (1970).

4. C. L. Tang and P. P. Bey, IEEE J. Quant. Electron. QE-9, 9 (1973).

5. J. P. van der Ziel, M. Ilegems, and R. M. Mikulyak, Appl. Phys. Lett. 28, 735 (1976).

6. A. Yariv, Appl. Phys. Lett. 25, 105 (1974).

7. B. W. Batterman, Rev. of Mod. Phys. 36, 681 (1964).

Chapter 6

WAVES IN CYLINDRICALLY LAYERED MEDIA

6.1 Introduction

Propagation of electromagnetic waves in cylindrically symmetric dielectric waveguides has become increasingly important in fiber optics communication. The guiding principle is similar to that of the planar slab waveguide. A dielectric fiber is capable of supporting confined modes provided the refractive index of the guiding region (core) is greater than that of the surroundings (cladding). This ensures the evanescent decay of optical waves as r goes to infinity. Instead of dealing with sine and cosine functions, we have to deal with Bessel functions of both kinds in the cylindrical regimes. A great deal of work has been done on optical propagation in conventional fibers [1,2,3] .

In this chapter we will show that, in principle, confined modes exist in a fiber with a low index core, provided the core is surrounded by a suitably designed alternating cladding of high and low refractive indices (see Fig. 6.1). A fiber with this kind of cladding is called a Bragg fiber and is similar to the situation with the Bragg planar waveguide, where the light is guided by a low index slab. To treat this problem properly we introduce an optimization procedure similar to the one discussed in Section 4.5. Instead of solving the confined modes of a given fiber structure, we search for the fiber structure such that the modes have some desired properties. The guiding of electromagnetic waves in a fiber with a low index core, especially the hollow waveguide, is not
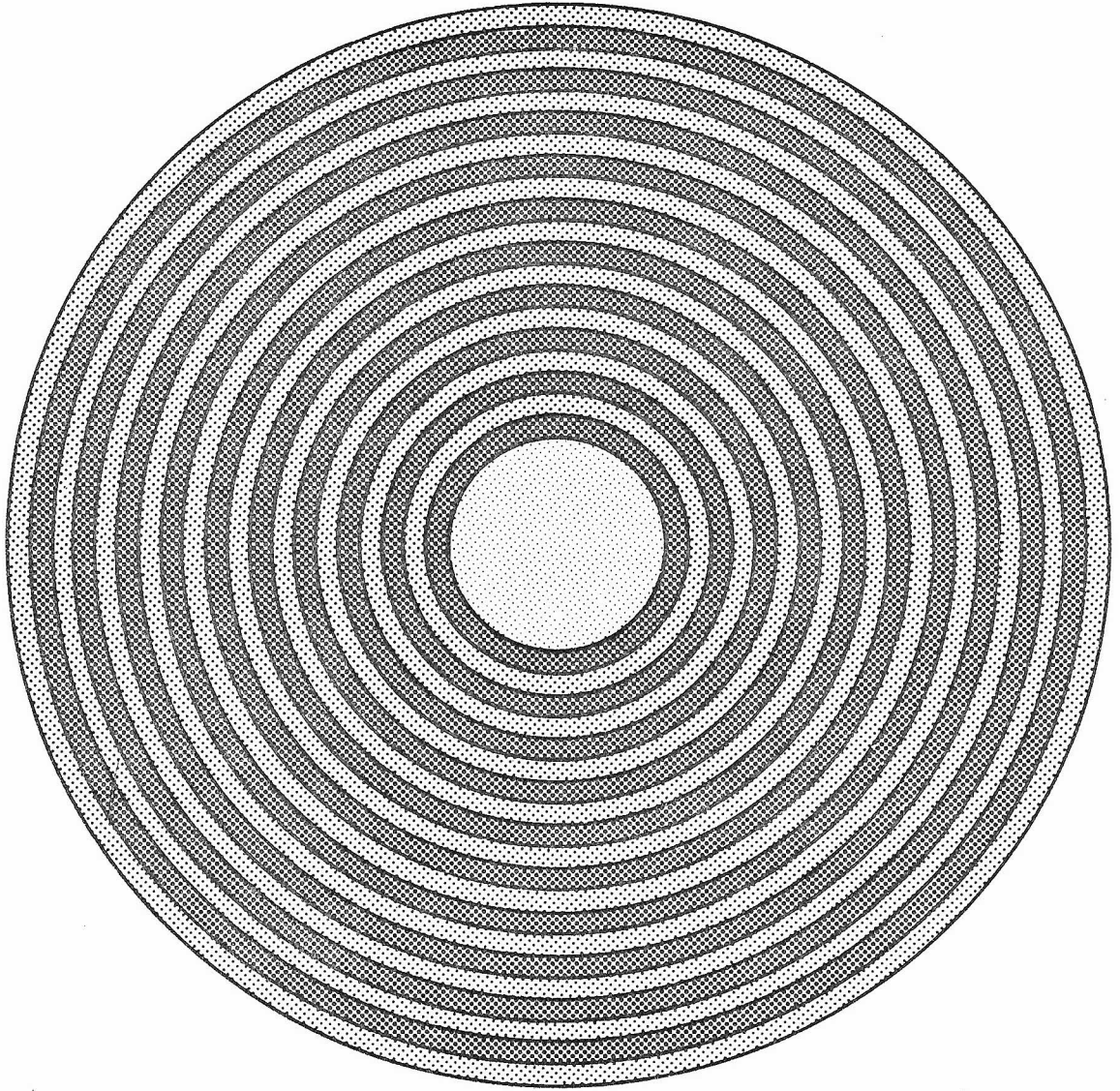
Fig. 6.1 A Bragg fiber

only important in optical communication, but also very useful in the guiding of high power infrared lasers [4]. Another novel application is the guiding of UV or soft x-ray in a hollow Bragg cylindrical waveguide where almost any material is too lossy in that frequency regime. Another important application in fiber optics communication is the design of a single mode fiber. We have shown that a single mode Bragg waveguide can be designed with a guiding layer thickness much larger than a wavelength.

A similar conclusion is derived for cylindrical Bragg waveguides. A single mode fiber is capable of transmitting a light pulse without broadening, due to modal dispersion [5]. Pulse broadening is a serious problem in digital fiber optics communication. It tends to reduce the pulse repetition rate.

6.2 Matrix Method in Concentric Stratified Fiber

In this section we will introduce a matrix method to compute the mode characteristics as well as the power flux of radially stratified fibers. The basic idea is to replace the boundary conditions by a matrix equation. Thus, each cladding interface is represented by a matrix. The introduction of this 4x4 matrix greatly simplifies the analysis.

We consider a fiber with the index profile given by

$$
n(r) = \begin{cases} n_g & 0 \leq r < r_1 \\ n_\nu & r_\nu \leq r < r_{\nu+1} \\ \nu = 1,2,3,\cdots,\infty \end{cases} \tag{6.1}
$$

In particular, we will consider a fiber with a low index core and alternating low and high index cladding. The geometry of this structure

is sketched in Figure 6.1. The index profile is then given by

$$
n(r) = \begin{cases}
n_g & 0 \le r < r_1 \\
n_2 & r_1 \le r < r_2 \\
n_1 & r_2 \le r < r_3 \\
n_2 & r_3 \le r < r_4 \\
n_1 & r_4 \le r < r_5 \\
\vdots & \\
etc. & etc.
\end{cases}
\tag{6.2}
$$

We take the z-axis as the direction of propagation, so that every field component has the form

$$
\psi(r,\theta,z,t) = \psi(r,\theta) \, e^{i(\beta z - \omega t)}
\tag{6.3}
$$

where ψ can be E_z, E_r, E_θ, H_z, H_r, H_θ. ω is the angular frequency and β is the propagation constant.

From waveguide theory we know that the transverse field components can be expressed in terms of E_z and H_z [6]:

$$
E_r = \frac{i\beta}{(\omega^2 \mu\varepsilon - \beta^2)} \left[\frac{\partial}{\partial r} E_z + \frac{\omega\mu}{\beta} \frac{\partial}{r\partial\theta} H_z \right]
\tag{6.4}
$$

$$
E_\theta = \frac{i\beta}{(\omega^2 \mu\varepsilon - \beta^2)} \left[\frac{\partial}{r\partial\theta} E_z - \frac{\omega\mu}{\beta} \frac{\partial}{\partial r} H_z \right]
\tag{6.5}
$$

$$
H_r = \frac{i\beta}{(\omega^2 \mu\varepsilon - \beta^2)} \left[\frac{\partial}{\partial r} H_z - \frac{\omega\varepsilon}{\beta} \frac{\partial}{r\partial\theta} E_z \right]
\tag{6.6}
$$

$$
H_\theta = \frac{i\beta}{(\omega^2 \mu\varepsilon - \beta^2)} \left[\frac{\partial}{r\partial\theta} H_z + \frac{\omega\varepsilon}{\beta} \frac{\partial}{\partial r} E_z \right]
\tag{6.7}
$$

$E_z(r,\theta)$ and $H_z(r,\theta)$ satisfy the wave equation

$$(\nabla_t^2 + (\omega^2\mu\varepsilon - \beta^2))\begin{Bmatrix} E_z \\ H_z \end{Bmatrix} = 0 \qquad (6.8)$$

where $\nabla_t^2 = \nabla^2 - \partial^2/\partial z^2$ is the transverse Laplacian operator. The general solutions can be written

$$E_z = [(AJ_\ell(kr) + BY_\ell(kr)] \cos(\ell\theta + \phi) \qquad (6.9)$$

$$H_z = [(CJ_\ell(kr) + DY_\ell(kr)] \cos(\ell\theta + \psi) \qquad (6.10)$$

where A, B, C, D, ϕ, and ψ are constants, ℓ is an integer, and

$$k = \sqrt{\omega^2\mu\varepsilon - \beta^2} \qquad (6.11)$$

We now consider the boundary conditions at a general cladding interface at $r = \rho$. The solution of the wave equation is taken as

$$E_z = \begin{cases} [A_1 J_\ell(k_1 r) + B_1 Y_\ell(k_1 r)] \cos(\ell\theta + \phi_1) & r < \rho \\ \\ [A_2 J_\ell(k_2 r) + B_2 Y_\ell(k_2 r)] \cos(\ell\theta + \phi_2) & r > \rho \end{cases} \qquad (6.12)$$

and

$$H_z = \begin{cases} [C_1 J_\ell(k_1 r) + D_1 Y_\ell(k_1 r)] \cos(\ell\theta + \psi_1) & r < \rho \\ \\ [C_2 J_\ell(k_2 r) + D_2 Y_\ell(k_2 r)] \cos(\ell\theta + \psi_2) & r > \rho \end{cases} \qquad (6.13)$$

where

$$k_i = \sqrt{\left(\frac{\omega}{c}\right)^2 \varepsilon_i \mu_i - \beta^2} \qquad i = 1,2 \qquad (6.14)$$

The boundary conditions at $r = \rho$ are: E_z, H_z, E_θ and H_θ continuous at

the interface. Thus a 4x4 matrix M can be found which relates A_1, B_1, C_1, D_1 to A_2, B_2, C_2, D_2, i.e.,

$$
\begin{pmatrix} A_2 \\ B_2 \\ C_2 \\ D_2 \end{pmatrix} = M \begin{pmatrix} A_1 \\ B_1 \\ C_1 \\ D_1 \end{pmatrix} \tag{6.15}
$$

Derivation of M

In terms of fields (6.12) and (6.13) the continuity of E_z gives

$$[A_1 J_\ell(k_1\rho) + B_1 Y_\ell(k_1\rho)] \cos(\ell\theta + \phi_1)$$

$$= [A_2 J_\ell(k_2\rho) + B_2 Y_\ell(k_2\rho)] \cos(\ell\theta + \phi_2) \tag{6.16}$$

This equation has to be satisfied for all θ which implies

$$\phi_1 = \phi_2 \tag{6.17}$$

and similarly from the continuity of H_z

$$\psi_1 = \psi_2 \tag{6.18}$$

Thus, continuity of E_z and H_z gives

$$A_1 J_\ell(k_1\rho) + B_1 Y_\ell(k_1\rho) = A_2 J_\ell(k_2\rho) + B_2 Y_\ell(k_2\rho) \tag{6.19}$$

$$C_1 J_\ell(k_1\rho) + D_1 Y_\ell(k_1\rho) = C_2 J_\ell(k_2\rho) + D_2 Y_\ell(k_2\rho) \tag{6.20}$$

In terms of the fields (6.12), (6.13), and (6.5), the continuity of E_θ gives

$$\frac{1}{k_1^2} \left[\frac{-\ell}{\rho} \{A_1 J_\ell(k_1\rho) + B_1 Y_\ell(k_1\rho)\} \sin(\ell\theta + \phi)\right.$$

$$\left. - \frac{\omega\mu_1}{\beta} k_1 \{C_1 J'_\ell(k_1\rho) + D_1 Y'_\ell(k_1\rho)\} \cos(\ell\theta + \psi)\right]$$

$$= \frac{1}{k_2^2} \left[\frac{-\ell}{\rho} \{A_2 J_\ell(k_2\rho) + B_2 Y_\ell(k_2\rho)\} \sin(\ell\theta + \phi)\right.$$

$$\left. - \frac{\omega\mu_2}{\beta} k_2 \{C_2 J'_\ell(k_2\rho) + D_2 Y'_\ell(k_2\rho)\} \cos(\ell\theta + \psi)\right] \qquad (6.21)$$

where the primed quantities are the derivatives with respect to their own argument. Again, this equation has to be satisfied for all θ . From (6.19) and (6.20) we have

$$\frac{1}{k_1^2} \{A_1 J_\ell(k_1\rho) + B_1 Y_\ell(k_1\rho)\} \neq \frac{1}{k_2^2} \{A_2 J_\ell(k_2\rho) + B_2 Y_\ell(k_2\rho)\} \qquad (6.22)$$

$$\frac{1}{k_1} \{C_1 J'_\ell(k_1\rho) + D_1 Y'_\ell(k_1\rho)\} \neq \frac{1}{k_2} \{C_2 J'_\ell(k_2\rho) + D_2 Y'_\ell(k_2\rho)\} \qquad (6.23)$$

provided $k_1 \neq k_2$. Thus we conclude from (6.21)-(6.23) that

$$\sin(\ell\theta + \phi) = \pm \cos(\ell\theta + \psi) \qquad (6.24)$$

or equivalently,

$$\phi = \psi \pm \frac{\pi}{2} \qquad (6.25)$$

Continuity of H_θ and eq. (6.7) gives

$$\frac{1}{k_1^2} \{\frac{-\ell}{\rho} [C_1 J_\ell(k_1\rho) + D_1 Y_\ell(k_1\rho)] \sin(\ell\theta + \psi)$$

$$+ \frac{\omega\varepsilon_1}{\beta} k_1 [A_1 J'_\ell(k_1\rho) + B_1 Y'_\ell(k,\rho)] \cos(\ell\theta + \phi)\} =$$

$$= \frac{1}{k_2^2} \left\{ \frac{-\ell}{\rho} \left[C_2 J_\ell(k_2\rho) + D_2 Y_\ell(k_2\rho) \right] \sin(\ell\theta + \psi) \right.$$

$$\left. + \frac{\omega\varepsilon_2}{\beta} k_2 \left[A_2 J_\ell'(k_2\rho) + B_2 Y_\ell'(k_2\rho) \right] \cos(\ell\theta + \phi) \right\} \quad (6.26)$$

From (6.24) or (6.25) we can classify the waves into two categories:

I
$$E_z = (A J_\ell(kr) + B Y_\ell(kr)) \cos \ell\theta$$
$$H_z = (C J_\ell(kr) + D Y_\ell(kr)) \sin \ell\theta$$
$$(6.27)$$

II
$$E_z = (A J_\ell(kr) + B Y_\ell(kr)) \sin \ell\theta$$
$$H_z = (C J_\ell(kr) + D Y_\ell(kr)) \cos \ell\theta$$
$$(6.28)$$

The boundary conditions for these two categories are summarized below:

I

$$A_1 J_\ell(k_1\rho) + B_1 Y_\ell(k_1\rho) + 0 + 0 = (1 \to 2) \quad (6.29)$$

$$\frac{\omega\varepsilon_1}{k_1\beta} A_1 J_\ell'(k,\rho) + \frac{\omega\varepsilon_1}{k_1\beta} B_1 Y_\ell'(k_1\rho) + \frac{\ell}{k_1^2\rho} C_1 J_\ell(k_1\rho) + \frac{\ell}{k_1^2\rho} D_1 Y_\ell(k_1\rho) = (1 \to 2) \quad (6.30)$$

$$0 + 0 + C_1 J_\ell(k_1\rho) + D_1 Y_\ell(k_1\rho) = (1 \to 2) \quad (6.31)$$

$$\frac{\ell}{k_1^2\rho} A_1 J_\ell(k_1\rho) + \frac{\ell}{k^2\rho} B_1 Y_\ell(k_1\rho) + \frac{\omega\mu_1}{k_1\beta} C_1 J_\ell'(k_1\rho) + \frac{\omega\mu_1}{k_1\beta} D_1 Y_\ell'(k_1\rho) = (1 \to 2) \quad (6.32)$$

where $(1 \to 2)$ means the same functional form with subscript 1 replaced by 2, and vice versa.

II - Similar equations for the second category, except that ℓ is replaced by $-\ell$.

Equations (6.29)-(6.32) can be written as a matrix equation

$$
M(1,\rho) \begin{pmatrix} A_1 \\ B_1 \\ C_1 \\ D_1 \end{pmatrix} = M(2,\rho) \begin{pmatrix} A_2 \\ B_2 \\ C_2 \\ D_2 \end{pmatrix}
\tag{6.33}
$$

with

$$
M(i,\rho) = \begin{bmatrix}
J_\ell(k_i\rho) & Y_\ell(k_i\rho) & 0 & 0 \\[2ex]
\dfrac{\omega\varepsilon_i}{\beta k_i} J'_\ell(k_i\rho) & \dfrac{\omega\varepsilon_i}{\beta k_i} Y'_\ell(k_i\rho) & \dfrac{\ell}{k_i^2\rho} J_\ell(k_i\rho) & \dfrac{\ell}{k_i^2\rho} Y_\ell(k_i\rho) \\[2ex]
0 & 0 & J_\ell(k_i\rho) & Y_\ell(k_i\rho) \\[2ex]
\dfrac{\ell}{k_i^2\rho} J_\ell(k_i\rho) & \dfrac{\ell}{k_i^2\rho} Y_\ell(k_i\rho) & \dfrac{\omega\mu_i}{\beta k_i} J'_\ell(k_i\rho) & \dfrac{\omega\mu_i}{\beta k_i} Y'_\ell(k_i\rho)
\end{bmatrix}
$$

$$
i = 1,2 \tag{6.34}
$$

We notice that when $\ell = 0$, the matrix is reducible. In other words, we can have pure TE or pure TM waves when $\ell = 0$.

The matrix in eq. (6.15) can be written, using (6.33), as

$$
M = M^{-1}(2,\rho) \, M(1,\rho) \tag{6.35}
$$

If we define $x = k_1\rho$, $y = k_2\rho$ and write M as

$$
M = \frac{\pi y}{2} \begin{pmatrix}
m_{11} & m_{12} & m_{13} & m_{14} \\
m_{21} & m_{22} & m_{23} & m_{24} \\
m_{31} & m_{32} & m_{33} & m_{34} \\
m_{41} & m_{42} & m_{43} & m_{44}
\end{pmatrix}
\tag{6.36}
$$

Using (6.34) and carrying out the matrix multiplication, the matrix elements m_{ij} in (6.36) are obtained as

$$m_{11} = J_\ell(x)\, Y'_\ell(y) - \frac{k_2\varepsilon_1}{k_1\varepsilon_2}\, J'_\ell(x)\, Y_\ell(y)$$

$$m_{12} = Y_\ell(x)\, Y'_\ell(y) - \frac{k_2\varepsilon_1}{k_1\varepsilon_2}\, Y'_\ell(x)\, Y_\ell(y)$$

$$m_{13} = \frac{\beta\ell}{\omega\varepsilon_2}\left(\frac{1}{y} - \frac{1}{x}\right) J_\ell(x)\, Y_\ell(y)$$

$$m_{14} = \frac{\beta\ell}{\omega\varepsilon_2}\left(\frac{1}{y} - \frac{1}{x}\right) Y_\ell(x)\, Y_\ell(y)$$

$$m_{21} = \frac{k_2\varepsilon_1}{k_1\varepsilon_2}\, J'_\ell(x)\, J_\ell(y) - J_\ell(x)\, J'_\ell(y)$$

$$m_{22} = \frac{k_2\varepsilon_1}{k_1\varepsilon_2}\, Y'_\ell(x)\, J_\ell(y) - Y_\ell(x)\, J'_\ell(y)$$

$$m_{23} = \frac{\beta\ell}{\omega\varepsilon_2}\left(\frac{1}{x} - \frac{1}{y}\right) J_\ell(x)\, J_\ell(y)$$

$$m_{24} = \frac{\beta\ell}{\omega\varepsilon_2}\left(\frac{1}{x} - \frac{1}{y}\right) Y_\ell(x)\, J_\ell(y)$$

$$m_{31} = \frac{\beta\ell}{\omega\mu_2}\left(\frac{1}{y} - \frac{1}{x}\right) J_\ell(x)\, Y_\ell(y)$$

$$m_{32} = \frac{\beta\ell}{\omega\mu_2}\left(\frac{1}{y} - \frac{1}{x}\right) Y_\ell(x)\, Y_\ell(y)$$

$$m_{33} = J_\ell(x)\, Y'_\ell(y) - \frac{k_2\mu_1}{k_1\mu_2}\, J'_\ell(x)\, Y_\ell(y)$$

$$m_{34} = Y_\ell(x)\, Y'_\ell(y) - \frac{k_2\mu_1}{k_1\mu_2}\, Y'_\ell(x)\, Y_\ell(y)$$

$$m_{41} = \frac{\beta\ell}{\omega\mu_2}\left(\frac{1}{x} - \frac{1}{y}\right) J_\ell(x)\, J_\ell(y)$$

$$m_{42} = \frac{\beta \ell}{\omega \mu_2} \left(\frac{1}{x} - \frac{1}{y} \right) Y_\ell(x) J_\ell(y)$$

$$m_{43} = \frac{k_2 \mu_1}{k_1 \mu_2} J_\ell'(x) J_\ell(y) - J_\ell(x) J_\ell'(y)$$

$$m_{44} = \frac{k_2 \mu_1}{k_1 \mu_2} Y_\ell'(x) J_\ell(y) - Y_\ell(x) J_\ell'(y) \tag{6.37}$$

Again we find that the transfer matrix M is block diagonalized when $\ell = 0$. In this case the matrix equation (6.15) can be written as two separate equations

$$\begin{pmatrix} A_2 \\ B_2 \end{pmatrix} = M_{TE} \begin{pmatrix} A_1 \\ B_1 \end{pmatrix} \tag{6.38}$$

$$\begin{pmatrix} C_2 \\ D_2 \end{pmatrix} = M_{TM} \begin{pmatrix} C_1 \\ D_1 \end{pmatrix} \tag{6.39}$$

The matrix method described above can be employed to obtain the mode dispersion relations for any conventional fibers. We will, however, use this technique to design a Bragg fiber in the next section.

6.3 Bragg Fibers

Recently, Bragg waveguiding in planar geometry has been successfully demonstrated in a GaAs-AlGaAs multilayer stack (grown by molecular beam epitaxy) [7]. The experimental results are consistent with theoretical calculations. This type of guiding is now extended to the cylindrical regime where we intend to guide the light in a fiber with a low index core. An optimization procedure similar to that of Section 4.5 will be introduced to design an optimum Bragg fiber. Without loss of generality

we will consider TE modes (ℓ = 0 and E_z = 0) only. The only nonvanishing components of the field for TE waves are

$$H_z = (CJ_0(kr) + DY_0(kr))\, e^{i(\beta z - \omega t)} \qquad (6.40)$$

$$E_\theta = -\frac{i\omega\mu}{k^2}\, \frac{\partial}{\partial r}\, H_z \qquad (6.41)$$

$$H_r = \frac{i\beta}{k^2}\frac{\partial}{\partial r}\, H_z \qquad (6.42)$$

where C,D are real constants. C and D are real because the field is normalized such that $H_z = e^{i(\beta z - \omega t)}$ at r = 0. The radial component of the Poynting vector is given by

$$S_r = \frac{1}{2}\, \mathrm{Re}[E_\theta H_z^*] \qquad (6.43)$$

$$= \frac{1}{2}\left\{\mathrm{Re}\,\frac{-i\omega\mu}{k}\,[CJ_0'(kr) + DY_0'(kr)][C^*J_0(kr) + D^*Y_0(kr)]\right\}$$

$$= 0 \qquad \text{for all } r \qquad (6.44)$$

This implies

$$\text{outflowing flux} = \text{inflowing flux} \qquad (6.45)$$

It can be shown that

$$\text{outflowing flux} = \text{inflowing flux} \propto [C^2+D^2]\,\frac{\omega\mu}{k^2} \qquad (6.46)$$

Optimization of Outflowing Flux.

Referring to Figure 6.2, we consider the fields on both sides of a general cladding interface. The z-component of magnetic field is taken as

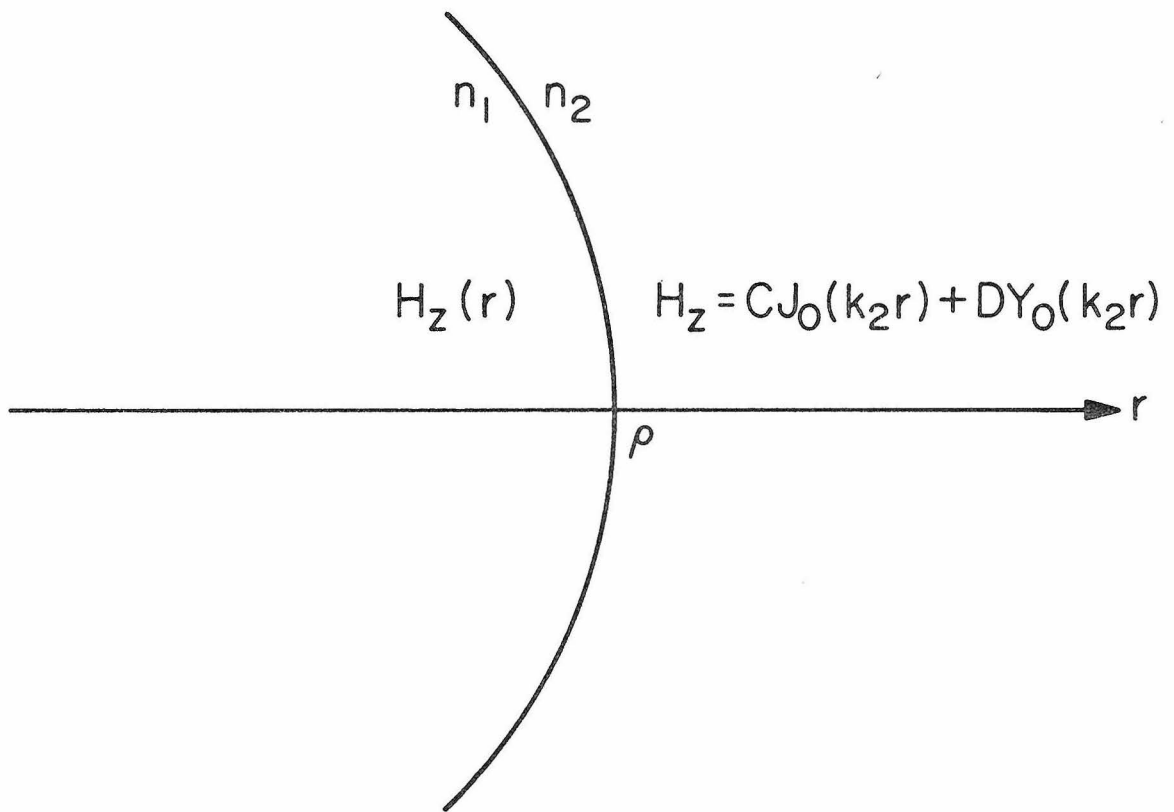$$H_z = \begin{cases} H_z(k_1 r) & r < \rho \\[2mm] CJ_0(k_2\rho) + DY_0(k_2\rho) & r > \rho \end{cases} \qquad (6.47)$$

Fig. 6.2 A general cladding interface at $r = \rho$

where $H_z(r)$ satisfies the wave equation

$$\{\frac{1}{r} \frac{\partial}{\partial r} (r \frac{\partial}{\partial r}) - k_1^2\} H_z(k_1 r) = 0 \tag{6.48}$$

and is determined by the boundary condition at $r = 0$. In terms of fields (6.40), (6.41), (6.42) and (6.47), the continuity of E_θ and H_z gives

$$CJ_0(k_2\rho) + DY_0(k_2\rho) = H_z(k_1\rho) \equiv H(k_1\rho) \tag{6.49}$$

$$\frac{\mu_2}{k_2^2} [Ck_2 J_0'(k_2\rho) + Dk_2 Y_0'(k_2\rho)] = \frac{\mu_1}{k_1^2} k_1 H_z'(k_1\rho) \equiv \frac{\mu_1}{k_1^2} k_1 H'(k_1\rho) \tag{6.50}$$

where primed quantities are the derivatives with respect to their own argument. For the sake of simplicity in algebraic manipulation, we will drop the functional arguments and the z subscript. Thus we have

$$CJ_0 + DY_0 = H \tag{6.51}$$

$$CJ_0' + DY_0' = (\frac{k_2\mu_1}{\mu_2 k_1}) H' \tag{6.52}$$

Solving for C and D from (6.51) and (6.52) we obtain

$$C = \frac{\pi k_2\rho}{2} (HY_0' - \frac{k_2\mu_1}{k_1\mu_2} Y_0 H') \tag{6.53}$$

$$D = \frac{\pi k_2\rho}{2} (\frac{k_2\mu_1}{k_1\mu_2} J_0 H' - J_0' H) \tag{6.54}$$

where we have used the Wronskian of Bessel functions

$$J_0(x) Y_0'(x) - J_0'(x) Y_0(x) = \frac{2}{\pi x} \tag{6.55}$$

The magnitude of C and D depends on ρ. The purpose of optimization procedure is to find a ρ such that

$$\frac{\partial}{\partial\rho} [C^2+D^2] = 0 \tag{6.56}$$

By carrying out the partial differentiation with respect to ρ, we obtain

$$\frac{\partial}{\partial\rho} [C^2+D^2] = \frac{1}{2} (\frac{\pi k_2\rho}{2})^2 \{[k_2(\frac{\mu_1}{\mu_2} - 1) H^2 - k_1 \frac{k_2\mu_1}{k_1\mu_2} (1 - \frac{k_2^2\mu_1}{k_1^2\mu_2}) H'^2]$$
$$\times (J_0 J_0' + Y_0 Y_0')$$
$$+ HH'[k_1(1 - \frac{k_2^2\mu_1}{k_1^2\mu_2})(J_0'^2 + Y_0'^2) - k_2(\frac{\mu_1}{\mu_2} - 1)\frac{k_2\mu_1}{k_1\mu_2} (J_0^2 + Y_0^2)]\} \tag{6.57}$$

A similar expression can be obtained for TM waves by replacing H by E and μ_i by ε_i, i=1,2.

Equation (6.57) is an exact general expression. If the fiber materials are pure dielectric, (6.57) can be simplified by using $\mu_2 = \mu_1$,

$$\frac{\partial}{\partial\rho} [C^2+D^2] = \frac{1}{2} (\frac{\pi k_2\rho}{2})^2 (1 - \frac{k_2^2}{k_1^2}) H'\{k_1 H(J_0'^2 + Y_0'^2) - k_2 H'(J_0 J_0' + Y_0 Y_0')\} \tag{6.58}$$

A further simplification can be made if we notice that

$$\frac{J_0(x) J_0'(x) + Y_0(x) Y_0'(x)}{J_0'^2(x) + Y_0'^2(x)} \quad \underset{x \gg 1}{\sim} \quad 0(\frac{1}{x}) \tag{6.59}$$

In practical application $x = k_2\rho$ is a large number (i.e., $k_2\rho \gg 1$) even in the first cladding interface. Therefore, the last term in (6.58) can

be neglected. Thus we obtain

$$\frac{\partial}{\partial\rho}\left[C^2+D^2\right] = \frac{1}{2}\left(\frac{\pi k_2\rho}{2}\right)^2 \left(1 - \frac{k_2^2}{k_1^2}\right) k_1\left[J_0'^2(k_2\rho) + Y_0'^2(k_2\rho)\right]H_z(k_1\rho)H_z'(k_1\rho)$$

(6.60)

Equation (6.60) looks similar to (4.32) which is the corresponding equation for planar geometry. The same arguments show that minimization of outflowing flux occurs at $E_\theta = H_z' = 0$ if $k_2 > k_1$, and $E' = H_z = 0$ if $k_2 < k_1$. In a transition through the interface the field amplitude decreases by a factor of (k_1/k_2) if $k_2 > k_1$ and $E_\theta = 0$. The field amplitude, however, does not increase for $k_2 < k_1$ provided the interface is located at the local maximum of E_θ, i.e., $E_\theta' = 0$. Thus by employing alternating claddings with different refractive indices, the field amplitude will decrease by a factor of (k_1/k_2) per pair of cladding, provided the interfaces are located according to the minimization procedure. As a result the field amplitude decreases exponentially as r increases. Theoretically, a confined mode is obtained if the alternating cladding is infinite. However, it is important to notice that the field decay is nearly complete in several pairs of claddings so that practical structures with, say, ten pairs of claddings, are a good approximation to the infinite alternating claddings.

The field distribution for a typical Bragg fiber mode is shown in Figure 6.3. We notice that each pair of claddings is exactly half-wave thickness. The half-wave thickness means that the cylindrical optical wave (Bessel functions) experiences a phase change of π in that thickness.
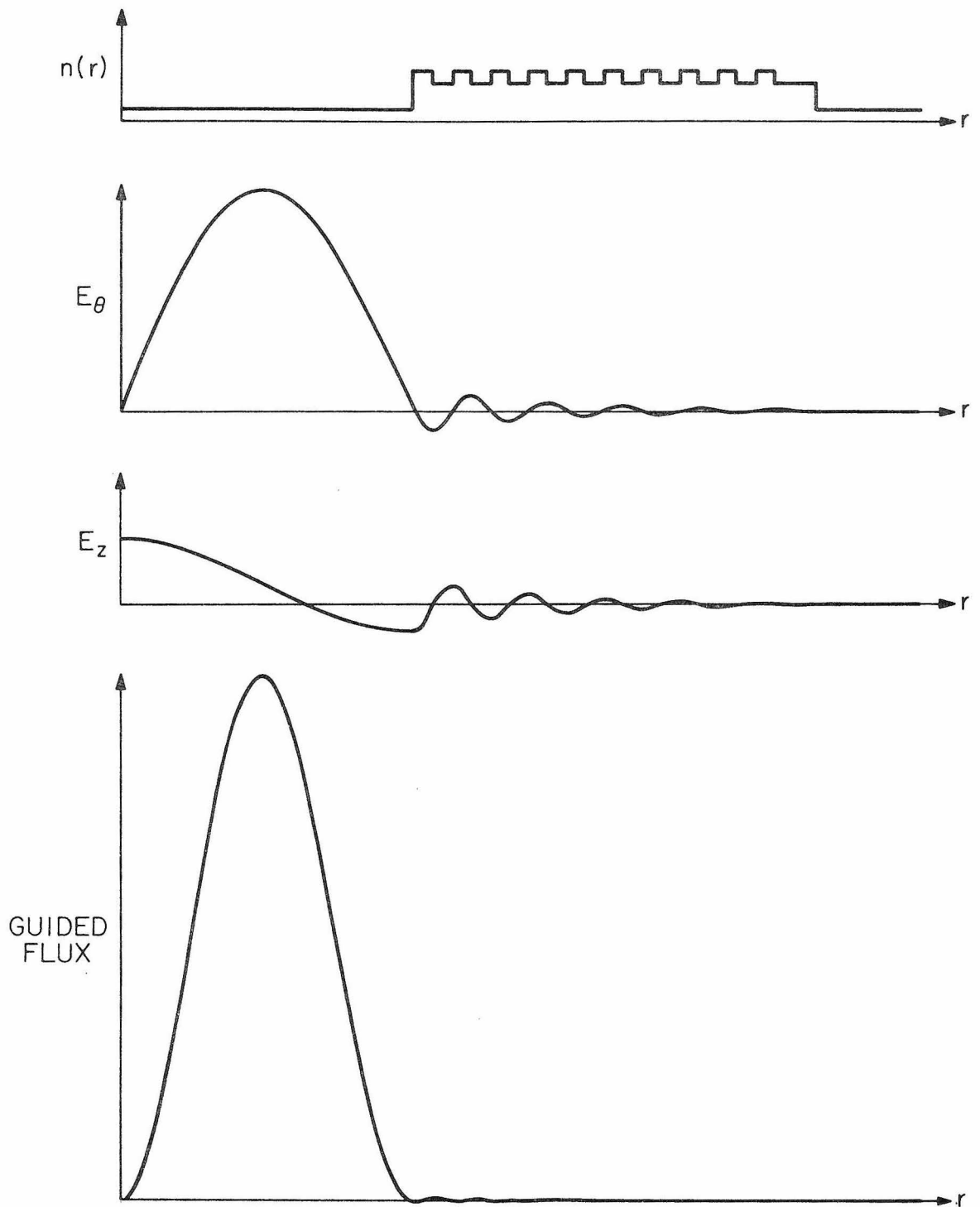
Fig. 6.3 Field distribution and guided flux of a typical Bragg fiber.

Because of the fact that the zeros of Bessel function are not equally spaced, the cladding thicknesses are not exactly identical. However, they tend to become identical as r becomes large. This is due to the asymptotic form of the Bessel functions which approach sine and cosine functions. The index profile shown in Figure 6.3 looks almost periodic in the cladding region.

The leakage due to finite number of claddings will be discussed in the next section.

6.4 Mode Characteristics and Leak Consideration

A Bragg fiber is usually designed to minimize the leakage for some particular mode. Again, we have the problem of leakage due to finite number of claddings. As a result, some higher order undesired modes may be supported by the same Bragg fiber with larger attenuation coefficients. However, it can be shown numerically that these undesired modes are very lossy. Therefore, Bragg fiber can be employed as a mode filter to select some particular mode from an ensemble of modes.

To study the mode characteristics and leakage problem, we start from a Bragg fiber structure optimized for some particular ray angle θ (or equivalently $\beta = \frac{\omega}{c} n \cos \theta$). Then we study the amplitude reduction factor for any other ray angle θ. The amplitude reduction factor is defined as

$$\eta \equiv \frac{[C^2+D^2]_{r=\infty}}{[C^2+D^2]_{r=0}} \qquad (6.61)$$

This quantity is proportional to the ratio of power flow in the last cladding region to the power flow in the core. Given a Bragg fiber structure,

η is a function of ray angle θ and number of pairs of claddings,

$$\eta = \eta(\theta, N) \qquad\qquad (6.62)$$

Figure 6.4 shows the curves of η vs θ for various N's. The structure is optimized for the fundamental mode. The minima in the curves are the virtual modes [8] of the structure. We can see that the fundamental mode has the best degree of confinement. All the higher order modes are less confined and hence more lossy. This is the basic property of a mode filter.
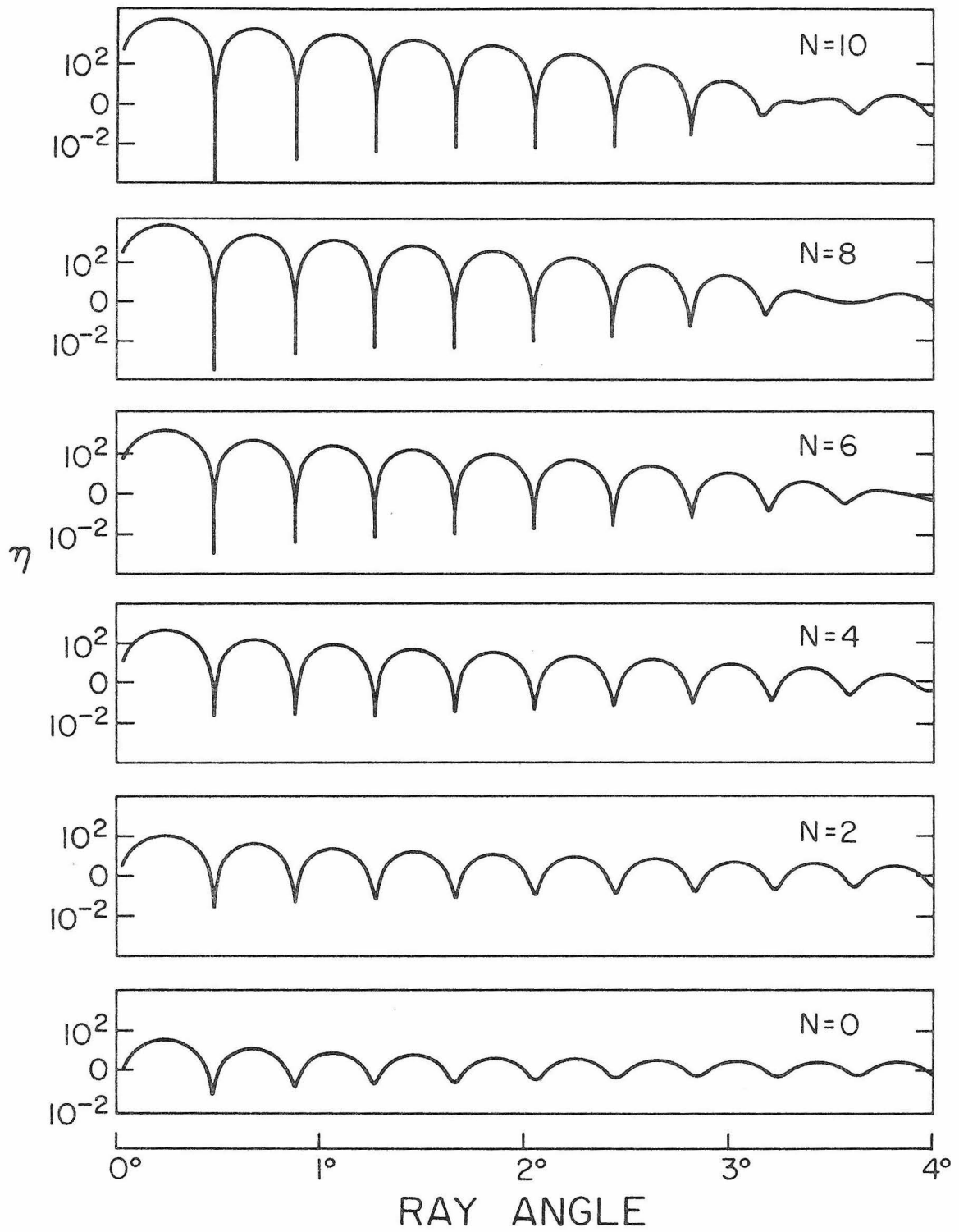
Fig. 6.4 η vs. ray angle for N = 0,2,4,6,8,10.

References - Chapter 6

1. D. Gloge, Optical Fiber Technology, IEEE, New York (1975).

2. E. Snitzer, J. Opt. Soc. Am. 51, 491 (1961).

3. E. Snitzer and H. Osterberg, J. Opt. Soc. Am. 51, 499 (1961).

4. E. Garmire, T. McMahon and M. Bass, Appl. Phys. Lett. 31, 92 (1977).

5. A. Yariv, Appl. Phys. Lett. 28, 88 (1976).

6. J. A. Stratton, Electromagnetic Theory (McGraw-Hill, New York, 1941).

7. A. Y. Cho, A. Yariv and P. Yeh, Appl. Phys. Lett. 30, 471 (1977).

8. They are called virtual modes because their energy is more or less confined.

Chapter 7

EXPERIMENTAL OBSERVATION

7.1 Introduction

We have predicted that Bragg reflection can be used in a new type
of dielectric waveguide in which the conventionally used substrate is
replaced by a periodic layered medium. We used a Bloch wave formulation
of propagation in periodic layered media to obtain the dispersion rela-
tion of a Bragg waveguide [1,2] and showed that, unlike ordinary dielec-
tric waveguides, confined propagation with arbitrarily low loss is
possible even when the guiding layer possesses an index of refraction
which is lower than that of the periodic layers.

The Bloch formulation of wave propagation in periodic layered media
is also applied to the special case of optical surface waves. These
waves, confined to the interface between a periodic layered medium and
a homogeneous medium, are formally analogous to electronic surface states
in crystals. Single mode surface wave propagation along the surface of
a GaAs-AlGaAs multilayer stack (grown by molecular beam epitaxy) has been
observed experimentally.

7.2 Experimental Apparatus

The experimental apparatus for observation of Bragg waveguiding and
optical surface waves is discussed with reference to Figure 7.1. A cw
He-Ne laser beam is focused onto the cleaned edge of the sample. The
output is magnified by the second objective and is scanned over a narrow
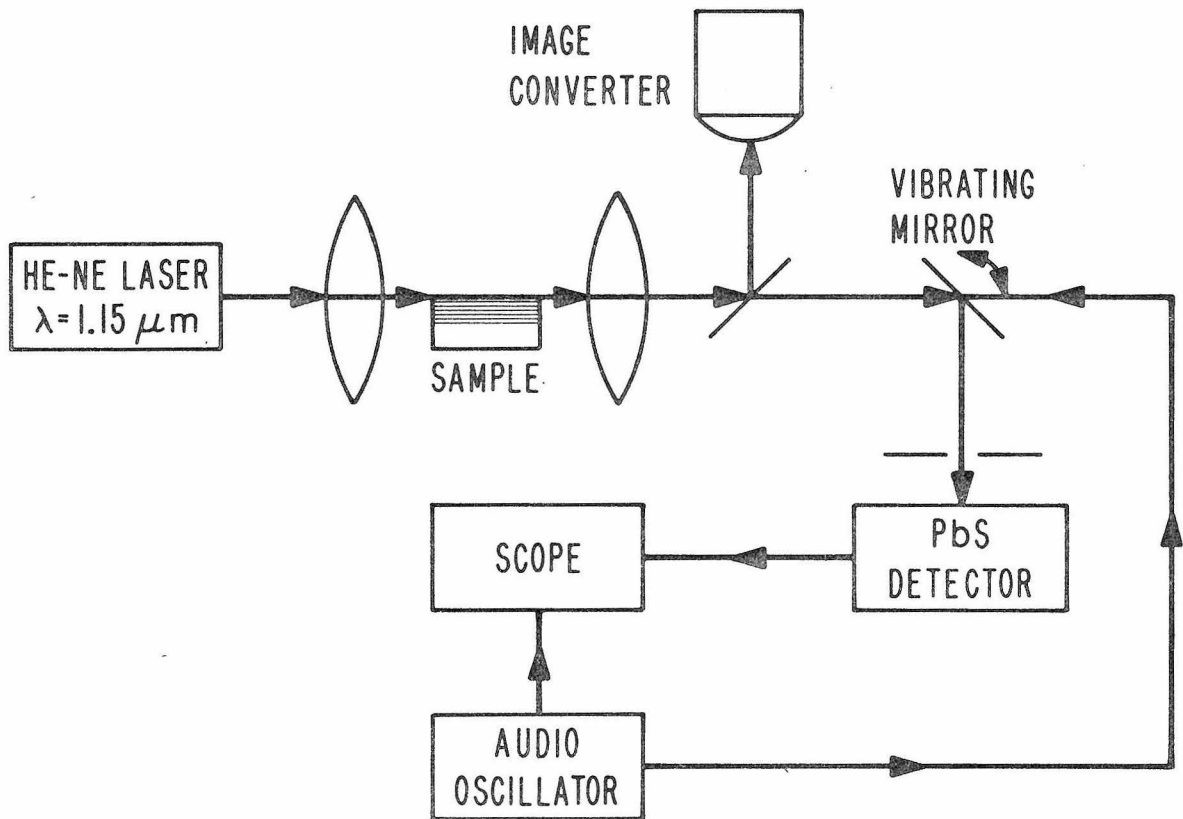slit and PbS photodetector combination [3,4]. The vibrating mirror is

Fig. 7.1 Experimental set-up.

driven by an audio oscillator at 28 Hz. The detector response is displayed on the screen of an oscilloscope.

7.3 Bragg Waveguiding Experiment

The waveguide structure (see Figure 7.2) consists of a guiding layer of $t = 1.37$ µm thick $Al_{0.38}Ga_{0.62}As$ and 8 pairs of alternating layers of $a = 0.26$ µm thick GaAs and $b = 0.26$ µm thick $Al_{0.2}Ga_{0.8}As$ on a GaAs substrate. The layer thicknesses were chosen so that only one mode can exist at the excitation wavelength of 1.15 µm and so that the propagation conditions correspond to the center of the first optical forbidden gap. The waveguide was grown by conventional molecular beam epitaxy (MBE) techniques on a GaAs substrate [5]. Layers were grown at a substrate temperature of 580-600°C at a rate of 1 µm/hr. Ion beam etching was employed subsequent to the growth in order to obtain different thicknesses of the guiding layer.

The resulting intensity distribution for a Bragg waveguide 2 mm long is shown in Figure 7.3. The oscillatory behavior in the layered medium, which has a period of ~ 0.52 µm, could not be resolved with the optics of our imaging system. Despite the resolution limit, we have demonstrated guiding in the Bragg waveguide and the experimental results are consistent with the calculated values.

Because the Bragg reflector has a finite number of periods, the reflection coefficient at the interface between the guiding channel and the Bragg reflector is somewhat less than unity (i.e., the waveguide is slightly "leaky"). The calculated attenuation coefficient of the Bragg waveguide due to the resulting losses into the substrate, but neglecting
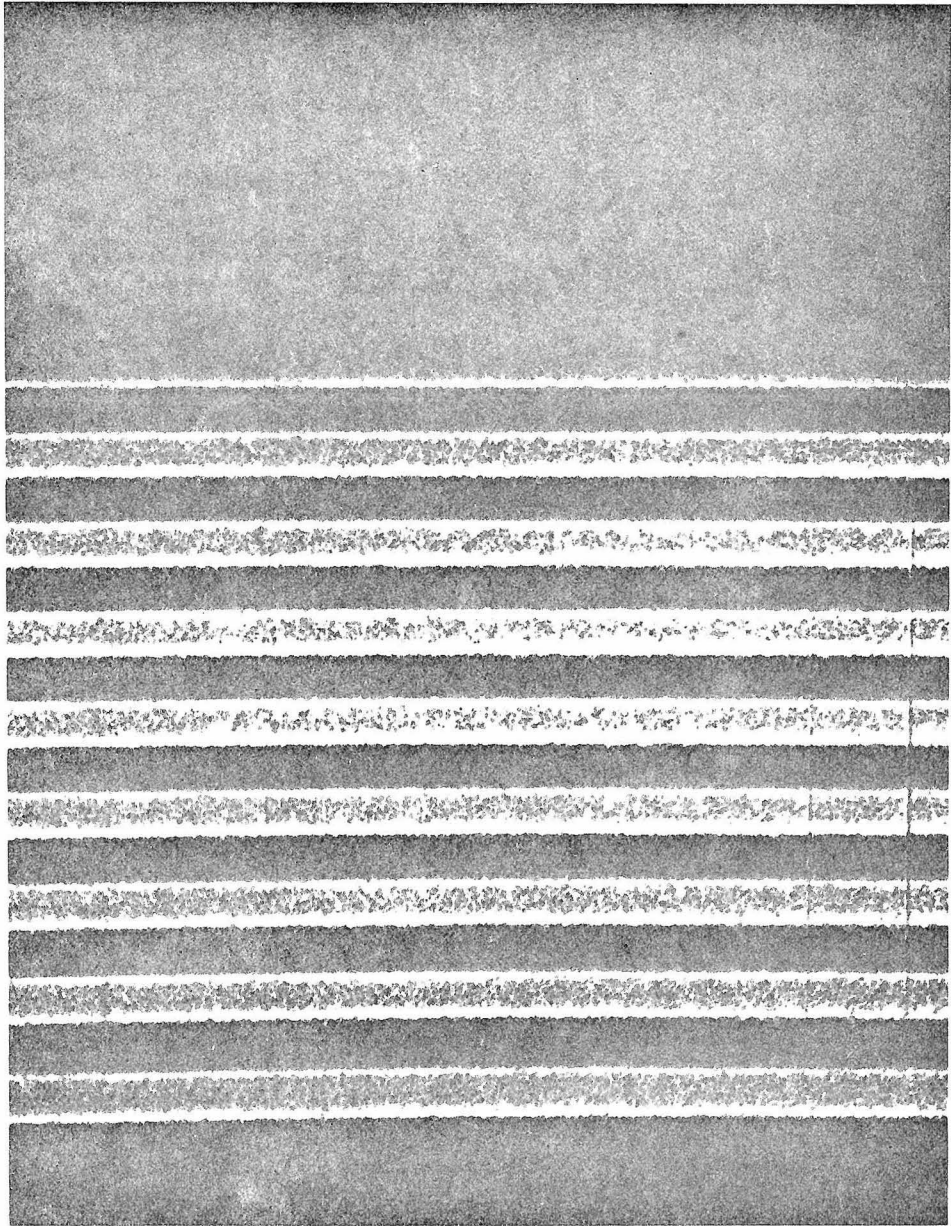
Fig. 7.2 A scanning electron micrograph of a cleaved section of a

Bragg waveguide composed of alternating layers of GaAs and

$Al_{0.20}Ga_{0.80}As$. ·
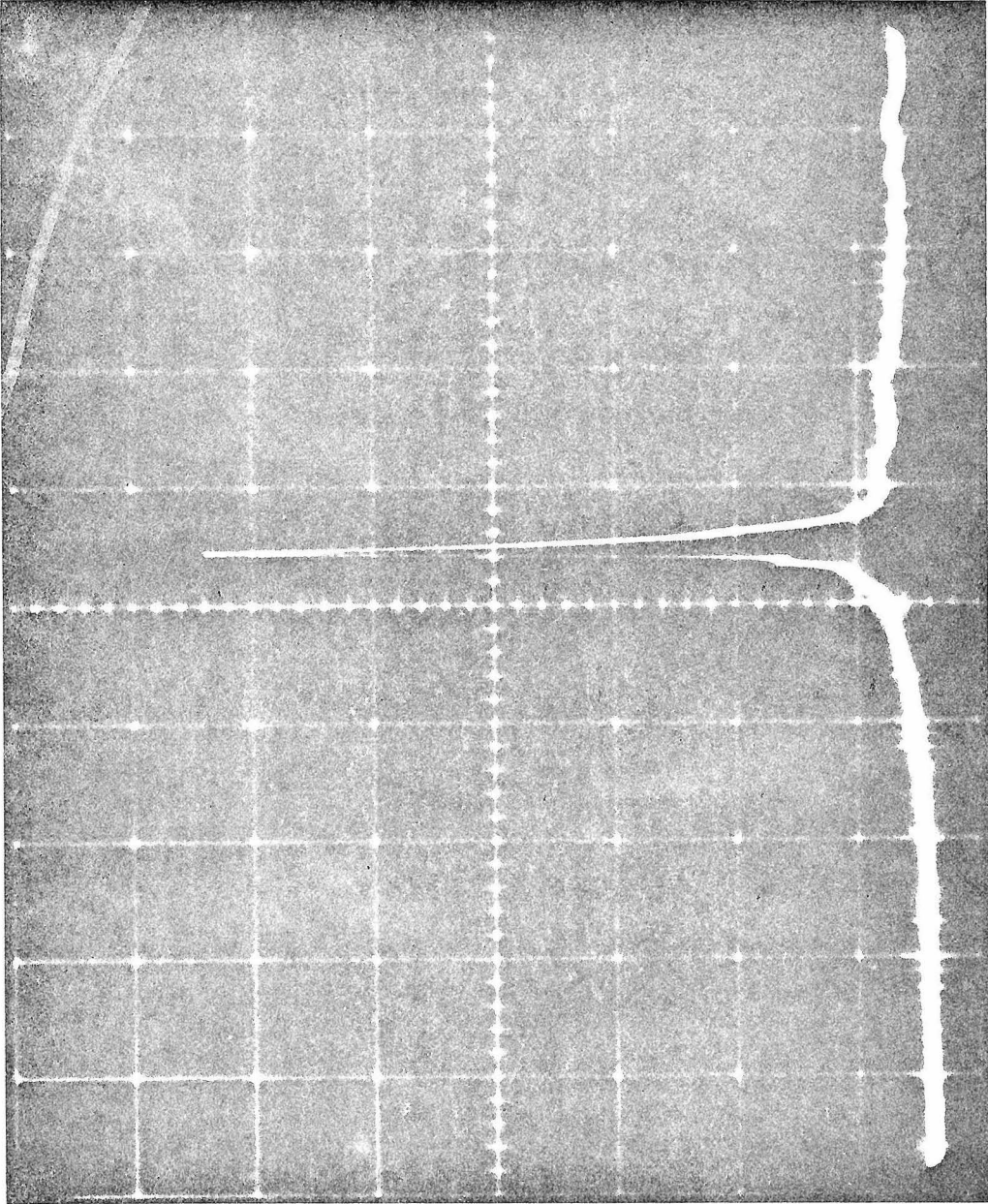
Fig. 7.3 Measured transverse intensity distribution of a confined mode in a Bragg waveguide 2 mm long. The horizontal scale is about 10 μm per (big) division.

the loss due to the bulk absorption [6], is α = 14.97 cm^{-1} and 0.355 cm^{-1} for 8 and 16 periods, respectively. The attenuation coefficient decreases rapidly as the number of periods in the Bragg reflector increases.

The demonstration of Bragg waveguiding described above suggests a number of possibilities: The need to satisfy simultaneously the transverse resonance condition [7] in the guiding layer (i.e., a transverse round trip phase delay equal to an integer times 2) and the Bragg condition in the periodic medium makes it possible to design Bragg waveguides with transverse dimensions large compared with wavelength which can support only one transverse mode. Conventional dielectric waveguides with similar dimensions and index discontinuities would support several transverse modes.

Symmetric Bragg waveguides (i.e., guides with periodic layers on both sides) could be used for guiding in the medium to long x-ray region of the spectrum. Such guiding should possess high wavelength selectivity. The novel Bragg waveguide discussed in this section is a selective transmission waveguide (band-pass filter) while a conventional periodic grating [8] is a selective reflector; these two different optical functions are therefore complementary to each other.

7.4 Optical Surface Wave Experiment

The Kronig-Penney [9] model was introduced in 1931 to demonstrate the band structure of electronic states in crystals. Tamm [10] considered a semi-infinite Kronig-Penney potential and showed that, under certain conditions, surface states appear. The existence of surface

states in a general one-dimensional periodic potential terminated at its potential maximum by a step was also examined by Shockley [11]. He showed that, under appropriate conditions, surface states appeared when the surface "perturbation" was sufficiently small.

The existence of electromagnetic surface waves was suggested by Kossel [12] and later considered in an approximate manner by Arnaud and Saleh [13]. Recently, the band theory of periodic media [14] was used in an exact analysis of the optical surface waves.

According to the Bloch formulation [14] of electromagnetic wave propagation in a layered medium, the electric field has the form of

$$\vec{E}(x,z,t) = \vec{E}_K(x)e^{iKx}e^{i(\beta z - \omega t)} \tag{7.1}$$

where the coordinate axis is oriented such that the wave is propagating in x-z plane and x-axis is normal to the layer interfaces. $\vec{E}_K(x)$ is a periodic function of x with a period equal to that of the medium.

At a given frequency, there are regions of β for which K is complex

$$K = m(\pi/\Lambda) \pm iK_i \tag{7.2}$$

where m is a non-negative integer.

In an infinite periodic medium, solutions with exponential intensity variation, as in eq. (7.1) cannot exist, and we refer to these regions as "forbidden." If the periodic medium is semi-infinite,

the exponentially damped solution is a legitimate solution near the surface. The electric field amplitude is described by a decaying exponential in the homogeneous medium and by a standing wave with an exponentially decaying envelope $\exp(-K_i x)$ in the layered medium. A detailed theory of surface waves in layered media can be found in Chapter 3.

The periodic layered structure in which we observed the surface wave consists of 12 pairs of alternating layers of 0.5 μm thick GaAs and 0.5 μm thick $Al_{0.2}Ga_{0.8}As$ on a GaAs substrate. Under these conditions and at the excitation wavelength of 1.15 μm, our theoretical calculation predicts that exactly four surface modes can be supported by the structure. The transverse intensity distribution for the fundamental mode is shown in Figure 7.4. The computed Bloch wave numbers of these four modes are given in Table I.

The periodic layered structure was grown by conventional molecular beam epitaxy (MBE) techniques [5] on a GaAs substrate. Layers were grown at a substrate temperature of 600° at a rate of about 1 μm/hr. A phase contrast photograph of the structure's cross section is shown in Fig., 7.5.

Our experimental set-up for measuring the mode intensity profiles has a resolution limit of ∿0.5 μm, consequently, in order to resolve the field distribution of the surface waves we need to choose a sample with a period Λ at least 1 μm. For samples with large period Λ, the number of surface modes increases linearly as a function of Λ. This introduces the difficulty of resolving admixtures of surface modes. As a compromise we chose a sample with a period Λ of 1 μm. This structure still supports four surface modes (see Table I). Fortunately, these higher order surface modes are extremely lossy in a sample with a finite number of periods.
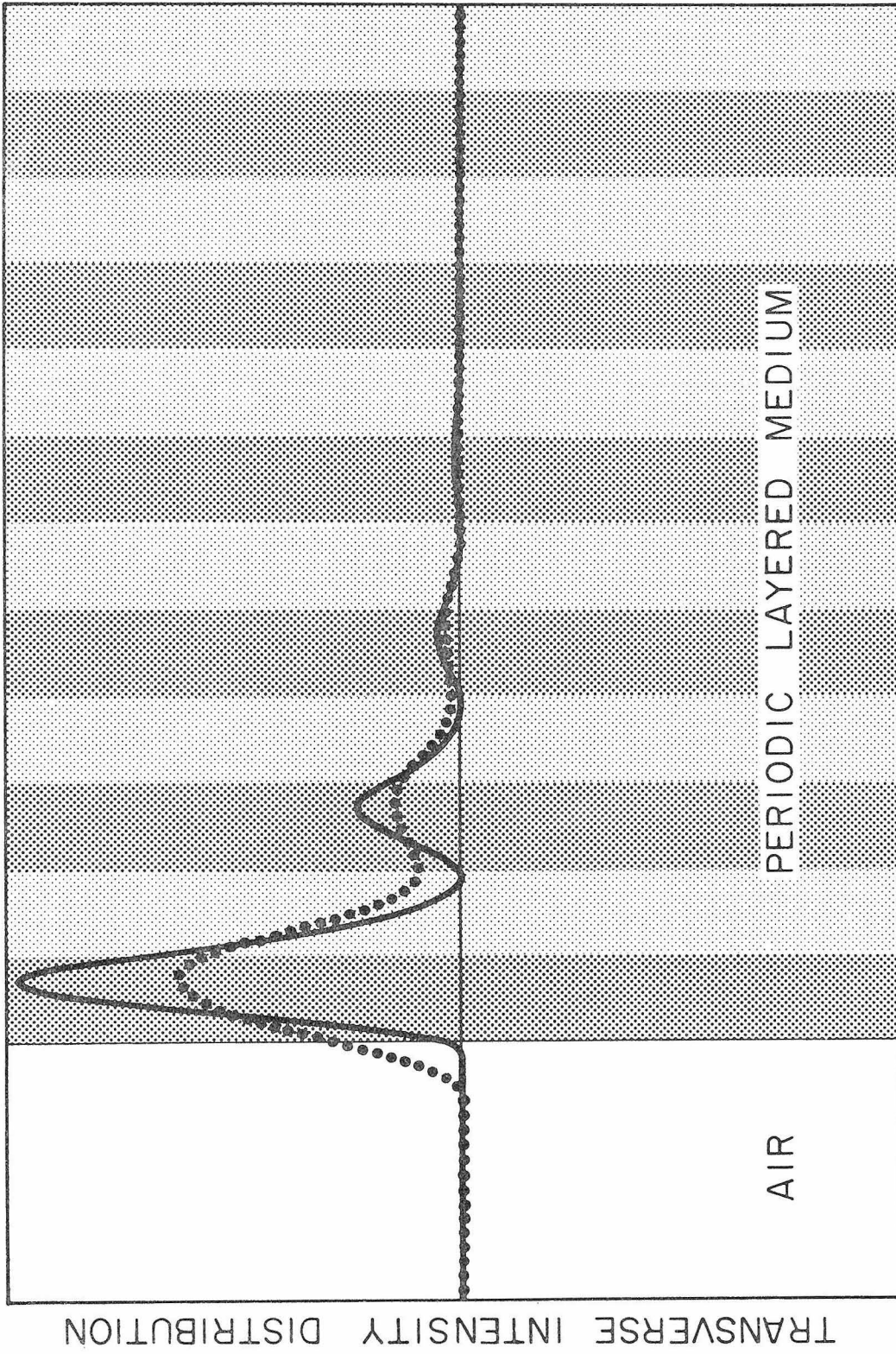
Fig. 7.4 The calculated transverse intensity distribution for the fundamental surface mode in a periodic layered medium. The dotted line is the convolved intensity distribution.

Even if we assume that the modes are excited equally, the lossy modes
will decay to relative insignificance provided the sample is long enough.
We chose a sample 15 mm long, and indeed observed the fundamental mode
(m = 1) only.

The intensity distribution of the surface waves was obtained by
focusing the output of a 1.15 µm He-Ne laser on the cleaved edge of the
sample and by scanning the magnified (x100) image of the output edge[8,9]
past a narrow slit ($\sim$ 50 µm) and detector combination. The resulting in-
tensity distribution is shown in Figure 7.6. This measured distribution is
in excellent agreement with the theoretical prediction, Figure 7.4, if we
convolve the latter with an instrumental window function $\sim$0.5 µm wide.
The result of this convolution is shown in Figure 7.4.

Because the number of periods in the structure is finite, the in-
tensity at the substrate is not exactly zero (i.e., the surface modes are
"leaky"). The calculated attenuation coefficient of each surface mode due
to the resulting losses into the substrate, but neglecting the loss due to
bulk absorption and surface scattering, is given in Table I. The attenua-
tion coefficient decreases exponentially as the number of periods
increases. A rough experimental determination of the mode loss based on
comparing the outputs of a number of samples with varying lengths under
similar input conditions yielded $\alpha < 10^{-2} \text{cm}^{-1}$ for the fundamental mode.
The higher order modes are too lossy to be seen even in a sample 1 mm
long. It is possible that continuum modes may be excited at the input sur-
face. However, these continuum modes are all leaky. For a sample 15 mm
long, the intensities of these modes are extremely small at the output
surface. Interference fringes due to surface reflections can hardly be
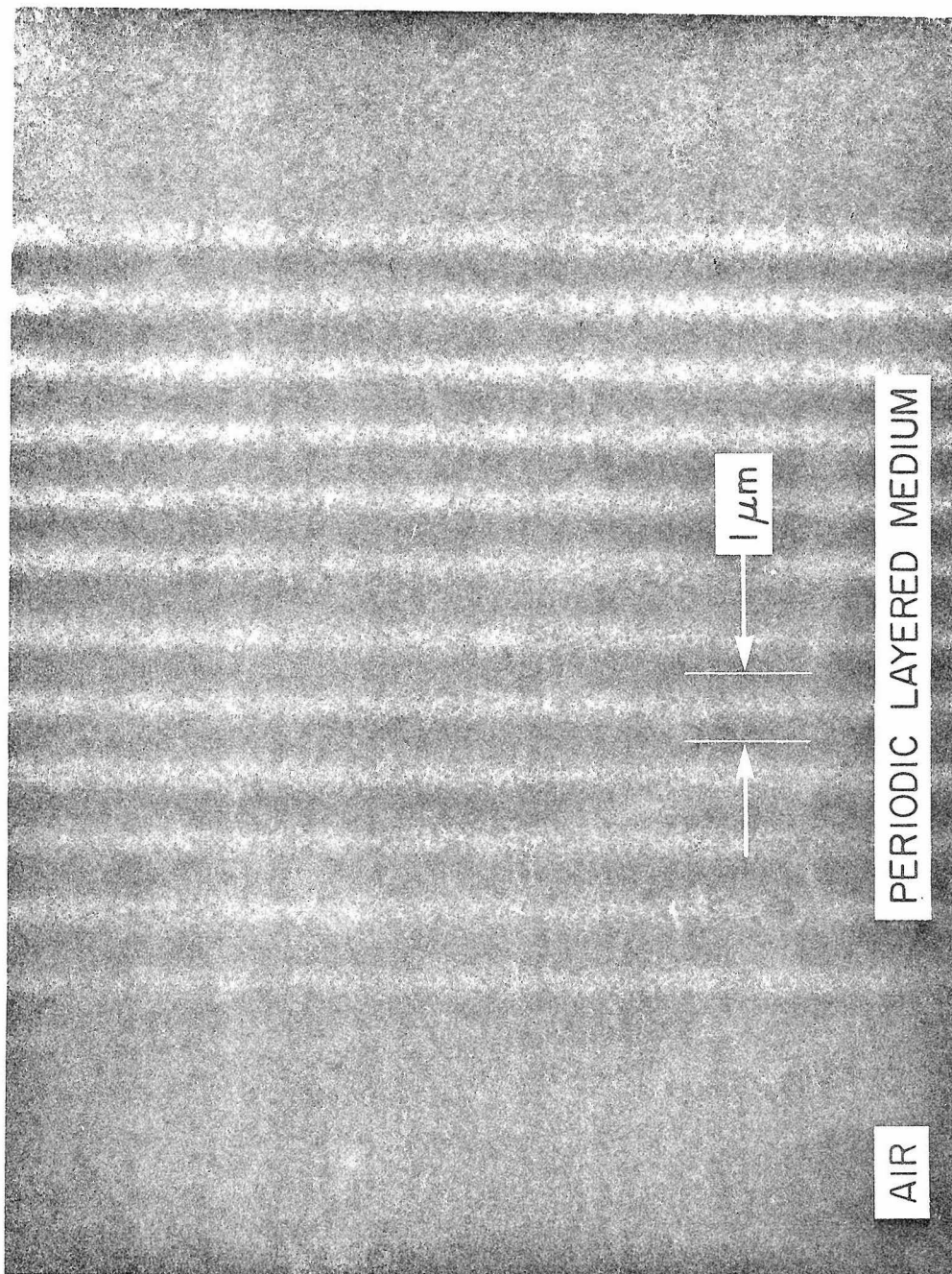
Fig. 7.5 A phase contrast photograph of a cleaved section of a layered medium composed of alternating layers of GaAs and $Al_{0.2}Ga_{0.8}As$.
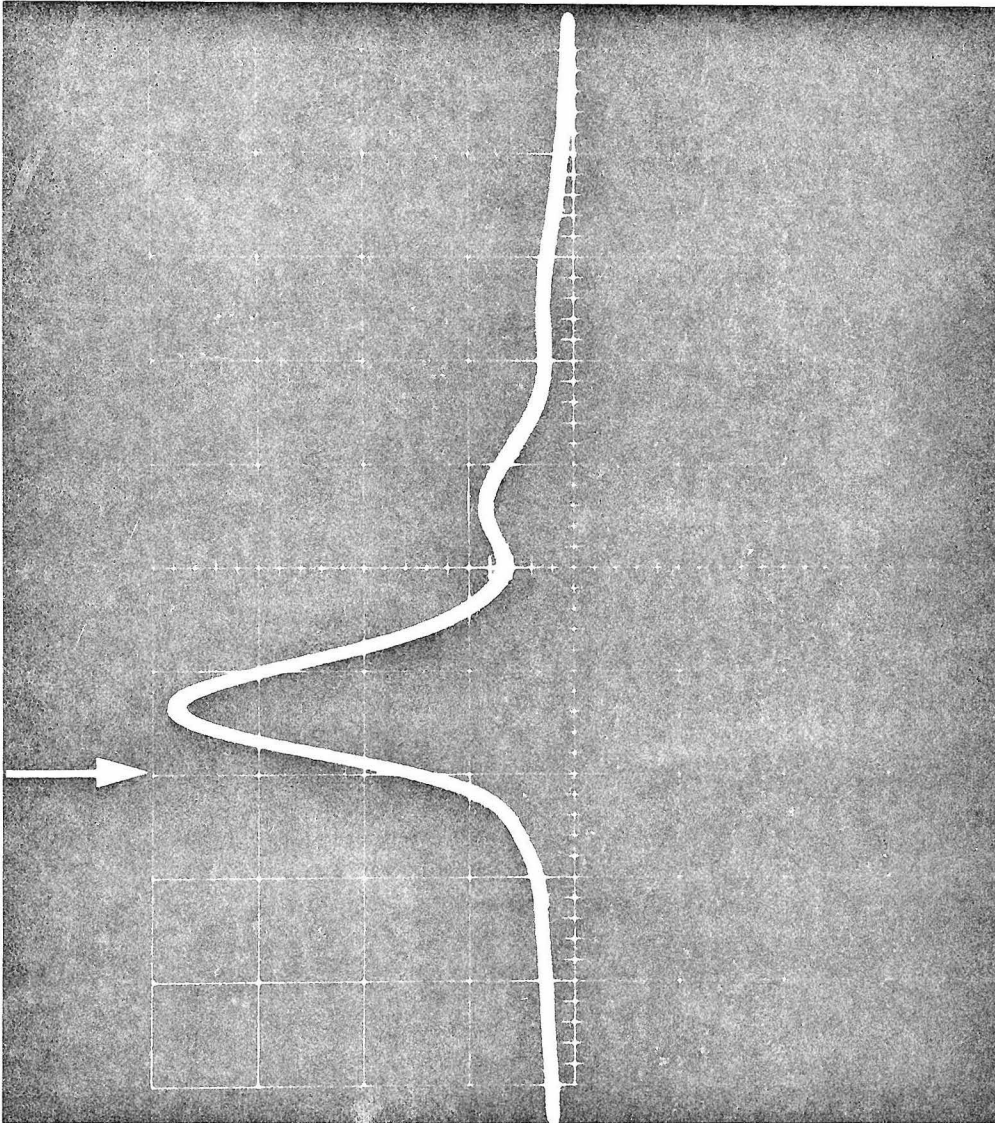
234

Fig. 7.6 Measured transverse intensity distribution of surface waves in a layered medium 15 mm long. The horizontal scale is about 0.5 μm per (big) division. The surface of the structure is indicated by the arrow.

seen in a sample 10 mm or longer. They are usually seen in a sample 5 mm or less whenever the sample is moved transversely across the focused laser beam.

In conclusion: the optical surface waves in a $GaAs-Al_{0.2}Ga_{0.8}As$ periodic layered medium have been observed. The experimental results are consistent with the theoretical calculations. This observation also demonstrates the optical analog of electronic surface states in crystals.

Table I. CHARACTERISTICS OF SURFACE MODES

Mode	β in units of $(\frac{2\pi}{\lambda})$	$K\Lambda$	η^*	α^+ cm^{-1}
1	3.357	$\pi + i(7.233 \times 10^{-1})$	2.89×10^{-8}	2.6×10^{-5} cm^{-1}
2	3.185	$2\pi + i(5.568 \times 10^{-2})$	2.63×10^{-1}	6.3×10^{1} cm^{-1}
3	2.927	$3\pi + i(2.183 \times 10^{-2})$	5.92×10^{-1}	1.7×10^{2} cm^{-1}
4	2.490	$4\pi + i(8.109 \times 10^{-3})$	8.23×10^{-1}	3.2×10^{2} cm^{-1}

$^*\eta$ = (Intensity at Substrate)/(Intensity at Surface)

$^+\alpha$ = attenuation coefficient

References - Chapter 7

1. P. Yeh and A. Yariv, Opt. Comm. $\underline{19}$, 427 (1976).

2. A. Y. Cho, A. Yariv and P. Yeh, Appl. Phys. Lett. $\underline{30}$, 471 (1977).

3. W. L. Bond, B. G. Cohen, R.C.C. Leite and A. Yariv, Appl. Phys. Lett. $\underline{2}$, 57 (1963).

4. E. Garmire, H. Stoll, A. Yariv and R. G. Hunsperger, Appl. Phys. Lett. $\underline{21}$, 87 (1972).

5. A. Y. Cho and J. R. Arthur, Progress in Solid State Chemistry, Vol. 10 (Pergamon Press, 1975), pp. 157-191.

6. J. L. Merz and A. Y. Cho, Appl. Phys. Lett. $\underline{28}$, 456 (1976).

7. P. K. Tien, Appl. Opt. $\underline{10}$, 2395 (1971).

8. D. C. Flanders, H. Kogelnik, R. V. Schmidt and C. V. Shank, Appl. Phys. Lett. $\underline{24}$, 194 (1974).

9. R. de L. Kronig and W. G. Penney, Proc. Roy. Soc. A $\underline{130}$, 499 (1930).

10. I. Tamm, Physik Zeits., Sowjetunion $\underline{1}$, 733 (1932).

11. W. Shockley, Phys. Rev. $\underline{56}$, 317 (1939).

12. D. Kossel, J. Opt. Soc. Am. $\underline{56}$, 1434 (1966).

13. J. A. Arnaud and A.A.M. Saleh, Appl. Opt. $\underline{13}$, 2343 (1974).

14. P. Yeh, A. Yariv and C. S. Hong, J. Opt. Soc. Am. $\underline{67}$, 423 (1977).

Appendix A

DERIVATION OF A GENERAL TRANSLATION MATRIX

Translation matrices of a general periodic layered medium with the index of refraction given by

$$
n(x) = \begin{cases} n_1 & x_0 < x < x_1 \\ n_2 & x_1 < x < x_2 \\ \vdots \\ n_M & x_{M-1} < x < x_M \end{cases} \tag{A.1}
$$

$$
n(x + \Lambda) = n(x) \quad , \qquad \Lambda = x_M - x_0 \tag{A.2}
$$

There are M layers in each period. The thickness of the mth layer is given by

$$
t_m = x_m - x_{m-1} \tag{A.3}
$$

The electric field distribution in the mth layer of the nth unit cell is given by

$$
E(x) = a_n^{(m)} e^{ik_{mx}(x-n\Lambda)} + b_n^{(m)} e^{-ik_{mx}(x-n\Lambda)} \tag{A.4}
$$

The translation matrix that relates the mth layers of two neighboring unit cells is designated as $T^{(m)}$

$$
\begin{pmatrix} a_{n-1}^{(m)} e^{ik_{mx}x_m} \\ b_{n-1}^{(m)} e^{-ik_{mx}x_m} \end{pmatrix} = T^{(m)} \begin{pmatrix} a_n^{(m)} e^{ik_{mx}x_m} \\ b_n^{(m)} e^{-ik_{mx}x_m} \end{pmatrix} \tag{A.5}
$$

$T^{(m)}$ is derived by employing the continuity conditions.

$$T^{(m)} = \frac{1}{2^m} \prod_{\alpha=m+1}^{M+m} \begin{pmatrix} (1 + C_\alpha)\, e^{-ik_{\alpha x} t_\alpha} & (1 - C_\alpha)\, e^{ik_{\alpha x} t_\alpha} \\ (1 - C_\alpha)\, e^{-ik_{\alpha x} t_\alpha} & (1 + C_\alpha)\, e^{ik_{\alpha x} t_\alpha} \end{pmatrix} \quad \text{(A.6)}$$

where

$$C_\alpha = \begin{cases} \dfrac{k_{\alpha x}}{k_{(\alpha-1)x}} & \text{TE waves} \\[2em] \dfrac{n_\alpha^2 k_{(\alpha-1)x}}{n_{(\alpha-1)}^2 k_{\alpha x}} & \text{TM waves} \end{cases} \quad \text{(A.7)}$$

Note that

$$C_{M+\alpha} = C_\alpha$$

$$t_{M+\alpha} = t_\alpha \quad \text{(A.8)}$$

and

$$\prod_{\alpha=1}^{M} C_\alpha = 1$$

$$\sum_{\alpha=1}^{M} t_\alpha = \Lambda \quad \text{(A.9)}$$

The translation operator $T^{(m)}$ is formed by a product of M matrices. A cyclic permutation of the order of multiplication yields $T^{(m+1)}$. The translation operators for different m values are different but have the same eigenvalues.

If $\mu \neq$ constant, then

$$C_\alpha = \begin{cases} \dfrac{k_{\alpha x} \, \mu_{\alpha-1}}{k_{(\alpha-1)x} \mu_\alpha} & \text{TE waves} \\[2em] \dfrac{n_\alpha^2 \, k_{(\alpha-1)x} \mu_{\alpha-1}}{n_{\alpha-1}^2 k_{\alpha x} \, \mu_\alpha} & \text{TM waves} \end{cases} \qquad (A.10)$$

Appendix B

ENERGY VELOCITY AND GROUP VELOCITY OF ELECTROMAGNETIC BLOCH
WAVES IN PERIODIC MEDIA

The equality of group velocity and energy velocity in periodic layered media was examined recently [1]. We will now show that this equality is true in an arbitrary periodic medium provided the medium is lossless. The electromagnetic susceptibility tensors, reflecting the translational symmetry of the medium, are periodic functions of $\vec{x}$,

$$\varepsilon_{ij}(\vec{x}) = \varepsilon_{ij}(\vec{x} + \vec{a}) \tag{B.1}$$

$$\mu_{ij}(\vec{x}) = \mu_{ij}(\vec{x} + \vec{a}) \tag{B.2}$$

where $\vec{a}$ is an arbitrary lattice vector. The propagation of the electromagnetic waves is described by Maxwell's equations

$$\nabla \times \vec{H} = -i\omega\varepsilon \cdot \vec{E} \tag{B.3}$$

$$\nabla \times \vec{E} = i\omega\mu \cdot \vec{H} \tag{B.4}$$

where we assume the $e^{-i\omega t}$ time dependence.

According to the translation symmetry of the medium (and/or Floquet theorem), the waves assume the following form:

$$\vec{E} = \vec{E}_K(\vec{x}) \, e^{i\vec{K}\cdot\vec{x}} \tag{B.5}$$

$$\vec{H} = \vec{H}_K(\vec{x}) \, e^{i\vec{K}\cdot\vec{x}} \tag{B.6}$$

where $\vec{E}_K(\vec{x})$ and $\vec{H}_K(\vec{x})$ are periodic,

$$\vec{E}_K(\vec{x}) \;=\; \vec{E}_K(\vec{x} + \vec{a}) \tag{B.7}$$

$$\vec{H}_K(\vec{x}) \;=\; \vec{H}_K(\vec{x} + \vec{a}) \tag{B.8}$$

The subscript K indicates that the functions $\vec{E}_K$ and $\vec{H}_K$ depend on K which is known as the Bloch wave vector. A dispersion relation exists between K and ω

$$\omega = \omega(\vec{K}) \tag{B.9}$$

The time averaged flux of energy in an electromagnetic field is given by

$$\vec{S} = \frac{1}{2}\,\mathrm{Re}[\vec{E} \times \vec{H}*] \tag{B.10}$$

The time averaged electromagnetic energy density is given by

$$U = \frac{1}{4}\,[\vec{E} \cdot \varepsilon \cdot \vec{E}* + \vec{H} \cdot \mu \cdot \vec{H}*] \tag{B.11}$$

The electromagnetic susceptibility tensors are assumed to be real. In the case of a propagating Bloch wave in a periodic structure, S and U are both periodic functions of space. It is desirable to define the energy velocity as

$$\vec{V}_e \;=\; \frac{\dfrac{1}{V}\displaystyle\int \vec{S}\, d^3\vec{x}}{\dfrac{1}{V}\displaystyle\int U\, d^3\vec{x}} \;\equiv\; \frac{\langle\vec{S}\rangle}{\langle U\rangle} \tag{B.12}$$

where the integration is over a unit cell and V is the volume of the cell. By substituting (B.5) and (B.6) into (B.10) and (B.11), we get from (B.12)

$$\vec{V}_e = \frac{\left\langle \dfrac{1}{2}\,\mathrm{Re}[\vec{E}_K \times \vec{H}_K]\right\rangle}{\left\langle \dfrac{1}{4}\,(\vec{E}_K \cdot \varepsilon \cdot \vec{E}_K^* + \vec{H}_K \cdot \mu \cdot \vec{H}_K^*)\right\rangle} \tag{B.13}$$

where the brackets < > denote unit cell average.

The group velocity $\vec{V}_g$ is defined as

$$\vec{V}_g = \nabla_K \omega = \left(\frac{\partial \omega}{\partial \vec{K}}\right) \tag{B.14}$$

which is a vector perpendicular to the normal surface. If we substitute the Bloch waves (B.5) and (B.6) into Maxwell's equations (B.3) and (B.4), we obtain

$$\nabla \times \vec{H}_K + i\vec{K} \times \vec{H}_K = -i\omega\varepsilon \cdot \vec{E}_K \tag{B.15}$$

$$\nabla \times \vec{E}_K + i\vec{K} \times \vec{E}_K = i\omega\mu \cdot \vec{H}_K \tag{B.16}$$

To prove that $\vec{V}_e$ and $\vec{V}_g$ are equal, we start from (B.15) and (B.16). Suppose now that $\vec{K}$ is changed by an infinitesimal amount $\delta\vec{K}$. If $\delta\omega$, $\delta\vec{E}_K$, and $\delta\vec{H}_K$ are the corresponding changes in ω, $\vec{E}_K$, and $\vec{H}_K$, respectively, we have

$$\nabla \times \delta\vec{H}_K + i\delta\vec{K} \times \vec{H}_K + i\vec{K} \times \delta\vec{H}_K = -i\varepsilon \cdot \vec{E}_K\delta\omega - i\omega\varepsilon \cdot \delta\vec{E}_K \tag{B.17}$$

$$\nabla \times \delta\vec{E}_K + i\delta\vec{K} \times \vec{E}_K + i\vec{K} \times \delta\vec{E}_K = i\mu \cdot \vec{H}_K\delta\omega + i\omega\mu \cdot \delta\vec{H}_K \tag{B.18}$$

We now consider $\vec{H}_K^* \cdot$ (B.18) $+ \vec{E}_K \cdot$ (B.17)*. Using the identity

$$\vec{A} \cdot (\vec{B} \times \vec{C}) = \vec{B} \cdot (\vec{C} \times \vec{A})$$

we get

$$\vec{H}_K^* \cdot \nabla \times \delta\vec{E}_K + \vec{E}_K \cdot \nabla \times \delta\vec{H}_K^* + i\delta\vec{K} \cdot (\vec{E}_K \times \vec{H}_K^*) + i\delta\vec{K} \cdot (\vec{E}_K \times \vec{H}_K^*)$$

$$+ i\vec{K} \cdot (\delta\vec{E}_K \times \vec{H}_K^*) + i\vec{K} \cdot (\vec{E}_K \times \delta\vec{H}_K^*) = i\omega[\vec{H}_K^* \cdot \mu \cdot \delta\vec{H}_K + \vec{E}_K \cdot \varepsilon \cdot \delta\vec{E}_K^*]$$

$$+ i\delta\omega[\vec{H}_K^* \cdot \mu \cdot \vec{H}_K + \vec{E}_K \cdot \varepsilon \cdot \vec{E}_K^*] \qquad (B.19)$$

The electromagnetic susceptibility tensors μ and ε are assumed to be symmetric so that

$$\vec{H}_K^* \cdot \mu \cdot \delta\vec{H}_K = \delta\vec{H}_K \cdot \mu \cdot \vec{H}_K^* \qquad (B.20)$$

$$\vec{E}_K \cdot \varepsilon \cdot \delta\vec{E}_K^* = \delta\vec{E}_K^* \cdot \varepsilon \cdot \vec{E}_K \qquad \text{etc.} \qquad (B.21)$$

If we multiply both sides of (B.3) by $\delta\vec{E}_K^*$ and both sides of the complex conjugate equation (B.4)* by $\delta\vec{H}_K$, we get

$$i\omega\delta \vec{E}_K^* \cdot \varepsilon \cdot \vec{E}_K = -\delta\vec{E}_K^* \cdot \nabla \times \vec{H}_K - i\vec{K} \cdot (\vec{H}_K \times \delta\vec{E}_K^*) \qquad (B.22)$$

$$i\omega\delta \vec{H}_K \cdot \mu \cdot \vec{H}_K^* = -\delta\vec{H}_K \cdot \nabla \times \vec{E}_K^* + i\vec{K} \cdot (\vec{E}_K^* \times \delta\vec{H}_K) \qquad (B.23)$$

Using (B.20), (B.21) and (B.22), (B.23), equation (B.19) can be written

$$\vec{H}_K^* \cdot \nabla \times \delta\vec{E}_K + \vec{E}_K \cdot \nabla \times \delta\vec{H}_K^* + \delta\vec{E}_K^* \cdot \nabla \times \vec{H}_K + \delta\vec{H}_K \cdot \nabla \times \vec{E}_K^*$$

$$+ 2i\delta\vec{K} \cdot (\vec{E}_K \times \vec{H}_K^*) + i\vec{K} \cdot (\delta\vec{E}_K \times \vec{H}_K^* + \vec{H}_K \times \delta\vec{E}_K^* + \vec{E}_K \times \delta\vec{H}_K^* + \delta\vec{H}_K \times \vec{E}_K^*)$$

$$= i\delta\omega[\vec{H}_K^* \cdot \mu \cdot \vec{H}_K + \vec{E}_K^* \cdot \varepsilon \cdot \vec{E}_K] \qquad (B.24)$$

The right hand side of (B.24) is a pure imaginary number; we take the imaginary part of (B.24) by considering (B.24)-(B.24)*

$$[\vec{H}_K^* \cdot \nabla \times \delta\vec{E}_K - \delta\vec{E}_K \cdot \nabla \times \vec{H}_K^*] + [\vec{E}_K \cdot \nabla \times \delta\vec{H}_K^* - \delta\vec{H}_K^* \cdot \nabla \times \vec{E}_K] +$$

$$[\delta\vec{E}_K^* \cdot \nabla \times \vec{H}_K - \vec{H}_K \cdot \nabla \times \delta\vec{E}_K^*] + [\delta\vec{H}_K \cdot \nabla \times \vec{E}_K^* - \vec{E}_K^* \cdot \nabla \times \delta\vec{H}_K]$$

$$+ 2i\delta\vec{K} \cdot [\vec{E}_K \times \vec{H}_K^* + \vec{E}_K^* \times \vec{H}_K]$$

$$+ i\vec{K} \cdot [\delta\vec{E}_K \times \vec{H}_K^* + \vec{H}_K \times \delta\vec{E}_K^* + \vec{E}_K^* \times \delta\vec{H}_K + \delta\vec{H}_K^* \times \vec{E}_K]$$

$$+ i\vec{K} \cdot [\vec{E}_K \times \delta\vec{H}_K^* + \delta\vec{H}_K \times \vec{E}_K^* + \delta\vec{E}_K^* \times \vec{H}_K + \vec{H}_K^* \times \delta\vec{E}_K]$$

$$= 2i\delta\omega[\vec{H}_K \cdot \mu \cdot \vec{H}_K^* + \vec{E}_K \cdot \varepsilon \cdot \vec{E}_K^*] \qquad (B.25)$$

The last two terms on the left hand side of equation (B.25) cancel each other.

Using

$$\nabla \cdot (A \times B) = B \times (\nabla \times A) - A \cdot (\nabla \times B) \qquad (B.26)$$

equation (B.25) can be written

$$\nabla \cdot \vec{F} + 2i\delta\vec{K} \cdot 2 \text{ Re}[\vec{E}_K \times \vec{H}_K^*] = 2i\delta\omega[\vec{H}_K \cdot \mu \cdot \vec{H}_K^* + \vec{E}_K \cdot \varepsilon \cdot E_K^*] \qquad (B.27)$$

where $\vec{F}$ is a periodic function of $\vec{x}$ and is given by

$$\vec{F} = \delta\vec{E}_K \times \vec{H}_K^* + \delta\vec{H}_K^* \times \vec{E}_K + \vec{H}_K \times \delta\vec{E}_K^* + \vec{E}_K \times \delta\vec{H}_K \qquad (B.28)$$

If we perform an integration over a unit cell on (B.27), we get

$$<\nabla \cdot \vec{F}> + 4i\delta\vec{K} \cdot <\text{Re}(\vec{E}_K \times \vec{H}_K^*)> = 2i\delta\omega <\vec{H}_K \cdot \mu \cdot \vec{H}_K^* + \vec{E}_K \cdot \varepsilon \cdot \vec{E}_K^*> \quad \text{(B.29)}$$

We notice that the first term in equation (B.29) is identically zero because of the periodic nature of $\vec{F}$,

$$<\nabla \cdot \vec{F}> = \int_{\text{unit cell}} \nabla \cdot \vec{F} \, d^3\vec{x} = 0 \quad \text{(B.30)}$$

Thus we have, from (B.13)

$$\delta\omega = \vec{V}_e \cdot \delta\vec{K} \quad \text{(B.31)}$$

From the definition of the group velocity we also have

$$\delta\omega = (\nabla_K\omega) \cdot \delta\vec{K} = \vec{V}_g \cdot \delta\vec{K} \quad \text{(B.32)}$$

Since $\delta\vec{K}$ is an arbitrary vector, we conclude that

$$\vec{V}_e = \vec{V}_g \quad \text{(B.33)}$$

Reference

1. P. Yeh, A. Yariv and C. S. Hong, J. Opt. Soc. Am. 67, 423 (1977).

APPENDIX C

Zeros of Mode Dispersion Relation

To prove that equation (3.14) have N zeros in each allowed band where $K\Lambda$ varies from $m\pi$ to $(m+1)\pi$, we need to show that the left hand side of the same equation changes sign N times in each allowed hand. We define

$$F(K\Lambda) = A \frac{\sin NK\Lambda}{\sin K\Lambda} - \frac{\sin(N-1)K\Lambda}{\sin K\Lambda} \tag{C.1}$$

Where A can also be considered as a function of $K\Lambda$. Let's now examine the sign of F at $K\Lambda = n\pi/N$, where $n = 0, 1, 2, \cdots N$. From (C.1) we obtain

$$F(\frac{n\pi}{N}) = \begin{cases} N[A(0) - 1] + 1 & n = 0 \\ (-1)^n & n = 1, 2, \cdots N-1 \\ (-1)^{N-1} N[A(\pi) + 1] - 1 & n = N \end{cases} \tag{C.2}$$

In order to show that F changes sign N times we need to show that

$$N[A(0) - 1] + 1 \quad > 0 \tag{C.3}$$

and

$$N[A(\pi) + 1] - 1 \quad < 0 \tag{C.4}$$

for all N.

Since N is arbitrary, we need to show that

$$A(0) > 1 \tag{C.5}$$

and

$$A(\pi) < -1 \tag{C.6}$$

From (2.37), (3.9) and (3.10), we obtain

$$\frac{A+D}{2} = \cosh qa \cos pb - \frac{1}{2}(\frac{p}{q} - \frac{q}{p}) \sinh qa \sin pb = 1 \quad \text{at } K\Lambda = 0 \quad (C.7)$$

$$\frac{A-D}{2} = \sinh qa \cos pb - \frac{1}{2}(\frac{p}{q} - \frac{q}{p}) \cosh qa \sin pb \qquad (C.8)$$

Using C.7, $(\frac{p}{q} - \frac{q}{p})$ can be eliminated from C 8. Thus we have, after a few mathematical steps

$$\frac{A-D}{2} = \frac{\cosh qa - \cos pb}{\sinh qa} \qquad \text{at } K\Lambda = 0 \qquad (C.9)$$

The right hand side of C.9 is always positive. Combining (C.7) with (C.9), we obtain

$$A(0) > 1 \qquad (C.10)$$

(C.6) can be proven in a similar way. Thus we have proven that F changes sign N times in the region where $K\Lambda$ varies from 0 to π. Since equation (3.14) is invariant under $K\Lambda \rightarrow K\Lambda + \pi$, our statement is proven.

Appendix D

Derivation of Chebyshev Identity

The Nth power of a unimodular matrix can be simplified as shown in the following equation

$$\begin{pmatrix} A & B \\ C & D \end{pmatrix}^N = \begin{pmatrix} AU_{N-1} - U_{N-2} & BU_{N-1} \\ CU_{N-1} & DU_{N-1} - U_{N-2} \end{pmatrix} \tag{D.1}$$

where

$$U_N = \frac{\sin(N+1)K\Lambda}{\sin K\Lambda} \tag{D.2}$$

with

$$K\Lambda = \cos^{-1}\left(\frac{A+D}{2}\right) \tag{D.3}$$

Proof:

Let $V_\pm$ be the normalized eigenvectors of the ABCD-matrix with eigenvalues $e^{\pm iK\Lambda}$ respectively.

$$\begin{pmatrix} A & B \\ C & D \end{pmatrix} V_\pm = e^{\pm iK\Lambda} V_\pm \tag{D.4}$$

It is evident that the two eigenvalues are inverse of each other because of the fact that the matrix in A.2-4 is unimodular. They are given by

$$e^{\pm iK\Lambda} = \left(\frac{A+D}{2}\right) \pm \sqrt{\left(\frac{A+D}{2}\right)^2 - 1} \tag{D.5}$$

with the corresponding eigenvectors given by

$$V_\pm = \begin{pmatrix} \alpha_\pm \\ \beta_\pm \end{pmatrix} \tag{D.6}$$

where

$$\alpha_\pm = \frac{B}{\sqrt{B^2+(e^{\pm iK\Lambda} - A)^2}} \quad , \quad \beta_\pm = \frac{e^{\pm iK\Lambda} - A}{\sqrt{B^2+(e^{\pm iK\Lambda} - A)^2}} \tag{D.7}$$

The Chebyshev identity (D.1) can be derived by employing the following matrix equation

$$\left\{ M \begin{pmatrix} A & B \\ C & D \end{pmatrix} M^{-1} \right\}^N = M \begin{pmatrix} A & B \\ C & D \end{pmatrix}^N M^{-1} \tag{D.8}$$

which says that the Nth power of a transformed matrix is equal to the transform of the Nth power of the original matrix. If a matrix M can be found such that

$$M \begin{pmatrix} A & B \\ C & D \end{pmatrix} M^{-1} = \begin{pmatrix} e^{iK\Lambda} & 0 \\ 0 & e^{-iK\Lambda} \end{pmatrix} \tag{D.9}$$

then the Nth power of the ABCD-matrix is immediately given by

$$\begin{pmatrix} A & B \\ C & D \end{pmatrix}^N = M^{-1} \begin{pmatrix} e^{iNK\Lambda} & 0 \\ 0 & e^{-iNK\Lambda} \end{pmatrix} M \tag{D.10}$$

The matrix M which transforms the ABCD-matrix into a diagonal matrix can be constructed from the eigenvectors (D.6) of the ABCD-matrix. M and its inverse M^{-1} are given by

$$M^{-1} = \frac{1}{\sqrt{\alpha_+\beta_- - \alpha_-\beta_+}} \begin{pmatrix} \alpha_+ & \alpha_- \\ \beta_+ & \beta_- \end{pmatrix} \tag{D.11}$$

$$M = \frac{1}{\sqrt{\alpha_+\beta_- - \alpha_-\beta_+}} \begin{pmatrix} \beta_- & -\alpha_- \\ -\beta_+ & \alpha_+ \end{pmatrix} \tag{D.12}$$

The two columns in (D.11)) are simply the eigenvectors of the ABCD-matrix. It can be easily seen by simple matrix multiplication that (D.9) is true as long as M and M^{-1} are given by (D.12) and (D.11) respectively. The Chebyshev identity (D.1) follows directly from (D.10) by carrying out the matrix multiplication.

$$
\begin{pmatrix} A & B \\ C & D \end{pmatrix}^N = \frac{1}{\alpha_+\beta_- - \alpha_-\beta_+} \begin{pmatrix} \alpha_+ & \alpha_- \\ \beta_+ & \beta_- \end{pmatrix} \begin{pmatrix} e^{iNK\Lambda} & 0 \\ 0 & e^{-iNK\Lambda} \end{pmatrix} \begin{pmatrix} \beta_- & -\alpha_- \\ -\beta_+ & \alpha_+ \end{pmatrix}
$$

$$
= \begin{pmatrix} \dfrac{A \sin NK\Lambda - \sin(N-1)K\Lambda}{\sin K\Lambda} & \dfrac{B \sin NK\Lambda}{\sin K\Lambda} \\[4mm] \dfrac{C \sin NK\Lambda}{\sin K\Lambda} & \dfrac{D \sin NK\Lambda - \sin(N-1)K\Lambda}{\sin K\Lambda} \end{pmatrix}
$$

$$(D.13)$$

The last step is left to the reader.